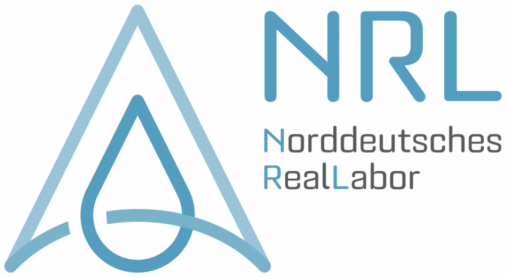

MASTER THESIS
Nicolas Neubauer

Model–Based Techno–Economic Optimization of a Grid Serving Electrolyzer on an Industrial Scale

FACULTY OF LIFE SCIENCES
Fakultät Life Sciences

DEPARTMENT OF PROCESS ENGINEERING
Department Verfahrenstechnik

HAMBURG UNIVERSITY
OF APPLIED SCIENCES
Hochschule für Angewandte
Wissenschaften Hamburg

The author would like to express his sincere and heartfelt gratitude to his parents who made his studies possible that gave him so much pleasure. It is now perfect, in the literal sense of the word.
Thanks Mum, thanks Dad!

Master Thesis

Model–Based Techno–Economic Optimization of a Grid Serving Electrolyzer on an Industrial Scale

Author:	Nicolas Neubauer (B.Eng.)
	[redacted]
Submitted:	January 4^{th}, 2023 in Hamburg
University:	Hamburg University of Applied Sciences (HAW)
Faculty:	Life Sciences
Department:	Process Engineering
Study Program:	Process Engineering (M.Sc.)
Institute:	Competence Center for Renewable Energies and EnergyEfficiency (CC4E)
Research Program:	Northern German Living Lab (NRL)
1. Supervisor:	Professor Dr. Marc Hölling
2. Supervisor:	Mike Blicker (Dipl.)
Tutor:	Carsten Schütte (M.Sc.)

Contents

List of Figures

List of Tables

List of Abbrevations

AEL	Alkaline Electrolyzer
AF	Anode Furnaces
AFLH	Annual Full Load Hours
aFRR	Automatic Frequency Restoration Reserve
A_r	Annuity factor
AuxS	Auxiliary Service
$AuxS_{int}$	Auxiliary Service Interval
Ba	Battery
BCM	Balancing Capacity Market
BEM	Balancing Energy Market
BNetzA	"Bundesnetzagentur"
CapEx	Capital Expenditures
CCfD	Carbon–Contracts–for–Difference
CH_4	Methane
$C_{h/int}$	Hours per Interval
ci	Gas component
Co	Compressor
CO_2	Carbon Dioxide
$CO_{2,eq}$	Carbon Dioxide Equivalents
DA	Day–Ahead
DSO	Distribution System Operator
EEX	Europan Energy Exchange AG
El	Electrolyzer
El_{AFLH}	El AFLH
El_{Grad}	El load gradient
El_{min}	El minimal load
Entso–E	European Network of Transmission System Operators for Electricity
EP	Electric Power
EPC	Electricity–Price–Compensation
EPEX	Epex Spot SE
η	Efficiency
ETS	Emission–Trading–System
EUA	European–Union–Allowances
EXAA	Energy Exchange Austria AG
$F_{CO2,H2}$	CO_2–Footprint of H_2
F_{CO2}	CO_2–Footprint
FCR	Frequency Containment Reserve
f_{FCO2}	Environmental weighting factor
$f_{weighting}$	weighting factor
FfE München	"Forschungsstelle für Energiewirtschaft München e. V."
f_{LCoH2}	Economic weighting factor
Fraunhofer ISE	"Fraunhofer–Institut für Solare Energiesysteme"
f_{red}	Reducing factor
GoO	Gurantees of Origin

Gr	Grid
H	Enthalpy
HHV	Higher Heating Value
H_2	Hydrogen
H_2O	Water
ID	Intraday
IDX	Index
Inf	Inflation
Inv	Investment
Inv_{re}	Reinvestment
$Inv_{Residual}$	Residual Investment
IRENA	International Renewable Energy Agency
LCoE	Levelized Costs of Energy
$LCoH_2$	Levelized Costs of H_2
LHV	Lower Heating Value
Li–Ion Ba	Lithium-Ion Battery
M	Maintenance
mFRR	Manual Frequency Restoration Reserve
MpY	Minutes per Year
MOO	Multi–Objective Optimization
NaN	Not–a–Number
NG	Natural Gas
NNI	Non–Negative–Integers
NNR	Non–Negative–Reals
NRL	Northern German Living Lab
N_2	Nitrogen
O_2	Oxygen
OpEx	Operating Expenditures
OTC	Over–the–Counter
PEMEL	Proton Exchange Membrane Electrolyzer
PPA	Power Purchase Agreement
$Price_{Cap}$	Capacity Price
$Price_{Op}$	Operating Price
$P_{kg(H2)/MW}$	specific H_2 production
Pr	Process
PtH_2	Power–to–Hydrogen
PYOMO	Python Open–source Modelling and Optimization
Q	Heat
r_{int}	Interest rate
RLI	Reiner–Lemoine–Institut
SOC	State–of–Charge
SOEL	Solid Oxide Electrolyzer
SRU	“Sachverständigenrat für Umweltfragen”
St	Storage
StD_{rel}	Relative Standard Deviation
t_{Comp}	Component lifetime
t_{int}	Interval
$t_{Project}$	Project lifetime
TRL	Technology Readiness Level
TS	Time–Stamp
TSO	Transmission System Operator
UTC	Coordinated Universal Time
w_{real}	real work
w_{rev}	reversible work
x	Volumetric concentration
ρ	Density

Chapter 1

Introduction

Embedded in the decarbonization ambitions of industrial actors and the transition to Hydrogen (H_2) as a feedstock for reducing processes, the installed capacity of Power–to–Hydrogen (PtH_2) units based on electrolysis is growing [41], [77]. These PtH_2 units come with two positive effects. They can, on the one hand, convert electrical energy into chemical energy, which is useful for all kinds of industrial processes and mobility applications. This allows the increasing amount of renewably sourced electricity to be coupled with other non–electric sectors. On the other hand, PtH_2 units offer the option of reacting flexibly to external factors such as the availability of renewable electricity generation or the demand for electric energy by market participants. This is possible primarily because the production of H_2 is decoupled from the consumer by means of storage units. This flexibility can be used to operate "grid serving" by reflecting the balance of supply and demand (e.g. indicated by the electricity price, discussed later) [22], [75]. These additional degrees of freedom induce a component sizing and dispatching issue for PtH_2 units.

The aim of this thesis is to compute optimal component sizes and dispatch based on different scenarios for such PtH_2 units including an electrolyzer, a battery and a pressurized H_2 storage with a compressor. Thereby, the thesis incorporates the local circumstances to source H_2 at the production facility of Aurubis AG (in the following Aurubis) in Hamburg as a case study. The optimum is defined by the case study to represent minimized Levelized Costs of H_2 ($LCoH_2$) in a first economic step and the CO_2–Footprint of H_2 ($F_{CO2,H2}$) based on the F_{CO2} of the converted electricity in a second environmental step. This thesis, therefore, develops a software–based optimization tool to compute optimal dimensions for flexible operating industrial–scale PtH_2 units. Moreover, this work assesses the option for flexible operating PtH_2 units to provide Auxiliary Service (AuxS). The optimization tool is based on deterministic mathematical optimization and makes optimized component sizes together with an optimized dispatch for the PtH_2 elements available. It is tested with generic data for validation. This is followed by applying the optimization tool to the case study based on an economic objective represented by the $LCoH_2$. First, the sensitivity of the obtained results is analyzed for the case study with respect to technical and economic input parameters. Second, the case study is analyzed with respect to different scenarios which are worked out in cooperation with the industry partner Aurubis. In addition, the resulting $F_{CO2,H2}$ is analyzed and targeted in a subsequent analysis within a combined objective approach.

Thereby this research is based on the findings of Schütte et al. (2022) and Röben et al. (2021) who

assessed the implementation of a PtH_2 unit at the production facility of Aurubis qualitatively and simulatively in a techno–economic manner [111], [117]. This thesis aims to extend these findings by collaborating closely with the industry partner to replicate the case study precisely. Further, this consideration includes a grid–serving operating strategy of the PtH_2 unit by reflecting the balance in the electricity grid based on the spot market prices. Thereby, the thesis extends a scheduling approach of Wagner et al. (2022) who focused on optimized energy procurement and showed that a flexible operating strategy based on a H_2 storage results in financial benefits [143]. Moreover, this work analyzes the possibility of providing AuxS and identifies the effects on the $LCoH_2$ together with effects on the optimized PtH_2 dimensions. The applied objective function is subsequently extended to include an environmental assessment based on the CO_2–Footprint (F_{CO2}) of the converted electric energy.

This thesis is worked out under the framework of the Northern German Living Lab (NRL) which is coordinated by the Competence Center for Renewable Energies and EnergyEfficiency (CC4E) at the University of Applied Sciences (UAS, German: HAW) in Hamburg. The research project NRL is a joint research program with industrial and scientific partners to develop solutions for the transition to a renewable–based energy system with a focus on industrial H_2 applications and sector coupling. The NRL is part of the funding initiative “Reallabore der Energiewende” and is funded by the Federal Ministry of Economics and Climate Protection (BMWK). This thesis is involved in a subordinated project with the industry partner Aurubis, which runs a primary copper smelter in Hamburg. The project aims to decarbonize a processing unit through the replacement of fossil natural gas by renewable–sourced H_2. The unit process takes place in the Anode Furnaces (AF), which includes the last pyrometallurgical refinement step of copper. In order to advance the energy transition, literature recommends extensive electrification to enable sector coupling as renewable energy is primarily available as electric energy [3], [30], [114]. However, the energy supply of the AF cannot be directly electrified as they consume energy carriers as feedstock to chemically reduce the intermediate copper product (blister copper). H_2 can work as a link between renewable energies and their application as a reducing agent. This fuel switch taking place in the AF is analyzed from a metallurgical point of view by Edens et al. (2022) at the production facility of Aurubis and in other projects [35], [46].

The structure of this thesis is as follows. The theoretical background is provided in chapter 2 right after this introduction. The fundamentals are distinguished in the sections energy markets, elements of the PtH_2 unit, optimization and the economic and environmental assessment. This section is followed by an analysis of the requirements for this thesis in chapter 3. After the requirements are analyzed, the technical and economic circumstances relevant to this thesis are analyzed in chaper 4. It is divided up into sections covering the energy markets, the PtH_2 unit itself, the case study, and the definition of grid services and a brief outlook on the used software. Thereafter, the design of the optimization tool is presented by addressing each element of the PtH_2 unit individually. The design chapter is followed by the implementation of the optimization tool, which demonstrates the operating procedure with generic test data. The optimization tool is then applied to the case study in chapter 7. This chapter includes a sensitivity study, a scenario analysis based on the $LCoH_2$ objective and a combined objective approach which factors in the $F_{CO2,H2}$. To conclude, the aspects concerning the case study are summarized and consequences are drawn in chapter 8.

Chapter 2

Theoretical Background

This section provides fundamental interrelationships upon which the further chapters build. Referring to energy and in particular chemical and electric energy, the word "convert" is used to address the conversion of one form of energy to another. Following the laws of thermodynamics, real conversions are affected by losses. These losses are considered within this thesis if not stated differently. This chapter on the theoretical background of this thesis addresses the aspects of the energy markets in the first place. This includes the function of the spot and Over–the–Counter (OTC) markets. In the second place, the fundamentals of a Power–to–Hydrogen (PtH_2) unit with its technical elements are described. Thereby, a special focus is on the power to hydrogen conversion by electrolyzers. The procedure of optimization and the environmental and economic assessment are discussed in the third and fourth place.

2.1 Energy markets

The electric power system connects electricity–generating units with electricity–consuming customers of all kinds. The correct function of such a system is constrained by physical means in the first place and by regulative means in the second place. The key physical challenge is to maintain the exact balance of generation and demand, as this balance determines the frequency of the alternating current. The key regulative and economic challenge is to reduce the costs related to the consumption and transmission of electric energy. The physical property of the electric power system is discussed in the first subsection. The regulating bodies, on the European and the national level, reflect this physical challenge in their regulation of the energy markets. The markets aim to allocate predicted energy generation to predicted energy consumption before the energy itself is flowing. The operation of these energy markets is described in the second subsection. To maintain the balance between generation and consumption for all points in time, additional measures are required which react to imbalances in the power system. These measures, summarized with the term Auxiliary Service (AuxS), are explained in the third subsection.

2.1.1 Balance of power generation and demand

The electric power system consists of three main elements which are the power–generating units, the power–transmission system and the power–consuming units. Power can be generated and consumed by a

variety of different participants from an industrial, commercial or private background. The power system in Germany itself is operated by four Distribution System Operators (DSO) on the upper level and on a smaller level by the Transmission System Operators (TSO). This system is defined in Germany by the federal law "Energiewirschaftsgesetz" [13]. The law issues the system operators to maintain a frequency of 50 Hz [15], [98].

Power generation The power generated by the generating units in the power system can be distinguished into two categories. On the one hand, there are conventional power plants based on fossil resources such as coal, gas and oil. The operation of these is based on the combustion of fossil hydrocarbons to run turbines which are connected to electricity generators. Their operation causes the emission of Carbon Dioxide (CO_2). Power–generating units based on nuclear fission are counted as conventional generators whereas their operation does not emit CO_2. Conventional plants are characterized by a predictable and constant output of electric energy [15].

On the other hand, there are renewable power generators such as photovoltaic panels and wind turbines which are considered to operate without the CO_2 emissions. Their power generation is more difficult to predict due to the nature of solar radiation and wind speed. In contrast to conventional power–generating plants, which generate electricity by heating up water and converting this thermal energy to rotational and then to electric energy, renewable power plants directly yield electric energy [15], [21]. Hydro power plants can be considered to be renewable while their electricity generation is predictable.

Frequency The frequency of the alternating current in the power system is governed by the balance of the generation and the consumption of electric energy within a power system. The frequency in Europe is at 50 Hz. The stability of the frequency is primarily provided by the inertial energy induced by the rotating masses within the electric power system. Such rotating masses are all kinds of synchronous generators and their respective turbines. In addition, there are dedicated spinning wheels that induce inertia in the power system, building up the operational reserve. An overview of the distinct AuxS is given in figure 2.1. As soon as the frequency derivates more than ± 0.02 Hz from the 50 Hz baseline, additional measures are in place to restore the frequency. These measures are gathered by the name AuxS and react opposite to the deviation. The AuxS can be divided into three different services which differ in their extent and response time [1], [98].

Frequency Containment Reserve (FCR) providing facilities monitor the current frequency in place and react contrary to a frequency derivation within seconds. Their participation in the frequency stability is compensated by the containment capacity they provide. Their actual operation is not measured by the Distribution System Operator (DSO) [21]. As soon as larger derivations occur, the DSO initiates the intervention by Automatic Frequency Restoration Reserve (aFRR) facilities in the required sense of operation. The aFRR has to deliver its operation within 5 minutes, see illustration 2.1. In contrast to the FCR which is a symmetrical product adjusting automatically to the derivation in either direction, the aFRR is split into negative and positive products. Negative aFRR counters the decrease of the amount of available electric energy in the grid either by reducing the generation or by increasing the consumption, positive aFRR reacts vice versa [21], [98].

The Manual Frequency Restoration Reserve (mFRR) is regulated similarly to the aFRR but is manually

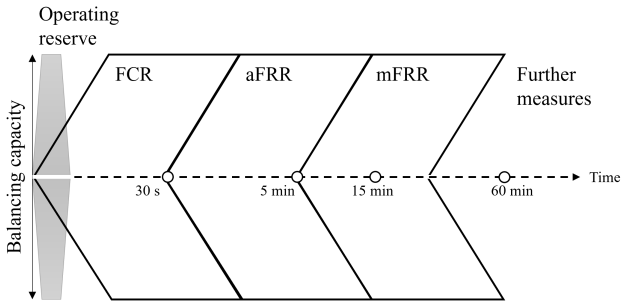

Figure 2.1: Comparison of the auxiliary services in place by their specific time of delivery. Own visualization based on [15], [98].

initiated by the DSO and has to deliver within approximately 12.5 minutes [98]. In the case that AuxS measures are not sufficient to reduce the frequency deviation, further measures have to be taken such as the disconnection of large consumers or the sectional decoupling of the electric grid. The regulations concerning the AuxS are discussed subsequently in section 2.1.3.

System–average emission factor Taking the power plant fleet generating a power mix into account, the specific CO_2 emissions can be calculated. This results in the system–average emission factor, or the CO_2–Footprint (F_{CO2}) of the electricity mix which is considered in this thesis with the unit t_{CO2}/MWh. This thesis bases its F_{CO2} on publications by the "Forschungsstelle für Energiewirtschaft München e. V." (FfE München) (2022) who base their calculations on daily publications by the European Network of Transmission System Operators for Electricity (Entso–E) and the "ecoinvent" database [34], [37], [47]. Further details can be found in the respective publication [47].

The marginal emission factor discussed by Seckinger (2021) takes the additional emissions into account which are caused by a load increase. This is done by incorporating the F_{CO2} gradient of the electricity mix [71], [118].

2.1.2 Excurse: Wholesale markets

Since 1996, the European Union gradually liberalizes the domestic markets for electricity. This effort was implemented in 2003, with the "*Directive [...] concerning common rules for the internal market in electricity and repealing Directive 96/92/EC [...]*" [44]. Therefore, a small excursion to the function of liberal markets is made within this section. First, the context of demand and offer in free markets is discussed by addressing the merit–order system. Second, the two price–setting principles pay–as–bid and pay–as–clear are explained [98].

Merit–Order The merit–order is typically used as an approach to creating a balance of supply and demand, in other terms: to allocate resources. It is summarized in a diagram like the one shown in figure 2.2 which includes the capacity on the horizontal axis and the prices on the vertical axis. This diagram is filled by the offers and demands of the market participants. The offers for the supply and the

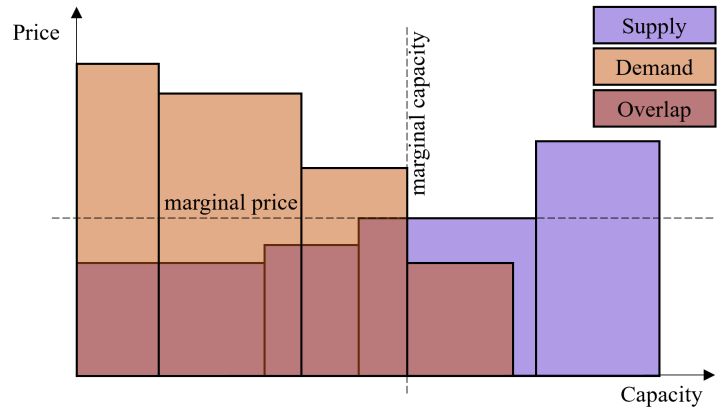

Figure 2.2: Schematic visualization of a wholesale market clearing mechanism and the merit–order. Own visualization based on [98].

consumption are placed on the graph according to their corresponding prices. The market is balanced right at the intersection of both curves in the diagram [15].

In the case of the energy markets, renewable power generation units operate cheaply due to low operating costs compared to conventional plants. Thus renewable bids are lined up at the left side of the capacity curve. Gas–fired power plants show high operating prices so they are lined up at the far right of the merit–order curve. As cheaper capacities are considered first, the renewable generation power units are selected more likely than gas–fired (or other fossil–based) plants [15], [49].

Based on the merit–order chart, there are two principles of price formation which are discussed in the subsequent paragraphs. First, prices can form as the pay–as–clear method which bases on the equilibrium price indicated by the intersection. Second, the price can be structured with the pay–as–bid method which assumes individual prices for each participant according to their bid. Further details are provided in a regulative elaboration by the "European Union Agency for the Cooperation of Energy Regulators" (ACER) (2022) and others [45], [121], [145].

2.1.3 Auxiliary service markets

As several AuxS products are auctioned, this section will provide insights into the auction procedures. Thereby, this section focuses on the FCR and the aFRR aspects since these are relevant to this thesis. In the first place, each AuxS product has a specific time span, which is defined by regulative bodies. Currently, there are 6 AuxS products per day with each covering a duration of 4 hours [1], [50], [98].

To participate at the AuxS, each facility has to conduct a prequalification. Since the prequalification procedure is not of relevance to this thesis, reference is made to relevant literature such as Paulus (2013) and the association of the German DSO [2], [102]. A summary of the AuxS regulations relevant for this thesis is given in table 2.1.

Balancing energy and capacity markets The capacities of AuxS are traded on the Balancing Capacity Market (BCM). The auctions on this market result in the Capacity Price (Price_{Cap}) for each

Table 2.1: Overview of the AuxS regulation covering FCR and aFRR based on [1], [2], [50], [98].

	FCR	**aFRR**
Activation	Local measurement	DSO
Maximal activation delay	30 s	5 min
Duration of the service	0 min to 15 min	30 s to 15 min
Auctions	BCM	BCM and BEM
Minimal size	±1 MW (symmetrical)	5 MW* (negative or positive)
Daily auctioned products	6, each 4 h	6, each 4 h
Price formation	pay–as–clear	pay–as–bid
Bidding limit	/	99,999,99 €/MW**
Pooling	possible	possible

*Minimum is 1 MW if only one bid is submitted per auction.

**Changed several times, this is the current (May, 2022) regulation [54].

product. The FCR and aFRR are based on a Price_{Cap} which implies that the AuxS providing facilities have reserved capacity to deliver their services. Based on the auctioned product, the FCR delivers its service as soon as the local frequency control unit detects a deviation. Unlike the nature of the FCR, the operation of aFRR is auctioned on an individual market.

Additional to the BCM and its Price_{Cap}, the actual delivery of aFRR is auctioned at a separate Balancing Energy Market (BEM). These auctions result in the Operating Price (Price_{Op}). Participants on the markets for aFRR have to offer for both BCM and BEM markets individually. The BEM market for aFRR (and mFRR) was introduced in November 2020. Due to legal conflicts in Germany, the bidding price cap for aFRR products of 9,999.99 €/MWh was changed to 99,999.99 €/MWh several times back and forth. Currently, the operational price bidding cap is set to 99,999.99 €/MWh which is expected to be changed to 15,000,00 €/MWh in June 2022 (information from May 2022) [54].

Pooling There is the option to combine different technical units to large–scale AuxS providing facilities (pools). Each technical unit would have to be prequalified individually. The participation in the wholesale markets of a pool consisting of technical units providing auxiliary services is possible and their relevance is expected to grow with the increasing implementation of renewable energy sources [2], [20].

2.1.4 Electric energy markets

The markets for electric energy are constrained by the exact balance of generation and consumption as discussed above. Basically, the markets focus on the price signal to allocate the amount of flowing electric energy. The European market for electricity is divided into regions with a uniform price, called price zone (sometimes: “bidding zone”). This thesis focuses on the price zone Germany and Luxemburg, as they incorporate a common zone in 2018 after Austria left the same zone [10].

The liberalized markets for electric energy in Europe can be subdivided by the application of two categories. First, there is the temporal aspect which divides the market into a spot and a future market. All contracts representing a timeframe of more than 24 h are considered to be futures. Second, the energy markets can be divided into the exchange market which considers supervised trades and the Over–the–

Counter (OTC) markets. In Europe, the volume of Electric Power (EP) traded on the OTC market outweighs that traded on the exchange markets [10], [15], [98]. The two trading principles taking place on the exchange market or at an OTC market are discussed subsequently in greater detail.

Over–the–Counter On the Over–the–Counter (OTC) market, two parties (sometimes supported by specialized brokers) agree on a contract to supply EP. The prices manifested in that contracts are the result of bilateral (or sometimes multilateral) negotiations and are not affected by exchange prices directly. Contractual details made at an OTC market are disclosed and therefore only accessible to the partners involved [10].

Exchange markets In contrast to the OTC market where only a few parties are involved to form a contract, the exchange market gathers numerous participants. These participants place their offers, either to generate EP or to consume EP. The exchange creates a merit–order list based on these offers. A high share of the consumption offers (79.2 %) is price unflexible while the share of unflexible generation offers is lower (9.1 %) [10]. The exchange markets for electric energy are operated by Europan Energy Exchange AG (EEX), Epex Spot SE (EPEX), Energy Exchange Austria AG (EXAA) and Nord Pool AS. The most relevant institution by traded volume is the EEX followed by the EPEX. While the EEX focuses on EP futures, the three other trading hubs consider the spot markets [15]. As the EPEX is the most relevant institution for spot markets in the price zone Germany and Luxemburg, this thesis focuses on the regulated products of the EPEX incorporating the Day–Ahead (DA) and Intraday (ID) auctions. There is a second continuous ID market offered by the EPEX allowing trades until 5 minutes prior to delivery which is not looked at in this thesis at the request of the industry partner [39].

The **Day–Ahead (DA)** market operated by EPEX covers hourly products which are traded at 14:00 o'clock on the day before delivery. Orders for each hour of the next day can be placed until noon the day before delivery and in smaller increments. The EPEX creates a merit–order list based on these orders and determines a clearing–price. In contrary to the OTC market, buyers and sellers are not matched one by one [39]. The **Intraday (ID)** market enables the trade of electricity more closer to the actual moment of delivery. The market covers products with a duration of a quarter–hour which are traded from 15:00 o'clock on the day before delivery. The ID market does not yield in a clearing price but in individual prices based on the pay–as–bid principle. The volume of electric energy traded on the ID market is smaller compared to the volume traded on the DA market [39].

Gurantees of Origin (GoO) Next to the electric energy markets, there is a separate market where certificates are traded that certify the source of electric energy to be renewable. As the power mix and its F_{CO2} are physically identical at all places, the GoO is a system to show on the balance sheet that the consumed electricity is "green" [28]. In September 2022 the EPEX launched a monthly auction for GoO in addition to the OTC market [39].

2.1.5 Emission–Trading–System

Based on the international treaty on climate protection negotiated in Kyoto 1997, the European Union established the Emission–Trading–System (ETS) in 2005. The system creates a framework in which cer-

tificates to emit Carbon Dioxide Equivalents ($CO_{2,eq}$) are auctioned. The certificates are called European–Union–Allowances (EUA). Enterprises in the aviation, power and industrial sector have to procure these certificates. By limiting the number of certificates on the auction and in the market, the system aims to reduce the amount of CO_2 emitted and increase the price of carbon–based fuels [26].

The phenomenon that industrial players respond to the price increase by relocating their production or upstream investments in regions which are not subject to the ETS rules outside the EU is called "carbon leakage" [11]. This aspect is mitigated by compensating electricity–intensive companies by a system called Electricity–Price–Compensation (EPC). This compensation is issued to decrease the additional costs due to the EUA related price increase in the power sector [42]. Industries can request financial compensation for increased electricity prices when they meet certain requirements. The compensation in Germany is managed by the "Deutsche Emissionshandelsstelle" which publishes equation 2.1 to determine the compensation extent [138].

$$\begin{aligned} EPC = \quad & Consumption_{EP} \cdot F_{Eligable} \cdot F_{Fallback} \cdot F_{CO2,EP} \cdot EUA_{Price} \\ & - Deductible_{EP} \cdot F_{CO2,EP} \cdot \mathrm{EUA}_{Price} \end{aligned} \tag{2.1}$$

Equation 2.1 considers on the one hand the consumed EP and on the other hand the deductible amount of EP. The consumed EP is multiplied by the eligible and the fallback factor which is individually negotiated to determine the amount of EP to be compensated. The $F_{CO2,EP}$ factors in the amount of indirectly emitted $CO_{2,eq}$ by the generation of the consumed EP. Further, the EUA_{Price} considers the related costs to procure the respective certificates. The amount of 1,000 MWh/a is deductible for each enterprise ($\mathrm{Deductible}_{EP}$) [138]. The EUA_{Price} is based on the previous year while the $F_{CO2,EP}$ is considered to be $0.72\,t_{CO2}/\mathrm{MWh}_{EP}$ [12]. To relieve the increased price pressure on European industry and to prevent carbon leakage, the national states have the option to compensate for the increased electricity prices.

2.2 Elements of a PtH_2 unit

The fundamentals concerning the PtH_2 elements are to be introduced in this section. This focuses on the aspects relevant to this thesis. A PtH_2 unit based on electrolysis converts electrical energy to chemical energy in the form of Hydrogen (H_2). The process takes place in an Electrolyzer (El). In addition, a PtH_2 unit in the manner of this thesis incorporates a Battery (Ba), a Compressor (Co) and a pressurized H_2 Storage (St).

2.2.1 Battery

The Battery (Ba) stores electric energy in an electro–chemical way by changing electrical charges. This section provides briefly the relevant aspects of the Ba unit, a more detailed description of Ba is for the example given in Kurzweil (2018) [88]. Ba consist of two electrodes which are enclosed by an electrolyte. Although there are different Ba technologies available, this thesis focuses on the Lithium-Ion Battery (Li–Ion Ba) technology. The charging and discharging process in Li–Ion Ba, transfers positively charged

Lithium kations in the electrolyte back and forth between the two electrodes. The charging and discharging process is affected by losses which are quantified by the Ba Efficiency (η). The efficiency implies that the discharged energy quantity is always smaller than the charged energy quantity [88].

The battery lifetime is restricted by the number of charging cycles and the depth of discharge. A high number of charging cycles contribute to the degradation of the Ba capacity. The depth of discharge is constrained by electrochemical circumstances. A discharge deeper than the specified limit causes irreparable cell damage [88].

2.2.2 Electrolyzer

The Electrolyzer (El) is the main component of a PtH_2 unit as the H_2 generation takes place here. H_2 is generated by splitting Water (H_2O) into its elements H_2 and Oxygen (O_2) by applying a current according to equation 2.6. Several aspects relevant to this thesis addressing the El design, the reactions taking place and technical circumstances are briefly introduced subsequently. For an extended theory concerning the El technologies and the electrolysis chemistry, this thesis refers for example to Kurzweil and Dietlmeier (2018) [88]. The distinct values to be implemented in the optimization tool are elaborated in the technical analysis in section 4.2.4.

Typically, El units are considered to consist out of a stack, where the electrolysis takes place, and the total system which includes peripheric apparatuses such as pumps [106], [111]. Electrolysis can be performed at atmospheric pressure or pressurized, while this thesis considers pressurized El [94].

Electrolyzer design There are three El technologies available on a considerable scale to that point in time. The most mature technology is the Alkaline Electrolyzer (AEL), followed by the Proton Exchange Membrane Electrolyzer (PEMEL) and the Solid Oxide Electrolyzer (SOEL) which is the latest development. SOEL are not considered in this thesis as their Technology Readiness Level (TRL) is not mature enough for a large–scale installation in the next years, although the technology seems to bear good opportunities for heat integration [16], [56], [106], [111], [122], [125].

The AEL technology is based on a liquid alkaline electrolyte which is circulating in the system and two Nickle–based electrodes. The electrolyte consists of 25 to 30 % potassium hydroxide which contains OH^- anions. H_2 evolves next to OH^- anions at the cathode. The OH^- anions permeate through the gas–tight diaphragm to release their electrons on the anode forming O_2 and water as equations 2.2 to 2.3 show. The moving OH^- anions close the electric circuit [88], [94]. The operating temperature is between 50 to 80 °C and at a pressure between 20 to 50 bar. Compared to the PEMEL technology, the spacial footprint is higher because of the electrolyte circulating system [6], [106].

$$Cathode: \quad 2\,H_2O + 2\,e^- \longrightarrow H_2 + 2\,OH^- \tag{2.2}$$

$$Anode: \quad 2\,OH^- \longrightarrow \frac{1}{2}O_2 + H_2O + 2\,e^- \tag{2.3}$$

The PEMEL consists of a polymer membrane that allows protons to permeate and two electrodes. O_2 evolves at the anode side together with protons. These protons permeate to the cathode where H_2 is formed according to equation 2.4 and 2.5 [88], [94]. In contrast to the AEL technology, the PEMEL

electrodes are based on precious metals (Iridium and Platin) which makes them more cost–intensive [6], [106].

$$Anode: \quad H_2O \longrightarrow \frac{1}{2}O_2 + 2\,H^+ + 2\,e^- \tag{2.4}$$

$$Cathode: \quad 2\,H^+ + 2\,e^- \longrightarrow H_2 \tag{2.5}$$

Both El technologies extract the two elements H_2 and O_2 in their gaseous state. Cross–permeation reduces the gas purity and causes a safety issue because an explosive H_2–O_2 mixture is created. Both technologies required desalinized water as feedstock. Commercially available plants, therefore, include a desalination process [106].

H_2 evolution reaction The H_2 evolution reaction is given in equation 2.6. This represents the summative reaction taking place at the anode and cathode of the El. The specific reaction Enthalpy (H) is about 33.35 kWh/kg based on gaseous water or 39.41 kWh/kg based on liquid water at standard conditions (298.15 K and 1,013 mbar) [120]. These two values equal the Lower Heating Value (LHV) and Higher Heating Value (HHV) of H_2.

$$1\,H_2O_{(l)} \longrightarrow 1\,H_{2(g)} + \frac{1}{2}\,O_{2(g)} \qquad \Delta_r H = 286.00\,\frac{kJ}{mol} \;=\; 39.41\,\frac{kWh}{kg} \tag{2.6}$$

According to equation 2.6 the production of 1 kg H_2 consumes 8.94 kg H_2O according to stoichiometry. Thus, 7.94 kg O_2 is produced per kg of H_2. Due to the means of desalination, the actual water consumption of electrolysis is higher [106], [120].

Efficiency and excess heat The reaction in equation 2.6 includes several energy losses, thus more energy has to be applied during electrolysis than chemical energy in the form of H_2 can be extracted. The losses result in incomplete reactions at the electrodes, chemical overpotentials and the operation of peripheric technical components such as pumps, desalination equipment and more [88]. The η of El is a function of the actual load or power. Kopp (2018) publishes a load–dependent system efficiency of a PEMEL which is visualized in figure 2.3 together with a constant η of 60 % as a reference [84]. In addition, the figure shows the stack efficiency of a PEMEL published by Schalenbach et al. (2016).

The data points of Schalenbach et al. (2016) are fitted by Tuschewitzki (2021) [115], [134]. Due to a lack of publicly available data, no efficiency curve for AEL systems is included in this thesis, although the load dependency is assumed by Schalenbach et al. (2016) to behave similar [115]. Figure 2.3 shows that the published stack efficiency of a PEMEL is larger than the system efficiency which can be explained by the additional components considered. The load dependency of the efficiency is pronounced for loads $<0.1\,MW/MW_{max}$. The curvature of the specific H_2 production rates is barely noticeable, thus a linear approximation (such as linear approximation with η=0.6 %) might be reasonable. This work does not consider overload behavior as done by Kopp (2018) and thus equates the maximum load to the nominal load [84]. According to the Danish Energy Agency (2017), approximately 5.0 % points (referenced to the HHV) of the excess heat have to be considered as unrecoverable heat whereas the remaining excess heat

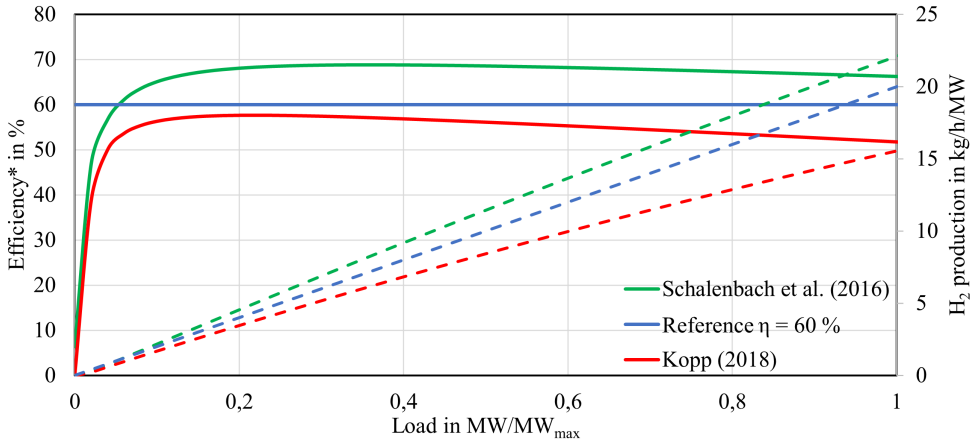

Figure 2.3: Comparison of the load–dependent PEMEL stack efficiency published by Schalenbach et al. (2016) and the PEMEL system efficiency published by Kopp (2018) with a constant efficiency* at η=60 % as a reference on the primary y–axis (straight lines) [84], [115], [134]. The specific H_2 production rates are shown on the secondary y–axis (dashed lines). *Efficiencies are referenced to the LHV.

can be further utilized [23]. This utilization is recommended by Schalling et al. (2022) among others to increase the overall efficiency [30], [107], [111].

Minimal load The El minimal load (El_{min}) is a restriction of the operational load range of an El. The El_{min} for AEL is considered due to the permeation of H_2 molecules on the O_2 evolution site, creating a possibly explosive mixture at low loads and causes H_2 losses according to Tjarks (2017) and Haug (2019) among others [29], [67], [133]. Further, the gas quality on the H_2 evaluating site decreases for low loads in the case of AEL and PEMEL systems [88]. At minimal loads, the share of the auxiliary components like pumps in the power consumption increases so that operation becomes unfavorable [17], [84], [88]. The decreased η can be identified in figure 2.3 for loads <0.1 MW/MW_{max}. Therefore, a minimal operational load for AEL and PEMEL has to be considered.

Load gradient The electrolysis taking place in PEMEL and AEL units can react immediately to changes in the electrical load, whereas auxiliary components are limited in their reaction time [84], [88], [133]. The load gradient is typically referenced to the possible change in % of the nominal load per second [17], [84], [107], [133].

Start–up PEMEL system have less mass to be heated up compared to AEL systems so that their cold–start behaviour is quicker [88]. Further, the pressure in the El systems has to be created. AEL systems are described by the literature to have cold–start times up to 2 h whereas the PEMEL technology can start–up within 10 minutes [23], [29], [107]. Nevertheless, warm–starts are considered according to load gradients at any overload.

Temperature and pressure Compared to high–temperature electrolysis, which is not considered in this thesis, the low–temperature El operates with liquid water below 100 °C. According to Tjarks (2017), the efficiency of the El is a function of the temperature and pressure [133]. This dependency is not considered in this thesis and thus is not further elaborated.

2.2.3 Pressurized H_2 storage

There are several options to store H_2 whereas this thesis focuses on pressurized storage. Other methods such as the storage of liquified H_2 or by other physical or chemical principles are not considered. A pressurized H_2 tank is typically constructed out of composite materials or steel [83]. The mass–based Storage (St) capacity corresponds to the pressure and the volume in accordance with the gas law and the compressibility factor of H_2 as shown in equation 2.7 [146].

$$\Delta p_{St,El} \cdot V_{St} = z_m \cdot \frac{m_{H2} \cdot R \cdot T_{St}}{M_{H2}} \tag{2.7}$$

$$\begin{aligned}
with: \quad & \Delta p_{St,El} = \text{ differential pressure between } p_{El,\ out} \text{ and } p_{St,\ max} \\
& V_{St} = \text{ St volume} \\
& z_m = 1.05\ \frac{1}{1},\ \text{mean real gas factor (compressibility)} \\
& m_{H2} = \text{ mass of hydrogen to be stored} \\
& R = 8.3145\ \frac{J}{mol \cdot K}\ \text{universal gas constant} \\
& T_{St} = \text{ St temperature in K} \\
& M_{H2} = 2.0159\ \frac{g}{mol},\ \text{molar mass}
\end{aligned}$$

The inaccuracy of this approach at pressures below 100 bar is accepted and a more precise consideration based on the *Beattie–Bridgemann Equation of State* as recommended by Kurzweil and Dietlmeier (2018) is not considered [88]. Note that the $\Delta p_{St,El}$ is the differential pressure which incorporates the required pressure of downstream processes and its maximal pressure. The T_{St} is assumed to be equal to the environment temperature. The compressibility factor z_M of H_2 is assumed to be ~1.05 at 30 °C and 50 bar [58], [69]. Upstream to the St tank is a Co unit which elevates the pressure level of the H_2 to match the pressure level of the St. Both, the compression and the storing process can be affected by a distinct leakage rate. Within this thesis, the specific reversible work (w_{rev}) performed by the Co is estimated to be reflected best by polytropic thermodynamic conditions. The applied calculations are outlined in equation 2.8 [146].

$$w_{real} = w_{rev} \cdot \frac{1}{\eta_{Co}} = \frac{z_m \cdot R \cdot T_{El}}{M_{H2}} \cdot \frac{n}{n-1} \cdot \left[\left(\frac{p_{St}}{p_{El}} \right)^{\frac{n-1}{n}} - 1 \right] \cdot \frac{1}{\eta_{Co}} \tag{2.8}$$

$$with: \quad n = 1.3\ \frac{1}{1},\ \text{polytropic coefficient}$$

$$\eta_{Co} = \text{efficiency of the compressor}$$

The inlet temperature T_{in} is assumed to equal the El temperature such as the inlet pressure p_{in}. As this thesis assumes polytropic compression conditions, the polytropic exponent n=1.3 is applied [146]. For an estimated inlet pressure $p_{in} = 50\,bar$ and an inlet temperature $T_{in} = 65\,°C$, both approximated to resemble a PEMEL, the specific w_{rev} can be calculated to be 0.3035 kWh/kg. This assumes a constant storage pressure of $100\,bar$. In addition, the efficiency of compressors η_{Co} is used to calculate the real work (w_{real}).

2.3 Optimization of technical systems

Optimization is the task of finding input parameters that determine an approximation of the most favorable outcome of an objective function. The task can either be approached in a stochastical, or in a deterministic manner. The procedure applied in this thesis is deterministic and is based on the mathematical representation of real–world systems [32], [126]. The representation of real systems in mathematical formulas can cause challenges in respect of complexity and certainty. Therefore, the performance of mathematical optimization is constrained to the precision of the formulated optimization problem. The complexity of the representation has to be in balance with the resources required to solve it which is often considered to be the computing time. The mathematical representation typically consists of several variables which are affected by constraints. Further, an objective is based on the variables and is typically minimized [66], [104].

Optima of mathematical functions can be differentiated in local or global optima. Global minima represent a local minimum as well. Within the framework of optimization, there is a distinction between feasible solutions which fulfill all constraints and optimal solutions which fulfill the constraints while representing an optimized outcome [104]. An optimization problem can be considered to be convex when all local minima correspond to the global minima [104].

Variables The core of an optimization model consists of a set of variables. By manipulating these variables, the outcome of an objective function can be influenced. Typically, these variables are constrained in some sort [104], [126]. When defining variables, there are several properties to specify. In the first place, the numeric quantity of a variable is from importance. A variable can consist of integers, floats or all other types of mathematical sets. The optimization tool developed for this thesis involves Non–Negative–Reals (NNR) and Non–Negative–Integers (NNI) variables whereas the thesis focuses on NNR [18]. Further, an initial value can be set for each variable which is used by the solving algorithm. Initial values play a significant role in optimization problems with multiple local extremes [104].

Constraints Constraints define the interrelationships between the variables. Sometimes, the numeric quantity of a variable is already considered to be a constraint. A constraint can force a variable to be either equal to another value or contain an inequality operator [104]. In the case of indexed or vector variables, the constraint can affect different indexes of the variable individually.

Objectives The objective is a mathematical equation set up to define a function to be minimized in favor of the operator. For the minimalization of an objective embedded in a set of variables and constraints, a solving algorithm is applied. The definition of the objective function takes the defined variables into account.

The optimization of real technical systems often implies more than one objective function, as real–world issues have to fulfill several criteria. The basic procedure to compute multi–objective optimization problems are called Pareto optimization. The Pareto optimum is defined as a trade–off, the minimization of one target function would increase the others. Thus, a set of feasible optima fulfilling all applied objectives is called a Pareto–set [104]. To determine the most favorable objective, additional efforts have to be taken. According to Pieper (2017) and others, there are numerous approaches to determining favorable solutions, while the method of weighted sums with a weighting factor ($f_{weighting}$) is the most known [59], [103], [104]. Pieper (2017) recommends normalizing the function values for objective functions with a different range of values. This can be done by the individual maxima according to equation 2.9 which assumes two objectives f_1 and f_2 with the variables $x_{0,1}$ [104].

$$f_{Combined}(f_1(x_{0,1}), f_2(x_{0,1})) = w_1 \cdot \frac{f_1(x_{0,1})}{f_{1,max}(x_{0,1})} + w_2 \cdot \frac{f_2(x_{0,1})}{f_{2,max}(x_{0,1})} \tag{2.9}$$

The factors $f_{weighting1}$ and $f_{weighting2}$ in equation 2.9 are representing the weighting factors for each objective.

Visualization To illustrate the nature of optimization problems, a small example is created subsequently and visualized.

$$\begin{aligned} f_{min}(x,y) &= x + y \\ C1 &: y \leq 4 \cdot x \\ C2 &: y \geq 2 \cdot x \\ C3 &: 2 \cdot y \leq -0.5 \cdot x + 20 \\ x, y &\in \text{NNR } or\ x, y \in \text{ NNI} \end{aligned} \tag{2.10}$$

Figure 2.4 visualizes the optimization problem described in equation 2.10. The figure compares two different characteristics of the variables x and y. In the continuous formulation of the optimization problem, the variables x and y can represent all Non–Negative–Reals (NNR). The variable can be set for any NNR during the optimization process. Further, the figure shows the inequality constraints C1, C2 and C3 and indicates the feasible range. The second plot in figure 2.4 visualizes the same optimization problem of equation 2.10 while considering Non–Negative–Integers (NNI) for the variables x and y. Comparing both

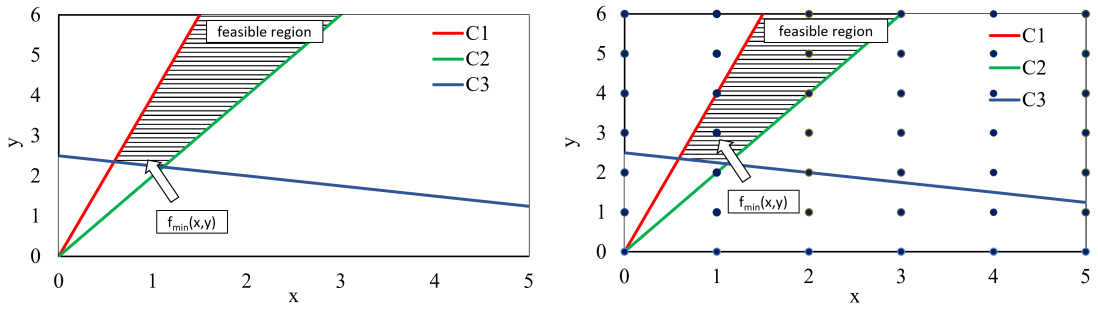

(a) Continious variables (NNR) (b) Discrete variables (NNI)

Figure 2.4: Visualization of an optimization problem described in equation 2.10. Own visualization inspired by [126].

plots, the difference between NNR and NNI becomes clear. While the results of an optimization can not be predicted in (a) as an applied algorithm has a wide feasible range of variables available, the outcome in (b) is obvious. The NNI conditions restrict the problem so that the minimization of f(x,y) results in x=1 and y=3. Optimization problems which are constrained to NNI are typically much more difficult to be solved, thus their computation time is longer [60].

Solving algorithm Technical literature describes a wide variety of different solving algorithms that can be differentiated into analytic, numeric and experimental solving techniques according to Snyman (2018) [126]. This thesis is based on numerical solving techniques which require the definition of a mathematical representation as explained before. The mathematical representation is written in a matrix which is then solved with respect to the integrated objective function [61].

Numerical solvers can not be applied to discrete NNI constraints as their method of solving is based on continuous variables. Although the principles of numerical solving are generally not applicable, there are a couple of procedures developed to cope with discrete optimization problems which are not discussed in this thesis. Reference is made to relevant literature such as Synman (2018) and the publisher of the Gurobi solving algorithm [61], [126].

2.4 Economic and environmental assessment

The optimization goals, defined by the objective functions, include an environmental and an economic assessment. These two assessments are about to be presented in this section. Thereby, the specifics applied within this master thesis are outlined. In the first place, the optimization of the PtH_2 unit addresses the Levelized Costs of Energy (LCoE), and the Levelized Costs of H_2 ($LCoH_2$) in particular. In the second place, the objective covering the F_{CO2} of the produced H_2 will be discussed which includes the amount of CO_2 exhausted due to the procurement of electricity by factoring in the electricity mix.

2.4.1 Levelized Costs of Energy

According to Sens et al. (2022) and Hölling et al. (2022), the LCoE factors in the total lifetime costs of a technical unit which are divided by the amount of produced energy [70], [122]. The LCoE is often used to compare different energy–generating technologies [70], [86], [111], [122]. This approach is applied by this master thesis to compute the $LCoH_2$ issued by the PtH_2 unit. The $LCoH_2$ are calculated by equation 2.11 which includes the annual Capital Expenditures (CapEx), the annual Operating Expenditures (OpEx) and the annual amount of hydrogen produced $m_{H2,a}$. The CapEx are considered according to the annuity method based on the norm DIN 2067 issued by the "Verein Deutsche Ingenieure" [142].

$$\mathrm{LCoH_2} = \frac{\mathrm{CapEx}_a + \mathrm{OpEx}_a}{\mathrm{m}_{H_2,a}} \tag{2.11}$$

$$\begin{aligned} with: \quad & \mathrm{CapEx}_a = \text{ Annual Capital Expenditures} \\ & \mathrm{OpEx}_a = \text{ Annual Operating Expenditures} \\ & \mathrm{m}_{H2,a} = \text{ Annual mass of produced hydrogen} \end{aligned}$$

Equation 2.11 takes the lifetime costs of a H_2–producing unit into account by summing up CapEx and OpEx on the fraction counter. The CapEx are multiplied by the Annuity factor (A_r) which accounts for the annual expenses based on the Interest rate (r_{int}) and the Project lifetime ($\mathrm{t}_{Project}$). The fraction denominator represents the amount of annual produced energy during that time frame. The CapEx consists of the sum of the individual investments, reinvestments, the residual value for each PtH_2 element and the A_r according to equation 2.12 [142].

$$\mathrm{CapEx}_a = \sum \Big((\mathrm{Inv}_{comp} + \mathrm{Inv}_{comp,re} - \mathrm{Value}_{comp,Residual}) \cdot \mathrm{A}_r \Big) \tag{2.12}$$

$$\begin{aligned} & comp \; \forall \; \{\text{Components of an investment}\} \\ with: \quad & \mathrm{Inv}, \mathrm{Inv}_{re} = \text{ Specific investment, specific reinvestment} \\ & \mathrm{Value}_{Residual} = \text{ Residual value after project lifetime} \\ & \mathrm{A}_r = \text{ Annuity factor} \end{aligned}$$

The Investment (Inv) in equation 2.12 considers the specific investment costs and the size of the corresponding component. The Reinvestment (Inv_{re}) considers necessary reinvestments according to equation 2.13, as soon as the Component lifetime (t_{Comp}) is shorter than the $\mathrm{t}_{Project}$. This thesis considers

not more than one reinvestment during the project's lifetime (n $\leq$1).

$$\mathrm{Inv}_{re} = \mathrm{Inv}_{re,raw} \left(\frac{\mathrm{inf}}{\mathrm{r}_{int}} \right)^{n \cdot t_{Project}} \tag{2.13}$$

$$\begin{aligned} with: \quad & \mathrm{Inv}_{re,raw} = \text{ Raw reinvestment} \\ & \mathrm{inf} = \text{ Inflation} \\ & \mathrm{r}_{int} = \text{ Interest rate} \\ & \mathrm{n} = \text{ Number of reinvestments } (\leq 1) \\ & \mathrm{t}_{Project} = \text{ Project time} \end{aligned}$$

The Residual Investment ($\mathrm{Inv}_{Residual}$) is taken into account as soon as the $\mathrm{t}_{Project}$ is shorter than the t_{Comp} by equation 2.14. The aspect is considered for each component individually.

$$\mathrm{Inv}_{Residual} = \mathrm{Inv} \cdot \mathrm{inf}^{\mathrm{t}_{Comp}} \cdot \frac{(\mathrm{n}+1) \cdot \mathrm{t}_{Comp} - \mathrm{t}_{Project}}{\mathrm{t}_{Comp}} \cdot \frac{1}{\mathrm{r}_{int}^{\mathrm{t}_{Project}}} \tag{2.14}$$

$$with: \quad \mathrm{t}_{Comp} = \text{Component lifetime}$$

The A_r factors the r_{int} and the $\mathrm{t}_{Project}$ in. The factor is applied to calculate the annual costs related to the investment according to equation 2.15.

$$\mathrm{A}_r = \frac{\mathrm{r}_{int}^{\mathrm{t}_{Project}} \cdot (\mathrm{r}_{int} - 1)}{\mathrm{r}_{int}^{\mathrm{t}_{Project}} - 1} = \frac{\mathrm{r}_{int} - 1}{1 - \mathrm{r}_{int}^{-\mathrm{t}_{Project}}} \tag{2.15}$$

By applying the equations above, the individual CapEx can be calculated which yield the summation for the overall annual CapEx in equation 2.12. The following explains the procedure to determine the annual OpEx making up the second part in the LCoH_2 calculations. The OpEx can be calculated by adding up maintenance exposures $\mathrm{OpEx}_{a,M}$ and exposures related to activities in the energy markets. The PtH_2 unit considered in this thesis can participate in different energy markets, such as the wholesale markets for EP OpEx_{EP} and the balancing markets for auxiliary services such as the OpEx_{FCR} and the OpEx_{aFRR}. Thereby, the variable i represents all observed Time–Stamp (TS). In addition, the CapEx_a factors in the costs related to Maintenance (M).

$$\mathrm{OpEx}_a = \sum \left(\mathrm{OpEx}_{EP,i} + \mathrm{OpEx}_{FCR,i} + \mathrm{OpEx}_{aFRR,i} \right) + \sum \mathrm{OpEx}_{a,M,comp} + \mathrm{OpEx}_{a,other} \tag{2.16}$$

$$i \; \forall \; TS \; ; \; comp \; \forall \; \{\text{Components of an investment}\}$$

The OpEx related to maintenance exposures are calculated by factoring the component–specific maintenance exposures referenced to the annual CapEx in. In addition, further OpEx related aspects are considered, that are related to regulatory aspects or the procurement of GoO for example.

The amount of H_2 (or energy in MWh in a general sense) produced during the time frame is the last aspect to calculate the LCoH_2. The mass of H_2 produced during the operation is calculated by summing

up all TS of the production timeline according to equation 2.17.

$$m_{H2} = \sum_{i \ \forall \ \text{TS}} \dot{m}_{H2,i} \tag{2.17}$$

By applying the equations 2.12 to 2.17, the $LCoH_2$ in equation 2.11 can be calculated. The sens of optimization is to minimize this function, as minimal $LCoH_2$ is the optimization target applied in this master thesis.

Annual Full Load Hours The Annual Full Load Hours (AFLH) is a typical value to quantitatively describe the dispatch of a technical unit (U). The value considers the total occupation related to the maximal installed capacity. It is calculated according to equation 2.18.

$$\text{AFLH} = \frac{\sum U_i}{U_{max} \cdot TS}_{i \ \forall \ \text{TS}} \tag{2.18}$$

A high AFLH indicates an operational dispatch close to the maximal capacity of the unit. A small AFLH describes a dispatch when the operational capacity does extend up to the maximal capacity

Adjustment for inflation As this thesis bases its assumptions on literature data published before the assumed investment in 2023, all prices are adjusted for inflation. The adjustment procedure is visualized in figure 2.5 and in the subsequent equations. The investment is issued in the beginning of the year 2023 as an example, thus $€_{2023,BoY}$ (Begin of Year) is assumed to be equal the $€_{2022}$ and the values for 2022 do not have to be adjusted.

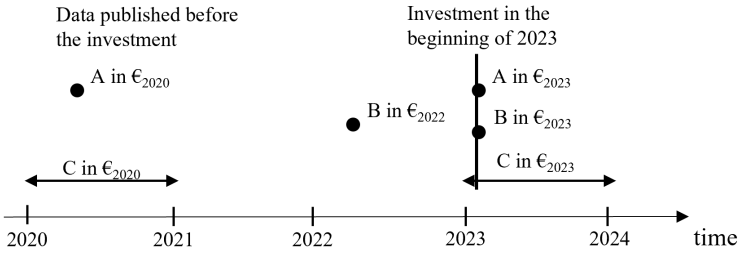

Figure 2.5: Schematic visualization of the procedure to adjust investment costs and time–series prices for inflation. Own visualization.

To adjust the price of A, B and C for inflation, equations 2.19 to 2.21 are applied. The Inflation (Inf) rates relevant for each price are factored in. This is done for both, constant values such as investment

costs (A, B) and time–series data (C) such as prices for electric energy.

$$A: \quad €_{2023,BoY} = €_{2020} \cdot (1 + \text{Inf}_{2022}) \cdot (1 + \text{Inf}_{2021}) \tag{2.19}$$

$$B: \quad €_{2023,BoY} = €_{2022} \tag{2.20}$$

$$C: \quad €_{2023,BoY} = €_{2020} \cdot (1 + \text{Inf}_{2022}) \cdot (1 + \text{Inf}_{2021}) \tag{2.21}$$

The inflation noted in table 2.2 is based on a data set published by the German Federal Statistical Office [128]. The inflation rates are published in change to the previous year. The total inflation of the year 2022 Inf_{2022} is estimated to settle down to 10 % by the end of the year. This assumption is supported by the fact that the inflation for November 2022 is expected to be at 10.0 % [128].

Table 2.2: Inflation rates based on the German Federal Statistical Office in change compared to the previous year in % [128].

	2013	2014	2015	2016	2017	2018	2019	2020	2021	2022
Inflation	1.6	0.8	0.7	0.4	1.7	1.9	1.4	0.4	3.2	10.0*

*Assumption made in this thesis.

2.4.2 CO_2–footprint of H_2

Next to the levelized costs discussed above, the model–based optimization is also assessed from an environmental perspective. The procured electricity, to be converted to H_2 by the electrolyzer, is affected by the carbon footprint of the electricity mix. The environmental assessment covers the cumulated amount of CO_2 related to the procurement of electricity EP_{in} and the produced mass of H_2 as the equation 2.17 shows.

$$\text{F}_{CO2,H2} = \sum_{i \ \forall \ \text{TS}} \frac{\text{F}_{CO2,Electricity,i} \cdot E_{in}}{\dot{m}_{H2,i}} \tag{2.22}$$

Chapter 3

Analysis of the Requirements

This chapter summarizes the required answers the thesis has to provide. First, the field of research is elaborated on, then the requirements of the optimization tool are described in greater detail. A brief outlook on the case study is given followed by the chapter closing with a brief summary of the derived research questions. To clarify the designation, the term "optimization tool" describes a software that imports data, performs calculations and outputs results. The "model", which consists of the mathematical representation of the Power–to–Hydrogen (PtH_2) unit, is embedded in the optimization tool.

3.1 Research question

This thesis aims to solve the component sizing issue of flexible operating PtH_2 units by considering techno–economic factors next to environmental aspects. The PtH_2 unit has the purpose of satisfying a Hydrogen (H_2) flow demand at any specific point in time while consuming power in a flexible manner. This behavior is achieved by implementing a means of energy storage. To solve the component sizing issue, a python–based tool is supposed to be set up to obtain optimal sizes together with an optimal dispatch schedule. Python is utilized, as it is well–known in the research group supervising this thesis. This thesis does not simulate the behavior according to a "battery first" or other approaches but optimizes the behavior mathematically. The nature of the optimum is supposed to be described by objective functions focusing on either economic or a combination of economic and environmental factors. Moreover, the tool aims to provide insights into the economic benefits of participation in auxiliary services such as Frequency Containment Reserve (FCR) and Automatic Frequency Restoration Reserve (aFRR) activities. Further, the surplus heat and Oxygen (O_2) generated by the PtH_2 unit is supposed to be identified.

The precise definition of a "grid serving behavior" applied in this thesis has to be worked out. It is expected to consider the electricity grid's current status when scheduling the dispatch. This could be done for example by reflecting the demand and generation of power and the option to provide auxiliary services. An extended interpretation of flexibility including dynamic scheduling of the H_2 demand itself should not be considered.

The thesis is supposed to make appropriate (historical) input data next to the optimization tool available. This includes the H_2 demand and electricity grid data (such as prices, auxiliary service compensation

and the carbon footprint) for the last four years (starting in 2019), summarized in figure 3.1. To validate the results provided by the tool and the simplifications made due to performance reasons, a model–specific sensitivity analysis is supposed to be done. Additionally, test cases have to be built up for validation.

The resulting component sizes and the corresponding dispatch schedule are supposed to be presented in an appropriate manner. To cope with the uncertainty of future developments and different setups of the PtH_2 unit, a set of scenarios is worked out based on the available data. Relevant parameters are to be discussed in a sensitivity study. The design of the optimization tool is expected to be documented. The optimization tool is supposed to be applied within a case study at the copper processing facility of Aurubis in Hamburg.

3.2 Optimization tool

The optimization tool is required to describe a PtH_2 unit consisting of the main components Electrolyzer (El), pressurized H_2 Storage (St) and Battery (Ba) by algebraic modeling equations in a techno–economic manner. The developed tool is supposed to optimize the dimensions of the PtH_2 unit components together with their dispatch schedule. As shown in figure 3.1, the tool draws several inputs which can be distinguished into constant, time–series and model–specific values.

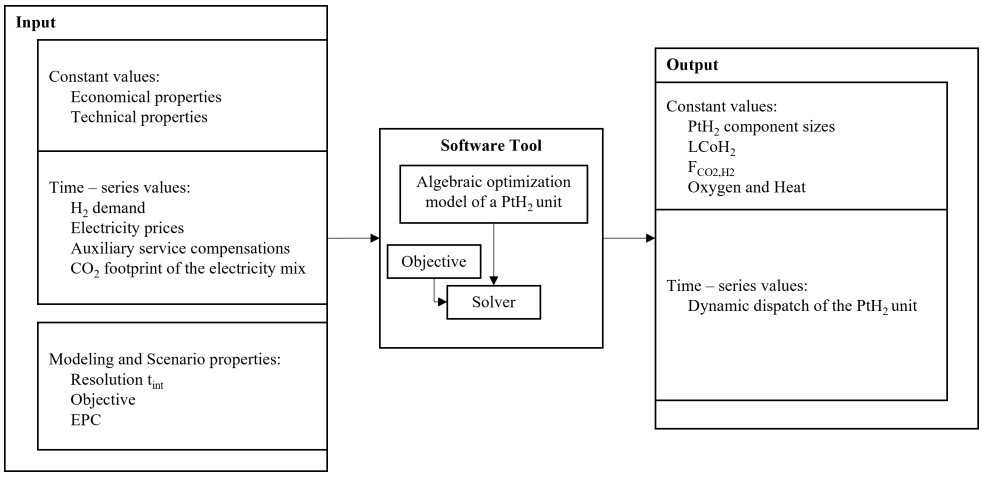

Figure 3.1: Graphical representation of the requirements to be fulfilled by this thesis and the framework of the optimization tool to be programmed with its input and output parameters. Own visualization.

Technical and economic properties are constant, such as the electrolyzer efficiency, the specific investment costs, or the expected maintenance costs. Data concerning the H_2 demand, electricity prices, or auxiliary service compensations have time–series character. Aspects like the resolution Interval (t_{int}) or the chosen objective of the variables are examples of modeling properties. There should be the possibility to draw different series by an import function and parameterize time–independent data and modeling properties in a user interface.

The input data is supposed to be processed by the software tool to construct an algebraic optimization model. The model reflects the technical behavior of the PtH_2 unit while stating necessary and reasonable

simplifications. The model is implemented to be able to satisfy a H_2 demand, rely on electric energy and H_2 storages and participate in the Auxiliary Service (AuxS) markets. Subsequently, the model is solved by a solver within the optimization tool. The solver is required to be capable of minimizing predefined objective functions such as either an economic or a combination of ecologic–economic objectives. Thereby, the economic consideration is supposed to be based on Schütte et al. (2022) [117]. The tool is supposed to output a set of values consisting of constant values such as the optimal component sizes and the obtained optimal objective according to the provided input data. Further, the output includes time–series data representing the dispatch of the PtH_2 unit elements.

3.3 Case study: Apply the tool at an Aurubis production site

The software tool is supposed to be applied in a case study at the production site of Aurubis in Hamburg. Aurubis aims to set up a PtH_2 unit at their production site in Hamburg to replace Natural Gas (NG) with H_2 in their Anode Furnaces (AF) in order to meet their climate targets established in 2021 [119]. Based on the current NG consumption, the corresponding H_2 demand in the case study is to be determined. Consequently, this thesis is supposed to compute the optimal component sizes and an optimal dispatch of a PtH_2 unit together with expected Levelized Costs of H_2 ($LCoH_2$) and CO_2–Footprint of H_2 ($F_{CO2,H2}$) for the case study based on different scenarios.

Such representative scenarios for the case study are supposed to be set up and agreed upon with the industry. The scenarios include perspectively different low–temperature El technologies, different energy market developments based on historical data and different grid serving aspects. The scenario–based optimization is supposed to consider the economic and a combination of the economic and the environmental objective functions. Consequential recommendations are supposed to be drawn from the obtained results.

3.4 Summary of the derived research questions

In the preceding sections, the research objective is formulated together with the requirements for the optimization tool. The main aspect of the thesis is to determine optimal component sizes of a grid serving PtH_2 unit based on an economic and an environmental objective. To do so, an optimization model of a PtH_2 unit is developed. The definition of a grid serving operation is supposed to be worked out. These derived questions summarized below are analyzed in the upcoming chapter 4 in greater detail.

a) How does the (historical) time–series describing the energy market look like?

b) Which techno–economic properties are suitable to describe the components of a PtH_2 unit?

c) Are there any special restrictions that have to be respected in the case study?

d) How to determine the H_2 demand in the case study?

e) How does this thesis define a grid serving operation?

f) Which application and software are used to set up the optimization tool?

Chapter 4

Techno–Economic Analysis

Within this chapter, the techno–economic framework of the thesis is analyzed. The first section of this chapter addresses the case study by assessing the Hydrogen (H_2) demand and classifying further specific considerations. This is followed by the description of the basic system design of the Power–to–Hydrogen (PtH_2) unit together with its technical and economic properties. Then, the power system is analyzed by discussing time–series data concerning the electricity prices, auxiliary service prices and the Carbon Dioxide (CO_2) footprint. In addition, the aspect of grid serving operations is discussed followed by a brief look at the used software.

4.1 Case study: Supplying Aurubis with hydrogen

This thesis is embedded in the joint research efforts of the Northern German Living Lab (in German: "Norddeutsches Reallabor", NRL) and the copper processing company Aurubis AG (in the following: Aurubis) in Hamburg. Based on this cooperation, this thesis applies its optimization tool to a case study based on data from the industry partner Aurubis. Within the decarbonization strategy of Aurubis, the reducing Anode Furnaces (AF), which consume Natural Gas (NG) as a feedstock, are to be retrofitted to operate with the reductant H_2. To supply these furnaces, a PtH_2 unit is planned to be installed at the production facility of Aurubis.

The aim of this thesis is to compute the optimal component sizes of this PtH_2 unit at the production facility of Aurubis. The PtH_2 unit includes potentially an electrolyzer, a battery, a pressurized hydrogen storage and a compressor. The study will be based on data covering the historic NG demand and historic prices on the energy markets. This section will discuss the specific parameters related to the case study. To put the case study into context, a rough overview of the copper process at Aurubis and its decarbonization strategy is given. This is followed by the analysis of the historic NG consumption and the calculation of the corresponding hydrogen demand. Furthermore, the way in which electricity is purchased by Aurubis is analyzed.

4.1.1 Copper production at Aurubis in Hamburg

Aurubis processes primary and secondary copper in several processing steps. An overview of the primary copper production is given in figure 4.1, the secondary copper production pathway is not discussed in this thesis.

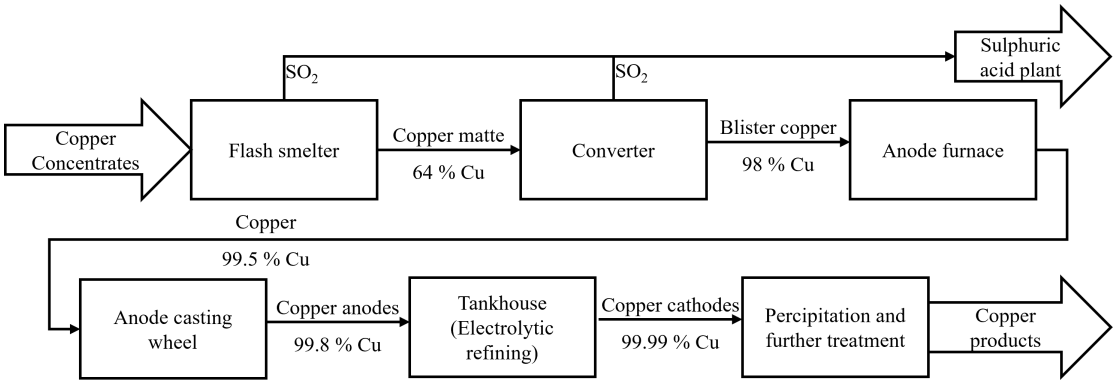

Figure 4.1: Graphical visualization of the processing steps applied for primary copper. The graphic is based on Schlesinger et al. (2011) among others [95], [112], [116].

The treatment of primary and secondary copper consists of a large number of processing steps, which involve heating, cooling and chemical reducing operations. For this thesis, the pyrometallurgical processing steps are focused, which are followed by electrometallurgical and mechanical steps. Each step aims to increase the purity of copper by precipitating the byproducts. The processing facility in Hamburg receives copper concentrates with roughly 30 % of copper and the elements iron and sulfur [112]. First, the raw copper is dried and treated in a flash smelting furnace to become copper matte, consisting of 64 % of copper. During the flash smelting process, sulfur is precipitated in a gaseous state while silica and limestone separate from the copper concentrate by forming a slag. This floating slag is precipitated so that copper matte with a copper portion of 64 % can be forwarded to the converter [112].

The exothermal reaction in the converted gives the option to treat copper scrap as shown in figure 4.1. The converter yields blister copper with a purity of 98 %. Within the converter, copper scrap can be added which is then called secondary copper. This is favorable, as the treatment in the two furnaces releases surplus heat, which can be used to melt the scrap [112]. The last pyrometallurgical processing step takes place in the Anode Furnaces (AF). These furnaces oxidize the blister copper in the first place to remove the remaining sulfur elements. Then, the melted copper is reduced to eliminate the remaining copper oxides. This reducing processing step requires reducing agent respectively energy carriers as a feedstock [35], [111], [112], [117].

The output of the anode furnace with 99.5 % copper is subsequently cast into anodes which are then electrolytically refined. This results in copper cathodes with a copper proportion of 99.99 % [112], [116]. The mechanical treatment steps followed are not discussed in this thesis.

Decarbonization at Aurubis Putting the copper industry into context, it is one of many contributors to the greenhouse gas budget illustrated in table 4.1. The Carbon Dioxide Equivalents ($CO_{2,eq}$) caused by the primary metallurgic industry for steel reflect a share of 18.4 % and for the aluminum industry of

0.6 % in reference to the industrial sector in Germany. Other metallurgical products, such as copper are responsible for 0.9 % of the emissions within that sector [24], [117], [136].

Table 4.1: $CO_{2,eq}$ emissions of the primary metallurgic industry distinguished in ferrous, aluminum and others in relation to total emissions caused by the industrial sector in Germany in 2021 [24], [117], [136].

	Ferrous	**Aluminum**	**other** (incl. Copper)	**Germany** (industrial sector)
in 10^6 $t_{CO2,eq}$	30.91	0.92	1.56	167.71
in %	18.43	0.55	0.93	100.00

Aurubis aims to become CO_2 neutral in 2050 [119]. This involves an electrification of thermal processes and the implementation of CO_2 neutral reductants for operations where energy carriers are consumed as feedstocks. The case study in this thesis addresses such a swap from fossil–based reductant NG to in–house produced H_2.

For the case study, it is considered that the consumed electric energy related to the production of H_2 is from CO_2–neutral origin. From a physical perspective, this would only be possible for a directly connected CO_2 neutral power generation unit. As this thesis assumes that the electric energy is drawn from the power grid, the CO_2 neutrality has to be ensured by Gurantees of Origin (GoO). As a consequence, the processing facility of Aurubis in Hamburg will experience a reduced consumption of NG and an increased consumption of electric energy if the case study is implemented. That leads to a decrease of CO_2 emissions as the procured electricity, hedged by GoO, is considered to be CO_2 neutral.

Local circumstances According to a sustainability report of Aurubis in 2019, Aurubis bases its electricity procurement on a virtual hard coal power contract on the Over–the–Counter (OTC) market [7]. Within this thesis, it is assumed that the agreement includes monthly prices for coal power including the procurement costs of coal, the respective costs of the European–Union–Allowances (EUA) certificates, transportation and investment costs.

In addition, discussions with Aurubis showed that the power consumption of the PtH_2 unit has to be limited to 7 MW_{EP}. Although this constraint might cut off the optimization tool in some scenarios, the value is considered in this thesis to reflect the limitations at the production facility.

The required pressure level for the supply of the AF is at ∼10 bar relative to the atmosphere in accordance with the industry partner Aurubis. A pressure throttling valve is not considered in this thesis as the pressure output of the PtH_2 unit is assumed to be always higher than the required AF pressure. Further, emergency storage is incorporated for the investment costs. The storage should provide the option to bridge eventual failures of the PtH_2 unit for 8 hours and supply the H_2 demanding processes. After 8 hours further measures have to be taken. The annual production of (anode–) copper of the production facility in Hamburg is published by Schütte et al. (2022) to be 427,818 t_{Cu} [117].

4.1.2 Coal power contract

As mentioned before, Aurubis procures its electric energy based on a coal power contract. Due to the fact that the prices defined in that contract are only accessible to the contracting parties, an approximation of the prices is made for this thesis. The applied calculations are shown in the following paragraphs by calculating the Levelized Costs of Energy (LCoE) of coal electricity.

Coal traded under the "CIF ARA" label is considered to be the most important indicator of coal prices in Europe as it represents the coal traded in the region of Amsterdam, Rotterdam and Antwerpen [79]. The Lower Heating Value (LHV) of the hard coal is normed at 6000 kcal/kg [79]. As the CIF ARA is traded in US–dollars, the prices are converted by the conversion ratio taken from the national bank of Austria [100]. The wholesale market prices for coal are taken from `investing.com` [79]. In a study, Lehmann and Lanzrath (2020) calculate the transport costs of coal in Germany to be 9.78 €$_{2022}$/t as an average [90]. This transportation cost is considered as a price component (Price$_{Transp.}$) valid for all years of observation.

Additional to the coal prices, the expenses related to the EUA are factored in. Daily EUA prices are drawn from investing.com [78]. The specific CO_2 emissions of coal $F_{tCO2/tcoal} = 93.5\,t_{CO2}/t_{coal}$ are based on publications of the German Environment Agency [137]. Investment (Inv) and Maintenance (M) costs are considered according to the "Fraunhofer–Institut für Solare Energiesysteme" (Fraunhofer ISE) who considers Inv$_{coal}$ at 1.5-2.2 $\cdot 10^6$ €$_{2021}$/MW$_{EP}$ [85]. This thesis will take the mean value of the span into account which is 2.00 $\cdot 10^6$ €$_{2023}$/MW$_{EP}$ adjusted to the beginning of the year 2023 [85]. Further, the M$_{coal}$ are considered with 3 % of the annual Capital Expenditures (CapEx) according to similar publication [85]. Table 4.2 analyzes the input data and the amount of Not–a–Number (NaN) values in the data sets.

Table 4.2: Tabular overview of the number of NaN values within the coal OTC describing time–series.

	Res.	2019	2020	2021	2022*
Total rows		365	366	365	334
NaN in EUA price	24 h	108 (29.6 %)	108 (29.5 %)	106 (29.0 %)	98 (29.3 %)
NaN in coal price (CIF ARA)	24 h	113 (31.0 %)	113 (30.9 %)	113 (31.0 %)	104 (31.1 %)
NaN in USD/EUR	24 h	110 (30.1 %)	109 (29.8 %)	107 (29.3 %)	98 (29.3 %)

*Covering TS between January 1st, 2022 and November 30th, 2022.

As the wholesale market does not trade on public holidays, the time–series are interpolated. An overview of the interpolation is given in the appendix on page XXXV. The figure 4.2 shows the resulting approximation of the LCoE for the coal OTC contract. The LCoE are later interpreted as prices from the perspective of the industry partner Aurubis.

These values in figure 4.2 are compared to publications from the International Energy Agency (IEA) in 2020 and Fraunhofer ISE in 2018 and 2021 for validation purposes [73], [85], [86]. The LCoE for lignite and hard coal in 2018 is published by the studies to be approximately in the area of 45.9 to 98.6 €/MWh$_{EP}$ as indicated in the figure 4.2 in pink. For the year 2021, the studies determine the LCoE for coal power between 108.3 and 200.4 €/MWh$_{EP}$, as indicated by the blue background color. The calculated LCoE of coal power plants displayed in figure 4.2 have an average of 104.4 €/MWh$_{EP}$ for the year 2021. The estimated LCoE of coal–based electricity is agreed with Aurubis.

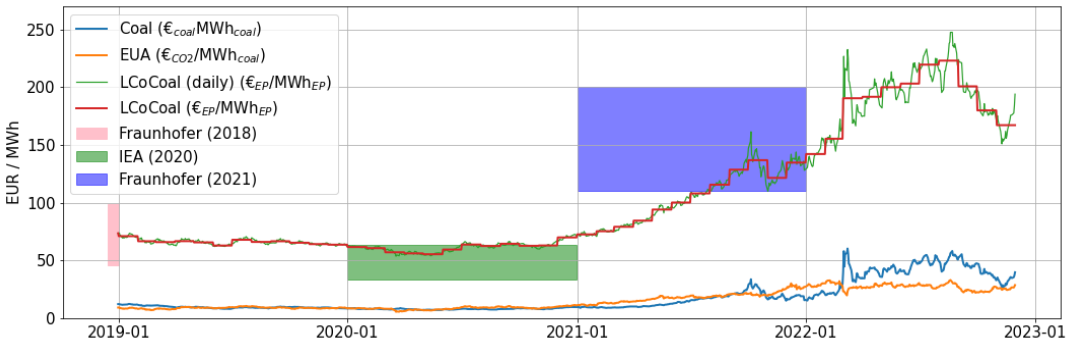

Figure 4.2: Monthly price series of a OTC coal contract based on NG and EUA price data provided by investing.com among others [31], [73], [78], [79], [85], [86], [100].

4.1.3 Determining the H_2 demand

The optimization tool bases its computations on a specified hydrogen flow demand. The determination of this time–series for the case study is shown in this section. The industry partner Aurubis provides a time–series of measurements performed in their primary smelter in Hamburg where two AF operate (called AF 8 and AF 9 by the industry partner). The currently used reductant NG is replaced with the reductant H_2 for this case study. To do so, the NG time–series data is used to compute the H_2 flow demand based on the specific Reducing factor (f_{red}).

The NG mass flow $\dot{m}_{NG}$ is affected by imprecise measurements and therefore filtered on behalf of Aurubis. Based on this mass flow, the respective hydrogen demand is calculated by applying stoichiometric and experimental considerations. As the downtimes periods of the production facility should be neglected, these periods are cut out of the respective time frame.

Process filters and downtimes gaps In correspondence to the industry partner Aurubis, the mass flow time–series is filtered by two criteria. The mass flow is only considered to be relevant when the measured mass flow $\dot{m}_{NG}$ is higher than 20 $\mathrm{Nm^3/h}$ and the measured angle α_{AF} of the furnace is higher than 80°. The angle indicates the position of the rotating anode furnaces and is applied in this filter to determine the process phase. These conditions are summarized in equation 4.1 and 4.2 and visualized in figure 4.3 later on.

$$\dot{m}_{NG} > 20\,Nm^3/h \tag{4.1}$$

$$\alpha_{AF} < 80° \tag{4.2}$$

Additional to the applied criteria, maintenance downtimes are removed from the time–series. Aurubis maintains its production facility in Hamburg several times during the observed time period. It can be expected that the PtH_2 unit would be switched off in these periods. Therefore the data points of the series have to be removed from the input data of the tool. As soon as there is an interval of 16 hours with no measured gas flows, it is removed. These periods are shaded red in figure 4.3. The nature of the filters is shown in figure 4.3 for both the positional condition and the minimal flow rate. The background color indicates the filters. Further, the maintenance downtime is shown in the third graph of the figure.

Calculating the H_2 demand Based on the filtered NG demand, the hydrogen demand is calculated. The applied procedure is shown for methane, representing the main component of Natural Gas (NG). Subsequently, the same procedure is worked out for NG as well, based on NG samples discussed in the appendix A on page XXIX.

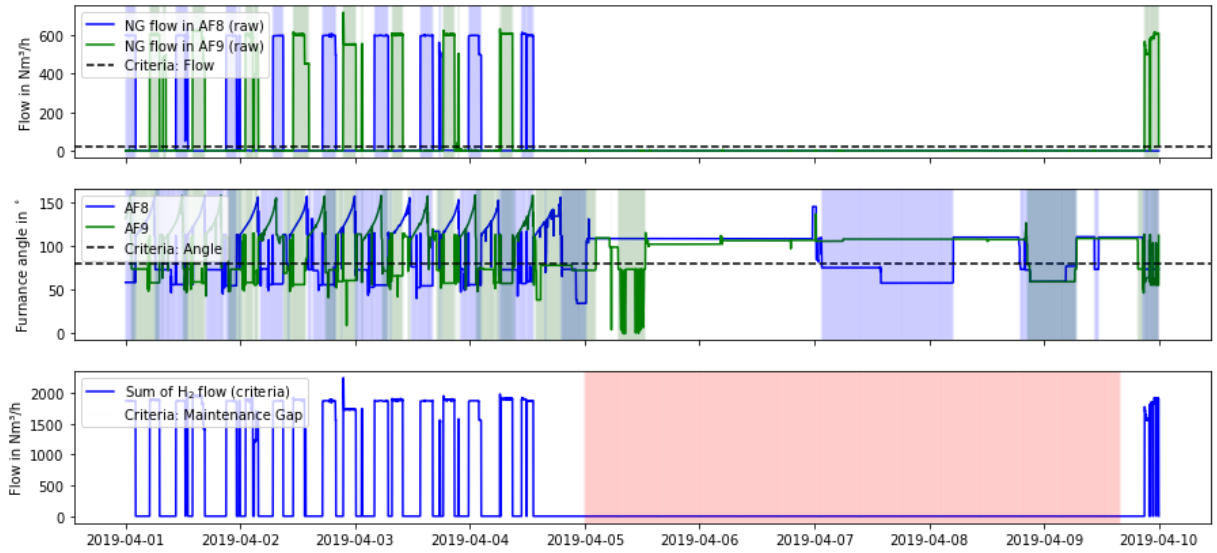

Figure 4.3: Visualization of the H_2 demand time–series determined for the case study and the applied process–related filters. In addition, the downtime treatment procedure is shown.

In the following, equation 4.3 and 4.4, the reaction equations for both H_2 and Methane (CH_4) are shown.

$$4\,Cu_2O + CH_4 \longrightarrow 8\,Cu + CO_2 + 2\,H_2O \tag{4.3}$$

$$Cu_2O + H_2 \longrightarrow 4\,Cu + H_2O \tag{4.4}$$

According to the equation 4.3 and 4.4, a mole of methane can reduce four times more copper molecules compared to hydrogen. Thus the f_{red} of CH_4 is four times higher than of H_2. This approach can also be applied to NG by adapting equation 4.3 to represent all the molecules present in the gas mixture. According to data of Gasnetz Hamburg GmbH, the NG consumed in Hamburg is composed of ∼94 % CH_4 and other hydrocarbons [55]. Taking the actual composition into account, the reducing potential f_{redNG} of one–mole NG can be determined to be 4.094 dicopper oxide molecules as equation 4.5 shows. The calculations are shown in the appendix within section A on page XXIX.

$$C_{1.044}H_{4.044}N_{0.013}O_{0.015} + 4.094Cu2O \longrightarrow 1.044CO_2 + 2.022H_2O + 0.013N_2 + 2 \cdot 4.094Cu \tag{4.5}$$

According to Edens et al. (2022) who worked out an experimental study at Aurubis primary smelter in Hamburg, the poling conversion is increased by the implementation of hydrogen [35]. The average conversion efficiency of NG η_{NG} is determined to be 69 %, while hydrogen showed a conversion efficiency of $\eta_{H_2} = 90\,\%$. This ratio must be considered next to the reducing factor ratio f_{red} when calculating the hydrogen demand based on NG according to equation 4.6. The density of H_2 is considered to be $\rho_{H_2} = 0.0899\,\mathrm{kg/m^3}$ [35], [83].

$$\begin{aligned}\dot{m}_{H_2} = \dot{V}_{H_2} \cdot \rho_{H_2} &= \dot{V}_{NG} \cdot \frac{f_{red,H_2}}{f_{red,NG}} \cdot \frac{\eta_{NG}}{\eta_{H_2}} \cdot \rho_{H_2} \\ &= \dot{V}_{NG} \cdot \frac{4.094 \frac{mol_{CH4}}{mol_{O2}}}{1 \frac{mol_{H2}}{mol_{O2}}} \cdot \frac{0.69}{0.90} \cdot 0.0899 \frac{kg}{m^3}\end{aligned} \tag{4.6}$$

Figure 4.3 summarizes the applied filters explained beforehand. The first graph shows the raw NG flow time–series with the flow–criteria indicated as a dashed line. The values for NG are drawn as a volume flow at standard conditions (1.013 bar and 0 °C). The second plot includes the corresponding angle of the AF, which determines its position with the respective threshold as a dashed line. The lower plot shows the H_2 consumption resulting from applying the equations discussed above. Additionally to that, the third graph includes the maintenance criteria. As the first graph shows, there is no consumption of NG measured between the 5^{th} and the 9^{th}, the developed algorithm detects a maintenance downtime. As explained beforehand, this time frame is going to be excluded during the simulation. Thus, the corresponding timestamps of all other time–series data such as electricity prices or the CO_2 factor are not considered.

Analyzing the hydrogen demand The resulting reductant demand is analyzed within this paragraph. To do so, the data series is analyzed for missing values. Further, the consequences implied by the filtering procedure explained beforehand are shown. Table 4.3 gives an insight into the data of the dataset used in the case study. Note that Aurubis provides the data set with a minute-by-minute resolution.

Table 4.3: Tabular overview of the number of NaN values within the case study NG measurements time–series.

	Res.	2019	2020	2021	2022*
Total rows		525600	527040	525600	367081
NaN in AF 8 NG_{raw}	1 min	2347 (0.4 %)	184 (0.0 %)	72 (0.0 %)	66 (0.0 %)
NaN in AF 9 NG_{raw}	1 min	1964 (0.4 %)	179 (0.0 %)	63 (0.0 %)	35 (0.0 %)
NaN in AF 8 α	1 min	2680 (0.5 %)	179 (0.0 %)	64 (0.0 %)	66 (0.0 %)
NaN in AF 9 α	1 min	2221 (0.4 %)	149023 (28.3 %)	78 (0.0 %)	55 (0.0 %)
NaN in NaN in $\sum$ NG	1 min	1964 (0.4 %)	179 (0.0 %)	63 (0.0 %)	35 (0.0 %)
NaN in $\sum$ H_2	1 min	1964 (0.4 %)	179 (0.0 %)	63 (0.0 %)	35 (0.0 %)

*Covering TS between January 1^{st}, 2022 and September 12^{th}, 2022.

Apart from values concerning the AF angle in 2020, the data are not affected by a large quantity of NaNs. The missing data points are filled with the annual average of the specific year. The values covering the angle of AF 9 are not filled by the average. The missing values are not considered in the filtering process.

As the reducant demand in the case study results from two furnaces that are either switched on or off, the data are visualized in a histogram. Before that, an overview of the applied filters is given in table 4.4.

Table 4.4: Overview of the annual reducant demand in $t_{Reductant}$ calculated for the study.

	2019	2020	2021	2022*
AF 8 NG_{raw}	783.0	936.0	872.0	452.3
AF 9 NG_{raw}	788.5	899.5	837.7	434.8
$\sum$ NG_{raw}	1571.6	1835.5	1709.8	887.1
$\sum$ NG_{filter}	1333.1	1493.5	1531.8	807.6
$\sum$ $H_{2,filter}$	492.4	551.6	565.8	298.3
$\sum$ $H_{2,filter,\ downtime}$	492.4	551.6	565.8	298.3

*Covering TS between January 1^{st}, 2022 and September 12^{th}, 2022.

The summative reductant demand[1] in $t_{Reductant}$ is gathered in table 4.4 for the four observed years 2019 to

[1]Note that the reductant consumption is measured at different measurement stations. Schütte et al. (2022) for example

2022. The rows in the table describe the step–wise treatment. First, the two raw reductant sums from AF 8 and 9 are indicated. These time–series beneath are filtered in the explained manner and results in the summative values for the specific year. The applied filter reduces the measured gas flow of AF 8 and 9 of approximately 1500 t_{NG} in 2019 to approximately 1300 t_{NG}, which is a reduction of ca. 15 %. To calculate the H_2 demand, the stoichiometry of equation 4.5 and the discussed experimental results from Edens et al. (2022) are applied [35]. The resulting H_2 demand is filtered for production interruptions. These downtimes are identified by searching reducant flow gaps larger than 16 hours. Therefore, there is no difference in the two last rows identifying the H_2 demand with downtimes considered and not. The values for the year 2022 are smaller compared to the previous years because 2022 is only partially observed.

To run the simulations, a normal year is used as a standardized H_2 consumption to simplify interpretations. This standardized year is considered to be 2020, the differences between these years are shown in figure B.1 in the appendix. Due to the alternating nature of the two AF, the H_2 demand is not constant but interrupted and is either on or off. This H_2 demand structure is in favor of the operation of PtH_2 plants, as the implementation of a pressurized H_2 tank can decrease the required Electrolyzer (El) capacity. The H_2 storage decouples the operation of the electrolyzer from the H_2 consumption, thus a smaller dimensioned electrolyzer could operate during decreased consumption.

4.2 Power–to–Hydrogen unit

The optimization model describes a PtH_2 unit in a techno–economic manner. The assumptions and estimates applied in this thesis are examined in this section. This is done by presenting the basic flow chart of the PtH_2 system and examining its elements in great detail. The structure and the components of the PtH_2 unit are discussed on the basis of two relevant publications by Sens et al. (2022) and Röben et al. (2021) who simulated PtH_2 units in a techno–economic manner [111], [122]. Additionally, assumptions made by Schütte et al. (2022), who worked out a qualitative assessment of PtH_2 units in the context of the case study at the production facility of Aurubis in Hamburg, are considered [117]. All costs mentioned in this section are adjusted for inflation according to section 2.4.1, assuming an investment at the beginning of 2023, if not stated otherwise. The focus of the subsequent section is the analysis of the El properties. A broad overview of the assumptions made in this thesis is provided in table 4.5 on page 38.

4.2.1 Flowchart

An overview of the PtH_2 unit is given in the basic flow chart displayed in figure 4.4. The displayed elements of the unit Grid (Gr), Battery (Ba), El, Compressor (Co) and Storage (St) are explained subsequently. Thereby, its economic properties such as the CapEx are identified together with the technical aspects. Moreover, the element Process (Pr) is not described in particular, as it stands for the production process which has to be fed with H_2. This specifically required mass flow is computed in the section 4.1 “Case study”.

The two elements Gr and Pr represent the intersections with the environment of the PtH_2 unit. The connection arrows in figure 4.4 indicate physical connections implying either a flow of electric energy (straight lines) or of H_2 (dashed lines). The Ba can be charged with electricity from the Gr while supplying both the electrolyzer and the compressor. Both electricity–consuming elements can be additionally supplied by a direct connection to the electricity grid. The El can be supplied with electric energy in several ways. Basically, the El is connected directly to the Gr and to the Ba. Further, an additional Gr to El connection is implemented which includes Auxiliary Service (AuxS) as shown in figure 4.4. These AuxS are provided by the electrolyzer alone without the Ba or any

consider 1,892 t_{NG} as an average without any process–related filters [117].

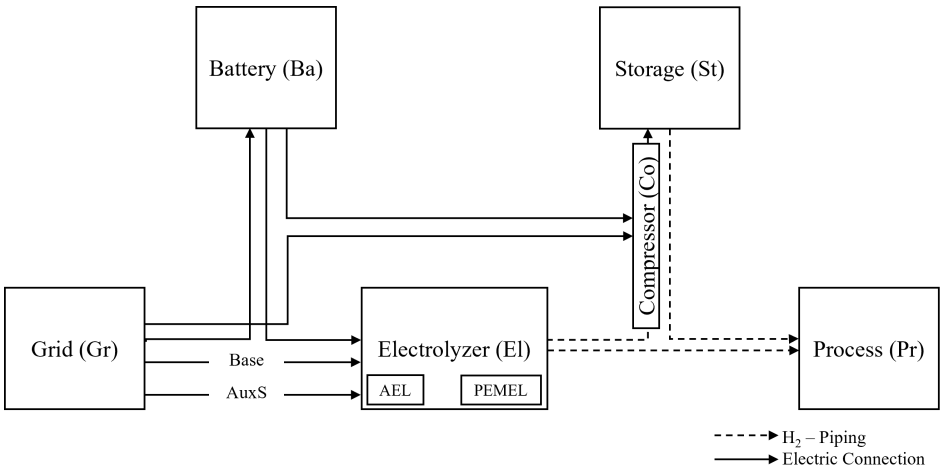

Figure 4.4: Basic flowchart of the modeled PtH_2 unit. Dashed lines indicate a H_2 flow and straight lines an electric energy flow.

other elements of the PtH_2 unit. This thesis considers either a Proton Exchange Membrane Electrolyzer (PEMEL) or an Alkaline Electrolyzer (AEL).

The H_2 storage can be charged by the El supported by a Co to elevate the pressure level. The compressor is supplied with electric energy directly by the grid or by the Ba. The process, reflecting the H_2 demand to be satisfied, itself can be supplied either by the electrolyzer directly or by the H_2 storage. The elements of the PtH_2 unit are about to be explained in the subsequent sections in greater detail.

4.2.2 Grid connection

The unit grid connection depends on local circumstances. Schütte et al. (2022) analyze the construction of a PtH_2 system at the production facility of Aurubis in Hamburg and assume that the investment costs to connect the PtH_2 unit with the electric grid has to be considered. This implies the need for transformer stations and construction work. Sens et al. (2022) and Röben et al. (2021) do not consider such expenses.

Specific investments and lifetime Schütte et al. (2022) assume costs of about $700\,€_{2023}/kW_{EP}$ which is depreciated for 20 years [117]. The value can not be confirmed directly, as the prices for medium and high voltage grid connections are negotiated by a Distribution System Operator (DSO) like "Stromnetz Hamburg GmbH" individually with customers. For comparison, a local DSO charges roughly $200\,€_{2023}/kW_{EP}$ for private customers (assuming low voltage grid connections based on Stromnetz Hamburg GmbH and own calculations) [129]. With this comparison in mind, the assumption made by Schütte et al. (2022) seems to be high. Therefore, this thesis considers a weighted average of $300\,€_{2023}/kW_{EP}$.

The lifetime of a Gr connection assumed by Schütte et al. (2022) can be justified by the German Federal Office of Finances which considers a lifetime for transformation units in the electricity sector of 20 years [8]. Thus, this thesis applies a lifetime of the grid connection for 20 years.

Maintenance The maintenance expenses estimated by Schütte et al. (2022) to contribute to the annual costs with 3 % of the CapEx are considered in this thesis as well [117].

4.2.3 Battery

The battery is implemented to store electrical energy. Necessary information is provided in section 2.2.1. As Iskeceli et al. (2020) state, Lithium-Ion Battery (Li–Ion Ba) batteries are the most suitable storage to store volatile renewable energy electrically [81]. Sens et al. (2022) implement this technology as well. Relevant properties for the implementation in the optimization tool such as the CapEx and the maintenance exposures are provided below.

Specific investments and lifetime The specific investments concerning the Ba value is based on the input properties of Sens et al. (2022) who refer their considerations on a publication of International Renewable Energy Agency (IRENA) in the year 2019 and others such as an overview of battery costs published by Cole et al. (2021) [19], [74], [105], [122], [141]. The investment is determined to be 362,100 €$_{2023}$/MWh$_{EP}$ when converted to actual currency exchange rates. Mauler et al. (2021) work out a comprehensive study on battery costs and projections. For 2020 costs for the battery pack itself were expected to be at an average of 308.7 €$_{2020}$/kWh$_{EP}$ (adjusted[2] to €$_{2020}$) [93]. The costs implemented by Sens et al. (2022) is considered to be more reasonable as Mauler et al. (2021) do not factor in all cost components (like revenues and the periphery of a battery pack). Therefore, this thesis applies the CapEx factor of 370,000 €$_{2023}$/MWh$_{EP}$ for its simulation. Whereby, it is assumed that this specific investment cost considers the operational capacity.

According to the German Federal Office of Finances, a battery has a Component lifetime (t_{Comp}) of 15 years [8]. Within this thesis, the same value is applied although this might lead to an underestimation of costs as the battery might experience many discharge cycles. As the lifetime of the Ba is shorter than the project lifetime (20 years), a Reinvestment (Inv_{re}) of the full extent is considered together with the consequential residual value of the Ba unit as explained in section 2.4.1.

Maintenance The annually expected maintenance exposure is expected to be about 3 % of the investment costs according to the literature mentioned in the paragraph above. This value is considered within the determination of the CapEx in this thesis.

Efficiency The efficiency of the battery is assumed to be 0.87 kWh_{out}/kWh_{in} according to Sens et al. (2022) and relevant literature [19], [74], [105], [122], [141].

4.2.4 Electrolyzer

The theoretical operating principle and specifics concerning the electrolyzer are already discussed in section 2.2.2. This section discusses the specific properties to be implemented in the optimization model. To do so, economic properties such as specific investment costs, maintenance exposures and technical properties such as the efficiency are analyzed by a literature review. As stated before, this thesis does not include the Solid Oxide Electrolyzer (SOEL) technolgy due to the compareably low Technology Readiness Level (TRL) [16], [56], [106], [125].

Literature does not agree on the technology suitable for PtH_2 applications. Röben et al. (2021) simulate their PtH_2 unit based on an AEL. They defend their decision by addressing the high TRL of the system. Sens et al. (2022) consider a PEMEL in their study and point out the advantages of the PEMEL properties in connection with volatile energy supply from wind and solar generating sources [122]. Thereby the aspect of load flexibility of PEMEL is highlighted in contrast to Roeben et al. (2021) who assume that AEL systems achieve a similar flexibility [111]. Sens et al. (2022) and Roeben et al. (2021) base their assumptions both on Buttler and Spielhoff (2018) and Smolinka et al. (2018), who summarize electrolyzer properties [17], [125]. Tuschewitzki (2021) draws the consequences from his simulations that PEMEL interacts better with the highly volatile power supply when

[2] $/€ in 2020: 1.14 [100]

compared to AEL. Thereby he identifies the minimal loads and the start–up times as the limiting operational factors for AEL [135]. Subsequently, the base parameters to be implemented in section 5.2.3 for the AEL and the PEMEL are discussed.

Specific investments Because electrolyzers are still under development and production capacity is increasing, investment estimates in the literature vary. Therefore, a literature study is conducted in the following. All costs are adjusted for inflation according to section 2.4.1. An overview of the literature values is given in figure 4.5.

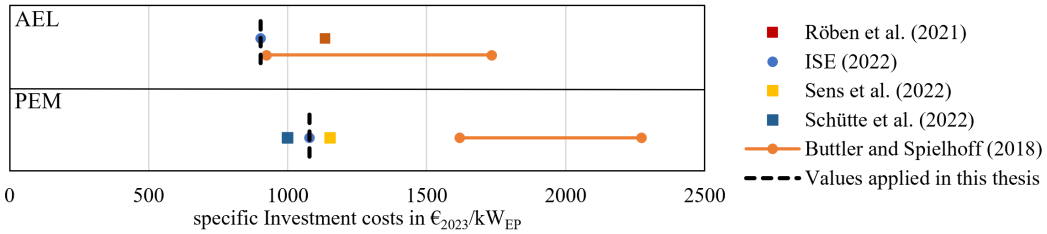

Figure 4.5: Summary of the conducted specific El investment literature research and the assumption made in this thesis indicated by a vertical dashed line. Circles represent distinct studies of El investments and squares indicate assumptions in other techno–economic assessments [17], [52], [111], [117], [122].

Buttler and Spielhoff (2018) determine a specific Inv range between 924 and 1,733 €$_{2023}$/kW$_{EP}$ for AEL systems and a higher cost range for the PEMEL technology of 1,162 to 2,273 €$_{2023}$/kW$_{EP}$ [17]. Röben et al. (2021) implement a linear investment function for their AEL system of 1,135 €$_{2023}$/kW$_{EP}$ well within the cost range mentioned before. Additionally, Röben et al. (2021) consider a Inv$_{re}$ of about 307 €$_{2023}$/kW$_{EP}$ or roughly a quarter of the initial Inv costs after ten years of operation for the El–stack [111]. Sens et al. (2022) draw their estimate for their PEMEL electrolyzer from a IRENA report in 2019 and the publication "Klimaneutrales Deutschland" supervised by the Prognos AG among others [74], [105], [106], [122], [148]. Their PEMEL electrolyzer is implemented with a linear cost function of 1,152 €$_{2023}$/kW$_{EP}$. Schütte et al. (2022) applies specfic investment costs for a PEMEL electrolyzer to be 1,000 €$_{2023}$/kW$_{EP}$ [117]. Compared to a recent publication by the Fraunhofer ISE in 2022, the mentioned values seem to be too high. The study considers the specific investment costs of PEMEL to be 980 €$_{2020}$/kW$_{EP}$ and for AEL 820 €$_{2020}$/kW$_{EP}$ in the year 2020 [52]. Note that the Fraunhofer includes the specific cost for the compression in the case of AEL which is excluded in this thesis as the thesis considers the compression separately.

Röben et al. (2021) and Sens et al. (2022) and Schütte et al. (2022) do not consider an investment cost reduction for larger module sizes and work with linear cost functions. This thesis follows this approach and assumes a linear relation between El capacity and El investment. Further, this thesis considers specific investments described by Fraunhofer ISE in 2022 for a PEMEL electrolyzer at 1,078 €$_{2023}$/kW$_{EP}$ and for an AEL at 902 €$_{2023}$/kW$_{EP}$. Both values consider inflation rates according to section 2.4.1. In addition, a stack replacement is considered for one–quarter of the initial Inv cost as applied by Röben et al. (2021).

Maintenance and lifetime Smolinka et al. (2018), expect higher annual maintenance costs for AEL than for PEMEL whereas both values settle down between 1.5 and 3 % of the CapEx [125]. Buttler and Spielhoff (2018) estimate maintenance costs of 2 to 3 % for AEL and of 3 to 5 % for PEMEL referenced to the CapEx. Sens et al. (2022) implement 3.5 % while Röben et al. (2021) and Schütte et al. (2022) use 3 % for theirs. This work expects annual maintenance costs to be at 3 % of the CapEx for both AEL and PEMEL following Röben et al. (2021) and Schütte et al. (2022).

According to Buttler and Spielhoff (2018), an AEL has a lifetime of about 55,000 to 120,000 h. In contrast, a PEMEL has a lifetime of 50,000 to 100,000 h [17]. Assuming a continuous operation (8,000 h p. a.), this would correspond to an operation between 6.8 and 15 years. Whereas Röben et al. (2021) distinguish between a stack lifetime of 10 years and a system lifetime of 20 years for their AEL, Sens et al. (2022) consider a deprecation time of 15 years [111], [122]. The study by the Fraunhofer ISE underlines the necessity of a stack replacement after typically ten years [52]. Within this thesis, a t_{Comp} of 20 years for both El systems is assumed. In addition, a stack replacement is considered after 10 years, following the assumption of Röben et al. (2021) [111].

Load Gradient Buttler and Spielhoff (2018) mention load changes within seconds at nominal operating temperatures for both PEMEL and AEL [17]. Tuschewitzki (2021) summarizes that load gradients do not have a relevant impact on the system behavior at minute resolution due to the fast dynamics [134]. According to Kopp (2018), a PEMEL can increase its operating power by 10.0 %/s of its nominal load whereas the total system can ramp up with 2.2 %/s [84]. This implies that load changes can not be described with a discretization of more than ∼30 min as their behavior becomes instantaneous. Buttler et al. (2018) and Kopp (2018) state that the flexibility of PEMEL is suitable to provide AuxS for both Frequency Containment Reserve (FCR) and Automatic Frequency Restoration Reserve (aFRR) [17], [29], [84]. This aspect is already demonstrated by a couple of projects for example by the H&R Group in Hamburg for aFRR and by "Energie des Nordens" for FCR [53], [63]. The capability for AEL is demonstrated by Kiaee et al. (2012) in a simulation [82].

This thesis assumes an instantaneous behavior for AEL and PEMEL units whereas it discusses the load gradients in a sensitivity study.

Start–up Sens et al. (2022) and Roeben et al. (2021) argue that start–up phases in cold conditions can be neglected either because of continuous H_2 supply or because of an intelligent control unit combining many small–scale electrolyzers [111], [122]. As this thesis does not consider downtimes in the production (or assumes that maintenance periods are carried out during the downtimes of the entire plant) this approach is followed and start–up phases are not considered.

Minimal Load Buttler and Spielhoff (2018) identify the El minimal load (El_{min}) for AEL to be 20 % although they mention a few examples with El_{min} of 10 %. Further, the minimum load for PEMEL is considered to be negligible [17]. Tuschewitzki (2021) identifies the El_{min} to be the main operational difference between AEL and PEMEL at nominal temperatures (together with the cold start behavior, which is not addressed in this thesis as stated above) [134]. Röben et al. (2021) implement a minimum load for their AEL at about 20 %. Sens et al. (2022) do not consider the minimum load for its PEMEL although a datasheet of the Silyzer 300 includes a El_{min} of 5 % [122], [123]. Data–sheets from H–TEC Systems GmbH include a El_{min} of ≥20 % wheras Kyros Hydrogen Solutions GmbH mentions a minimal range of ≥10 to 20 % in their PEMEL data-sheet [62], [89].

As three suppliers consider an El_{min}, this thesis will implement the AEL and the PEMEL with El_{min} of 20 % and 5 % respectively although literature does not implement them. Additionally, this value will be discussed in a sensitivity study.

Efficiency Tuschewitzki (2021) shows that the assumption of static efficiencies, applied in Röben et al. (2021) (60 % for AEL) and Sens et al. (2022) (60 % for PEMEL), leads to an underestimation of the hydrogen production [134]. Whereas the consideration of non-linear efficiencies implies high computing times of the optimization tool due to the non–linearity of the resulting constraints [60]. According to the H_2 production curves discussed in section 2.2.2 the uncertainty due to the assumption of a static efficiency is considerably small. This assumption is

confirmed by Varela et al (2021) who set up a scheduling algorithm for AEL systems based on a static efficiency of 66 % due to computing time [140]. An overview of the literature data is given in figure 4.6.

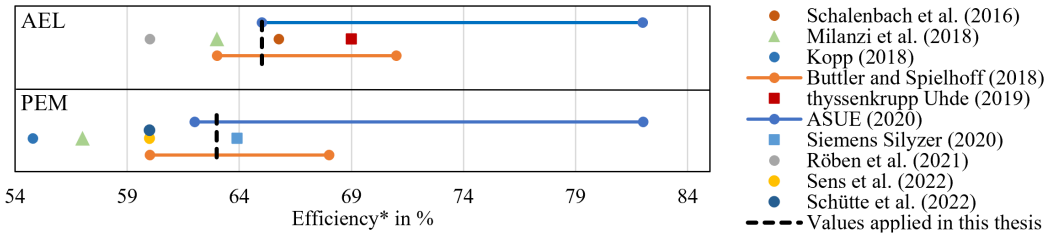

Figure 4.6: Summary of the conducted El efficiency literature research and the assumption made in this thesis indicated by a vertical dashed line. Circles show averages and ranges, squares indicate data sheets and triangles a median value. *Efficiencies are based on the LHV [6], [17], [84], [94], [111], [115], [117], [122], [123], [132].

Buttler and Spielhoff (2018) summarize the efficiency of AEL to be in between 63 and 71 % whereas PEMEL settles in between 60 and 68 % based on the LHV [17]. The tendency of higher efficiencies for the AEL is supported by Milanzi et al. (2018) whereas they find a lower median in their literature review of ∼63 % for AEL and ∼57 % for PEMEL (grey) [94]. The "Arbeitsgemeinschaft für sparsamen und umweltfreundlichen Energieverbrauch e. V." (ASUE, 2020) sees potentials for both technologies from 78 % (AEL) and 74 % (PEMEL) up to 84 % based on the LHV (blue) [6]. A datasheet from the Siemens Silyzer 300 (PEMEL) claims an efficiency of 63.9 % referenced to the LHV, which is lower compared to a datasheet of thyssenkrupp Uhde for an AEL system with 69.3 % (at 300 mbar differential pressure, whereas the other values are based on pressures >30 bar) [123], [132]. Note that Kreidelmeyer et al. (2020) conclude, in contrast to the literature mentioned beforehand, that PEMEL have a higher system efficiency compared to AEL whereas they do not state any distinct values [106]. The relation of the El efficiency and pressure discussed by Tjarks (2017) are not considered in this thesis [133]. Tjarks notes, that an increased pressure reduces the electrolysis efficiency while it has the potential to increase the system efficiency due to lower compression work.

The different efficiencies found in literature and in data sheets (summarized in figure 4.6) show a slightly higher efficiency of AEL compared to PEMEL systems. This thesis takes that into account and assumes approximated efficiencies of 65 % for AEL and 63 % for PEMEL systems.

Temperature and pressure Smolinka et al. (2018) show that the pressure of PEMEL is ≤70 bar and for AEL the pressure is ≤30 bar which is similar to the findings of Buttler and Spielhoff (2018) [17], [125]. The two stimulative studies from Röben et al. (2021) and Sens et al. (2022) assume an electrolyzer outlet pressure of 30 bar (AEL) and 50 bar (PEMEL), both in the range of the previously stated article [111], [122]. These values are applied in this thesis.

The cell temperature of the electrolyzer is not considered in the articles of Röben et al. (2021) and Sens et al. (2022). Literature such as Smolinka et al. (2018) show that typical temperatures for PEMEL are within 50 to 80 °C and for AEL 70 to 90 °C [125]. The temperature applied in this thesis for the PEMEL is about 65 °C and for the AEL is about 80 °C.

Water consumption The electrolyzer consumes approximately 8.94 kg_{H2O}/kg_{H2} according to stochiometry elaborated in section 2.2.2. Schütte et al. (2022) consider the consumption of 17 kg_{H2O}/kg_{H2} as aspects like the desalination process and excess water usage has to be incorporated [117]. Thus, sewage water is factored in with

$8.06\,kg_{H2O}/kg_{H2}$. The study includes water and sewage prices of $2\,€/m^3$ such as Schütte et al. (2022) who base their prices on the local water supplier "HAMBURG WASSER" [64], [117].

4.2.5 Compressor

The relevant theory addressing the compressing unit is discussed in section 2.2.3. In the following, the implemented parameters of the compressor are briefly outlined. The pressure ratio between the electrolyzer and the storage is not simulated, thus a constant pressure ratio is assumed. This fact leads to an overestimation of the necessary compression work, as the real compression ratio would not extend to the maximal storage pressure. The impact of the compression ratio will be discussed in a sensitivity study.

Compression work and efficiency The thermodynamic reversible work (w_{rev}) to compress the hydrogen in the case it is filled to the storage is calculated according to the formula introduced in section 2.2.3. The formula takes the electrolyzer temperature and its outlet pressure into account. In addition, it considers the maximal storage pressure. Based on the computed compression work, the required work is calculated by the electrical efficiency of the compressor. Equation 2.8 in that mentioned section takes the electrical efficiency into account which is assumed to be η_{Co}= 0.79 % by Sens et al. (2022) among others [122], [135]. This assumption fits well in the range of 50 % to 80 % assumed in a report concerning compressor costs from the "National Renewable Energy Laboratory" (2014) in the USA [96]. A compressor efficiency of 79 % is applied in this thesis to compute the real work (w_{real}).

Specific investments and lifetime The specific CapEx of the compressor is discussed within this section. Sens et al. (2022) implement a linear cost function based on the maximal mass flow of H_2 [122]. The specific investment cost of the compressor for the year 2023 is determined to be $2{,}021\,€_{2023}/(kg_{H2}/h)$ when considering inflation according to section 2.4.1 [122]. Röben et al. (2021) implement a fixed cost for the Co of approximately $567{,}600\,€_{2023}$ combined with a linear cost function of $2{,}770\,€_{2023}/(kg_{H2}/h)$ [111]. A publication of the "Fraunhofer–Institut für Solare Energiesysteme" in 2022 takes specific compressor costs between 2270 and $7719\,€_{2023}/(kg_{H2}/h)$ into account [52]. This thesis bases its assumption on the previously mentioned values and implements specific Co costs of $2500\,€_{2023}/(kg_{H2}/h)$.

According to the German Federal Office of Finances, compressors have a lifetime of 15 years, which is identical to the assumptions implemented by Schütte et al. (2022) and Sens et al. (2022) [8], [117], [122]. Therefore, this thesis assumes a lifetime of 15 years as well with a full reinvest after that lifetime and the consequential residual value after the project lifetime of 20 years as explained in section 2.4.1.

Maintenance Sens et al (2022) consider annual maintenance costs of 5 % based on Reu et al. (2019), whereas Röben et al. (2021) estimate lower annual maintenance exposures [109], [111], [122]. This thesis assumes maintenance costs of 5 % following the assumptions of Reu et al. (2019) and Schütte et al. (2022).

H_2 leakage In contrast to Röben et al. (2021), Sens et al (2022) do consider hydrogen losses at the compression stage of $0.005\,kg_{H2,loss}/kg_{H2,in}$. This fact is considered within this thesis as well.

4.2.6 Pressurized storage

The pressurized tank working as hydrogen storage is described in this section by discussing the parameters to be implemented in the optimization tool. The maximum pressure level of the tank will be determined in the post–processing step following the simulations.

Table 4.5: Applied techno–economic parameters of the PtH_2 unit within this thesis. The prices are adjusted to €$_{2023}$ according to inflation and currency exchange rates discussed in section 2.4.1 [100], [128].

Component	Parameter	Unit	Value	Reference
Grid	specific Inv	€/MW_{EP}	300,000	[117], [129]
	Maintenance	$\%_{of\ CapEx}/a$	3.0	[117]
	Depreciation	a	20	[117]
	Max. Capacity	MW_{EP}	7	assumption*
Li-Ion battery	CapEx	€/MWh_{EP}	370,000	[19], [74], [105], [122], [141]
	Maintenance	$\%_{of\ CapEx}/a$	3.0	[19], [105], [122]
	Lifetime t_{Comp}	a	15	[8]
	Efficiency	$kWh_{el,out}/kWh_{el,in}$	0.87	[19], [74], [105], [122], [141]
PEMEL	specific Inv	€/MW_{EP}	1,078,000	[52], [122], [123]
	specific Inv_{re}**	€/MW_{EP}	0.25 · Inv	[8], [52], [111]
	Lifetime Inv,Inv_{re}**	a	20, 10	[8], [52], [74], [105], [122]
	Maintenance	$\%_{of\ CapEx}/a$	3.0	[52], [74], [105], [122]
	Efficiency	$kWh_{H2,LHV}/kWh_{el,in}$	0.63	[84], [106], [122], [148]
	Outlet pressure	bar_{out}	50	[17], [122]
	Outlet temperature	$°C$	65	[17], [122]
	Minimal load El_{min}	$kWh_{H2,LHV}/kWh_{el,in}$	0.05	[17], [122]
	Load gradient***	$\%(kW_{el,max})/min$	100	[17], [84]
AEL	specific Inv	€/MW_{EP}	902,000	[17], [52], [77], [111]
	specific Inv_{re}**	€/MW_{EP}	0.25 · Inv	[8], [52], [111]
	Lifetime Inv,Inv_{re}**	a	20, 10	[8], [52], [111]
	Maintenance	$\%_{of\ CapEx}$/a	3.0	[17], [111]
	Efficiency	$kWh_{H2,LHV}/kWh_{el,in}$	0.65	[17], [111]
	Outlet pressure	bar_{out}	30	[17], [111]
	Outlet temperature	°C	80	[17], [111], [125]
	Minimal load El_{min}	$kW_{el,in}/kW_{el,max}$	0.20	[17], [111]
	Load gradient***	% $kW_{el,max}$/min	100	[17], [111]
Compressor	specific Inv	€/(kg_{H2}/h)	2,500	[101], [109], [122]
	Maintenance	$\%_{of\ CapEx}/a$	5.0	[109], [122]
	Lifetime t_{Comp}	a	15	[109], [122]
	Efficiency	kWh_{ideal}/kWh_{real}	0.79	[97], [101], [108], [122]
	Compression work	kWh_{real}	w_{real}+	[97], [101], [108], [122]
	H_2 losses	$kg_{H2,loss}/kg_{H2,in}$	0.005	[109], [122]
Pressure tank	specific Inv	€/kg_{H2}	530	[87], [108], [110], [122]
	Maintenance	$\%_{of\ CapEx}$/a	2.0	[108], [122]
	Lifetime t_{Comp}	a	30	[108], [122]
	H_2 loss	$kg_{H2,loss}/kg_{H2,in}$	0	[108], [122]
	Storage pressure	bar	100	assumption
Other	Labor	€/a	195,000	[117]
	GoO	€$_{H2O}$/MWh_{EP}	3	[117]
	EPC++			
	Water consumption	l_{H2O}/kg_{H2}	17	[117]
	Water price	€/m^3_{H20}	2	[117]
	Interest rate	%/a	6	[25], [111]
	Inflation+++	%/a	2	[40], [128]

*See case study in section 4.1.1; **Inv_{re} considers only the El stack; ***At nominal temperatures.
+w_{real} = f(p_{St}, p_{El}, T_{EP}); ++See section 4.2.7; +++Assumption for the project lifetime.

Specific investments and lifetime Sens et al. (2022) expect an investment of 524 €$_{2023}$/kg$_{H2}$ for a pressure tank with a maximum pressure of 200 bar based on Reu et al. (2017) [108], [122]. Röben et al. (2021) assume a similar value (534 €$_{2023}$/kg$_{H2}$) for the same maximal pressure [111]. Therefore, this investment cost factor of 530 €$_{2023}$/kg$_{H2}$ is considered in this thesis.

According to the German Federal Office of Finances, pressure tanks can be depreciated within 15 years, Sens et al. (2022) assume a longer lifetime of 30 years [8], [122]. Within this thesis, the lifetime of the pressurized St is expected to be 30 years.

Maintenance The expected annual maintenance exposures of the pressure tank are assumed to be 2 % of the CapEx according to Reu et al. (2017) [108]. This value is applied within this thesis.

4.2.7 Further aspects

This section is dedicated to costs and aspects that can not be referenced to a specific PtH_2 element but are important to be considered. Costs for the periphery of the PtH_2 unit are not considered. In contrast to Schütte et al. (2022), this thesis assumes that the necessary costs are already included in the individual costs of the PtH_2 elements [117].

This section addresses aspects like the labor costs and financial parameters such as the interest rate and the expected inflation for the project lifetime.

Labor costs According to Schütte et al. (2022), the staff hired to take care of operations of a PtH_2 plant can be considered to cost 195,000 €$_{2023}$/a [117]. This factor will be included in the simulation tool within the objective function.

Interest rate The interest rate assumed in this thesis is 6 % to determine the annual CapEx based on the Anode Furnaces (AF). The value is orientated on Röben et al. (2021) who calculate with 5.2 % in 2021 and the recently increased Interest rate (r_{int}) [25], [111].

Project lifetime and inflation For the calculation of the investment costs, a project's lifetime and inflation rate have to be considered. This thesis assumes a Project lifetime ($t_{Project}$) of 20 years similar to assumptions by Röben et al. (2021) [111]. The annual inflation during these 20 years is assumed to be 2 %. The inflation rate is taken from the targeted inflation rate by the European central bank [40].

Gurantees of Origin This thesis considers GoO of 3 €/MWh$_{EP}$ according to Schütte et al. (2022). The price is considered in the case study for the procurement of renewable certified electricity.

Electricity–Price–Compensation As explained, the Electricity–Price–Compensation (EPC) is a regulative system to release the price pressure on energy–intense enterprises. Schütte et al. (2022) publishes values for the $F_{Eligable}$ = 80 %, the $F_{Fallback}$ = 80 % and the $F_{Intensity}$ = 75 % [117]. The EUA prices are reflected by the average of the previous year respectively. The CO_2–Footprint (F_{CO2}) is defined to be 0.72 t_{CO2}/MWh$_{EP}$ and 1 GWh is considerd to be deductible within the respective law [12], [26].

4.3 Energy markets

To describe the power system in this thesis, several time–series of relevant properties are presented and analyzed. The applied data–treatment procedure is summarized in figure 4.7. The Time–Stamp (TS) and the data format

of the respective series are adjusted. Then, the Not–a–Number (NaN) values in the time–series are parsed and the time–series are merged with respect to their common TS. This is followed by a technical analysis by visualizing their developments in the last four years. First, the commodity prices on the spot markets for electricity are discussed. Then, the compensation allowances for the AuxS and the specific F_{CO2} of the electricity mix (sometimes called: system–average emission factor [71]) are analyzed. The section closes with a look at the correlation between the time–series. Concerning the different observed years, it is important to mention that 2020 is a leap year. All the TS of time–series data are converted to the Coordinated Universal Time (UTC) timezone format.

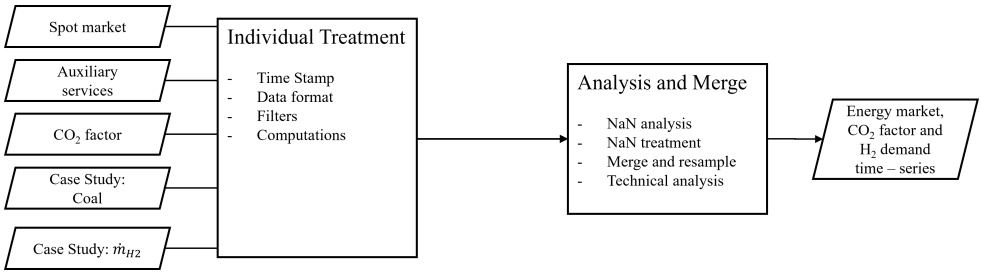

Figure 4.7: Schematic visualization of the time–series data treatment process applied in this thesis.

4.3.1 Electricity prices

This section analyzes the implemented commodity prices for electric energy in the last four years. As already described in the section 2.1, electric energy can be procured in several ways. This section focuses on the spot market in Germany which is operated by the Epex Spot SE (EPEX) among others [5]. It consists out of the Day–Ahead (DA) and the Intraday (ID) markets [38]. The ID continuous market is not considered within this thesis, as the quantity is considerably small [38].

Table 4.6: Tabular overview of the number of NaN values within the respective DA and ID related time–series. Based on EPEX [38].

	Res.	2019	2020	2021	2022*
Total rows		35040	35136	35040	32156
NaN in DA	60 min	26280 (75.0 %)	26352 (75.0 %)	26280 (75.0 %)	24117 (75.0 %)
NaN in ID	15 min	0 (0.0 %)	0 (0.0 %)	0 (0.0 %)	0 (0.0 %)

*Covering TS between January 1^{st}, 2022 and December 1^{st}, 2022.

Table 4.6 gives an overview of the dataset consisting out of the spot market prices. For an overview, the beginning and the end of the time–series are listed together with the number of rows. Further, a quantitative overview of NaN values is given. In the case of the DA prices, the share of NaN values of 75 % is explainable by the fact that the ID market clears every 15 minutes whereas the DA market clears every hour. Therefore, the DA values are valid for the full hour whereas the ID values only represent a quarter–hour.

Figure 4.8 compares the DA and the ID spot markets with an OTC coal power contract by a box–plot visualization. Note that the box–plot is built up by the box itself, which represents the interquartile range (representing the inner 50 % of the values) and the whiskers next to the box indicate the minimal and the maximal value. Thus, the conventional outlier indication is not applied within this thesis. The median is indicated by a

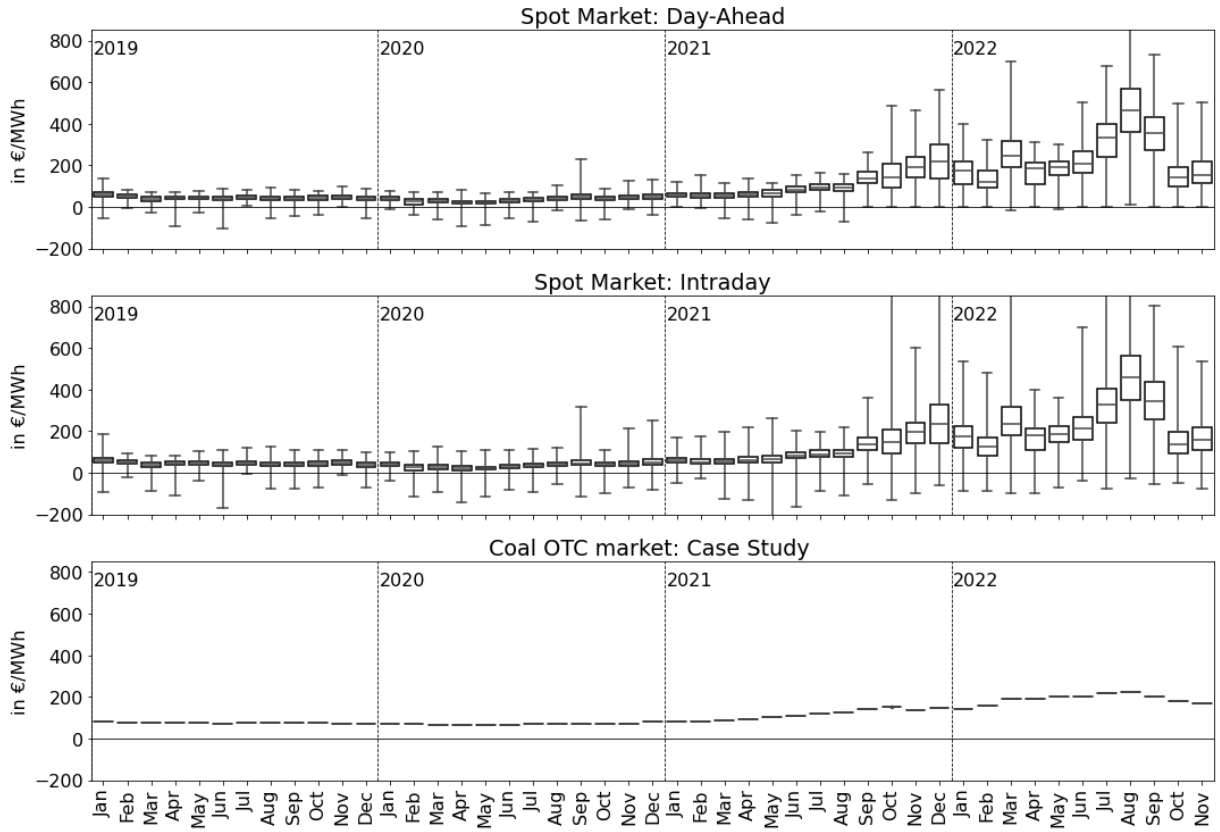

Figure 4.8: The prices for electric energy traded on the spot markets (ID and DA) and the estimated costs of a monthly altering coal PPA visualized in a monthly box–plot. Based on data provided by EPEX and investing.com among others [38], [78], [79], [100].

horizontal line splitting the box into two parts. A key difference between the DA and ID market is the bandwidth indicated by the length of the whiskers. Whereby the DA prices only show a small difference between the maximal and the minimal price, the ID prices have an increased spread. The DA market experiences an increased spreading since the winter of 2021, indicating higher fluctuating prices. The time–series considering ID and DA prices show an increase in the median value starting in the winter of 2021. This price increase is explained by the increasing gas prices by Consentec GmbH and several reports of the European Commission each analyzing the gas and electricity markets [20], [43]. Gas power plants are often the price setter as they are used to deliver the marginal capacities and therefore set the marginal price of the merit–order [43]. According to reports of the European Commission, the price increases in 2022 can be explained by the Russian invasion of Ukraine followed by announcements of Russian gas suppliers to throttle their deliveries. The market reactions forcing the price up and down in 2022 are attributed to policy announcements in Europe. Further, the reports underline the relevance of a decreased supply by french nuclear power plants as they experience outages [43].

The coal power contract is discussed in section 4.1 addressing the case study in further detail. Nevertheless, it is compared with the spot prices in this paragraph briefly. As the coal contract consists of monthly prices, there are no whiskers in the figure. The price increase of the coal power contract starting in 2021 can be explained by raising EUA prices and the switch from gas to coal power generating plants. Consequently, the spot markets for coal react to the higher demand with increasing prices as the European Commission summarizes in its report for

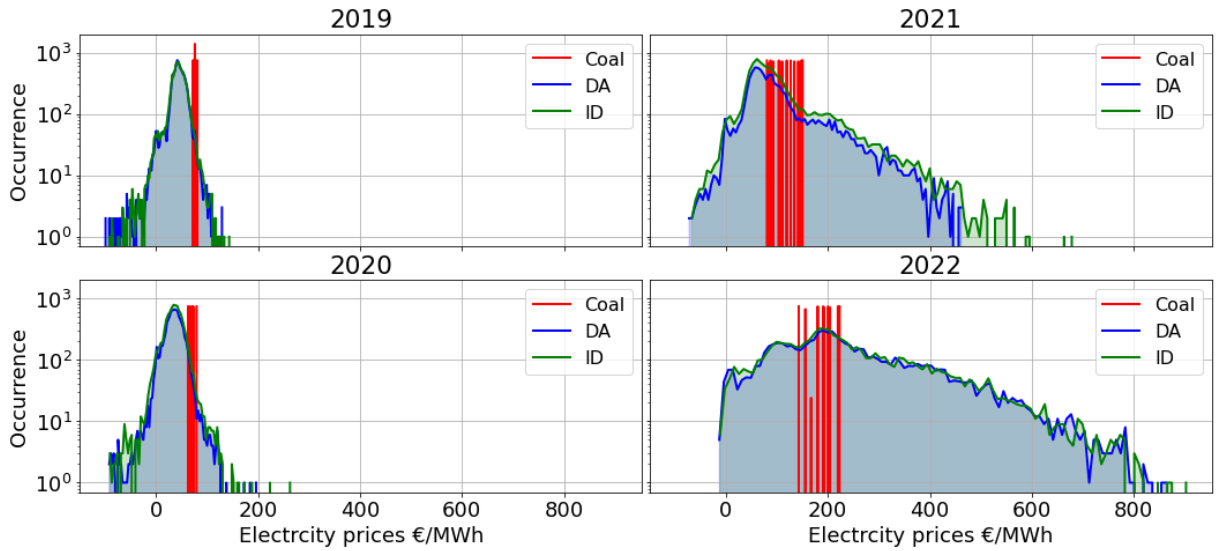

Figure 4.9: The prices for electric energy traded on the ID and DA markets visualized in a histogram with a logarithmically scaled y–axis. Based on data provided by EPEX [38].

the second quarter of 2022 [43]. According to the histogram in figure 4.9, the coal prices are slightly higher than the median spot market prices but not for the year 2022.

According to quarterly publications of the European Commission, the number of hours with a negative price for electricity on the spot DA market increased in 2020 due to the pandemic. The number of negative prices decreased in 2021 to the level of 2019 [43]. This effect can be identified for the DA market in figure 4.9, note the logarithmic scaling of the y–axis. The ID market experiences more hours with negative prices and could therefore be of special interest for the operation of PtH_2 units. Further, figure 4.9 shows the wide distribution of prices for the years 2021 and 2022. In the case of 2021, the publications of the European Commission and the boxplot in figure 4.8 show that the first quarters behaved similarly to the years 2019 and 2020 while the last quarter is driven by high gas prices [43]. This can plausibly explain the peak in the histogram of 2021 similar to the previous years while showing a wide distribution for higher prices similar to 2022.

4.3.2 Auxiliary service prices

According to the description in section 2.1, AuxS such as the FCR and the aFRR are auctioned by the Transmission System Operator (TSO). In contrast to the FCR which considers only a Capacity Price ($Price_{Cap}$), the auction of aFRR consists of a $Price_{Cap}$ and a Operating Price ($Price_{Op}$) for positive and negative services respectively. This thesis focuses on the $Price_{Cap}$ as already explained in section 4.2. It is assumed, that the PtH_2 unit participates at the $Price_{Op}$ auction with a "high price strategy" or "capacity–only". Therefore it is expected that this will never be chosen to operate. These auction results for the $Price_{Cap}$ are analyzed in table 4.7.

Table 4.7: Tabular overview of the number of NaN values within the AuxS related time–series.

	Res.	2019	2020	2021	2022*
Total rows		35048	35144	35048	32164
NaN in FCR	15 min	288 (0.8 %)	780 (2.2 %)	8352 (23.8 %)	960 (3.0 %)
NaN in aFRR(+)	15 min	360 (1.0 %)	24 (0.1 %)	0 (0.0 %)	384 (1.2 %)
NaN in aFRR(-)	15 min	408 (1.2 %)	204 (0.6 %)	0 (0.0 %)	384 (1.2 %)

*Covering TS between January 1^{st}, 2022 and December 1^{st}, 2022.

The time–series data drawn from the website `smard.de` operated by the "Bundesnetzagentur" (BNetzA) are analyzed in table 4.7 and in figure 4.10 [14]. The quantity of NaN values occurring in the positive and negative aFRR series is small and therefore not elaborated further. The situation for the FCR time–series is different as it is affected by a large quantity of NaN values in the years 2021 and 2022. All NaN values of the time-series considering the FCR and both aFRR prices are filled by interpolated values. The interpolation is exemplarily shown in figure C.1 on page XXXV in the appendix for the FCR values.

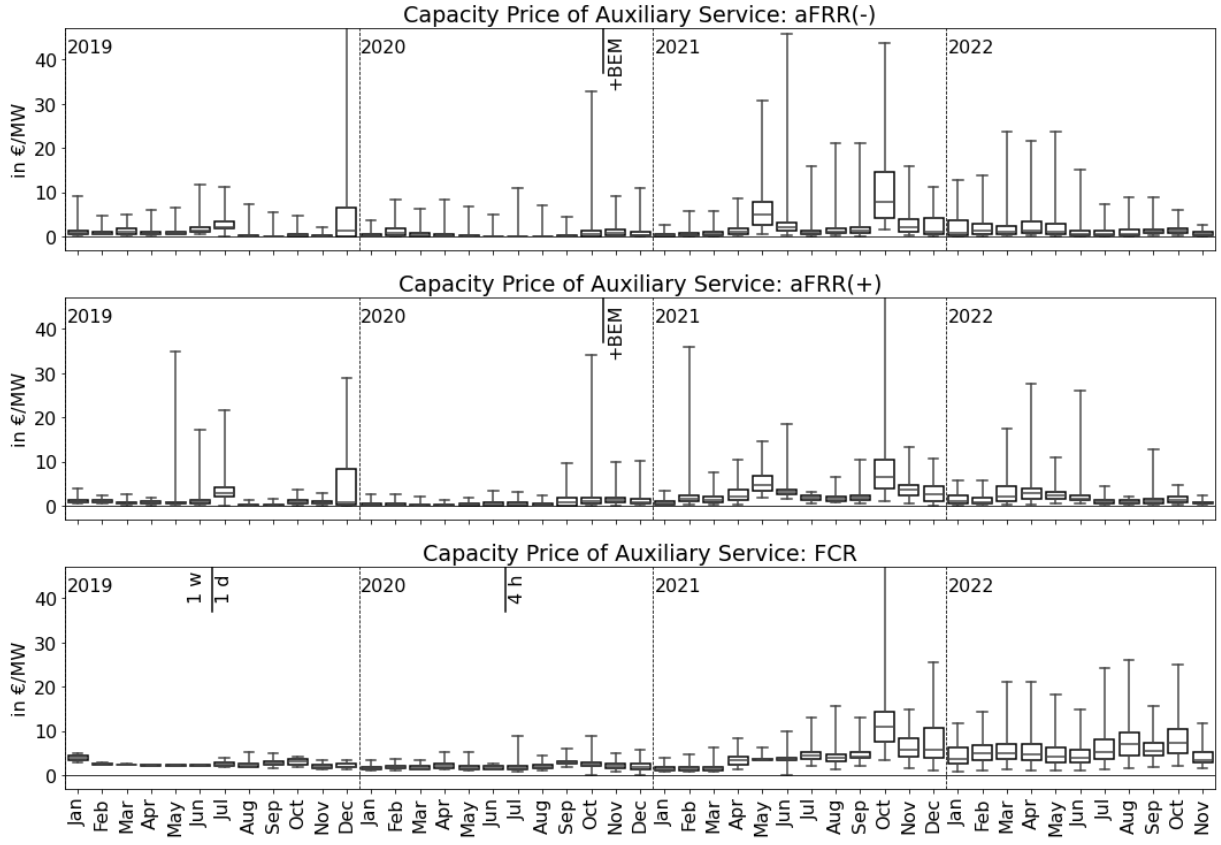

Figure 4.10: Price_{Cap} per 15 min interval for the FCR and the aFRR displayed as a monthly boxplot based on data provided by the BNetzA referenced to a quarter of an hour [14].

The time–series of the AuxS prices visualized as a box–plot in figure 4.10 give an overview on the trends and the bandwidth of the values for the last four years. At the beginning of the observed time frame, a very small

spread of the values (length of the whiskers) can be identified. This can be explained by a regulatory change. In July 2019, the FCR auction was adjusted so that daily rather than weekly periods were traded. A similar regulatory adjustment was performed on the first of July 2020 when the auctioned FCR period was reduced to represent 4 hours. These adjustments can be seen in the spread, which increased in July 2019. Consequently, more auctions per month take place which makes the chance for an increased spread more likely. Similar to the FCR prices, the aFRR market is affected by regulatory changes as well. According to Consentec, the bidding system for aFRR services was changed in November 2020 by implementing a second Balancing Energy Market (BEM) next to the existing Balancing Capacity Market (BCM). This led to an increase in the Price_{Cap} displayed in figure 4.10 [20]. Note that each displayed value represents the price referenced to a quarter of an hour [14].

The end of the three whiskers is not shown in figure 4.10. The aFRR(-) experiences its peak on December 8^{th}, 2019 which extended up to 81.41 €/MW while the aFRR(+) rises on November 13^{th}, 2021 up to 82.26 €/MW. The FCR service experiences its peak on November 2^{nd}, 2021 which extends up to 102.6 €/MW. A price increase can be identified in October 2021 for all AuxS capacity prices. According to Consentec GmbH, the rising prices for the FCR services starting in October 2021 can be explained by the rising gas prices [20].

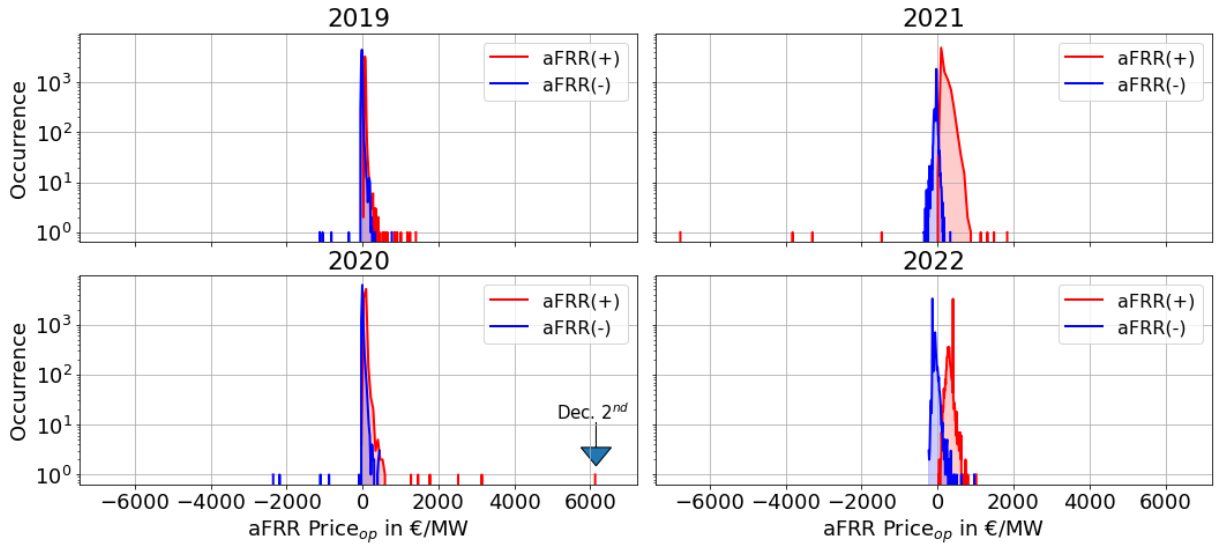

Figure 4.11: Histogram describing the scattering of the aFRR operating prices with a logarithmic notation of the y–axis based on smard.de [14].

Due to the high price strategy which assumes bidding prices for the operational market Price_{Op} as high as the regulations allow, this thesis assumes that the El participates as a capacity reserve for aFRR but never delivers aFRR. This assumption is strengthened by figure 4.11 which shows a histogram of the bidding results in the operational market. The horizontal axis shows the respective bidding results in €/MW while the vertical axis indicates the occurrence of the price on a logarithmic scale. Bidding prices higher than approximately 3,000 €/MW are never reached apart from December 2^{nd}, 2020, when the Price_{Op} for aFRR(+) climbed up to 17,021.49 €/MW. Assuming maximal bidding prices (the maximal Price_{Op} depends on the regulation in force, which constrained it either to 9,999 €/MW or to 99,999 €/MW), it is very unlikely that the El is chosen to deliver aFRR.

4.3.3 System average emission factor

The system average emission factor or the F_{CO2} of the power mix is an indicator of which power generation units are operating. A high CO_2 emission factor indicates a high share of coal (lignite or hard coal), oil and gas power plants whereas a lower CO_2 value indicates a high share of renewable generation [48], [92], [99], [113].

Table 4.8: Tabular overview of the number of NaN values within the F_{CO2} related time–series.

	Res.	2019	2020	2021	2022*
Total rows		8760	8784	8760	8015
NaN in F_{CO2}	60 min	0 (0.0 %)	0 (0.0 %)	0 (0.0 %)	0 (0.0 %)

*Covering TS between January 1^{st}, 2022 and November 30^{th}, 2022.

The CO_2 data properties are analyzed in table 4.8. There are no NaN values present in the data set provided by the "Forschungsstelle für Energiewirtschaft München e. V." (FfE München) [47]. The carbon footprint of the electricity mix is displayed in figure 4.12 whereby the data are taken from a publication by FfE München which is based on data of the European Network of Transmission System Operators for Electricity (Entso–E) [37], [47]. Wörner et al. (2019) published their methodology to determine the F_{CO2} in an article [147].

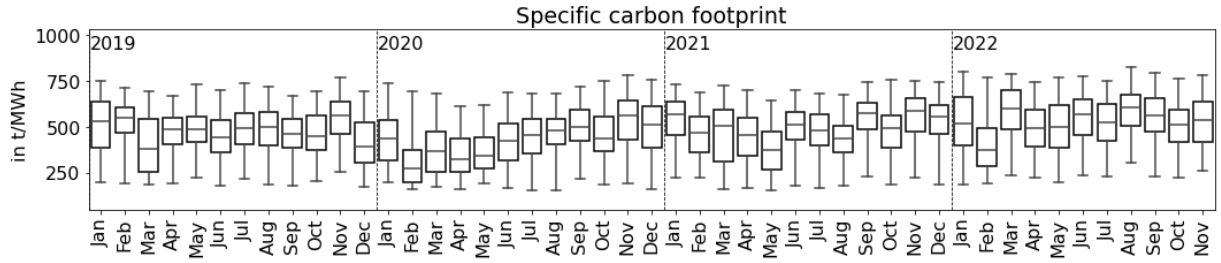

Figure 4.12: The carbon footprint of the electricity mix is visualized as a box–plot. Based on data provided by FfE München [47].

The figure 4.12 shows monthly boxplots of the time–series while the box indicates the interquartile range. The end of the whiskers indicates the maximal and the minimal values. Basically, a seasonal effect can be observed. The summer months have a lower specific CO_2 factor compared to the winter months. It is noticeable that the spread of each month extends roughly from 200 to 600 t_{CO2}/MWh. Thus, it seems that nearly all possible constitutions of power–generating units are present every month. The average footprint in 2022 was about 517 t_{CO2}/MWh, which is an increase compared to the previous years 2019 (470 t_{CO2}/MWh), 2020 (427 t_{CO2}/MWh) and 2021 (481 t_{CO2}/MWh) which can be compared to publications by the Federal Environment Agency [136].

4.3.4 Correlation

The presented data is analyzed for correlation within this section. First, a possible correlation of the electricity prices with the specific CO_2 emissions is analyzed. Second, a possible correlation between the electricity prices and the auction results for FCR and aFRR are is examined.

F_{CO2} and electricity prices According to Nicolosi et al. (2009), Makalska et al. (2018) and Ryota Keeley et al. (2020), there is a correlation between the share of renewable energy in the electricity mix and the spot

market price [48], [92], [99], [113]. This aspect is of high interest, especially when applying multi-objectives to the optimization tool. Figure 4.13 shows a scatter plot where specific CO_2 values of "15 min" slices, are plotted next to the corresponding spot market prices. Note that the DA dataset is resampled so that the NaN values are filled with the previous value which is placed on the last sharp hour representing the whole hour.

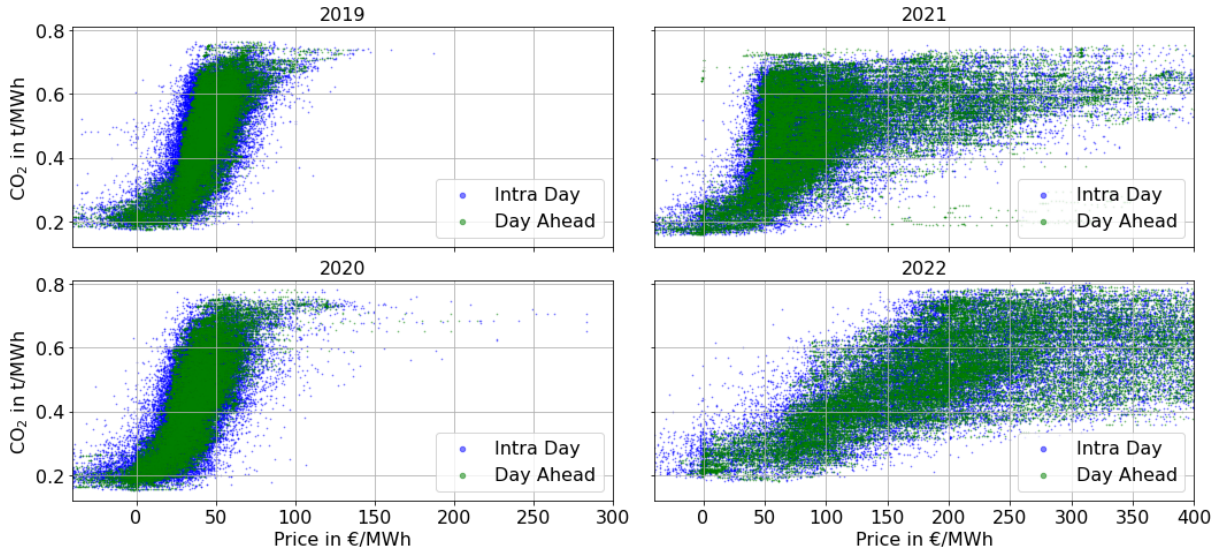

Figure 4.13: Correlation between the carbon footprint of the electricity mix and the spot market price based on data from FfE München and EPEX [38], [47]. Note the different x–axes scales.

The plots in figure 4.13 show a correlation for the spot market prices, as pointed out in the literature mentioned in the preceding paragraph. Low specific emission factors of the electricity grid correlate with low spot market prices. This relationship counts for both observed markets whereas the effect is more pronounced in the DA market as the scattering bandwidth is smaller. Considering the year 2022, there are fewer data points, as only the 11 months of the year are visualized. Therefore, fewer points are drawn in the plot. It is to point out, that the figures for 2019 and 2020 differ in contrast to the years 2021 and 2022. In the last two years, there are much higher prices on the spot markets corresponding with specific CO_2 factor above $0.5\,t_{CO_2}/MWh$.

Zakeri et al. (2022) analyze the spot market by determining the responsible price–setting power generation unit (marginal pricing) considering data between 2015 and 2019 [149]. They conclude that roughly two third of the spot market clearing prices are set by fossil–fueled power generating units. Assuming that this fact is still applicable today, the distribution in the years 2021 and 2022 could be explained. For a CO_2 factor of 0.5 in 2022, the spot prices scatter between ca. 50 and more than 400 €/MWh, whereas the same CO_2 factor in 2020 shows a scatter between ca. 10 and 90 €/MWh. High gas prices, as reported by the European Commission in their quarterly energy market report, might cause the high marginal prices at the spot market [43].

The correlation of the spot market prices and the CO_2 factor is in favor of the combined objective optimization applied to the PtH_2 unit within this thesis. Instead of the optimization with a single objective addressing the LCoE, the combined optimization considers both the CO_2 factor and the LCoE. Whereas the LCoE optimization of the PtH_2 unit based on the DA and ID prices might already have an impact on the CO_2 factor of the consumed power mix, as there is a correlation between the two input time–series.

Auxiliary service prices and electricity prices As there is a correlation between the CO_2 and the spot market prices, a similar correlation is analyzed for the AuxS. According to Consentec GmbH, auxiliary services

providing FCR and aFRR (+) have a correlation with the prices as the bidders of AuxS have to procure energy on the spot markets in the first place [20]. aFRR (-) is not mentioned here in particular, as the PtH_2 unit would run at throttled speed to increase its power consumption when ordered. Therefore, it does not procure its (balancing-) energy on the spot markets beforehand.

Figure C.2 in the appendix on page XXXV aims to show correlations by plotting the auxiliary service auction results next to the prices of the spot market. The upper three plots show the DA market results, while the lower plots show the ID results. Most of the data points accumulate at low auxiliary prices but scatter without any correlation. High auxiliary service prices do not appear together with high spot market prices.

4.4 Grid serving electrolyzers

The criteria for designing a grid serving operating strategy for El are not well defined in the literature [51]. Therefore, a distinct definition is derived subsequently for this thesis. Note the differences between the terms grid serving and system serving. FfE München publishes an overview of these terms in 2021. They consider system serving operations to include measures to stabilize the electricity grid for example by providing AuxS to maintain grid–frequency. The same publication considers grid services to contribute to equalizing the grid load. Further, the FfE München notes that the grid serving aspect negates power grid expansions caused by the additionally installed load [51].

Literature distinguishes between geographical and temporal criteria for a grid serving operation [36], [51], [107], [114], [118]. The Reiner–Lemoine–Institut (RLI) (2022) and the "Sachverständigenrat für Umweltfragen" (SRU) (2019) underline the geographic proximity of electricity generation and consumption, especially in the context of grid congestion that could be mitigated [107], [114]. As the location of the electrolyzer is predefined within the case study, this aspect is not implemented within the optimization tool. However, the temporal aspect is considered in the design of this thesis. In order to take the temporal aspect into account, there are two options. On the one hand, a publication by Energy Brainpool on behalf of the Green Planet Energy eG in 2019 presents a "trigger price"–based dispatch strategy for electrolysis–based PtH_2 units [36]. This consideration has similarities to Schalling et al. (2022) who assessed the grid serving potential of El. They conclude, that a grid serving operating strategy is given when El functions as a flexible consumer of renewable electricity [107]. A similar recommendation is drawn by the SRU (2021) based on Drunert et al. (2019) [33], [114]. The F_{CO2} of the electricity mix can be considered on the other hand due to its correlation with the electricity price as shown in section 4.3.4 and recommended by the RLI [107].

Based on the mentioned literature, this thesis considers an operating strategy optimized with respect to electricity prices as grid serving. The price–based optimization is then extended to include the F_{CO2} of the electricity mix. Whereas the marginal emission factor recommended by Seckinger (2021), which considers the consequences of an increase in load on the F_{CO2}, is not considered in this thesis [118]. In addition, this thesis implements system serving aspects by including the participation at the AuxS markets. This definition lacks the consideration of local circumstances because of identical EPEX prices within the price zone (Germany and Luxemburg). A more focused definition could be worked out and implemented in subsequent work.

4.5 Software

The optimization tool is a software–based application developed to provide insights concerning the research question derived in section 3.1. The tool itself is written in the language "Python", published by van Rossum et al. (2010) [139]. Thereby, the application programming interfaces "Spyder" and "Jupyter Notebooks" are used [9],

[127].

The optimization tool is based primarily on the Python Open–source Modelling and Optimization (PYOMO) library published by Bynum et al. (2011), and Hart et al. (2021) [18], [66]. It is used to design the computational representations of the PtH_2 unit. The PYOMO library provides the "concrete model" class which can be used to define variables and constraints. Further, this class can be used to define an objective function representing the target of the optimization issue. By the help of the PYOMO library the constructed "concrete model" is transferred to the solver application "Gurobi" published by the Gurobi Optimization, L. L.C. [60]. The "Gurobi" solver (version number 9.5.2) is used within the framework of an academic license.

Additionally to that, the library "Pandas" published by the "pandas development team" and the library "Numpy" published by Harris et al. (2020) are applied [65], [130]. "Pandas" is used for data and table management and "Numpy" for numerical computations. Visualizations are done with the help of the Python library "Matplotlib" by Thomas A. Caswell et al. (2022) [131]. Some visualizations are based on the python library "Seaborn" by Waskom et al. (2021) [144].

Chapter 5

Design of the Optimization Tool

This chapter addresses the design of the optimization tool and its integrated optimization model of the Power–to–Hydrogen (PtH_2) unit. The thesis implements a deterministic optimization model–based on a mathematical representation of the technical system. This approach, often called "linear programming", is used by Röben et al. (2021) and Sens et al. (2021) among others to solve similar optimization problems [111], [122], [135], [140]. The optimization tool is fed with techno–economic parameters discussed in the section before. This chapter includes a structural overview of the optimization tool which draws the input parameters, constructs the model, sends it to the solver and extracts the solved data. Furthermore, this chapter includes the construction procedure of the optimization model. Thereby, each step required to implement the PtH_2 elements is discussed individually by defining the variables and constraints applied to represent its technical and economic properties. Subsequently, the design of the objective functions, addressing economic and environmental parameters, is explained.

5.1 Structure of the optimization tool

The structure of the optimization tool is visualized in figure 5.1 in a schematic flow diagram. Basically, the optimization tool involves several procedures to draw data, and to construct and to solve an optimization model. Further, it processes the obtained results. With the start of the optimization tool, the script *PY_Optimization_Tool_main* is called to construct an optimization model instance. The script draws input data including static PtH_2 properties such as the specific Electrolyzer (El) and Battery (Ba) parameters for example. Additionally to that, time–series data concerning the energy markets, the CO_2–Footprint (F_{CO2}) of the electricity mix and the Hydrogen (H_2) demand specified in the case study are imported. These data sets are discussed within chapter 4 beforehand. Further, the construction procedure takes modeling and scenario properties into account such as the discretization intervals or information concerning the offer of Auxiliary Service (AuxS) in the current scenario.

Based on these input data sets, the script defines each PtH_2 element with functions gathered in the script *PY_Optimization_Tool_Functions*. These definitions yield variables and constraints implemented in the Python Open–source Modelling and Optimization (PYOMO) "ConcreteModel" class. The properties of each PtH_2 element are summarized in a Python dictionary which is used to store all relevant parameters.

Based on the variables implemented for the PtH_2 elements, the objective functions are defined and implemented in the respective PYOMO subclass. As soon as the implementation procedure is finished, the "ConcreteModel" is sent as a matrix to the Gurobi solver application. The solver applies numerical algorithms to retrieve an optimal configuration of the input variables with respect to the implemented objective function [60]. The data of the solved

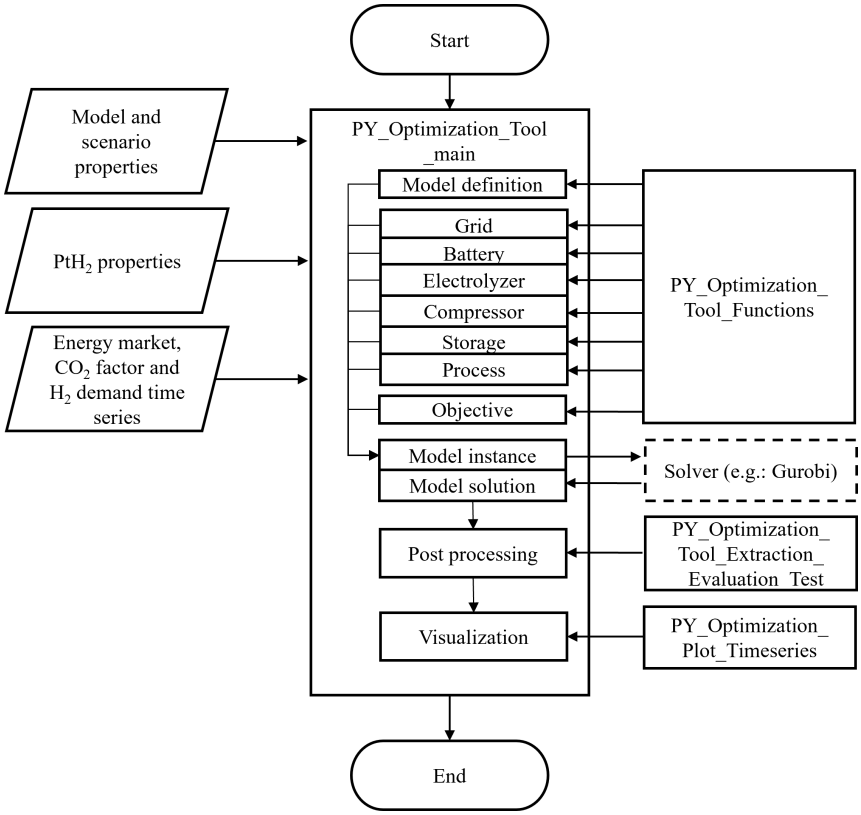

Figure 5.1: Schematic block diagram visualizing the structure of the optimization tool with the main script in the middle which draws input data, and additional functions to solve, process and plot the results from further scripts.

model are then extracted and evaluated from a technical, economic and environmental perspective with the help of functions in the script *PY_Optimization_Tool_Extraction_Test*. The retrieved data set is saved and visualized by the *PY_Optimization_Plot_Timeseries*. To apply the tool for sensitivity studies or scenario analyses, a higher–level routine must be designed specifically for the issue of interest. Typically, such a higher–level routine would include several independent calls of the optimization tool each based on adjusted input data.

5.2 Optimization model construction

The construction of the optimization model is elaborated in this section, based on the structure discussed before in figure 5.1. As explained above, the model construction includes the data sets discussed in chapter 4 which discusses the techno–economic parameters.

The model construction procedure is described in the following subsections. The model is created by implementing the "ConcreteModel" class in the first place. Based on this PYOMO class, each PtH_2 element is defined based on a number of variables and constraints. Within the optimization tool, all variables are defined with their unit stated at the end of the variable name by underscores. As many indexed variables are based on an adjustable time Interval (t_{int}), the chosen discretization period in minutes is indicated with the abbreviation t_{int}.

Variables in PYOMO can be distinguished into indexed and non–indexed. Indexed variables have an individual

value for each simulated point in time, non–indexed variables are constant throughout the simulation. All indexed variables of the PYOMO "ConcreteModel" class are based on the "RangeSet" subclass, which provides a common index. It is defined by the Time–Stamp (TS) of the H_2 time–series data set which does not include production downtimes as discussed in section 4.1.

Within the model creation, a factor is defined which allows the transformation of continuous variables such as MW or kg/h to time–based variables such as MWh/t_{int} or kg/t_{int} by considering the amount of t_{int} per hour. The factor Hours per Interval ($C_{h/int}$) is shown in the equation 5.1. Note that the term min_{int} represents the length of each interval in minutes which is defined within the model properties input–data.

$$MW \cdot \frac{min_{int} \cdot h}{int \cdot 60\ min} = MW \cdot C_{h/int} = \frac{MWh}{int} \quad ; \quad \frac{kg}{h} \cdot \frac{min_{int} \cdot h}{int \cdot 60\ min} = \frac{kg}{h} \cdot C_{h/int} = \frac{kg}{int} \tag{5.1}$$

As each PtH_2 element accesses previously defined variables, thus the order of the implementation is of relevance. The "ConcreteModel" with its implemented Index (IDX) and $C_{h/int}$ variables is used to construct each PtH_2 element. Constraints are implemented by adding them to a variable–specific list within the PYOMO subclass "ConstraintList". Constraints of indexed variables can be defined for every index individually. The design of the variables and constraints representing the PtH_2 unit are discussed in the next sections starting with the grid connection.

5.2.1 Grid

The PtH_2 element Grid (Gr) is defined by an individual function drawn from the function file shown in figure 5.1 in the section 5.1 before. Its definition includes several variables and constraints which are elaborated subsequently. Table 5.1 gives an overview of the implemented variables, whether they are indexed, which unit they have and of which numerical domain they consist. The variables placed on the arrows in figure 5.2 define the in– and out–flowing electric energy.

Within the modeling properties, the energy flows providing AuxS can either be selected individually or neglected. As soon as Frequency Containment Reserve (FCR) or Automatic Frequency Restoration Reserve (aFRR) are not considered, the value of their respective variable is set to zero for all indices.

The non–indexed variable *Gr_Capacity_MW* defined as a Non–Negative–Reals (NNR) variable, represents the maximal capacity of the grid connection. Therefore, it is a constant value valid for all points in time. The variable *Gr_Capacity_MW* is later applied in the economic objective function to calculate the total investment costs and the corresponding maintenance expenses discussed in section 4.2 and summarized in table 4.5. The second internal variable, displayed in figure 5.2, *Gr_out(i)* is used as a helper variable within the function Gr itself. It combines the distinct out–flowing variables such as the power flowing to the Ba and to the Compressor (Co), both are implemented as indexed variables based on NNR. The direct power supply to the electrolyzer is designed in a different manner. It consists of a NNR variable *Gr_to_El_Base* and three constrained variables representing the power input implemented to perform AuxS by the El. These energy flows involved in AuxS are implemented as continuous NNR for simplicity reasons. This thesis assumes that the AuxS are managed by AuxS–pooling providers, as the direct participation is restricted to the bidding quantities of 1 MW as explained in section 2.1.3.

Equation 5.2 to 5.4 constraints the out–flowing energy for AuxS by adding each equation to the variable *Gr_ConsList*. The constraints are applied for all TS relevant in the case study (IDX) as explained beforehand. According to the considerations in section 2.1.3, the provision of AuxS is split up into six separate periods each day consisting of four hours. Within an AuxS period, the value of the provided AuxS has to be constant. This behavior is implemented within the Gr construction by considering adjustable discretization intervals. For simplicity reasons, this work considers only the current regulative circumstances although the bidding process changed in the past.

The helper variables s, t, and k in equation 5.2 to 5.4 are used to represent the regulatory nature of the AuxS.

Table 5.1: Modelling properties of the variables defined within the Gr unit.

Variable	Ind.	Unit	Domain
Gr_Capacity	/	MWh	NNR
Gr_out	i	MWh/t_{int}	NNR
Gr_to_Ba	i	MWh/t_{int}	NNR
Gr_to_Co	i	MWh/t_{int}	NNR
Gr_to_El_Base	i	MW	NNR
Gr_to_El_FCR	i	MW	NNI
Gr_to_El_aFRRn	i	MW	NNI
Gr_to_El_aFRRp	i	MW	NNI

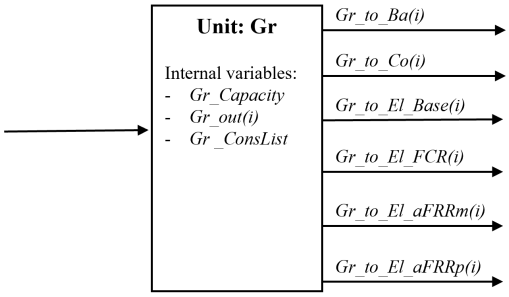

Figure 5.2: Graphical representation of the Gr unit and its variables.

The range $\{k \cdot 4/C_{h/int} | k \in \text{IDX}\}$ creates a set of integers representing each starting TS of an AuxS period by looping through all IDX with the specific increment $4/C_{h/int}$. The increment $4/C_{h/int}$ equals the number of TS within a four–hours AuxS interval. The points in time within the four–hours bidding period, represented by the helper variable t, are constrained to be equal to the first value of the AuxS interval (s). The range applied for these constraints during each AuxS period is represented by $\{1, ..., 4/C_{h/int}\}$ which considers all indices within a four–hour Auxiliary Service Interval (AuxS_{int}).

$$Gr\_to\_El\_FCR\_MWh\_t_{int}(s) = Gr\_to\_El\_FCR\_MWh\_t_{int}(s+t) \tag{5.2}$$

$$Gr\_to\_El\_aFRRp\_MWh\_t_{int}(s) = Gr\_to\_El\_aFRRn\_MWh\_t_{int}(s+t) \tag{5.3}$$

$$Gr\_to\_El\_aFRRn\_MWh\_t_{int}(s) = Gr\_to\_El\_aFRRn\_MWh\_t_{int}(s+t) \tag{5.4}$$

$$s \; \forall \left\{ k \cdot \frac{4}{C_{h/int}} | k \in \text{IDX} \right\}; t \; \forall \left\{ 1, ..., \frac{4}{C_{h/int}} \right\}$$

The internal variable *Gr_out_MWh_t_{int}(i)* is defined to be the sum of out–flowing energy streams shown in equation 5.5. The variable is used to determine the Operating Expenditures (OpEx) within the economic and the F_{CO2} within the environmental objective function. In contrast to the non–AuxS containing variables, the AuxS variables contribute to the *Gr_out_MWh_t_{int}(i)* according to their regulative nature. The energy stream implemented for aFRR(-) services is not considered to deliver energy since it must reserve capacity to increase consumption. The implementation of the AuxS variables is explained in section 5.2.3, which addresses the construction of the El element, in greater detail.

$$\begin{aligned} \text{Gr}\_out\_MWh\_\text{t}_{int}(i) = \; & 1 \cdot \text{Gr}\_to\_Ba\_MWh\_\text{t}_{int}(i) \\ & + 1 \cdot \text{Gr}\_to\_Co\_MWh\_\text{t}_{int}(i) \\ & + 1 \cdot \text{Gr}\_to\_El\_Base\_MW(i) \cdot \text{C}_{h/int} \\ & + 1 \cdot Gr\_to\_El\_\text{FCR}\_MW(i) \cdot \text{C}_{h/int} \\ & + 0 \cdot \text{Gr}\_to\_El\_\text{aFRR}n\_MW(i) \cdot \text{C}_{h/int} \\ & + 1 \cdot \text{Gr}\_to\_El\_\text{aFRR}p\_MW(i) \cdot \text{C}_{h/int} \\ & i \; \forall \; \text{IDX} \end{aligned} \tag{5.5}$$

The component size *Gr_Capacity_MW* has to be always larger than the individual out–flowing power streams,

as shown in equation 5.6. It defines the maximum capacity to be larger or equal to the individual indexed out–flowing variables. The electricity flow implemented for FCR services is considered with the factor 2 to reflect its symmetrical behavior.

$$\begin{aligned} Gr\_Capacity\_MW \cdot \mathrm{C}_{h/int} \geq \; & 1 \cdot Gr\_to\_Ba\_MWh\_t_{int}(i) \\ & + 1 \cdot Gr\_to\_Co\_MWh\_t_{int}(i) \\ & + 1 \cdot Gr\_to\_El\_Base\_MW(i) \; \cdot \mathrm{C}_{h/int} \\ & + 2 \cdot Gr\_to\_El\_FCR\_MW(i) \; \cdot \mathrm{C}_{h/int} \\ & + 1 \cdot Gr\_to\_El\_aFRRn\_MW(i) \; \cdot \mathrm{C}_{h/int} \\ & + 1 \cdot Gr\_to\_El\_aFRRp\_MW(i) \; \cdot \mathrm{C}_{h/int} \\ & i \; \forall \; \mathrm{IDX} \end{aligned} \tag{5.6}$$

5.2.2 Battery

Within the function to construct the Ba, several variables and constraints are defined to reflect the technical behavior of the PtH_2 element. Thereby, the construction of the Ba specific constraints takes variables into account which are already defined in the preceding Gr function. All variables are implemented as NNR. The unit of the variables is based on MWh as it is summarized in table 5.2. Figure 5.3 shows the in– and out–flowing variables of the Ba. Internally, the Ba is constructed as an energy integrator based on the common State–of–Charge (SOC) approach recommended by Sioshansi et al. (2022) [124]. The SOC is a function of time and therefore indexed such as the in– and out–flowing variables *Ba_to_El* and *Ba_to_Co*. In case the battery should not be considered as a component for the PtH_2 unit, it can be deselected by setting a parameter within the model properties input data set. The implemented variables would then be fixed to zero.

Table 5.2: Modelling properties of the variables defined during the construction of the Ba.

Variable	Ind.	Unit	Domain
Ba_Capacity	/	MWh	NNR
Ba_SOC	i	$\mathrm{MWh/t}_{int}$	NNR
Ba_to_El	i	$\mathrm{MWh/t}_{int}$	NNR
Ba_to_Co	i	$\mathrm{MWh/t}_{int}$	NNR

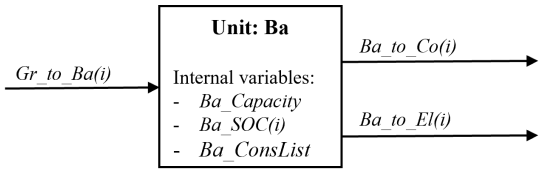

Figure 5.3: Graphical representation of the Ba unit and its variables.

The variable *Ba_Capacity_MWh*, measured in MWh, is not indexed, as it is the constant component size valid for all points of time. Its value is considered in the economic objective function to compute the respective Capital Expenditures (CapEx) and maintenance costs.

$$Ba\_Capacity\_MWh \geq Ba\_SOC\_MWh(i) \tag{5.7}$$

$$Ba\_to\_El\_MWh\_t_{int}(i) + Ba\_to\_Co\_MWh\_t_{int}(i) \leq Ba\_SOC\_MWh(i) \tag{5.8}$$

$$\begin{aligned} Ba\_Capacity\_MWh - Ba\_SOC\_MWh(i) \cdot \eta_{Ba} \geq & Gr\_to\_Ba\_MWh\_t_{int}(i) \\ & i \; \forall \; \mathrm{IDX} \end{aligned} \tag{5.9}$$

Equation 5.7 to 5.9 define the component sizes of the Ba. These constraints are added to the PYOMO

constraint list *Ba_ConsList*. First, the maximum capacity must always be larger than the indexed SOC. Second, the out–flowing energy streams are constrained to be smaller or equal then the SOC at any given IDX. Third, the in–flowing energy coming from the Gr has to be smaller or equal to the remaining capacity within the Ba for any IDX.

$$\begin{aligned} Ba\_SOC\_MWh(i+1) = \quad & Ba\_SOC\_MWh(i) - Ba\_out\_MWh\_t_{int}(i) \\ & + Gr\_to\_Ba\_MWh\_t_{int}(i) \cdot \eta_{Ba} \\ & i \; \forall \; \{1, ..., \mathrm{IDX}_{[-2]}\} \end{aligned} \tag{5.10}$$

Equation 5.10 defines the behavior of the SOC. Basically, the SOC is constructed to integrate the in– and out–flowing energy streams. Therefore, the successive SOC(i+1) corresponds to the current SOC(i) and the current in– and out–flowing energy flows. As discussed in section 4.2.3 the efficiency η_{Ba} of the Ba is considered for the charging process. The range expression in equation 5.10 does not cover the last simulated point of time.

As the initial SOC value of the Ba should not be set by the operators, but by the optimization algorithm, to achieve optimal results the first and last SOC are constrained to be identical.

5.2.3 Electrolyzer

With the two energy sources Gr and Ba supplying the El with electrical energy already defined, the necessary variables to construct the El are defined within this section and summarized in table 5.3 and in figure 5.4. The component size of the El is represented by the non–indexed variable *El_Capacity_MW* which is later used in the economic objective function. All variables defined within the El construction emerge from the domain NNR. Within the El, the unit changes from MWh to kg, as electrical energy is converted to a mass flow of H_2 in an electrolytic process discussed in section 2.2.2.

Table 5.3: Modelling properties of the variables defined during the construction of the El.

Variable	Ind.	Unit	Domain
El_Capacity_MW	/	MW	NNR
El_in_Pr._MWh_t$_{int}$	i	MWh/t$_{int}$	NNR
El_to_Co	i	kg/t$_{int}$	NNR
El_to_Pr	i	kg/t$_{int}$	NNR

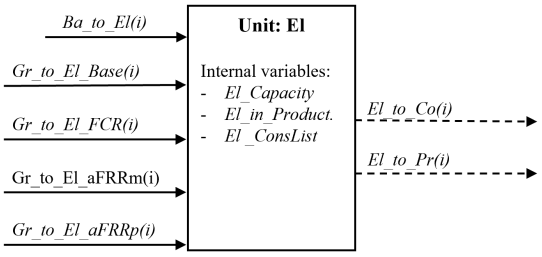

Figure 5.4: Graphical representation of the El unit and its variables.

Similar to the implementation function of the Gr, the capacity of the *El_Capacity_MW* is constrained to be always larger than its indexed energy flows. This constraint is shown in equation 5.11 which takes the in–flowing energy from the Ba and the "Base" flow originating at the Gr into account. In–flowing energy streams incorporating AuxS are factored in as well. In contrast to the aFRR, the symmetrical nature of the FCR is reflected with factor two in the third line of equation 5.11. The respective constraints affecting the construction of the El are stored in the PYOMO variable *El_ConsList*.

$$
\begin{aligned}
El\_Capacity\_MW \cdot \mathrm{C}_{h/int} \geq \quad & Ba\_to\_El\_MWh\_t_{int}(i) \\
& + 1 \cdot El\_to\_El\_Base\_MW(i) \ \cdot \mathrm{C}_{h/int} \\
& + 2 \cdot El\_to\_El\_FCR\_MW(i) \ \cdot \mathrm{C}_{h/int} \\
& + 1 \cdot El\_to\_El\_aFRRn\_MW(i) \ \cdot \mathrm{C}_{h/int} \\
& + 1 \cdot El\_to\_El\_aFRRp\_MW(i) \ \cdot \mathrm{C}_{h/int} \\
& i \ \forall \ \mathrm{IDX}
\end{aligned}
\tag{5.11}
$$

The consequences of equation 5.11 for each *Gr_to_El* variable are visualized in figure 5.5. The figure aims to show the maximum capacity constraint and the amount of electrical energy consumed in the H_2 production for different operational modes. The straight black line indicates the maximum capacity while the straight red line indicates the constraint to determine the maximum capacity. The amount of energy consumed to produce H_2 is indicated with the dashed green line.

The first sub–figure on the left shows the dispatch of an El without any AuxS offered at the time of observation. The constraint and the *El_in_Production(i)* are similar as only *El_to_El_Base(i)* is consumed. The second figure on the left takes the same basic case into account while adding the FCR ±1 MW service for one AuxS_{int}. The constraint to determine the maximum capacity considers the "Base" energy flow and the symmetric FCR capacity service. In contrast to that, the *El_in_Production(i)* variable defining the H_2 output assumes that the symmetric nature of the FCR service equals out statistically as the real consumption oscillates within the symmetrical range of the offered FCR.

In the case of positive and negative aFRR services, the capacity constraint and the consumption determining the H_2 are implemented according to the two sub–figures in the right of figure 5.5. The offered aFRR shown in the figure is about 1 MW. As described in section 2.1.3, negative aFRR is defined to reduce the amount of power generated in the electric grid from a grid–based viewing angle. This implies that the El has to be able to increase its consumption when necessary. As the third sub–figure 5.5 shows, the capacity constraint (straight red line) takes the full aFRR service into account, while the production curve *El_in_Production(i)* (dashed green line) does not include the negative aFRR. The opposite is the case for the positive aFRR which is defined to increase the available power in the electric grid, thus decreasing the production rate of the El.

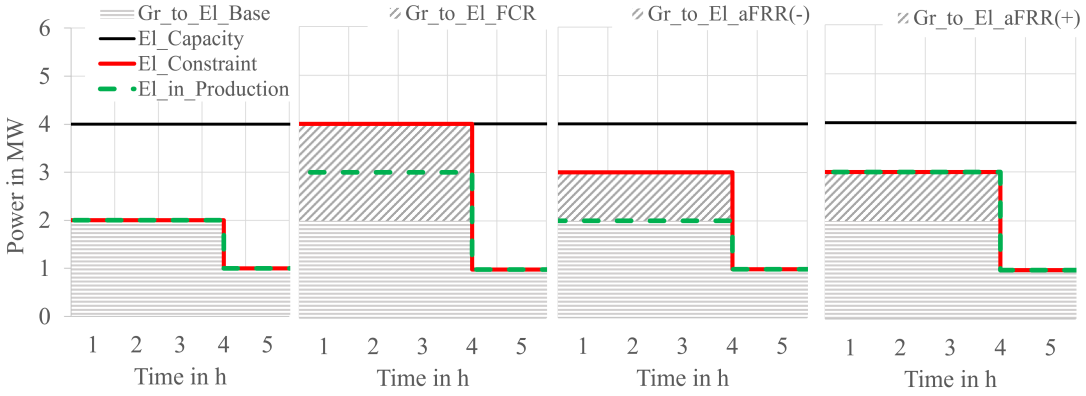

Figure 5.5: Visualization of the AuxS implementation by a maximal capacity and the ($El\_in\_Production\_MWh\_t_{int}(i)$) variable for the "Base", "FCR" and "aFRR" cases.

This thesis considers the El taking part at the capacity auctions for FCR and aFRR services as a price taker, thus it is assumed that its participation in the bidding process would not have influenced the outcoming prices. Based on the assumption that the El participates with a "high prices" strategy on the aFRR operational auction, it is assumed that the El is never chosen to deliver its capacities (capacity–only). This assumption is supported by the fact that higher prices than 5,000 €/MW have not been discovered (although there is one exception for aFRR(+) operational prices on December 2^{nd}, 2020 with prices up to 17,021.9 €/MW) within the analysis of the aFRR operational price times series in section 4.3.2. The maximal price was between 9,999.99 and 99,999.99 €/MW depending on the regulation which is significantly higher compared to typical auctioned prices [1], [14], [50].

The variable *El_in_Production_MWh_t_{int}(i)* is considered to be internal, as it is defined to determine the amount of in-flowing electrical energy available to be converted to H_2. The variable is later applied to calculate the amount of produced H_2 based on the efficiency (η_{El}) and the respective specific H_2 production ($P_{kg(H2)/MW}$). Equation 5.12 sums up in–flowing energy streams while taking the nature of the different AuxS properties into account.

$$\begin{aligned} \text{El\_}in\_Production\_MWh\_\text{t}_{int}(i) = \; & 1 \cdot \text{Gr\_}to\_Ba\_MWh\_\text{t}_{int}(i) \\ & + 1 \cdot \text{El\_}to\_Co\_MWh\_\text{t}_{int}(i) \\ & + 1 \cdot \text{El\_}to\_El\_Base\_MW(i) \cdot \text{C}_{h/int} \\ & + 1 \cdot \text{El\_}to\_El\_\text{FCR}\_MW(i) \cdot \text{C}_{h/int} \\ & + 0 \cdot \text{El\_}to\_El\_\text{aFRR}n\_MW(i) \cdot \text{C}_{h/int} \\ & + 1 \cdot \text{El\_}to\_El\_\text{aFRR}p\_MW(i) \cdot \text{C}_{h/int} \\ & i \; \forall \; \text{IDX} \end{aligned} \tag{5.12}$$

Based on *El_in_Production_MWh_t_{int}(i)*, the amount of H_2 is computed in equation 5.14. The electrolyzer production capacity $P_{kg(H2)/MW}$ in kg/(MWh/h) is based on the efficiency (η_{El}) and the Lower Heating Value (LHV) according to equation 5.13.

$$P_{kgH2/MW} = \frac{\eta_{El}}{LHV} \tag{5.13}$$

$$\begin{aligned} P_{kgH2/MWh} \cdot El\_in\_Production\_MWh\_t_{int}(i) = \; & El\_to\_St\_kg\_t_{int}(i) \\ & + El\_to\_Co\_kg\_t_{int}(i) \\ & i \; \forall \; \text{IDX} \end{aligned} \tag{5.14}$$

To reflect the dynamics of the El, additional constraints are implemented. First, the El minimal load (El_{min}) of the electrolyzer is implemented as a constraint for *El_in_Production_MWh_t_{int}(i)* by equation 5.15. It is assumed, that the El starts at a dynamic load which is determined within the simulation. Therefore *El_in_Production_MWh_t_{int}(1)* is not fixed to an distinct value.

$$\begin{aligned} El\_in\_Production\_MWh\_t_{int}(i) \geq & El\_Capacity\_MW \cdot El_{min} \cdot \text{C}_{h/int} \\ & i \; \forall \; \text{IDX} \end{aligned} \tag{5.15}$$

Second, the El load gradient (El_{Grad}) of the electrolyzer is implemented within the optimization model as soon

as the load gradients are relevant for the discretization intervals. The relevance is determined by an "if statement". As soon as the product of the El_{Grad} based on minutes and the interval length (t_{int}) is larger than one, the El_{Grad} becomes obsolete.

$$if\ El_{laod} \cdot t_{int} \leq 1:$$

$$El\_in\_Production\_MWh\_t_{int}(i+1) \leq (1 + El_{load} \cdot t_{int}) \cdot El\_in\_Production\_MWh\_t_{int}(i) \quad (5.16)$$

$$El\_in\_Production\_MWh\_t_{int}(i+1) \geq (1 - El_{laod} \cdot t_{int}) \cdot El\_in\_Production\_MWh\_t_{int}(i) \quad (5.17)$$

$$i\ \forall\ IDX_{[1:-2]}$$

Equation 5.16 and 5.17 are valid for all indices but not the last one, indicated by the index [1;-2 as the term (i+1) would set a constraint outside the range of the IDX variable.

The produced H_2 in the El can then either be fed in the process directly or can be stored in the pressurized storage. To elevate the outlet pressure of the El, which depends on the type of electrolyzer as discussed in section 4.2.4, a Co is implemented. The construction procedure of the Co and the Storage (St) is explained in the upcoming paragraph.

5.2.4 Compressor

The Co unit compresses the H_2 mass flow to be stored in the St. Thereby, a constant pressure ratio between the El outlet and the St inlet is assumed. This simplification is made as the optimization tool does not calculate the real St pressure in dependence on the actual SOC, thus the differential pressure incorporates the maximal St pressure. The necessary variables to implement the St unit are summarized in table 5.4 and figure 5.6.

Table 5.4: Modelling properties of the variables defined during the construction of the Co.

Variable	Ind.	Unit	Domain
Co_Capacity	/	kg/t_{int}	NNR
Co_to_St	i	kg/t_{int}	NNR

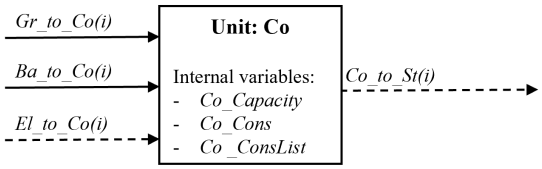

Figure 5.6: Graphical representation of the Co unit and its variables.

The capacity variable $Co\_Capacity\_kg\_t_{int}$ is constrained by equation 5.18 to be larger or equal to the inflowing amount of H_2 originating from the El.

$$Co\_Capacity\_kg\_t_{int} \geq El\_to\_Co\_kg\ \_t_{int}(i) \quad (5.18)$$

$$i\ \forall\ IDX$$

As leakages have to be incorporated for the compression process, equation 5.19 implements the leakage factor $Co_{Leakage}$. The leakage factor of the compressor units is discussed in section 4.2.5.

$$Co\_to\_St\_kg\_t_{int}(i) = (1 - Co_{Leakage}) \cdot El\_to\_Co\_kg\ \_t_{int}(i) \quad (5.19)$$

$$i\ \forall\ IDX$$

The energy consumed by the Co is defined by the equation 5.20. This definition is based on the Electric

Power (EP) consumed by the Co_{EP} which is calculated according to section 2.2.3 for each scenario individually. In addition, the equation 2.2.3 includes the efficiency Co_{EP}.

$$El\_to\_Co\_kg\_t_{int}(i) \cdot \frac{Co_{EP}}{Co_{\eta}} = Gr\_to\_Co\_MWh\_t_{int}(i) + Ba\_to\_Co\_MWh\_t_{int}(i) \quad (5.20)$$
$$i \; \forall \; \text{IDX}$$

5.2.5 Storage

The St is constructed in a similar manner as the Ba explained in section 5.2.2 with a constant capacity variable *St_Capacity_kg*, an indexed SOC variable *St_SOC_kg* and a set of constraints implemented in the *St_ConsList*. A summary of the variables is given in table 5.5 and figure 5.7.

Table 5.5: Modelling properties of the variables defined during the construction of the St.

Variable	Ind.	Unit	Domain
St_Capacity	/	kg	NNR
St_SOC	i	kg/t_{int}	NNR
St_to_Pr	i	kg/t_{int}	NNR

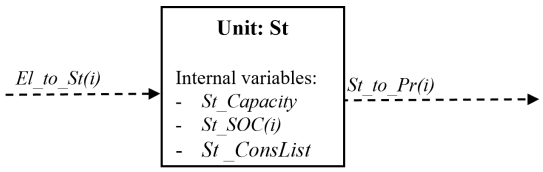

Figure 5.7: Graphical representation of the St unit and its variables.

Additionally to that, additional storage is considered to function as an emergency option *Storage_Emergency* for potential failures of the PtH_2 unit. The capacity is dimensioned to supply the average H_2 demand for at least 8 hours. Equation 5.21 to 5.23 constraint the SOC for all IDX.

$$St\_Capacity\_kg \geq St\_SOC\_kg(i) \quad (5.21)$$
$$Co\_to\_St\_kg\_t_{int}(i) \leq St\_Capacity\_kg - St\_SOC\_kg(i) \quad (5.22)$$
$$St\_to\_Pr\_kg\_t_{int}(i) \leq St\_SOC\_kg(i) \quad (5.23)$$
$$i \; \forall \; \text{IDX}$$

Equation 5.24 defines the integrating nature of the SOC for all IDX but not the last one as indicated by the series of values until the next–to–last [-2] index.

$$St\_SOC\_kg(i+1) = St\_SOC\_kg(i) + Co\_to\_St\_kg\_t_{int}(i) - St\_to\_Pr\_kg\_t_{int}(i) \quad (5.24)$$
$$i \; \forall \; \{1, ..., \text{IDX}_{[-2]}\}$$

Similar to the Ba unit, this thesis allows the optimization tool to set the initial SOC of the storage to achieve optimal results but constraints the last SOC to be equal to the first SOC.

5.2.6 Process

The Process (Pr) represents the balance boundary of the PtH_2 unit displayed in figure 5.1. The H_2 time–series to be satisfied by the PtH_2 unit is implemented within that PtH_2 element. As table 5.6 and 5.8 indicate, there are

no additional variables constructed to define the process apart from an additional *Pr_ConsList* which gathers the implemented constraints.

Table 5.6: Modelling properties of the variables defined in the Pr construction.

Variable	Ind.	Unit	Domain
/	/	/	/

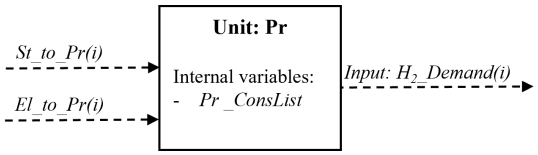

Figure 5.8: Graphical representation of the Pr unit and its variables.

The process is configured in the way, that the H_2 demand has to be satisfied. This is done by applying equations 5.25 for all IDX. The equation considers the mass flow of H_2 from the St and from the El.

$$El\_to\_Pr\_kg\_t_{int}(i) + St\_to\_Pr\_kg\_t_{int}(i) = \mathrm{H_2\_Demand}(i) \quad i \; \forall \; \mathrm{IDX} \tag{5.25}$$

5.3 Objective

To determine the optimal component sizes of the elements discussed beforehand and an optimized dispatch of the PtH_2 unit, the nature of the optimum itself has to be defined by objective functions in the first place. These functions are implemented during the model creation phase within the optimization tool. The solver treats the numeric optimization model by solving the numeric equation of the model by minimizing the objective function.

This thesis considers two kinds of objectives that are defined within this chapter. On the one hand, an economic objective is implemented which considers the Levelized Costs of H_2 ($LCoH_2$) as an economic measure. On the other hand, this objective should be combined with an environmental objective, based on the F_{CO2} of the produced H_2 calculated with the F_{CO2} of the consumed electricity. The economic objective is going to be applied directly, whereas the environmental objective is only considered in combination with the economic assessment. The objective functions are explained subsequently followed by a description of the multi–objective approach.

5.3.1 Economic objective

Economic parameters can be used to determine the optimal dimensions of a PtH_2 unit. As explained in section 2.4.1, a typical economic evaluation considers the Levelized Costs of H_2 ($LCoH_2$) shown in equation 5.26.

$$Optimum(LCoH_2) = min \; f_{LCoH2}(\mathrm{CapEx}_a, \mathrm{OpEx}_a, \dot{m}_{H_2,a}) \tag{5.26}$$
$$f_{LCoH2}() = \frac{CapEx_a + OpEx_a}{\sum \dot{m}_{H_2,a}}$$

Note that equation 5.26 does consider the annuity method which includes a potential Reinvestment (Inv_{re}) and a potential Residual Investment ($\mathrm{Inv}_{Residual}$) defined within section 2.4.1 depending on the project lifetime (20 years in this thesis). The terms in equation 5.26 are filled with several subordinated calculations addressed in the following. First, the determination of CapEx is shown in equation 5.27. The investment costs are the summation of the $CapEx_{Unit,\ specific}$ which is a factor unique to every PtH_2 element reflecting the CapEx costs. Additionally

to that, the external emergency storage has to be considered. Each summative term in equation 5.26 is depreciated according to the findings of section 4.2 to reflect the expenses for the year of observation. Further, these annual expenses are multiplied with the factor Minutes per Year (MpY) to represent the CapEx for the observed period of time.

$$\begin{aligned}\frac{\text{CapEx}_a}{\text{MpY}} = &\sum (\text{Inv}_{Unit,\ sp.} + \text{Inv}_{Unit,\ re,\ sp.} - \text{Value}_{Unit,\ Residual,\ sp.}) \cdot \text{Capacity}_{Unit} \cdot \text{A}_r \\ &+ (\text{Inv}_{St,\ sp.} + \text{Inv}_{St,\ re,\ sp.} - \text{Value}_{St,\ Residual,\ sp.}) \cdot \text{Capacity}_{\text{St\_Emergency}} \cdot \text{A}_r \\ &Unit\ \forall\{\text{Gr},\ \text{Ba},\ \text{El},\ \text{Co},\ \text{St}\} \\ with: \quad &\text{MpY} = \frac{min_{Scenario}}{min_{Annum}}\end{aligned} \tag{5.27}$$

Furthermore, the OpEx are calculated by equation 5.28. The OpEx considers the annual maintenance expense Maintenance (M) for each unit according to the literature study in section 4.2. These expenses are added to the costs involved with procuring electric energy and subtracted by the revenues providing AuxS to the grid. Note that the AuxS have to be affected with a factor reflecting the number of t_{int} per AuxS period. In addition, the prices for the Gurantees of Origin (GoO) are factored in. Depending on the settings, the aspect of Electricity–Price–Compensation (EPC) can be considered.

$$\begin{aligned}OpEx = \quad &\text{Labour} \cdot \text{MpY} \\ &+ \sum \left(\text{CapEx}_{a,\ Unit} \cdot M_{a,\ Unit}\right) \\ &+ \dot{m}_{H_2} \cdot \frac{\text{water} + \text{sewage}}{\text{m}_{H_2}} \cdot \text{Price}_{water} \\ &+ \sum (Gr\_out(i)) \cdot GOO \\ &+ \sum (Gr\_out(i) \cdot Price\_Electricity(i)) \\ &- \sum (Gr\_to\_El\_FCR(i) \cdot Price\_FCR(i)) \\ &- \sum (Gr\_to\_El\_aFRR(\text{-})(i) \cdot Price\_aFRR(-)(i)) \\ &- \sum (Gr\_to\_El\_aFRR(+)(i) \cdot Price\_aFRR(+)(i)) \\ if\ EPC = True: \\ &- \sum (Gr\_out(i)) \cdot \text{F}_{Eligable} \cdot \text{F}_{Fallback} \cdot \text{F}_{Intensity} \cdot \text{F}_{CO2} \cdot \text{EUA}_{annual} \\ &- \text{Deductible}_{MWh} \cdot \text{MpY} \cdot \text{F}_{CO2} \cdot \text{EUA}_{annual} \\ &\text{Unit}\ \forall\{\text{Gr},\ \text{Ba},\ \text{El},\ \text{Co},\ \text{St}\}; i\ \forall\ \text{IDX}\end{aligned} \tag{5.28}$$

In order to complete the definition of equation 5.26, computing the LCoH_2, the sum of produced H_2 has to be calculated. This is done by summing up the two variables entering the Pr unit *St_to_Pr(i)* and *El_to_Pr(i)* as shown in equation 5.29.

$$\begin{aligned}\sum m_{H2} = &\sum (St\_to\_Pr(i) + El\_to\_Pr(i)) \\ &i\ \forall\ \text{IDX}\end{aligned} \tag{5.29}$$

The economic objective does not include any environmental considerations apart from a correlation of the wholesale prices and the F_{CO2} of the electricity mix discussed in section 4.3.4. The environmental objective, which is explained subsequently, emphasizes the F_{CO2} by including it directly in the optimization model.

5.3.2 Environmental objective

To assess the optimization problem economically, the CO_2–Footprint of H_2 ($F_{CO2,H2}$) is used as a measure. The cumulative Carbon Dioxide (CO_2) exhaust of the consumed electricity mix is calculated according to equation 5.30 and minimized by the solving algorithm. The amount of H_2 produced during the observed period is calculated according to equation 5.29.

$$Optimum(F_{CO2}) = min\ f_{CO2}(Gr\_out\_MWh\_t_{int}, CO_2\_Factor(i), m_{H2}) \tag{5.30}$$

$$f_{CO2}() = \sum \frac{Gr\_out\_MWh\_t_{int}(i) \cdot CO_2\_Factor(i)}{\sum \dot{m}_{H2}}$$

$$i \ \forall \ \text{IDX}$$

As shown in equation 5.30, the environmental assessment only considers operational aspects. This fact leads to unrestricted dimensions of the PtH_2 elements as the sizing itself (constrained in the economic assessment by the CapEx term in the determination of the $LCoH_2$) is not considered in the environmental objective.

Therefore, the environmental assessment is always considered as a combination with the economic objective within this thesis as environmental optima are required to be economically feasible to sustain. This multi–objective approach is explained in the upcoming section.

5.3.3 Multi-objective optimization

Technical systems are often optimized in perspective of several different objectives. As addressed in section 2.3, this thesis follows the weighted–sum approach to carry out the Multi–Objective Optimization (MOO) considerations.

A pure environmental objective does not consider any economic factors such as investments and therefore the expected output is not considered to be feasible. Although the technical analysis in section 4.3.4 shows a relation between the F_{CO2} of the electricity mix and wholesale prices, this relationship only encounters for the OpEx and not for the total economic indicator $LCoH_2$. Therefore, a combination of the two objectives is used by adding them up to compute the MOO $Optimum_{MOO}$.

$$Optimum_{MOO} = f_{weighting,LCoH2} \cdot \frac{Optimum(\text{LCoH}_2)}{LCoH_{2,\ Base}} + (1 - f_{weighting,LCoH2}) \cdot \frac{Optimum(F_{CO2})}{F_{CO2,\ Base}} \tag{5.31}$$

Equation 5.31 weights the two objective factors $LCoH_2$ for the economic objective and the F_{CO2} for the economic objective with the weighting factor ($f_{weighting}$). Each objective is referenced to a "Base" run which normalizes both objectives into one. The "Base" run in this thesis is considered to be represented by an economic objective.

The designed PtH_2 is implemented in the next chapter. Further, the implementation is tested for specific test cases, covering different aspects of the optimization tool. In the first place, a single–objective is applied to the test data followed by a multi–objective test case.

Chapter 6

Implementation and Tests

The optimization model embedded in the tool is constructed according to the design, described in chapter 5, and filled with techno–economic input data discussed in chapter 4. Within this chapter, the optimization tool is tested with generic test data for validation. This test includes a 16 h period with a resolution period of 5 min.

First, the economic objective including the Levelized Costs of H_2 ($LCoH_2$) is analyzed by discussing the respective results of the optimization tool for different test cases. Second, the Multi–Objective Optimization (MOO) approach combining economic and environmental parameters with different Environmental weighting factor (f_{FCO2}) is discussed. To do so, the input parameters are described together with the individual dispatch and component sizes of each Power–to–Hydrogen (PtH_2) unit. Third, the sensitivity of model–specific parameters on the objective values such as the resolution Interval (t_{int}) is discussed.

6.1 Evaluation of the single objective ($LCoH_2$)

To prove the optimization tool working, noncomplex generic time–dependent data are chosen. The aim is to show that basic functions such as the import, the model construction, and the solving procedure are working. Within this section, the economic objective is discussed which addresses the $LCoH_2$ with a Economic weighting factor (f_{LCoH2}) of 1.0. Thereby, the correct operation of the optimization tool and its embedded PtH_2 model is demonstrated. This demonstration includes the presentation of the input data and a discussion of the dispatch of each PtH_2 element. Further, the resulting component sizes will be shown in addition to the values of the objective functions.

The model parameters such as the electrolyzer efficiency and the individual investment costs are taken from the analysis carried out in section 4.2. The electrolyzer type is assumed to be a Proton Exchange Membrane Electrolyzer (PEMEL) for the following test cases. As the optimization tool bases its results on numerical optimization, the interpretation of the results can be complex. Nevertheless, this section tries to explain the findings of the optimization tool since the tests are run with generic input data.

6.1.1 Input

The time–series input for the validation of the economic objective is shown in figure 6.1. In addition, relevant input data are shown in each subsequent figure addressing the PtH_2 units within the first row of plots to provide a common reference point. The test cases (A), (B) and (C) represent input data sets with increased complexity. The input for case (A) consists of constant values for the Day–Ahead (DA) market price, the Carbon Dioxide (CO_2)

factor of the electricity mix and the Frequency Containment Reserve (FCR) price. Test case (B) goes a step further and includes a DA price peak between 3 and 6 hours. The third test case (C) combines that peak with a system serving operation by providing optional FCR. The assumed time–series for the FCR market prices increase between 9 and 12.5 hours The Hydrogen (H_2) demand is designed to reflect a batch–wise consumption similar to the consumption in the case study analyzed in section 4.1.

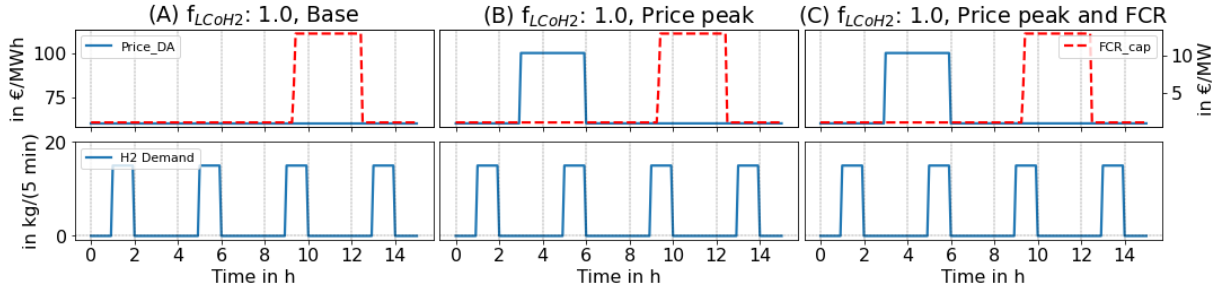

Figure 6.1: Graphical definition of the input data including the electricity prices, the FCR prices and the H_2 demand of three economic objectives ($LCoH_2$) test cases.

6.1.2 Grid and battery

Figure 6.2 plots the DA and the FCR prices as a reference next to the dispatch of the PtH_2 units Grid (Gr) on the second row. The Battery (Ba) dispatch is plotted on the third and the fourth row including the energy flows and the State–of–Charge (SOC) of the Ba.

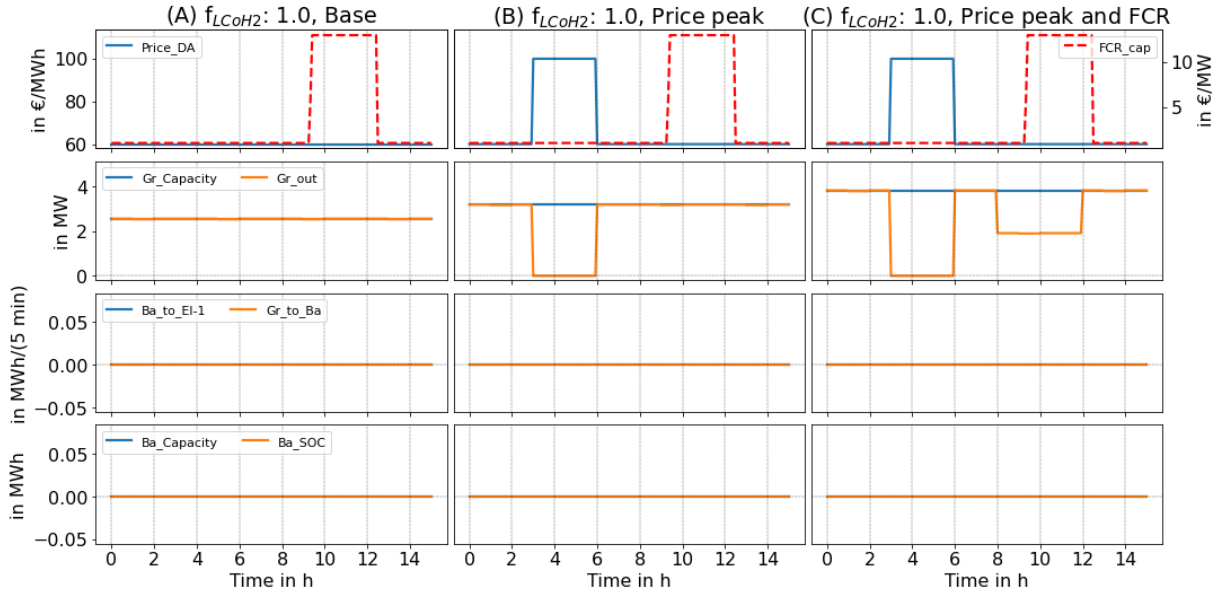

Figure 6.2: Graphical evaluation of the results concerning the Gr and the Ba dispatch for three defined test cases with an economic objective ($LCoH_2$).

Focusing on the test case (A) in the first place, it is shown that the optimization tool considers a static

consumption of electric energy. As there are no fluctuations in the input parameters apart from the Auxiliary Service (AuxS) price which is not choosen for case (A), the lowest $LCoH_2$ can be achieved with small components and maximal utilization. To cope with such a non–flexible power procurement and a batch–wise H_2 demand, a means of storage is required to fulfill the batch–wise demand. In this case, the optimization tool does not consider the implementation of a battery. Instead, a H_2 pressurized tank with a compressor is chosen which will be presented later on. In case (B), the optimization tool computes that the best objective is reached when the high price phase during 3 and 6 hours is skipped, indicated by the deceased variable *Gr_out*. In total, the maximum capacity of the grid connection *Gr_Capacity* is increased as the energy required to be converted to H_2 remains the same. Note that the out–flowing variable *Ba_to_El* in figure 6.2 is plotted with a negative prefactor to indicate its out–flowing behavior.

Similar to case (B), the occupation of the *Gr_out* in case (C) reflects the input parameters. There is a decrease in the power consumption during a high price phase of FCR which will be explained in the next section. Again, the increased maximum capacity of the Gr connection can be explained by the second phase of reduced power consumption. Again, the solving algorithm does not consider the Ba to decrease the $LCoH_2$.

6.1.3 Electrolyzer and compressor

Analyzing the dispatch of the electrolyzer and the compressor, presented in figure 6.3, provides additional information on the dynamics of the PtH_2 unit. For reference, the prices on the DA and FCR markets are displayed in the first row of the figure. Further, rows two and three show the in–flowing energy to the electrolyzer and the mass flow of H_2. The last row shows the in–flowing electric energy to the Compressor (Co).

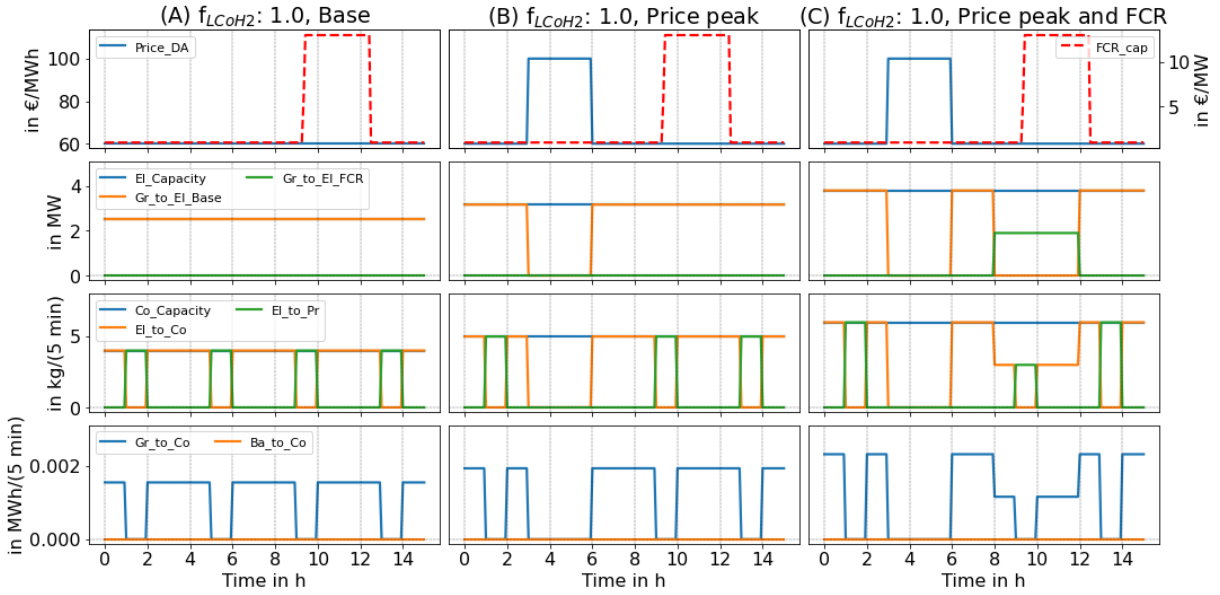

Figure 6.3: Graphical evaluation of the results concerning the El and the Co dispatch for three defined test cases with an economic objective ($LCoH_2$).

Similar to the Gr connection, the electrolyzer experiences a constant in–flow of power which is converted to H_2 for case (A). The resulting mass flow is either directed to the Co and consequentially to the H_2 storage or to the Process (Pr) itself. This circumstance can be explained by the alternating H_2 demand. The compressor

is supplied with electric energy by the Gr, as the Ba is not considered by the solving algorithm. The Co power dispatch corresponds to the mass flow originating at the Electrolyzer (El).

Case (B) involves an increased DA market price which leads the El to throttle down during hour three and hour six. This leads to an increased component size as already mentioned in the section above. During that H_2 production gap, the compressor throttles down as well. Test case (C) alters the FCR price between 9 and 12.5 hours which causes the El to provide FCR capacity. This participation at the FCR capacity is indicated with an increase of the variable *Gr_to_El_FCR*. The increase starts after eight hours and lasts for exactly four hours which fits the FCR regulations explained in section 2.1.1 and added to the model constraints in section 5.2.1.

Within test case (C), the operation of the Gr and El capacity constraint due to the particpation at the AuxS markets can be observed. It constrains the sum of the variables *Gr_to_El_Base* and *Gr_to_El_FCR* to be always smaller than the maximum capacity of the electrolyzer. Thereby, the constraint takes the symmetrical nature of the FCR capacity regulation into account by considering it twice. Consequently, the El does not consume the maximum amount of energy during the FCR phase but sets a consumption value that allows spontaneous ups and downs according to the frequency–containment efforts. The extent of these ups and downs is defined by the symmetrical *Gr_to_El_FCR* variable. As explained beforehand in section 5.2.1, it is assumed that the electrolyzer sets its electrical consumption dedicated to AuxS according to the grid frequency so that real consumption can be represented by the *Gr_to_El_FCR* variable itself by statistical means. As the consumption of electric energy is decreased during the FCR period, less H_2 is flowing to the compressor and thus the Co draws less energy from the Gr.

6.1.4 Storage and process

The analysis of the dispatch time–series closes with the consideration of the storage and the H_2 consuming Pr shown in figure 6.4. The first row indicates the input data for each test. The second row of graphs in the figure shows the in and out–flowing mass flow of H_2 to and from the Storage (St). These flows determine the SOC of the storage unit in the third row of figure 6.4. The fourth row shows the in–flowing amount of H_2 to the Pr unit. Within the PtH_2 system, the Pr represents the H_2 consuming process which has to be satisfied with a certain amount of H_2 at specific points in time.

Note that the variable *St_to_Pr* is added to figure 6.4 with a negative prefactor as it represents the discharging flow in the perspective of the St. As the storage is charged during H_2 demand gaps (shown in the fourth row of the figure), and discharged during H_2 demand, the SOC oscillates between a high and a low state. The initial filling level of the St is computed within the optimization tool. In order to realize this, the initial SOC is constrained to be equal to the last SOC of the St as explained in section 5.2.5. This constraint is fulfilled for the SOC after the displayed last Time–Stamp (TS), as there is still H_2 flowing to the TS at the last TS. As there is no production of H_2 during the high DA price phase in case (B), the storage can not be charged between hour three and hour 6, whereas the demand is satisfied complety by the St. The optimization tool determines a smaller St capacity for test case (C) compared to case (B). In detail, there are two maxima in the SOC curve of (B) and (C) right before the first batch of H_2 is required and right before the last batch. As the amount of H_2 flowing from the El to the Pr (indicated in the second and the fourth row in figure 6.4) is larger in (C) during the last H_2 batch, the storage can be smaller in size. The storage capacity of (A) remains the smallest since no gaps in the El operation must be compensated and the SOC timeline is periodical. The SOC in case (A) is rising slightly over time so that the inital and the last SOC match. The fourth row of plots in figure 6.4 shows the resulting amount of H_2 flowing to the Pr to satisfy the H_2 demand. The total demand assumed for this test scenario is shown as well. For case (A), there is always a small share of H_2 originating directly from the El and a larger share coming from the St. The ratio between El and St differe in the other two cases. The second peak of H_2 demand in test cases (B) and (C)

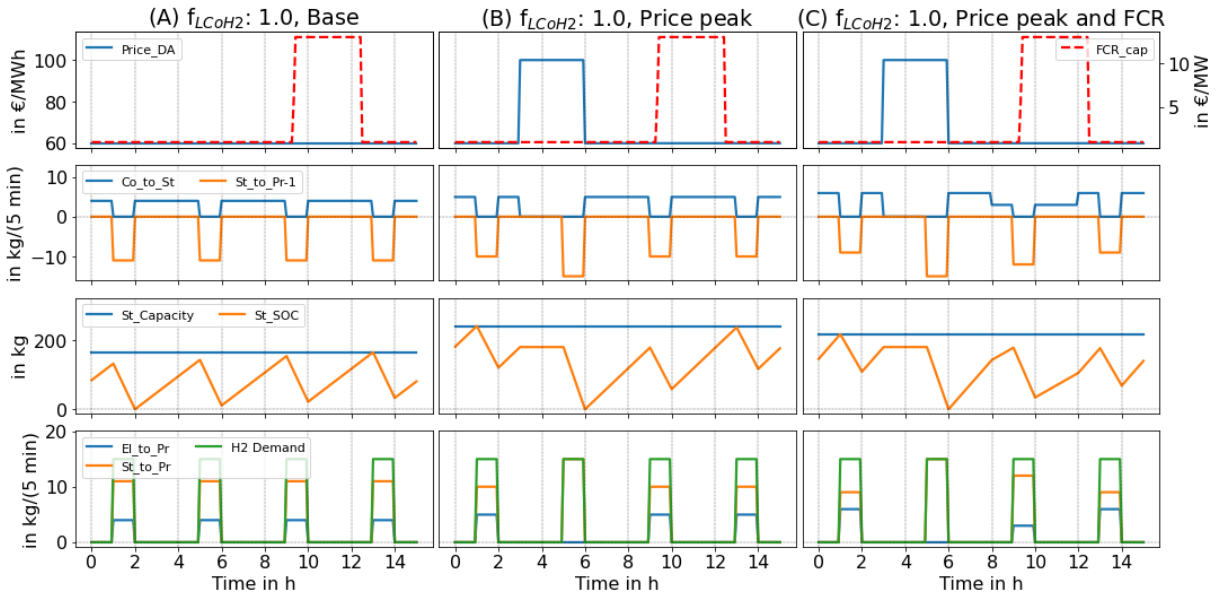

Figure 6.4: Graphical evaluation of the results concerning the St and the Pr dispatch for three defined test cases with an economic objective ($LCoH_2$).

is satisfied to its full extent by the storage as the electrolyzer throttles down. The third H_2 demand peak in case (C) comes in a large part from the St, due to the performed FCR measure at this point in time.

6.1.5 Objective values and component sizes

The dispatch time–series shown in the figures 6.2 to 6.4 beforehand can be summarized in a number of key values. Figure 6.5 gives an overview of the resulting objective functions and the determined capacities of each PtH_2 unit. In addition, the Annual Full Load Hours (AFLH) are plotted in % for the El. Each value is shown for the test cases (A), (B) and (C) respectively.

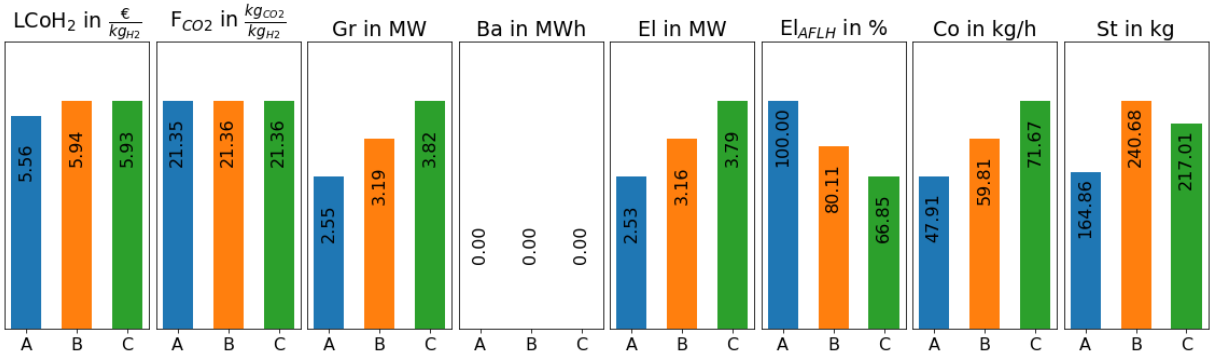

Figure 6.5: Summary of the objective values and the PtH_2 component sizes computed by the optimization tool for three defined test cases with an economic objective ($LCoH_2$).

The values $LCoH_2$ and CO_2–Footprint (F_{CO2}) addressed by the two objective values are plotted to the left of figure 6.5. The factor F_{CO2}, addressed by the environmental objective, is not considered in the implemented

objectives for these test cases and its value is assumed to be constant. The resulting PtH_2 unit dimensions sized by the optimization tool are shown on the left. In the first place, figure 6.5 shows that the determined $LCoH_2$ for test case (B) and (C) remains similar although the El size capacity changes. This can be explained by the revenues made by participating at the FCR capacity. In the second place, the data show that the optimization tool does not consider the battery to be implemented in all cases. Further, the PtH_2 components Gr and El are scaled accordingly as the El is the dominant consumer of electric energy and determines the necessary Gr size. At the same time, the maximum power consumption of the El is slightly smaller than the Gr, as the Gr has to satisfy the power demand of the Co as well. With lower El AFLH (El_{AFLH}), the capacity of the El increases as the same amount of H_2 has to be made available for the process. The amount of H_2 flowing through the compressor changes analog to the El dimensions. Further, the St dimensions are larger for the flexible test cases (B) and (C). Although the El_{AFLH} is smaller in case (C), the St is determined to be smaller in case (C) compared to (B). This might be explained by the fact, that the larger electrolyzer can satisfy the required H_2 demand to a larger extent directly, without relying on the storage. The considerations for the economic objective presented in the paragraphs are worked out for the MOO approach as well in the subsequent passages.

6.2 Evaluation of the combined objective ($LCoH_2$ and $F_{CO2,H2}$)

The MOO approach incorporates the F_{CO2} objective next to the $LCoH_2$ objective. This MOO analysis is validated by a set of test cases demonstrated in this section. The validation of the MOO does not particularize the behavior of the individual PtH_2 units, as was done in the section before. It is assumed, that the optimization tool with a combined–objective is operating identically to the single–objective. The resulting time–series for the El and the St for the MOO validation are visualized in figure 6.6. For an overview of the MOO dispatches, reference is made to the figures D.1 to D.5 in the appendix on page XXXVII and following.

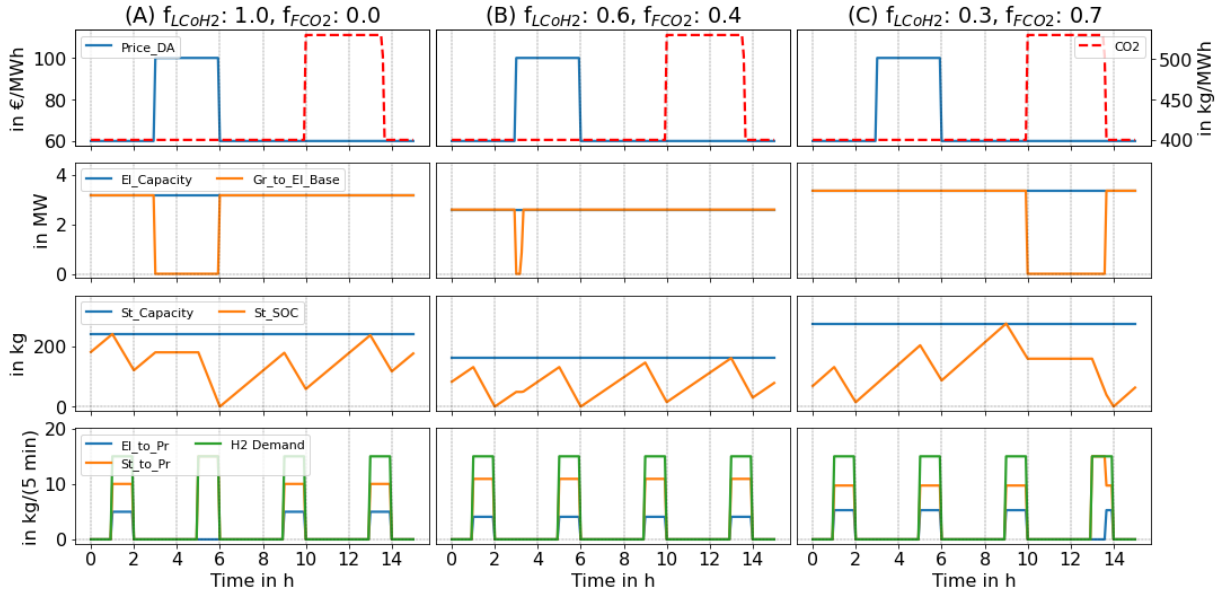

Figure 6.6: The optimized dispatch of the El, the St SOC and the H_2 demand visualized as timelines for three defined test cases with a combined objective ($LCoH_2$ and $F_{CO2,H2}$).

The operating procedure is briefly discussed by means of figure 6.6 which includes dispatch of the El, the SOC

of the St and the Pr respectively the H_2 demand. The first row shows the input time–series covering the DA market and the assumed system average emission factor, respectively the F_{CO2}. The corresponding El timeline is given next to the SOC of the H_2 pressurized storage in rows two and three. The fourth row of diagrams shows the H_2 flows to satisfy the assumed H_2 demand for this validation.

The MOO approach is based on the f_{FCO2} and f_{LCoH2}. To implement the weighting factors, the particular objectives are referenced to the results of a single–objective analysis according to the weighted sum approach explained in section 2.3 and implemented in section 5.3.3. The test cases (B) and (C) consider the environmental objective F_{CO2} by different weighting factors. The weighting factor in case (B) is $f_{LCoH2} = 0.6$ and $f_{LCoH2} = 0.3$ in case (C). To implement the weighted sums, each objective is normalized to the pure $LCoH_2$ driven reference case (A) ($f_{LCoH2} = 1.0$). The effects of this multi–objective combining environmental and economic measures are discussed subsequently.

In case (A), the price peak is excluded by the optimization tool as already discussed in figure 6.3. The optimization tool decreases the El capacity for case (B) and throttles shortly during the price peak yielding reduced electricity costs and a decreased F_{CO2} at the same time. This results in an increased AFLH. As test case (C) weighs the environmental objective higher, the optimization tool does not exclude the DA price peak anymore but excludes the F_{CO2} peak. Thus, the El capacity is larger for (C), resulting in smaller AFLH. The St corresponds to that behavior. Whereas case (B) shows nearly periodical SOC due to the H_2 demand, cases (A) and (C) are balancing the decreased El_{AFLH} out and have larger St capacities. Further aspects such as the corresponding dispatch of the Co and more are displayed within the appendix as mentioned above. The fourth row in figure 6.6 shows the H_2 demand and how it is satisfied. Test case (B), representing the largest El, supplies more H_2 directly compared to the two other test cases. This is only possible as the two excluded peaks do only partly overlap with a H_2 peak. In an optimization with many more TS, this influence is expected to decrease statistically. Addressing the possible influence of model–related sensitivities lead to the relevance of the resolution t_{int} which is discussed subsequently.

6.3 Sensitivity of the resolution interval

This section is dedicated to analyzing the impact of the temporal discretization, respectively the resolution. The left side of figure 6.7 plots the sensitivities of the discretization related to the objective values $LCoH_2$ and F_{CO2} besides the computing time on the secondary y–axis. The right side of figure 6.7 shows the resulting component sizes for the different discretization t_{int}. The graphic is based on a test data set discussed in the section beforehand. The optimizations run for that sensitivity study are based on the economic objective function minimizing the $LCoH_2$. The symmetrical ($\pm$) StD_{rel} is given in the legend.

In the first place, a decrease of the computing time for large discretization t_{int} can be observed in figure 6.7. Note that the test data set covers only 16 hours and the displayed absolute time is therefore not representative of a whole year that is going to be simulated for the case study. The objective values $LCoH_2$ and F_{CO2} are normalized by dividing each element with the average of the respective set of results. Basically, a trend can be detected. A smaller discretization period leads to smaller objective values since the simulation is based on more data points. The increased number of points gives more flexibility for optimizing the dispatch of the components.

The normalized objective values scatter with a Relative Standard Deviation (StD_{rel}) of roughly $\pm 1\,\%$ in reference to the average which seems to be a good approximation for all applied resolutions. Shifting to the right side of figure 6.7, a different conclusion has to be made. The plot shows the resulting normalized dimensions for each element of the PtH_2 unit, calculated by the optimization tool. Note that the battery is not included in the plot, as the optimization tool does not consider the implementation of a battery for this generic test scenario.

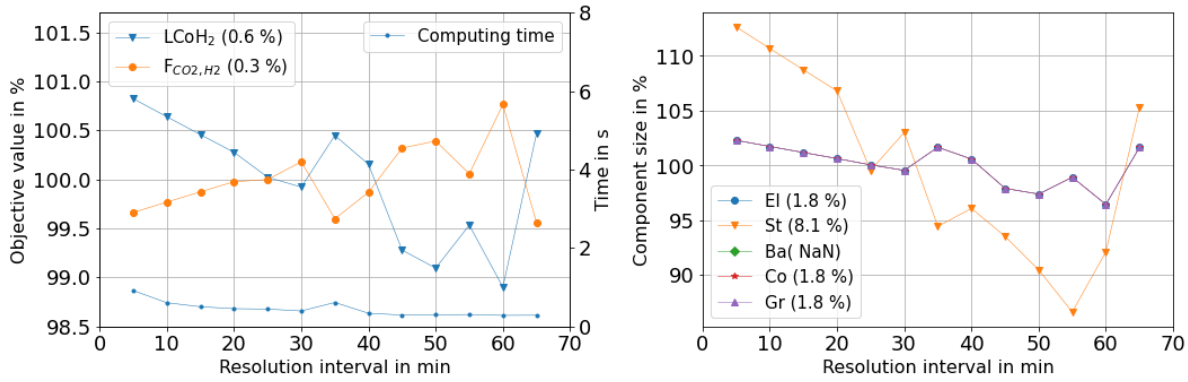

Figure 6.7: Sensitivity of the temporal resolution related to the objective values $LCoH_2$ and F_{CO2} on the primary y–axis and the computing time on the secondary y–axis of the left plot. The right plot shows the PtH_2 component sizes. The symmetrical (±) StD_{rel} is given in the legend.

While the component sizes for the El, the Gr and the Co scatter about roughly ±2 %, the St capacity behaves differently and scatters with a StD_{rel} of ±8.1 %. Taking the research question of this thesis into account, which includes the determination of optimized component sizes, such high deviations decrease the certainty of the results. As the resolution has a considerable effect on the St component size, it has to be discussed further. Figure 6.8 aims to give reasons for the high deviation by showing the dispatch computed by the tool for three PtH_2 elements and the input price (assumed to represent the DA) time–series.

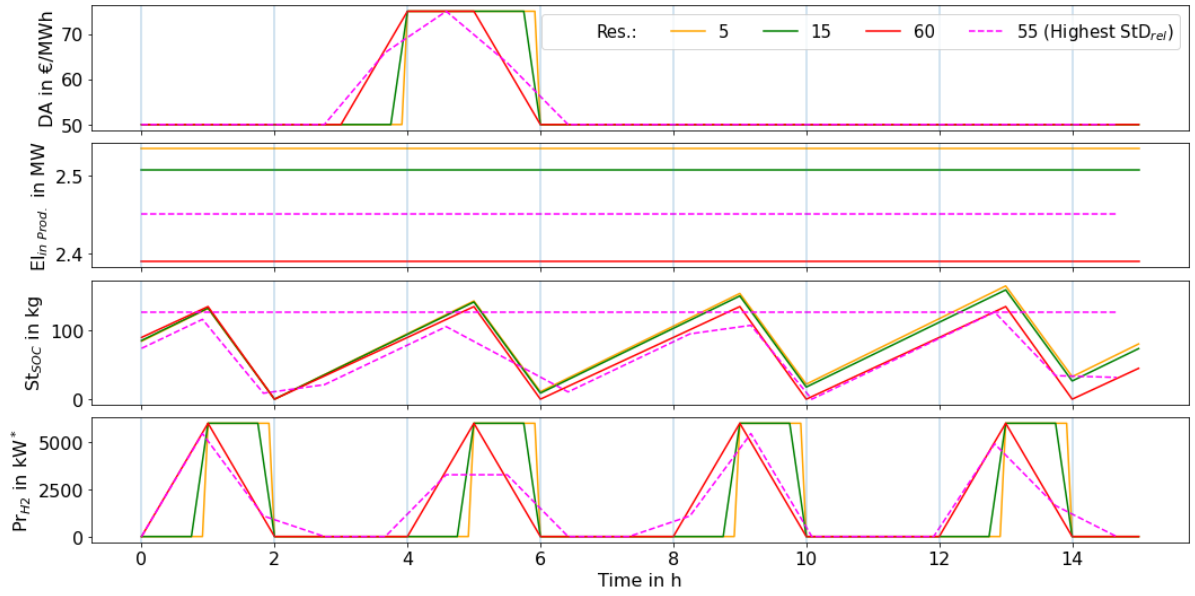

Figure 6.8: Influence of the resolution t_{int} on the optimized component sizes in respect to the dispatch of the El, the St and the Pr units. *The H_2 demand is represented as an energy stream in kW_{H2} based on the LHV.

The figure only includes the time–series for the resolutions 5, 15, and 60 min for clarity. The 5 min resolution

represent a considerably large amount of TS and the 15 and 60 min resolution represent the trading interval on the spot markets. Additionally, the resolution corresponding to the highest outlier of the St capacity in figure 6.7 is plotted as a dashed line for comparison. The first graph in figure 6.8 shows the price time–series for the selected resolutions. The lower plot in figure 6.8 defines the required amount of H_2 represented by the Pr element. The DA price series and the H_2 demand function as the input to the optimization tool. For each performed optimization, the optimization tool receives input data based on the resolution t_{int} of one minute. Depending on the chosen simulative resolution, the discretization time of the input data is adjusted. To do so, the Python library Pandas which includes the "resample" function to upsample time–series data is used. In the case of time–based data (such as kg/min), the average has to be multiplied with a factor to represent their cumulative value. Based on these two input time–series, the dispatch of the PtH_2 components is calculated. The figure aims to explain the different component sizes for different resolutions and only shows the *El_in_Production* and the *ST_SOC* variables. The outliers of the St capacity detected in figure 6.7 are represented by the most severe outlier in figure 6.8 by a dashed line together with the corresponding SOC. The outliers can be explained by the relation between the resolution and frequency of characteristic events within the input data. Figure 6.8 shows clearly the impact of the data value position on the resulting values. First, it can happen that the position of the data points does not fit the position of the event, and thus the actual circumstances are even out. Second, the data points of the dashed lines do not represent the full extent of the original peaks, as their average considers an extended resoution t_{int}.

As this consideration only includes 16 h and just four peaks of the H_2 demand and only one rise in the DA spot market prices, the datapoint position is likely to cause uncertainties. As the case study considers an entire year, the impact of the resolution is assumed to be smaller. Nevertheless, the temporal resolution is supposed to be analyzed for the case study and has to be chosen adequately to ensure that the obtained results are reasonable.

Chapter 7

Case Study: Results and Discussion

This chapter addresses the case study and applies the optimization tool to the questions laid out in chapter 3. The leading question raised in the case study is to compute the optimal component sizes for a grid serving Power–to–Hydrogen (PtH_2) unit. To answer that, the optimization tool is applied to optimize the dispatch together with the component sizes of the PtH_2 unit for the case study scenarios.

These results are shown and discussed subsequently for optimal Levelized Costs of H_2 ($LCoH_2$) starting with an analysis of the resolution sensitivity and the impact on the computing time. This section is followed by a sensitivity study covering the techno–economic input parameters of the case study. After assessing the optimization tool and the case study for its sensitivities, different scenarios are run with respect to the economic objective. This thesis distinguishes the scenario analysis into two parts with the first part covering different energy markets without participating in the Auxiliary Service (AuxS) markets. The second analysis compares the consequences of a system serving behavior by participation in the AuxS markets with the previously discussed base scenarios. This scenario–based assessment is complemented by the additional consideration of the environmental objective covering the CO_2–Footprint of H_2 ($F_{CO2,H2}$).

7.1 Resolution sensitivity

The optimization tool is based on several input variables which can be distinguished between model–specific or PtH_2 related parameters. This section addresses the sensitivity of model–specific parameters and aims to justify the significance as the analysis in the preceding sections identified the influence of the resolution to be relevant. Figure 7.1 addresses the sensitivity of the normalized objective values and the normalized component sizes with respect to the resolution interval.

The figure is based on several optimization runs while each run is performed with a varied resolution Interval (t_{int}). It incorporates the standard Hydrogen (H_2) demand discussed in section 4.1.3 and a Proton Exchange Membrane Electrolyzer (PEMEL) based PtH_2 unit operating with electricity prices of the year 2022. Similar figures for other scenarios are placed in the appendix on page XL and following. The corresponding results addressing the $LCoH_2$ and the CO_2–Footprint (F_{CO2}) of the produced H_2 are plotted on the primary y–axis of the left diagram as normalized values. Additionally to that, the computing time with its Relative Standard Deviation (StD_{rel}) for a t_{int}=15 min indicated by whiskers is displayed on the secondary y–axis. The plot on the right covers the resulting component sizes of the PtH_2 units Grid (Gr), Battery (Ba), Electrolyzer (El), Storage (St) and Compressor (Co). Each value is normalized by division through the mean of the actual series. In addition,

the symetrical (±) StD_{rel} of the values are given in the figure legend.

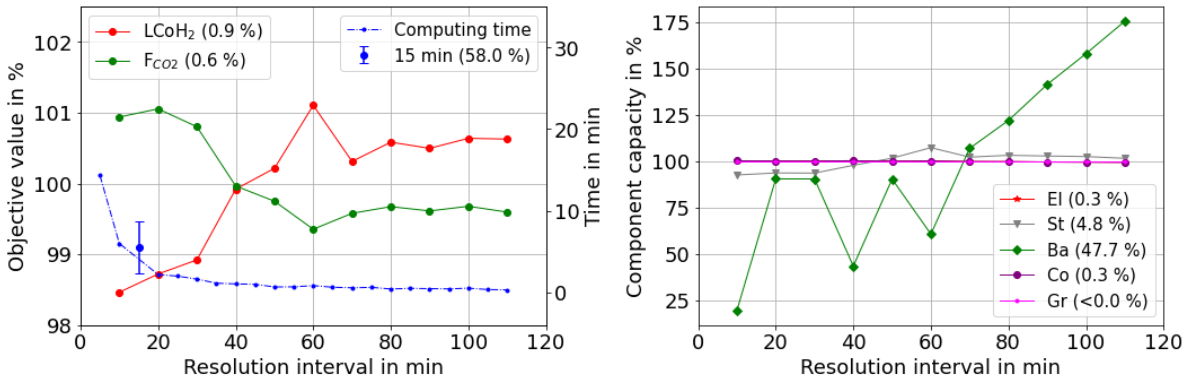

Figure 7.1: The sensitivity of the normalized objective values $LCoH_2$ and F_{CO2} on the primary y–axis and the corresponding computing time on the secondary y–axis related to the resolution t_{int} (left). The resulting normalized component sizes (right). Both diagrams are based on an PEMEL operating in the year 2022. The respective StD_{rel} (±) for each objective value and component size is shown in brackets.

The performed optimization runs are based on the economic objective which minimizes the $LCoH_2$. The resulting objective value $LCoH_2$ (red line) does not vary more than ±1 % as the StD_{rel} in the legend of figure 7.1 and the figures E.1 to E.3 in the appendix show. The relative F_{CO2} on the same y–axis (not targeted by the optimization tool in this case, but calculated) scatters in a similar order of magnitude. The results calculated by the optimization for identical inputs are supposed to lead to identical results according to the manual of the applied Gurobi solver [60]. Thus, the experienced StD_{rel} for the objective values originate in the varied resolution t_{int}. The left plot in figure 7.1 allows the conclusion, that the length of the resolution interval has a neglectable effect on the objective results. The computing time is expected to be influenced by the resolutions, thus only the StD_{rel} for several optimizations with a resolution of 15 min is shown. The computing time shows a significant increase for a resolution t_{int} smaller than 20 min.

The optimization tool results are further analyzed in the right graph of figure 7.1 which includes the computed PtH_2 component sizes. Apart from the Ba, the dimensions show almost constant averaged values for all resolutions with StD_{rel} smaller than $< \pm 5\,\%$. Whereas the integrating PtH_2 units St and Ba show relatively high StD_{rel} taking the figures E.1 to E.3 in the appendix on page XL into account. Their capacities show maximal StD_{rel} around ±7 % for the St and up to ±48 % for the Ba. The figure 7.1 visualizes the strong dependency of the Ba capacity to the resolution t_{int}. The normalized values do not show a plateau which would identify constant values. Therefore the StD_{rel}, especially for the Ba, has to be kept in mind in the following interpretations of the optimization tool results. The reasons for the high StD_{rel} of the integrating PtH_2 units are already discussed within the previous section 6.3 and relates to the position of the demand peaks and the Time–Stamp (TS).

Consequently, this thesis applies a resolution interval of t_{int}=15 min for all performed optimizations. An interval of 15 min seems to be a good compromise between computing time and precision while representing the shortest product traded at the Intraday (ID) spot market.

7.2 Techno–economic parameter sensitivities

In the subsequent sections, the optimization tool will be applied to the case study while varying individual techno–economic input parameters. These conducted optimization runs are analyzed in a sensitivity study similar to the procedure applied by Röben et al. (2021) [111]. Each performed optimization is based on the basic parameters of an PEMEL operating at the ID market.For the sensitivity study, the PtH_2 unit and the El are considered to not participate in the AuxS markets. The H_2 demand is based on the "standard" H_2 demand for the case study elaborated in section 4.1.3. The capacity constraint of the Gr connection ($7\,MW_{EP}$) relevant in the case study is not considered for this sensitivity study. The same applies to the Electricity–Price–Compensation (EPC) and the procurement of Gurantees of Origin (GoO) which are not implemented in this sensitivity study. The sensitivities are analyzed for the electricity prices in 2020 and 2022 as these represent the price extremes for PtH_2 units. The resulting figures F.1 to G.6 are placed in the appendix on page XLII and following. A combination of varied parameters is not discussed. First, investment–related sensitivities are analyzed by altering the specific investment costs. Second, technology–related parameters such as efficiencies and pressure levels are varied and discussed in a similar manner.

7.2.1 Investment related sensitivities

The findings of the sensitivity study addressing specific investment costs are summarized in figure 7.2. As the figure visualizes several aspects at once, it is explained before the actual results are discussed themself. The diagrams in figure 7.2 are based on identical x–axes while each diagram has an individual y–axis. In the case of the specific investment sensitivities addressed within this section, all considered investment costs are multiplied by an individual variation factor. Specific investment costs relevant to the PtH_2 unit itself which can not be assigned to a PtH_2 element are not considered (such as expenditures on labor). The two–row plot on the left–hand side covers the resulting $LCoH_2$. At the same time, the two diagrams below show the effects of the variation on the electrolyzer capacity (in MW) and on the Annual Full Load Hours (AFLH) of the El (in %).

The capacities of the other PtH_2 units are displayed on the right side of figure 7.2. This includes the capacity of the Gr, the St, the Ba and the Co. The legend on the upper left is applicable to all seven plots shown in the figure. Each line–color represents the variation of a specific PtH_2 element investment costs. The PtH_2 elements are gathered in the legend on the left–hand side. Note that this scenario with an PEMEL in the year 2022 is chosen because all PtH_2 elements including the Ba are implemented by the optimization tool so that the behaviour can be analyzed best. To interpret the figure 7.2, the variation of the components El, St and Ba are discussed in particular. In the first place, the effects of varying specific El investment costs are considered. These specific costs have a clear positive relation to the $LCoH_2$ as the ascending line in the upper left plot shows. Reduced El costs lead to a larger dimensioned capacity which correlates directly to a decreased amount of El AFLH (El_{AFLH}). The optimization tool seems to conclude that the direct production of H_2 becomes advantageous as TS with high electricity prices can be partly avoided. This circumstance can also be found in the optimized dimensions of the PtH_2 elements shown on the right side of figure 7.2. The Gr capacity increases with the El capacity. The St is dimensioned smaller in size because the El tends to supply the Process (Pr) directly. The Co capacity increases with reduced El investment costs and increased El capacity. The Co compresses more H_2 in TS with higher El production.

The effects implied by varied specific St costs are discussed in the second place based on figure 7.2. The $LCoH_2$ reduces with reduced St costs while an increase results in a smaller capacity and which is reflected by a minor change of the $LCoH_2$. The St capacity increases with reduced investment costs. Further, halved St costs double the implemented St capacity. The El capacity is not affected by varied Co investments. In the third place, the

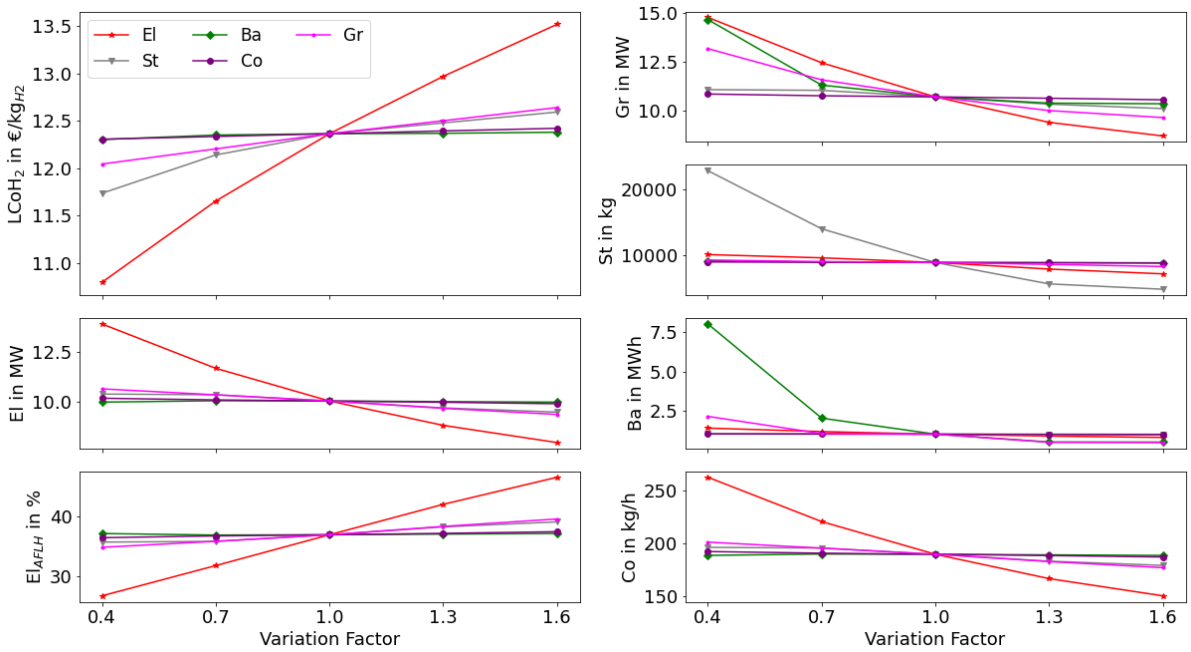

Figure 7.2: Sensitivity of the optimization tool results in respect to an economic objective with regard to individual varied specific investment costs of the PtH_2 elements. Based on the year 2022 and a PEMEL system.

$LCoH_2$ does correspond to the specific Ba investment costs. Whereas reduced the reduction of the Ba costs, its implemented capacity and the implemented Gr capacity rise. The Ba investment costs do not have an effect on the El capacity, nor on its AFLH as the straight green line in two left–foot diagrams show. Varied specific Gr investment costs affect the $LCoH_2$ and the optimized Ba capacities proportionate. These conclusions concerning the Ba have to be handled with care as the Ba capacity shows a high StD_{rel} for different resolution t_{int}.

7.2.2 Technology related sensitivities

After discussing sensitivities related to specific investment costs, the sensitivity of technical parameters is about to be discussed within this section. The technical sensitivity study includes two figures while the first figure 7.3 addresses El related parameters. The second figure 7.4 includes parameters related to the compression of H_2 and the storage of electric energy. The sensitivities displayed in this section are based on a PEMEL electrolyzer with an El minimal load (El_{min}) of 0.05 MW/MW_{max}, an efficiency of El_{η} = 63 % referenced to the Lower Heating Value (LHV) and an El load gradient (El_{Grad}) = 1.0 MW_{max}/min. The sensitivity studies based on different scenarios are placed in the appendix as mentioned previously. The time–series includes the standard H_2 demand of the case study determined in section 4.1.3. The electricity price time–series is represented by the ID market prices in 2021.

Figure 7.3 and figure 7.4 give an overview of the $LCoH_2$ and PtH_2 element capacity sensitivities in a manner similar to the investment sensitivities. Thereby, the $LCoH_2$ is plotted on the left–hand corner and the El capacity and its El_{AFLH} are shown on the left–foot corner. The related capacities of the further PtH_2 elements are shown on the right. Each subplot is defined by its y–axis label. This plot includes three x–axis due to individual units of each varied parameter. The three x–axis are applicable to the plots above.

Hydrogen production sensitivites Figure 7.3 covers the sensitivities implied by the parameters El_{min}, the El_{Grad} and the El_{η} as the three x–axes indicate. The El_{min} is defined in section 2.2.2 and implemented in section 5.2.3. It considers the minimal operating power in relation to the maximal power. The value is relevant for Alkaline Electrolyzer (AEL) units which have a minimal load of 0.20 MW_{min}/MW_{max} and play only a minor role for PEMEL (0.05 MW_{min}/MW_{max}). An increased El_{min} leads to higher $LCoH_2$ as the PtH_2 unit is forced to procure electric energy to all points of time by the El_{min}. TS with expensive electricity prices can not be excluded by throttling the El down. For an El_{min}, the optimization tool does not implement a battery whereas increased El_{min} leads to the implementation of a Ba unit to exclude moments of high electricity prices. This thesis will later show that a battery is not reasonable for lower electricity prices as happened in 2021 or earlier. An increased El_{min} corresponds to smaller El and Gr with a corresponding increase of the El_{AFLH}. Further, the necessary St capacity decreases because less H_2 has to be stored when the El is operating at a high El_{min}.

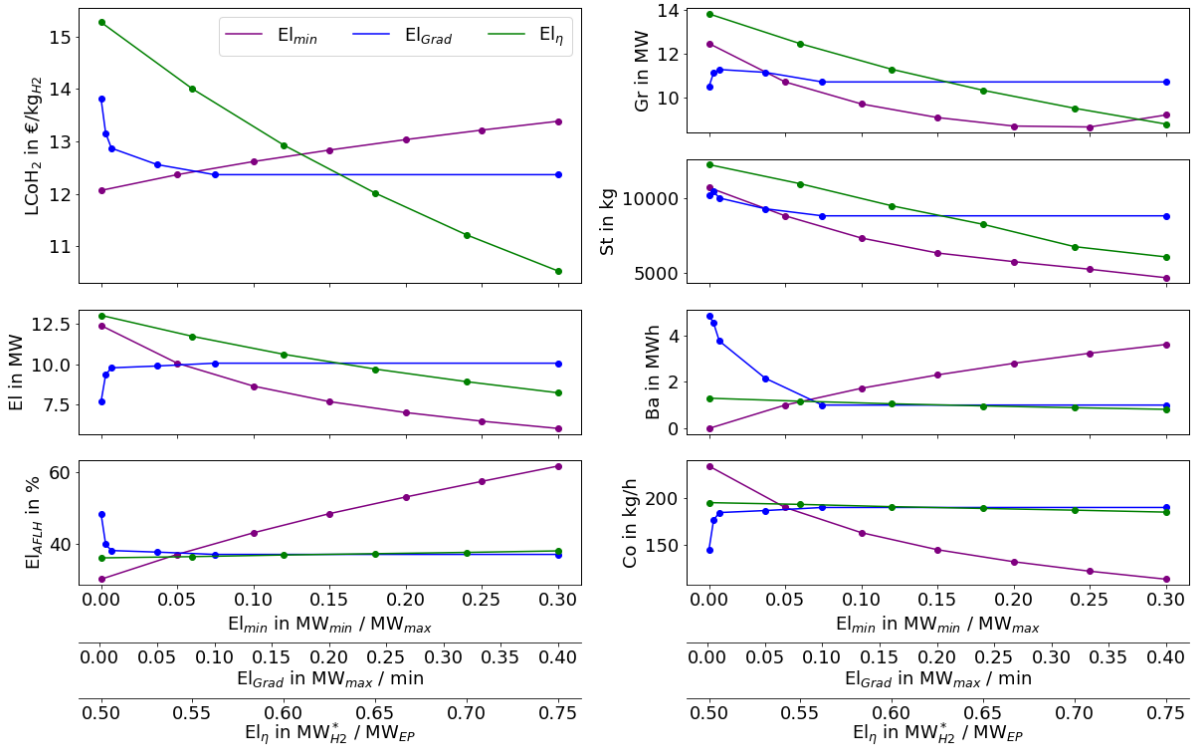

Figure 7.3: Sensitivity of the optimization tool results for an economic objective with regard to the technical parameters of the El such as the El_{min}, the El_{Grad} and the efficiency El^*_{η} based on the LHV. Incorporating a PEMEL and electricity prices of the year 2022.

The El_{Grad} on the secondary x–axis considers the change in operating power in MW_{max}/min. Due to the chosen resolution size, this aspect can become obsolete. For example, the maximal relevant gradient for a 5 MW El and time intervals of 15 min is about ∼0.067 MW_{max}/min as higher gradients would reflect an instantaneous behavior. This is reflected by the results shown in figure 7.3 where an increase of the $LCoH_2$ for El_{Grad} smaller than 0.05 MW_{max}/min can be identified. The El and Gr sizes are significantly decreased by the El_{Grad}. The El_{AFLH} increases as load–reduction potential is reduced. Further, the St and especially the Ba is dimensioned larger with a reduced El_{Grad}. AEL and PEMEL can adjust their power consumption a lot faster (within 0.10 MW_{max}/s) as

shown in section 4.2.4 and therefore this gradient is not of practical relevance in this thesis.

The efficiency El_η is plotted on the third x–axis in figure 7.3. It is defined as the ratio between the required amount of input energy and the energy of the resulting H_2 mass flow. A typical efficiency for an El is between 60 and 70 % referenced to the LHV. The El_η has a drastic effect on the resulting $LCoH_2$ as an increased efficiency corresponds to less electric energy required for the conversion. Increased efficiency leads to a smaller El and Gr while the El_{AFLH} remain roughly constant. The data show, that an increased efficiency corresponds to slightly reduced St capacities, the other components are not affected.

The sensitivities based on other scenarios such as electricity prices for the year 2020, annexed on page XLIV, show different $LCoH_2$ prices. The optimization tool does not consider the Ba for these scenarios, as the lower electricity prices do not justify a high investment in a Ba. This counts for all analyzed El_{min} values.

H_2 compression and battery sensitivites Figure 7.4 considers parameters related to the compression and storage of H_2 within the same PEMEL scenario with energy market data from 2022. This involves the efficiencies Co_η and the Ba_η, the maximal St pressure, and the pressure and temperature at the El outlet. Similar to the sensitivities discussed in figure 7.4, only one parameter is altered while the others represent the parameters derived in section 4.2. Note that this thesis only includes the maximal storage pressure to calculate the work of the Co. Thus, a decreased pressure ratio for proportionate State–of–Charge (SOC) is not considered.

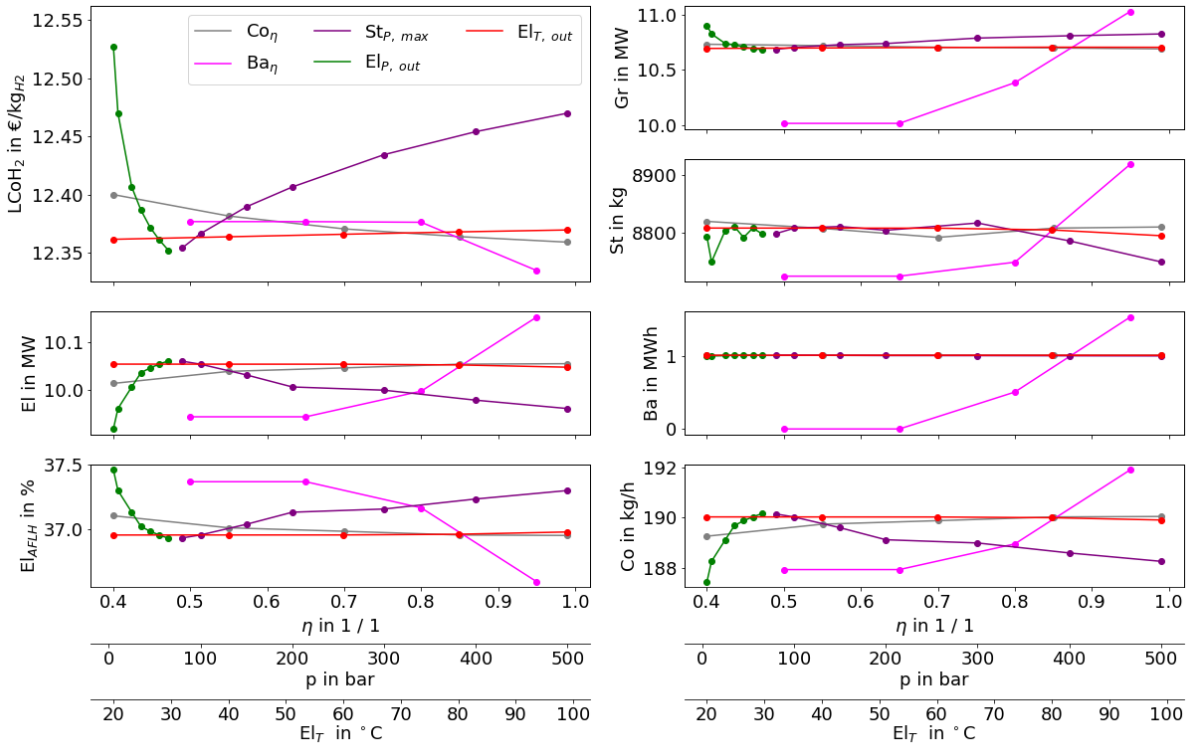

Figure 7.4: Sensitivity of the results incorporating an economic objective with regard to the technical parameters of the compression stage covering the input and output pressures of the Co, its efficiency Co_η and the output temperature of the El. In addition, the Ba_η is analyzed. Incorporating a PEMEL and electricity prices of the year 2022.

The sensitivity study displayed in figure 7.4 shows that the simulated parameters only have a minor effect

on the resulting $LCoH_2$, as the y–axis on the left–hand corner only covers $\Delta LCoH_2$=0.2€/kg_{H2}. This indicated range is in a similar order of magnitude as the StD_{rel} (∼1 %) based on different resolutions discussed in section 7.1. Therefore, the analysis of figure 7.4 can only identify aspects of interests but no reasonable findings.

The dominant factor for the compression process can be identified to be the El outlet pressure. Tjarks (2017) studied the relation between electrolyzer efficiency El_η and outlet pressure El_P and concluded that the two parameters influence each other. An increased pressure comes with a decreased El_η, thus the parameters build up a tradeoff. He recommended El with a high outlet pressure as this decreases the resulting work performed by the Co unit although the corresponding El_η might decrease [133]. This master thesis considers both parameters separately and does not include their interference. Nonetheless, the sensitivity study shows that the altered El_η has a much more significant impact compared to the outlet pressure El_P.

In addition to the El_P, the St_P influences the pressure ratio, relevant for the compression work. Typically, the Co_η would be a function of this pressure ratio as well, which is not implemented in the optimization tool. An increased compression ratio leads to the increase of H_2 storage costs. A relevant factor for the Ba capacity is its efficiency Ba_η. The Ba unit is not installed for small Ba_η, whereas small Ba_η below 90 % have no relevant effect on the resulting $LCoH_2$. In general, the analyzed and discussed sensitivities show, that the optimization tool reacts in a reasonable sense to the varied input parameters. Therefore, the actual scenario–based optimization can be performed. The obtained results are depicted and analyzed in the following section. It incorporates a grid–serving PtH_2 unit in the first step. Further, the system serving aspects is added by analyzing the changed $LCoH_2$ and component sizes due to participating in the AuxS markets in a second step.

7.3 Scenario analysis

To assess the case study and the related component sizing issue, this thesis conducts two scenario analyses summarized in figure 7.5. One of them relates to the Epex Spot SE (EPEX) spot markets Day–Ahead (DA), ID and the Over–the–Counter (OTC) market representing the case study with a coal–power contract. Thereby, the spot market scenarios are considered by this thesis to be grid serving, as they reflect the balance in the electricity grid. Contrary to that, the OTC scenario can not be considered to be grid serving as the electricity prices are only a function of the costs related to the procurement and conversion of coal to electricity. The second analysis includes scenarios addressing the possible benefits of participation at the AuxS markets resulting in a system serving operation. Thereby, it focuses on the ID market as it is the most flexible market and compares the obtained PtH_2 dimensions for the AuxS scenarios with the non–AuxS scenario (called “Base” in the following). The optimization tool is run with the techno–economic data analyzed in section 4.2.

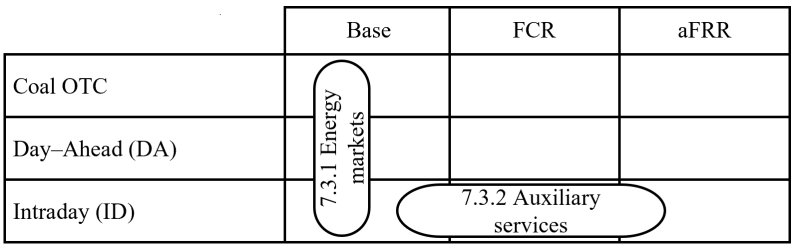

Figure 7.5: Overview of the optimized scenarios on the energy markets and the AuxS markets. Each analysis is performed for a PtH_2 unit based on an AEL and on a PEMEL respectively.

In order to address different possible developments in the energy markets, each scenario is optimized for the

price–related time–series of the last four years respectively. This includes the electricity price and the AuxS price time–series of the years 2019 to 2022. All price–related data are adjusted for inflation, while the H_2 demand is represented by the standard year 2020 elaborated in section 4.1.3. The influence of different H_2 demands represented by different years is shown in figure H.1 in the appendix on page L. Within the optimization tool, downtime periods are excluded as discussed in the same section. The scenario analysis considers the procurement of GoO and the EPC issued by the "Deutsche Emissionshandelsstelle", a subordinate authority of the Federal Environmental Agency. Thus, the procured electricity is certified to be of green origin.

Each scenario in both analyses is performed for an AEL and a PEMEL based PtH_2. The analysis is evaluated by discussing the composition of the resulting $LCoH_2$, the calculated PtH_2 component sizes and the optimized dispatch. Further, the $LCoH_2$ and the corresponding $F_{CO2,H2}$ are compared to the as–is situation operating with Natural Gas (NG).

7.3.1 Energy markets analysis

The energy market analysis covers the performance of the PtH_2 unit for different scenarios. The scenarios consider either a PEMEL or an AEL while the PtH_2 units procure their energy in different energy market scenarios such as an OTC coal contract and two EPEX spot markets. As figure 7.5 shows, the markets DA, ID with quarterly and hourly prices are considered alongside the monthly coal OTC contract. An overview of all resulting component sizes is given n figure H.2 on page LI in the appendix. The scenario analysis is divided into the expected $LCoH_2$, the optimized component sizes and dispatch followed by a balance including an environmental assessment.

Estimated $LCoH_2$ Figure 7.6 shows the computed $LCoH_2$ for an optimal PtH_2. The figure includes the share of the Operating Expenditures (OpEx) and Capital Expenditures (CapEx) summing up to the $LCoH_2$. Note that the terms OpEx and CapEx consider the specific exposures referenced to the mass of produced H_2 (kg_{H2}). The figure covers the PEMEL and the AEL operating at three different energy markets. On the left, their operation based on a coal–power contract is shown next to their operation on the DA market in the middle and on the ID market at the right. The price volatility of the markets differs as shown in section 4.3.1 and in addition, the coal–power contract includes monthly values while the DA and ID markets are divided up into 60 min and 15 min t_{int} respectively. Each scenario is analyzed for the four years of observation. The year 2022 is only considered until November 30^{th}, thus the annual CapEx are only considered proportionately as shown in section 5.3.1.

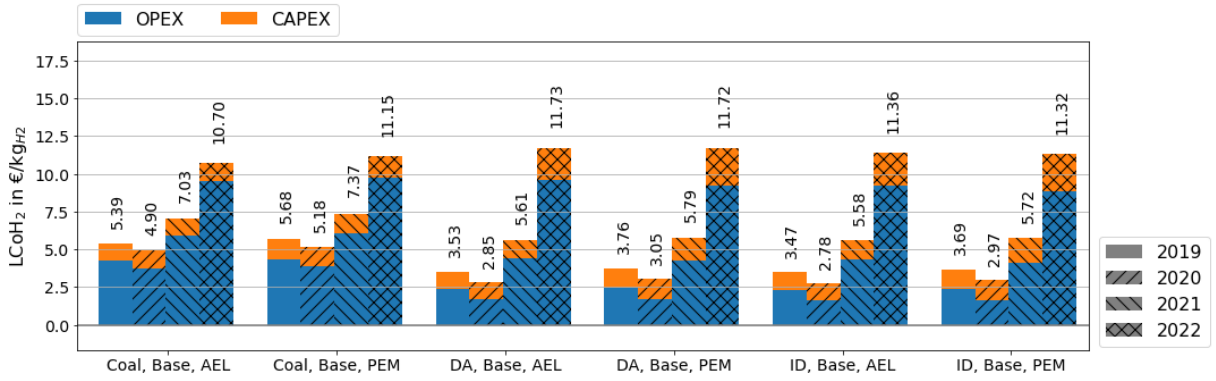

Figure 7.6: The resulting $LCoH_2$ distinguished in OpEx and CapEx of the scenario analysis focusing on the energy markets incorporating a coal–power contract and the DA and ID markets. AEL and PEMEL are considered without the participation at the AuxS markets.

The figure 7.6 shows two clear trends. In the first place, the OpEx contribute for the most part to the $LCoH_2$. In the second place, the results in the figure indicate the highest costs for the year 2022 with 11.73 €/kg_{H2}, and the lowest costs for the year 2020 with 2.78 €/kg_{H2}. The year 2022 is clearly an outlier in the perspective of H_2 costs caused by difficulties in the energy markets related to global politics discussed in the technical analysis in section 4.3.1. The predominant relevance of the OpEx is also described in the literature by the International Renewable Energy Agency (2020) among others [72], [76], [91]. The $LCoH_2$ determined in this work can be verified with a literature–based publication of the "Sachverständigenrat für Umweltfragen" (SRU) in 2021, who depicted $LCoH_2$ for the years 2018 to 2020 to be in the range of 2.01 to 4.97 €/kg_{H2}. Note that these values do not incorporate the high energy prices in 2022 or inflation.

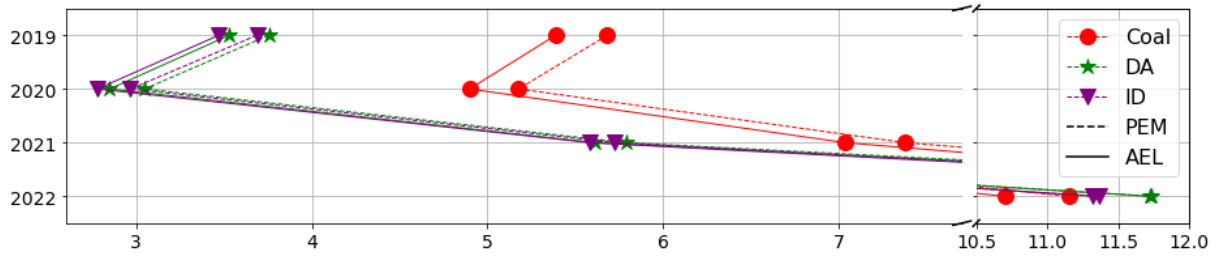

Figure 7.7: The resulting $LCoH_2$ of the scenario analysis focusing on the energy markets incorporating a coal–power contract and the DA and ID markets. AEL and PEMEL are considered without the participation at the AuxS markets.

The resulting $LCoH_2$ of the 6 analyzed scenarios are compared to each other in figure 7.7. It shows the four years represented by electricity prices on the y–axis and the corresponding $LCoH_2$ on the x–axis. The plot shows, that the spot market scenarios result in smaller $LCoH_2$ before 2022 due to the lower average electricity prices. Whereas the ID market results in lower optimized $LCoH_2$ compared to the DA. The AEL operating on the ID market results in the lowest $LCoH_2$ for the year 2020 which experienced the lowest electricity prices. The $LCoH_2$ in 2022 are four–times higher than the minimum prices in 2020. Consequently, the ID spot market with an AEL performs best from the economic perspective for the analyzed case study. The constitution of the $LCoH_2$ is analyzed in the upcoming figure 7.8 and figure 7.9 in further detail.

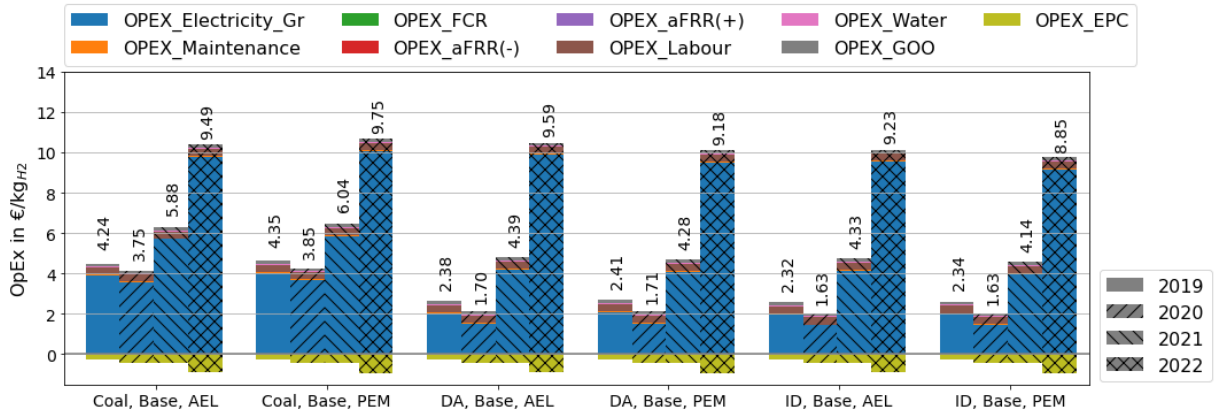

Figure 7.8: Levelized OpEx of the scenario analysis focusing on the energy markets incorporating a coal–power contract, the DA and the ID market. AEL and PEMEL are considered without the participation at the AuxS markets.

The specific OpEx, identified as the main contributor to the $LCoH_2$ in the figure 7.6, are visualized in figure 7.8. The predominant OpEx component is the costs to procure electric energy on the respective energy markets. The other contributor, mainly the labor and maintenance exposures, are not significant as their contribution is small. Further, the GoO contribute with $\sim 0.15\,€/kg_{H2}$ and the labour with $\sim 0.34\,€/kg_{H2}$ to the $LCoH_2$. The industry partner is expected to receive EPC of about 0.26 to $0.95\,€/kg_{H2}$, depending on the year of observation (and thus the European–Union–Allowances (EUA) prices according to section 2.1.5). The AuxS related components are not present as the scenarios do not include participation in these markets.

An overview of the CapEx is given in figure 7.9. The largest contributor to these costs is the El investment followed by the Gr and the St investments. The St investments and thus the capacity of the spot market scenarios in the year 2022 is increased compared to the other years. In addition, the Ba is considered for the ID scenario in the same year. Note that these values show a high StD_{rel} for different resolutions as discussed in section E. The ID scenario includes an extensive price spread forcing the El with the implemented El_{min} to procure electricity at all TS. Consequently, the high electricity price makes storing H_2 more reasonable and a high price spread favors the storage of electric energy. The Co unit does not contribute significantly to the costs. Table 7.1 compares the computed costs with the currently used NG.

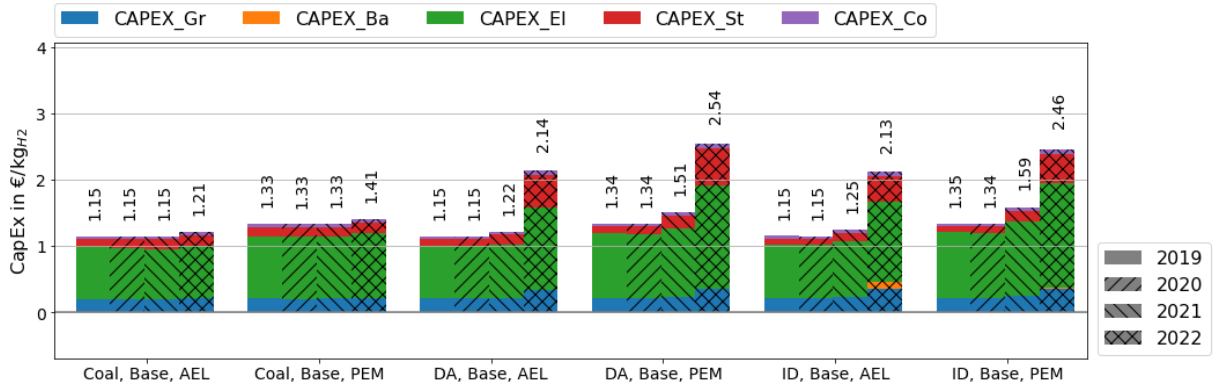

Figure 7.9: Levelized CapEx of the scenario analysis focusing on the energy markets incorporating a coal–power contract, the DA and the ID market. AEL and PEMEL are considered without the participation at the AuxS markets.

To reference the values calculated by the optimization tool, table 7.1 compares the PtH_2 scenarios to the as–is situation at the production facility of Aurubis. The values are referenced to a ton of copper for comparability similar to the procedure performed by Schütte et al. (2022) [117]. The table includes the three energy market scenarios while the two PtH_2 unit configurations consisting of a PEMEL or an AEL are averaged. In addition, the table includes prices for the procurement of NG which is based on the *Dutch TTF Natural Gas* index retrieved from investing.com [80]. The value considers only OpEx related to the procurement and includes no maintenance or investment related expenses. Therefore, this comparison aims to show a qualitative increase in costs and does not include a proper quantitative assessment.

Nevertheless, the poling of copper with H_2 is clearly ~ 2.1 to ~ 5.0 times more expensive compared to NG per ton of Cu (maximal ratio between the spot market scenarios and the NG consumption). According to a market analysis by the European Commission, the coal, electricity and especially the gas markets experienced a serious price increase in 2022 due to the war in Ukraine and the resulting tensions in the energy markets [43]. Figures describing the markets are shown in section 4.3.

Table 7.1: Comparison of the averaged $LCoH_2$ computed by the optimization tool based on the energy markets' scenarios with the currently used NG. The values are given in €/t_{Cu}, the gas prices are from investing.com [80].

	Coal–power	Day–Ahead	Intraday	Natural Gas
2019	7.12	4.69	4.61	1.06
2020	6.49	3.80	3.71	0.74
2021	9.27	7.33	7.27	2.61
2022	14.57	15.63	15.12	7.28

Optimized component sizes It is noticeable that the CapEx for the years 2019 to 2021 remain roughly on a constant level while the OpEx vary. The figure 7.10 includes reasons for that by plotting the resulting component sizes of the El and the corresponding AFLH for each scenario.

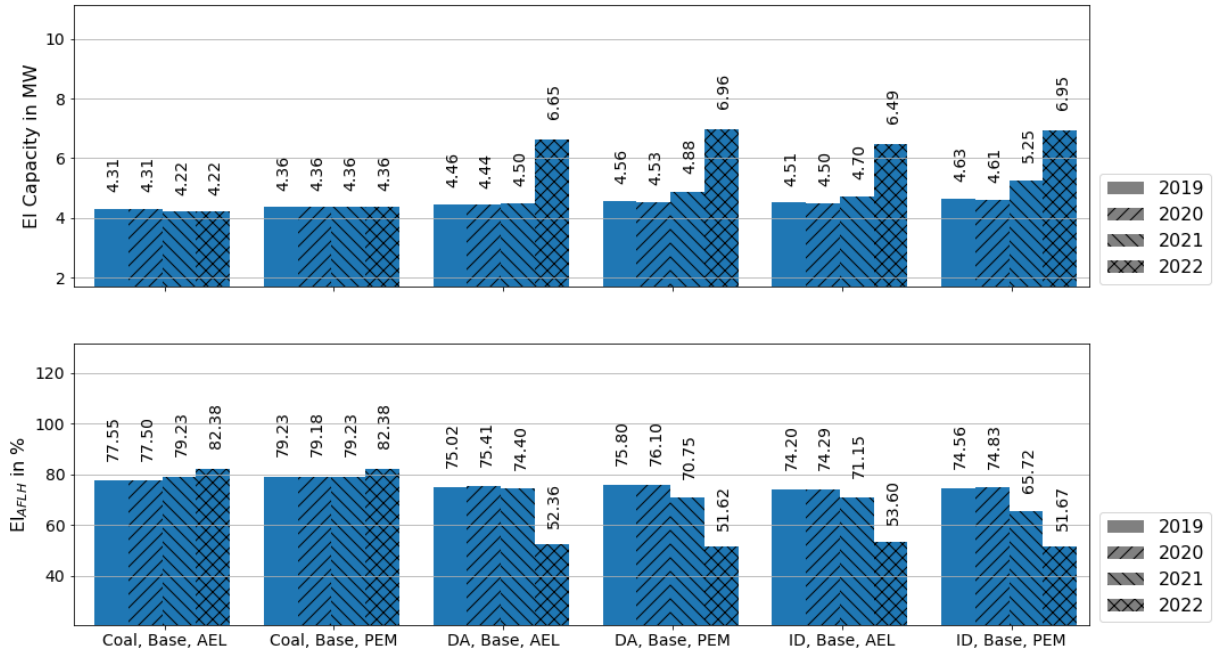

Figure 7.10: Resulting El dimensions and corresponding El_{AFLH} of the scenario analysis focusing on the energy markets incorporating a coal–power contract, the DA and the ID market. AEL and PEMEL are considered without the participation at the AuxS markets.

The El capacity is shown in figure 7.10 together with the corresponding El_{AFLH} for all analyzed scenarios. The El capacity optimized for the coal–power contract remains constant for the years 2019 to 2022. Comparing the PEMEL and the AEL to each other, the PEMEL is dimensioned a bit larger although it is affected by higher specific investment costs. This difference is in a similar order of magnitude as their difference in efficiencies. The sensitivity study in section 7.1 shows a similar influence, an increased efficiency leads to smaller El capacities. The component sizes calculated for the spot market scenarios in the years 2019 and 2020 show a slightly increased El capacity and a corresponding decreased AFLH that can be identified in comparison to the coal–power scenario.

Contrary to the coal–power scenarios, the optimization tool calculates slightly increased PEMEL capacities for the electric energy spot market prices. The increased capacity might be explained by the increasing price volatility in 2021. Probably, the PEMEL can make more use of this volatility in contrast to the AEL which is restricted by a larger El_{min}. In general, the two graphs in figure 7.10 show that the high electricity prices in 2022 lead to increased El capacities. Oversizing becomes advantageous as TS with low electricity prices can be used to store H_2 and throttle the El for TS with high prices. Note that the El capacity of the year 2022 is close to the maximal available power of the Gr constrained in the case study to 7 MW_{EP}. Thus, the resulting $LCoH_2$ might not reflect the global optima but the optima related to the case study. The relative SOC of the pressurized H_2 St is shown in figure 7.13 on the next but one page. The figure gathers the relative SOC for all scenarios of the year 2021.

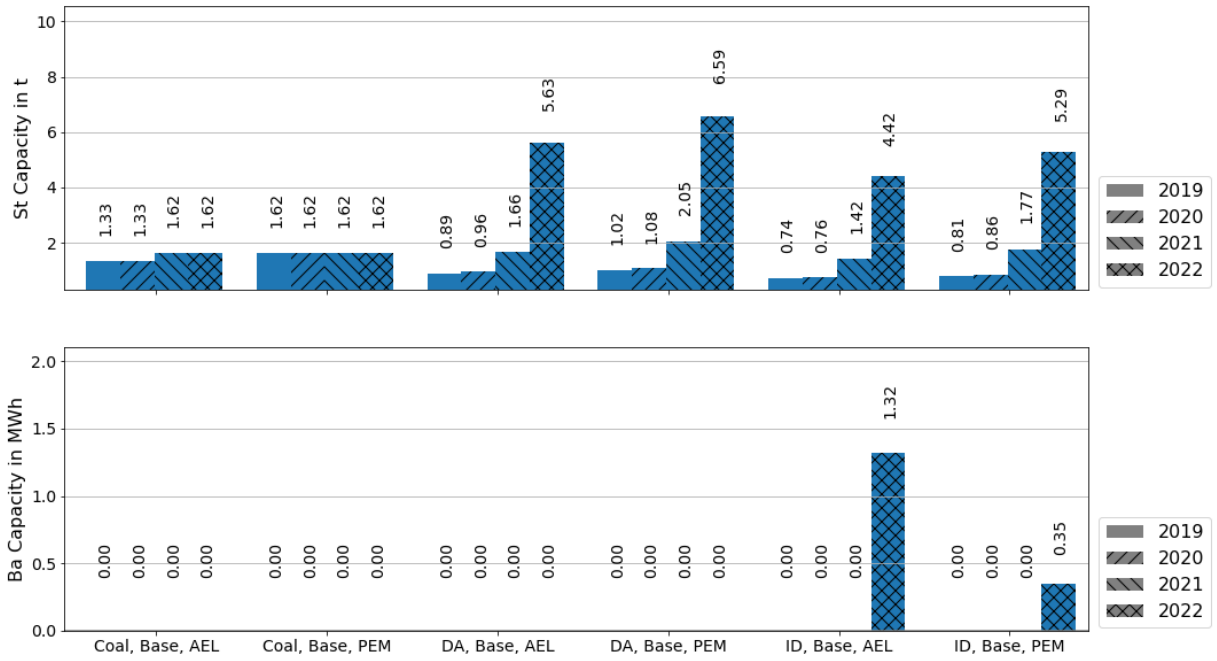

Figure 7.11: Resulting Ba and St dimensions of the scenario analysis focusing on the energy markets incorporating a coal–power contract, the DA and the ID market. AEL and PEMEL are considered without the participation at the AuxS markets.

Figure 7.11 gives an overview of the implemented capacities of the two energy and H_2 storing PtH_2 elements Ba and St. All in all, the St is clearly favored by the optimization tool in contrast to the Ba. The specific costs, elaborated in the techno–economic analysis in section 4.2, for the storage of energy and in a St and a Ba vary. The costs for a pressurized St is about 16 €/kWh_{H2} in contrast to a Ba which is affected by about 370 €/kWh_{EP}, excluding costs related to compression and the Ba efficiency. Thus, the investment in a pressurized St is more than ten times smaller compared to a Ba. Only high electrcity prices or a high El_{min} justify a Ba as also shown in the sensitvity study in figure 7.4. This explains the rare implementation of the Ba by the optimization tool.

The St calculated for the coal–power contract is larger compared to the cost–convenient years 2019 and 2020 at the spot markets. The St sizes calculated for the PEMEL scenario are higher compared to

the AEL scenarios. The St sizes calculated for the year 2022 are larger which comes hand in hand with the increased El dimensions. According to the theory of section 2.2, a St capacity of $1\,t_{H2}$ corresponds to a volume of $141.1\,m^3$ at 100 bar relative. This incorporates the relative Anode Furnaces (AF) inlet pressure of 10 bar.

Optimized PtH_2 dispatch To compare the optimized dispatches for the scenarios, the time–series data for a PEMEL based scenario at the beginning of August 2021 is exemplarily shown in figure 7.12. A similar plot is shown in figure H.3 in the appendix on page LI with the AEL based scenarios. It includes the prices of the coal OTC–market ("LCoCoal"), and the EPEX ID and the DA spot market prices. Further, the second row of diagrams shows the dispatch of the El while the third row identifies the corresponding SOC of the H_2 storage. The fourth row of diagrams represents the H_2 mass flows to the AF which represents the reductant demand in the case study. To visualize the values, the time–series are resampled to a resolution of t_{int}=1 h. Differences between the DA and ID are very small in this plot, as they are balanced out by the applied average.

In the first place, the figure indicates the different bandwidths of the electricity prices on the monthly based OTC and the hourly (and quarter–hourly) spot markets. Both spot markets show negative prices at the 31^{st} and 7^{th} of August. The figure shows in the second place, that the dispatch of the El for the spot and OTC markets is designed in a different manner. The El throttles on the ID market in a larger bandwidth while the El operates at the OTC market closer to its maximum.

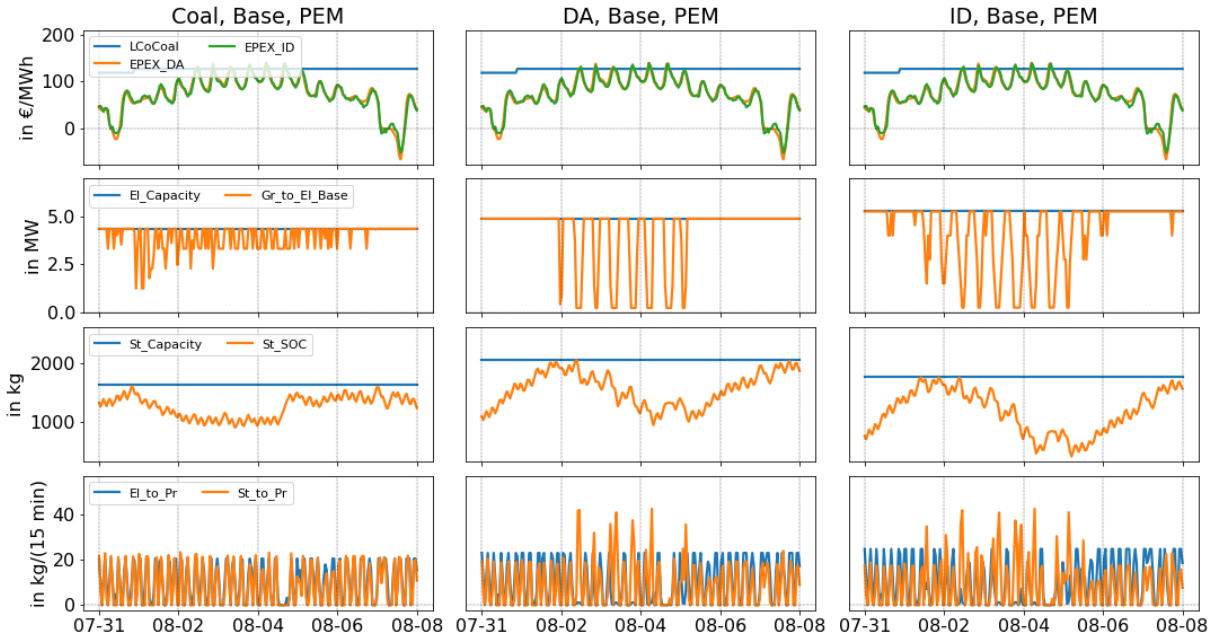

Figure 7.12: Comparision of three PEMEL based scenarios in 2021 with the specific electricity prices, the dispatch of the El and the SOC of the H_2 St. The price time–series are retrieved from EPEX among others [38], [78], [79].

The optimization tool excludes the TS with high electricity prices by reducing the consumed power of

the PEMEL in the spot market scenario, while TS with low or negative prices are exploited. For PtH_2 units with an AEL system, the dispatch of the El is similar whereas the higher El_{min} load is incorporated as the figure H.3 on page LI shows. The SOC of the H_2 St is analyzed in the third place. In the OTC scenario, the SOC has a smaller amplitude compared to the spot market scenarios. A larger price bandwidth results in a more volatile SOC timeline. This aspect is further elaborated in figure 7.13, which shows the SOC for a full year.

The H_2 flow supplying the AF of Aurubis is coming either directly from the El or indirectly from the St. Comparing the OTC to the spot market scenario, several spikes of the *St_to_Pr* variable between the 2^{nd} and the 5^{th} of August can be identified. The spikes indicate, that the optimization tool satisfies the PtH_2 demand at expensive TS with the St and to a smaller extent by the El directly. The share of indirectly supplied H_2 from the St increases for an AEL based system. This is caused by the higher El_{min} and the resulting accumulated H_2 in the St. This is the case although the compression process for an AEL system is more energy intensive due to the lower outlet pressure, whereas this circumstance is identified to be not significant in the sensitivity study.

To understand the dispatch further, the annual dispatch of the El and the SOC are visualized for the 2021 scenarios in two subsequent figures 7.13 to 7.14. The displayed figures are resampled to a resolution of t_{int}=1 h and their values are represented by the color intensity indicated by the bar on the right. The production downtimes in July and November which are excluded by the optimization tool can be identified by the white gaps in the figures.

Figure 7.13: Optimized dispatch of the St represented by the *St_SOC* variable in the year 2021 for the three energy–markets and both El technologies.

Comparing the SOC of the H_2 St in figure 7.13, it can be identified that the St reaches its full capacities less frequently. The annual values for the two spot market scenarios do not show significant differences. The same counts for the PEMEL and AEL scenarios. The figure shows, that storing H_2 for long periods of time, for example for the winter season is not considered by the optimization tool as the storage is discharged frequently.

The annual dispatch of the El is shown in figure 7.14, represented by the *El_in_Production* variable. The variable is the summative input electric power covering the connection to the Gr and to the Ba unit. The consequences drawn in the focused figure 7.12 can be extended. The El operates close to its maximum in the case of the OTC scenario while the El throttles down more frequently in the two spot

market scenarios, Further, the volatility of the dispatch is more pronounced in the ID scenario. The differences between the AEL and the PEMEL system implied by the El_{min} can not be identified in that figure. The H_2 demand identified in the case study decreases in the middle of September and so does the electricity consumption of the El. As discussed in section 4.3.1, the energy markets experienced increased price volatility in the autumn of 2021 which correlates with decreased production and decreased demand for reductants.

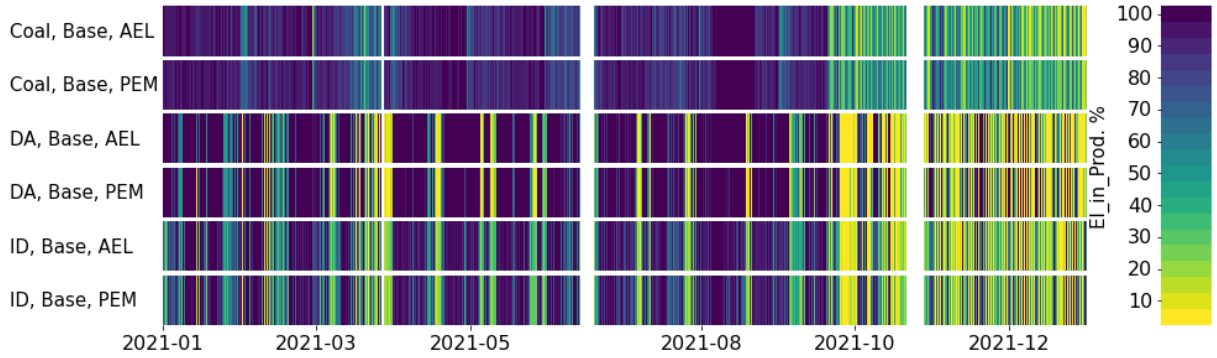

Figure 7.14: Optimized dispatch of the El represented by the *El_in_Production* variable in the year 2021 for the three energy–markets and both El technologies.

Environmental assessment and balances The procurement of electric energy comes together with a specific F_{CO2} related to its generation. Whereas the procured electricity is considered to be certified by GoO, the following analysis quantifies the physical applicable F_{CO2}. The H_2 produced by the PtH_2 is affected by a $F_{CO2,H2}$ of approximately 20.01 to 24.69 kg_{CO2}/t_{H2}, depending on the annual F_{CO2} of the electricity mix. These values are in the range of a publication issued by the SRU who conducted literature research in 2021 which shows that the $F_{CO2,H2}$ is about 14.00 to 26,00 kg_{CO2}/t_{H2} [114]. The $F_{CO2,H2}$ resulting from the procurement of a coal–power contract is higher with an approximate $F_{CO2,H2}$=45 kg_{CO2}/t_{H2}. The emissions related to the production with a PEMEL are larger compared to AEL due to its lower efficiency. To compare these values with the currently used reductant NG[1] and its related F_{CO2}, all values are referenced to a ton of copper as demonstrated by Schütte et al. (2022) [117]. The values are gathered in table 7.2 which distinguishes the PtH_2 scenarios based on the ID, the DA and the OTC options and the direct use of NG. The values for the PEMEL and AEL are averaged. For the computation of the Carbon Dioxide (CO_2) caused by NG, the CO_2 factor of 201.2 kg_{CO2}/MWh is applied which is determined for the case study in the appendix on page XXIX.

The procurement of electric energy to produce H_2 performs clearly worse compared to the direct use of NG. The amount of CO_2 emitted by the production based on the electricity mix is roughly ∼3 times more than the NG as–is situation. Further, a PtH_2 unit consuming coal–power emits ∼6 times more CO_2 per ton of copper. Thus, in physical terms, the direct consumption of the reductant NG is favorable compared to the H_2 sourced by electrolysis in a PtH_2 plant. This aspect is cured by the procured GoO which certifies the consumed electricity to be CO_2 neutral. This leads to a F_{CO2} reduction

[1] Note that Schütte et al. (2022) for example consider a different NG consumption of 1,892 t_{NG} as an average without any process–related filters due to different measurement stations [117].

Table 7.2: Comparison of the averaged F_{CO2} computed by the optimization tool based on the coal–power and the spot market scenarios with the currently used NG. The data is referenced to a ton of copper in kg_{CO2}/t_{Cu}.

	Coal–power	Day–Ahead	Intraday	Natural Gas
2019	58.26	30.48	30.72	9.35
2020	58.39	26.79	27.11	9.37
2021	58.27	30.55	30.49	9.35
2022	60.38	31.96	32.75	9.71

by approximately $9.4\,kg_{CO2}/t_{Cu}$ on the balance sheet based on the currently consumed NG. The one but next section 7.4 extents the objective function and considers the $F_{CO2,H2}$ criteria during the optimization next to the $LCoH_2$ and assesses the effects on the PtH_2 dimensions.

During the operation of a PtH_2 unit excess Oxygen (O_2) and Heat (Q) are generated. These two figures are proportionate to the amount of produced H_2 which equals $551{,}613.8\,kg_{H2}$ in the standard year 2020. According to the theoretial considerations of section 2.2, an annual O_2 mass of about $\sim$4,378.3 t_{O2}/a is generated due to stochiometry. The overall consumtion of Water (H_2O) including sewage water is $\sim$9,377.4 t_{H2O}/a. Schalling et al. (2022) and others recommend considering the use of the excess O_2 [30], [107], [111]. The production facility of Aurubis in Hamburg is suitable for this as a process upstream of the AF is operated with O_2 enriched process air as Röben et al. (2021) assess [111]. In addition, the production of H_2 yields in $\sim$9.0 GWh_Q/a excess heat at a temperature level between 55 to 80 °C depending on the temperature level of the El. The usage of excess heat can yield an overall energy utilization of $\sim$90 % based on the Higher Heating Value (HHV) according to Buttler et al. (2018) and the Danish Energy Agency (2017) [17], [23]. The integration of excess heat origin in the PtH_2 unit in the case study circumstances should be further discussed in a subsequent project.

The subsequent section analysis how participation at the AuxS, namely the Frequency Containment Reserve (FCR) and the Automatic Frequency Restoration Reserve (aFRR) markets, influence the $LCoH_2$ and the optimal component sizes of a PtH_2 unit. To do so, it compares the results to the non AuxS (Base) scenario on the ID market discussed within this section.

7.3.2 Auxiliary services analysis

Referring back to the economic assessment in the previous section, a supply of the AF with locally produced H_2 in a PtH_2 unit is not competitive with NG. Thus, this section analysis how the participation at the AuxS markets can decrease expectable $LCoH_2$ and how the optimization tool sizes the PtH_2 elements based on the additional revenue option. As shown in the figure 7.5, which gives an overview of the performed analyses, this assessment is based on the ID market and includes the participation at the FCR and the aFRR capacity markets (capacity –only). The results are calculated for the AEL and the PEMEL respectively. Note the simplifications made for the implementation of AuxS. In the first place, the PtH_2 unit is assumed to offer its services in an AuxS pool and not directly in the markets which might decrease the expectable revenues. Further, the published prices are averaged prices for the pay–as–bid market. Therefore, the resulting values discuss subsequently only indicate the order of magnitude.

The ID–Base scenario assessed in the section beforehand is used as a reference in the subsequent figures. The figures indicated the deviating (Δ) costs and component sizes related to the participation on the FCR and aFRR markets referenced to the ID–Base scenario. An overview of the obtained results for the AuxS scenario is given in the appendix on page LIII.

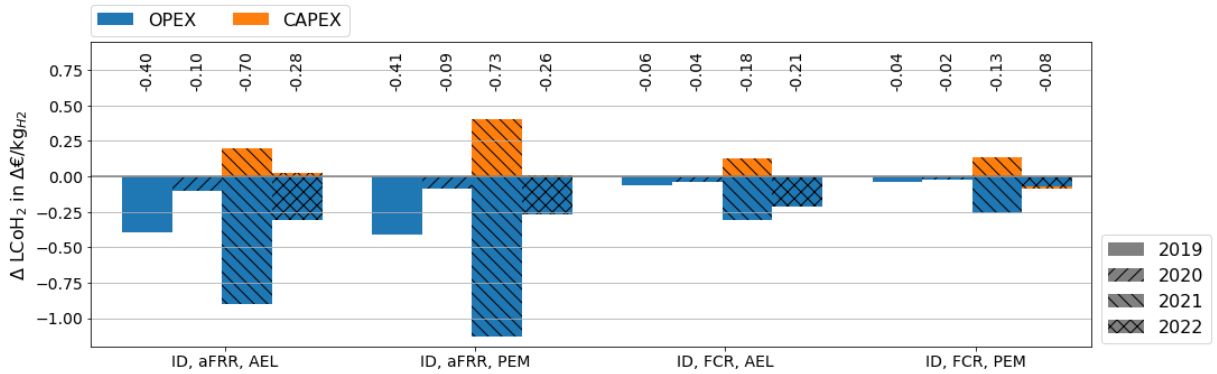

Figure 7.15: Resulting ΔLCoH$_2$ of the AuxS scenarios in reference to the ID–Base scenario distinguished in an AEL and a PEMEL based PtH$_2$ setup.

Figure 7.15 addresses the deviation of the LCoH$_2$ for a PtH$_2$ unit participating at the aFRR and the FCR capacity services. The figure distinguishes the resulting ΔLCoH$_2$ in the ΔOpEx and ΔCapEx by different colored bars. The value noted above each bar in the figure indicates the total cost deviation. As in the section beforehand, the years 2019 to 2022 are compared for each run.

All analyzed AuxS involving scenarios show a decreased LCoH$_2$ although the extent differs clearly from -0.04 to -0.73 €/kg$_{H2}$. The LCoH$_2$ decrease in 2020 is the smallest, whereas the absolute values for the ID–Base scenario shows already the lowest prices. The highest decline for the aFRR scenario is expected for the year 2021, which would result in a LCoH$_2$ for an AEL setup of 4.88 €/kg$_{H2}$ and for a PEMEL setup of 5.00 €/kg$_{H2}$. The cost reduction is approximately 12 to 13 % for both El technologies.

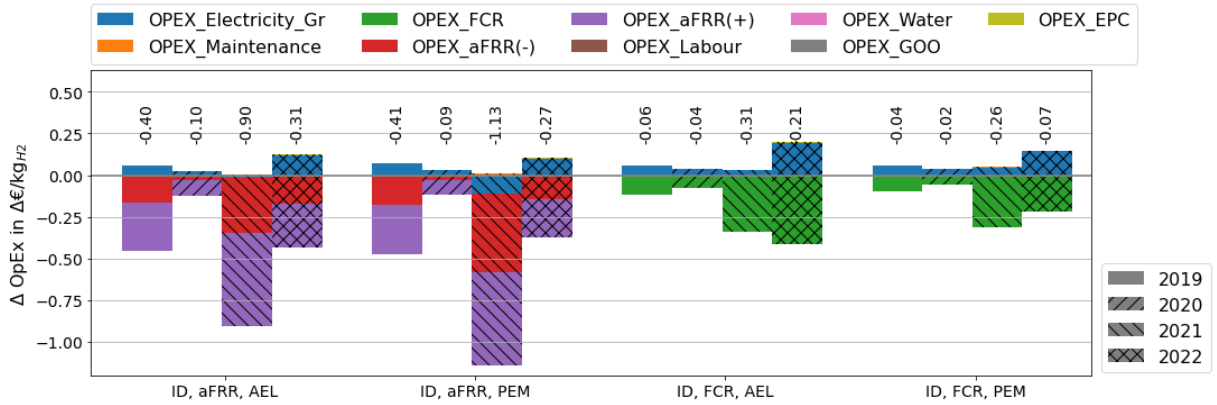

Figure 7.16: Resulting ΔOpEx of the AuxS scenarios in reference to the ID–Base scenario distinguished in an AEL and a PEMEL based PtH$_2$ setup.

The PEMEL is sized larger in the aFRR scenario for 2021 while it receives more aFRR revenues

compared to the AEL which results in similar $\Delta LCoH_2$ due to different specific investment costs. Further effects related to the El technology can not be identified. The $LCoH_2$ cost decrease due to the participation at the aFRR capacity market is larger compared to the FCR market. The bars in figure 7.15 show that the reduced $LCoH_2$ can be assigned to reduced OpEx as they incorporate the AuxS revenues. The revenues can be made without increased CapEx costs for all years but 2021. In the 2022, FCR, AEL scenario for example, a slight increase in the CapEx is also possible. Note that the maximal Gr capacity is constrained by the case study to 7 MW_{EP} which is already reached in the Base scenario for the year 2022. Therefore, an increase El capacity can only be achieved by downsizing other components, such as the Ba, to be able to participate more in the AuxS markets. The two figures below distinguish the OpEx and CapEx in their respective components.

Figure 7.16 focuses on the ΔOpEx deviation discussed above. The OpEx decrease is mainly caused by the revenues from the participation at the AuxS markets. This requires additional expenses for the procurement of electrical energy. The aFRR capacity market consists of two products aFRR(-) and aFRR(+) as explained in section 2.1.3 whereas the primary cost reduction is related to the aFRR(+). The positive sign indicates the PtH_2 or the El respectively allows to decrease its consumption, increasing the available energy in the power–grid. This behavior might favor the El operation as there is no need for oversizing but only the constraint to keep a constant value for four hours.

In addition to the analyzed ΔOpEx, the figure 7.17 gives an overview of the CapEx. Whereas the years 2019 and 2020 do not show any significant variation in the CapEx, the years 2021 and 2022 do. The El is enlarged compared to the ID–Base scenario which causes the increased investment costs. Further, the optimization tool downsizes the Ba for the year 2022.

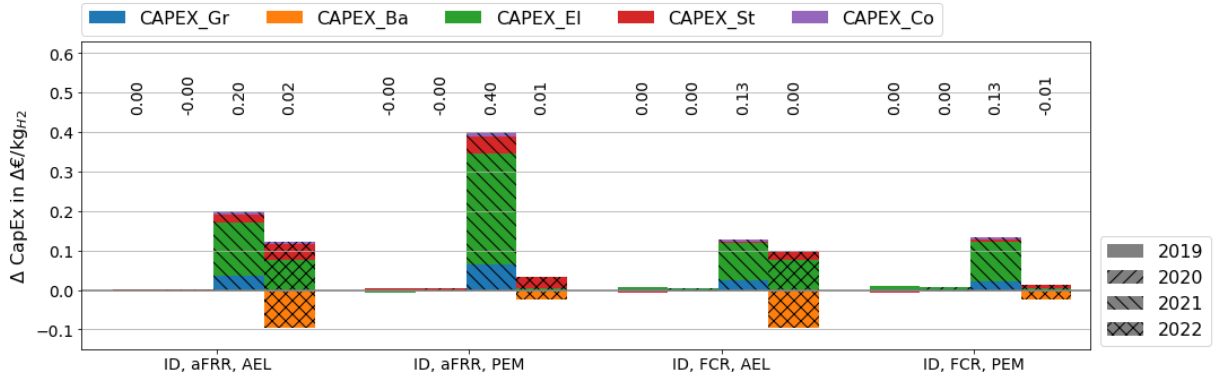

Figure 7.17: Resulting ΔCapEx of the AuxS scenarios in reference to the ID–Base scenario distinguished in an AEL and a PEMEL based PtH_2 setup.

All PtH_2 component sizes calculated for the AuxS scenario are shown in the appendix on page LIII. This figure H.4 shows that the corresponding El dimensions for the years 2021 and 2022 are increased. This comes together with decreased El_{AFLH}. The Ba, which is implemented in the ID–Base scenario for the year 2022 due to the high electricity prices and the El_{min} are downsized to <10 kWh_{EP} for the aFRR and FCR scenarios which is well within the StD_{rel} error. The pressurized St sizes increase by 0.32 to 0.58 t for the aFRR case while the FCR does not show a significant St capacity change. The optimization tool makes full use of the Gr capacity (7.0 MW_{EP}) limited for the case study in 2022.

7.4 Multi–objective optimization

Within this section, the scope of optimizing a PtH_2 unit with respect to its component sizes and dispatch is extended. The environmental assessment in the section beforehand showed that implementing a PtH_2 unit increases the F_{CO2} per ton of copper if the electricity mix is considered. Although the procurement of GoO to certify the electric energy to be green is considered in the case study, this section implements an environmental objective represented by the F_{CO2} in addition to the economic $LCoH_2$ objective. Thereby, the EPC is not implemented. This results in a Multi–Objective Optimization (MOO) approach based on the Pareto–principle as discussed in the preceding sections 2.3 and implemented in section 5.3.3. The objective functions for $LCoH_2$ and F_{CO2} are normalized with the results of an optimized single–objective based on the $LCoH_2$. Then, the weighted sum of the two objectives is implemented in the model. Figure 7.18 visualizes the Environmental weighting factor (f_{FCO2}) on the x–axes. The y–axes of the left diagram display the resulting objective values ($LCoH_2$ and $F_{CO2,H2}$) on individual y–axis. Further, the right–sided diagram shows the resulting El dimension in MW with its AFLH in %.

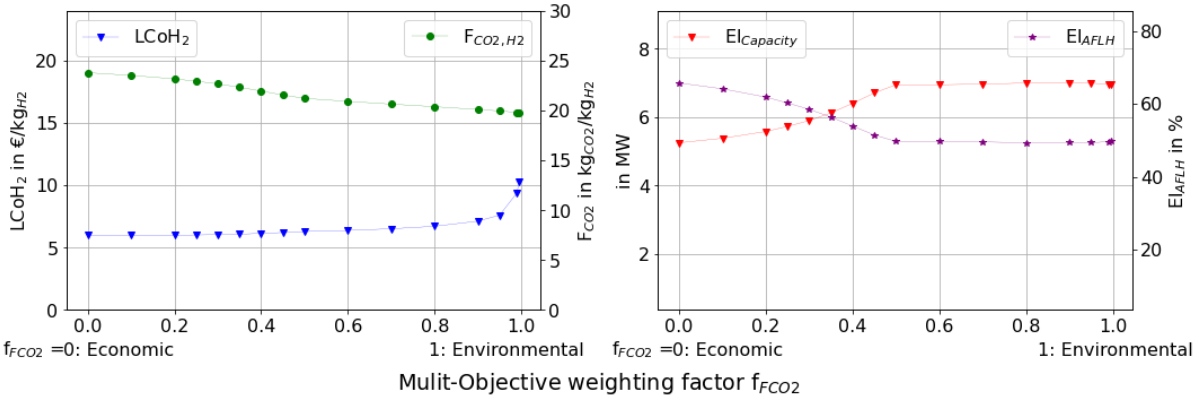

Figure 7.18: Results of the MOO analysis of the PtH_2 unit with a PEMEL operating at the ID market in the year 2021. The objective values are displayed on the left and the computed El dimensions with its El_{AFLH} on the right based on the f_{FCO2}.

The first reductions of the $F_{CO2,H2}$ in figure 7.18 can be achieved without compromising for the $LCoH_2$. Further reductions increase the $LCoH_2$. This corresponds to increased El dimensions and decreased El_{AFLH}. The environmental objective does not consider any investments or component sizes so that only the TS of operation is of interest. For f_{FCO2} larger than 0.6, the PtH_2 components are sized primarily in favor of the operating strategy.As the case study constraints the Gr capacity to $7\,MW_{EP}$, the El does not increase for higher environmental factors which would be the case for unconstrained capacities. This would lead to drastic increased $LCoH_2$ due to the large oversizes El up to $>20\,MW_{EP}$ depending on the scenario and f_{FCO2}. The resulting $F_{CO2,H2}$ would approach the $\sim 10\,kg_{CO2}/_{H2}$ asymptotically.

The MOO analysis with multiple weighting factors is conducted for a PtH_2 unit operating at the ID market for all four years of observation. The analysis includes an AEL and a PEMEL respectively. The resulting weighting factor figures I.1 to I.8 are displayed in the appendix on page LIV. Figure 7.19 includes all the resulting data points of figure 7.18 and the other performed MOO analyses in a Pareto–chart. The Pareto–chart combines the objectives on each chart axis. The connected lines form the Pareto–front,

which is defined to include the optimal relations between the two implemented objectives. Note that the Pareto–front was developed for all kinds of simulation procedures which can yield in none–optimal but feasible results. These results would form a cloud of data points in a Pareto–chart. The optimal edge of that cloud would represent the Pareto–front which is directly obtained by the optimization procedure applied in this work.

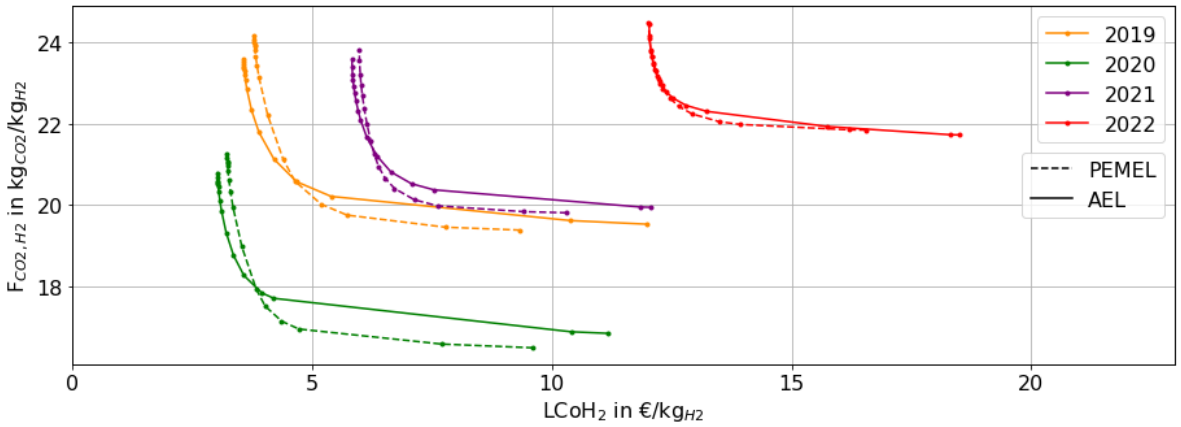

Figure 7.19: Visualization of the results for the four years of observation and a PEMEL and an AEL respectively computed by the optimization tool for the MOO approach combining $LCoH_2$ and $F_{CO2,H2}$ in a Pareto–chart.

Figure 7.19 summarizes the MOO results computed for all four years of observation based on the AEL and the PEMEL respectively. The environmental objective value $F_{CO2,H2}$ is plotted on the y–axis and the economic objective is represented by the $LCoH_2$ on the x-axis. The pure economic result of each year and PtH_2 configuration is shown by the left-hand corner points, indicating the lowest $LCoH_2$. A reduction of the $F_{CO2,H2}$ yields increased $LCoH_2$ in all cases. The first reduction steps do not contribute significantly to the $LCoH_2$ as the optimization tool can make use of the correlation between the spot market prices and the F_{CO2} discussed in section 4.3.4. An extended decrease comes hand in hand with increased $LCoH_2$ for both El types. Figure 7.19 shows that the PEMEL is advantageous compared to the AEL as it can reduce the $F_{CO2,H2}$ further. The PEMEL is able to exclude TS with high F_{CO2} of the electricity mix due to its lower El_{min}. In general, the F_{CO2} reduction is the most pronounced one in the year 2020, which shows low electricity prices and a low F_{CO2} of the electricity mix in the technical analysis in section 4.3.1. Further, the correlation between the spot market prices elaborated in section 4.3.4 shows that there are more TS in 2020 with a low F_{CO2} compared to the other years. Note that the lines in figure 7.19 do not stretch in a similar range of values as the objectives are weighted only within the individual scenario. Thus, a similar f_{FCO2} can result in different absolute values in other scenarios.

The CO_2 abatement costs calculated based on figure 7.19 are ~1,500 €/t_{CO2}. Typical values for CO_2 abatement costs are in between 60 to 230 €/t_{CO2} as for example “Agora Energiewende” (2019) shows [4]. The costs implied by a CO_2 influenced dispatch scheduling are several magnitudes higher than other measures. Thus, F_{CO2}–optimized PtH_2 units can only contribute in a limited way to the decarbonization of H_2.

Chapter 8

Conclusion

This section is about to conclude the analysis performed and the results obtained in the previous chapters. First, the results are summarized. Subsequently, recommendations for the industry partner Aurubis are elaborated. Third, global consequences are drawn by relating the flexible operation of Power–to–Hydrogen (PtH_2) units to the energy transition. An overview of further development possibilities for the created optimization tool is elaborated to close the work.

8.1 Summary

This thesis developed an optimization tool to determine optimal component sizes of a grid serving PtH_2 unit for different scenarios with respect to the Levelized Costs of H_2 ($LCoH_2$). The scenarios incorporate different energy markets, the participation at the Auxiliary Service (AuxS) markets and a Multi–Objective Optimization (MOO) analysis including the CO_2–Footprint of H_2 ($F_{CO2,H2}$). In a preceding analysis of the energy markets, this thesis shows that the year 2022 is clearly an outlier with respect to energy prices while the year 2020 experienced the lowest prices. Further, this work shows that a capacity–only strategy for the Automatic Frequency Restoration Reserve (aFRR) market is reasonable due to the high bidding price limit. The correlation between the system average emission factor (F_{CO2}) and the electricity prices shown in the literature are confirmed for the years 2019 to 2021. A definition of a grid serving operation is worked out and differentiated from a system serving operation strategy. In addition, this work conducts a literature review to determine reasonable parameters to model a PtH_2 unit and its elements Grid (Gr), Battery (Ba), Electrolyzer (El), Compressor (Co), and the pressurized Hydrogen (H_2) Storage (St). Thereby the optimization tool includes the option to choose either a Proton Exchange Membrane Electrolyzer (PEMEL) or an Alkaline Electrolyzer (AEL). The economic evaluation is based on the "VDI 2067" and incorporates Gurantees of Origin (GoO) and the Electricity–Price–Compensation (EPC) as demonstrated by Schütte et al. (2022) [117]. The optimization tool is implemented and tested with generic test data to confirm its operation. It can be shown that especially the integrating PtH_2 elements (Ba and St) are sensitive to the resolution Interval (t_{int}).

Subsequently, the optimization tool is applied to a case study which is about a fuel switch at the production facility of Aurubis where the Anode Furnaces (AF) are supposed to be supplied by H_2 instead

of Natural Gas (NG). This master thesis calculates the resulting H_2 reductant demand based on the NG consumption and sets up an additional electricity price reference scenario based on an Over–the–Counter (OTC) coal contract. The case study is then analyzed with respect to its sensitivities to the input parameters, followed by a scenario–based assessment focusing on the $LCoH_2$.

The conducted sensitivity studies show, that the $LCoH_2$ and the $F_{CO2,H2}$ are not depending on the chosen resolution interval, whereas the Ba and the St capacities show a Relative Standard Deviation (StD_{rel}) of about ±48 % and ±6 % for different resolution t_{int}. The analyses are run with resolution t_{int} of 15 min as this indicates a compromise between the computing time and the trading periods of the Intraday (ID) spot market. The conducted sensitivity study addressing the specific investment costs, the H_2 production and the parameters related to (energy) storages show that the El parameters have the most relevant impact on the resulting $LCoH_2$. The efficiency of the El influences the $LCoH_2$ as an increased efficiency leads to a smaller installed El capacity. Less electric energy has to be converted to yield the same amount of H_2. The specific investment costs of the El play a major role next to the efficiency. Increasing costs lead to a smaller El and a higher $LCoH_2$. The smaller El is compensated with a larger St unit and increased Annual Full Load Hours (AFLH). Moreover, the El minimal load (El_{min}) influences the installed St and Ba capacity and forces the PtH_2 unit to run the El at all Time–Stamp (TS). An increased El_{min} contributes to the required St and Ba capacity. The increased storage capabilities correspond with higher $LCoH_2$ and a smaller installed El capacity. Further, the sensitivity studies show that the El load gradient (El_{Grad}) and the compression parameters do not influence the resulting $LCoH_2$ nor the PtH_2 component dimensions significantly. The implementation of the Ba is highly influenced by the El_{min} and the level of the electricity prices.

The performed energy market and AuxS scenario analyses for the case study show that the $LCoH_2$ are highly dependent on the design of the scenarios. In the first place, the computed $LCoH_2$ by the optimization tool are between 2.78 €/kg_{H2} for 2020 electricity prices and rise up to 11.73 €/kg_{H2} in the year 2022. The computed values take the EPC and the procurement of GoO into account. The drastic deviation for different price time–series can be explained by the high relevance of the Operating Expenditures (OpEx) costs, primarily related to the procurement of electricity. Whereas Capital Expenditures (CapEx) are the sum of the El, the Gr and the St. A battery is only economically feasible for years with high electricity prices such as the year 2022 and a high El_{min}, although the capacity itself showed a high StD_{rel}. Further, the analysis shows that the locally produced H_2 in the framework of the case study is not competitive with the direct use of NG and shows ∼2 to ∼5 times higher costs per ton of copper. In addition, this research determines the excess amount of Oxygen (O_2) to be ∼4,378.3 t_{O2}/a and excess heat of approximately 9.0 GWh/a.

Participating at the AuxS can reduce the specific costs of H_2 up to 13 % for the energy market time–series of the year 2021. Whereas the AuxS covers the optimal potential with a number of underlying assumptions. For example, the simplified participation on the AuxS market in an AuxS pool and the assumption of averaged prices on the AuxS market although the prices are formed according to the pay–as–bid principle. The actual reduction potential for an optimal setup might be smaller than indicated by this optimizing approach. Thus, the expectable cost reductions related to participation are considerably small.

Taking the CO_2–Footprint (F_{CO2}) into account, the locally produced H_2 is affected by higher $F_{CO2,H2}$

compared to the direct application of NG. Locally sourced PtH_2 in a PtH_2 unit is only advantageous if the procured electricity is certified to be renewable by GoO. A combined optimization incorporating the $LCoH_2$ and the $F_{CO2,H2}$ shows that there is a tradeoff between the two objectives. Whereas minor improvements of the $F_{CO2,H2}$ cause only minor cost increases because the two time–series correlate. A significant improvement of the $F_{CO2,H2}$ leads to increased $LCoH_2$. The resulting Carbon Dioxide (CO_2) abatement costs are at least 6 times higher compared to alternative CO_2 abatement technologies. Within the case study, the potential to decrease the $F_{CO2,H2}$ is limited due to the constrained Gr connection capacity ($\leq 7\,MW_{EP}$).

8.2 Case Study: Recommendations for Aurubis

The performed simulations show that the resulting $LCoH_2$ is highly dependent on the assumed scenario, with electricity prices having the greatest relevance. Based on the assumptions made within this thesis, the lowest $LCoH_2$ are computed for inflation–adjusted electricity prices of the year 2020. These would settle at about $\sim 3\,€/kg_{H2}$ for spot market prices. The coal–power contract yields higher costs of about $\sim 5\,€/kg_{H2}$. Based on the assumptions made, the highest $LCoH_2$ is computed for the 2022 electricity prices which would result in up to $\sim 11\,€/kg_{H2}$. These values factor in the issued EPC of about 0.26 to $0.95\,€/kg_{H2}$ depending on the observed years (mainly influenced by the respective European–Union–Allowances (EUA) prices).

To fulfill the constraints of the case study, the optimized El should have a capacity of about 4.31 to $\sim 5\,MW_{EP}$ for energy–market data in 2019 to 2021. This results in AFLH of about 80 %. The optimization tool considers large overcapacities and the implementation of a Ba only for the year 2022 which experienced high electricity prices. Note that a sensitivity study shows that especially the Ba capacity depends on the resolution t_{int} and shows a StD_{rel} of ∼48%. The optimized storage capacities are between 0.81 and $1.42\,t_{H2}$ for all scenarios except 2022. The Co unit has a maximal capacity of about $\sim 90\,kg_{H2}/h$. The storage values and the mass flow to be compressed increase in the 2022 scenarios. The AEL scenarios result in slightly reduced $LCoH_2$ compared to the PEMEL scenarios due to the higher El_η and lower specific investment costs. The conducted sensitivity study shows that these two parameters, the El_η and the El investment costs, are the most relevant parameters in regard to the $LCoH_2$. An increased El_{min} emphasizes the implementation of a Ba and shows a proportionate trend with respect to the $LCoH_2$. Parameters related to the storage of electric energy or H_2 in a pressurized storage show only minor effects on the resulting $LCoH_2$.

The participation at the aFRR markets could decrease the $LCoH_2$ by a factor of up to ∼13 % for the 2021 energy markets' scenarios. The reductions for Frequency Containment Reserve (FCR) and the other observed years are smaller. Whereas the assumptions made in this thesis might overestimate the potentials, for example, due to the assumed participation in a AuxS pool and the focus on the capacity markets. The optimization tool concludes that especially the installed El, St and Gr capacities increase when participating in the AuxS markets. Consequently, an optimal sized PtH_2 unit can contribute to reduced $LCoH_2$ only in a limited way. Nevertheless, an oversized PtH_2 unit could make better use of the AuxS markets.

Compared to the currently used NG, the implementation of H_2 in the AF of the case study is eco-

nomically not feasible. The prices per ton of copper are increased by the factor of up to ∼6, even with the EPC. The same holds for the environmental assessment, which shows that the F_{CO2} related to the consumption of the reductants increases by a factor of at least ∼3 to ∼6. Due to the procured GoO, this effect does not have to count on the balance sheets. The optimization of the PtH_2 unit with respect to an environmental objective based on the $F_{CO2,H2}$ results in $LCoH_2$ of up to 10 €/MWh_{H2} which leads to higher CO_2 abatement costs compared to alternative measures.

8.3 Consequences

The production of H_2 for an onsite PtH_2 unit is economically not competitive compared to the currently used NG, which is ∼2 to ∼5 times less expensive. Consequently, political measures have to be in place to decrease costs related to electrolysis. This thesis emphasizes the introduction of incentives for CO_2 neutral production. This includes the call for higher EUA prices in order to make the consumption of fossil fuels less economically feasible. In addition, political measures such as the Carbon–Contracts–for–Difference (CCfD) discussed by the German Energy Agency need to be put in place to compensate for the additional costs and reduced competitiveness related to the CO_2 neutral production [27].

H_2 based on electrolysis is only environmentally reasonable on the balance sheet by the procurement of GoO as the $F_{CO2,H2}$ based on the electricity mix is up to ∼6 times higher compared to the direct consumption of NG. An optimized dispatch and sizing of PtH_2 units with respect to the F_{CO2} of the electricity mix involve much higher costs than alternative CO_2 abatement technologies. Thus, the decarbonization of the electricity mix itself must proceed.

Further, a grid serving, flexible demand for electricity has to be stimulated. The current regulation of standing charges (German: “Netzentgelte”) penalizes flexible operation. This does not favor the flexible procurement of electricity on spot markets. Although especially electrolyzers are excluded from standing charges, industries are reluctant to increase their demand–side flexibility which is required for the integration of renewable energy [57], [68].

8.4 Further development options

The optimization tool can be extended in its functionality in several ways. In the first place, more technical units could be implemented in the optimization tool. Such as a high–temperature Solid Oxide Electrolyzer (SOEL) connected to excess heat from possible industry partners to analyze whether alternative El technologies are beneficial. Further, additional consumers could be implemented such as Direct–Air–Capture units, heat pumps or others that consume the excess (low–temperature) thermal energy or the excess O_2 of a PtH_2 unit. A special remark is made on the scheduling of the H_2 demand itself. Although the scheduling of the demand might interfere with the production constraints of the industry partners, an elaboration of the degrees of freedom yielding in an optimized demand schedule can be of economic and environmental interest.

In the second place, the representation of the technical units could be enhanced to represent their real behavior more closely. This could include the degradation of the El stack or the interaction of the El outlet–pressure and the El efficiency, as assessed by Tjarks (2017) [133]. In addition, the battery lifetime

could be made dependent on the charging cycles. All adjustments should be assessed in perspective of their sensitivity and put in contrast to the deviated computing effort. As the resulting values are highly dependent on the input parameters, it is recommended to update the respective data continuously in the third place. To increase the significance of the results, technical offers from component suppliers could be requested and implemented into the tool. In the fourth place, the scope of the objective functions can be extended to reflect more parameters than the $LCoH_2$ and the $F_{CO2,H2}$. For example, technical parameters such as reduced degradation (indicated by charging cycles or load changes) can provide further findings.

To increase the comparability of the results, additional regulative aspects could be represented in the tool in the sixth place. An extended optimization tool could for example assess the implications due to the delegated act based on the Renewable Energy Directives issued by the European Commission to certify the origins of H_2 [41]. Alternatively, CCfD such as those mentioned above could be added to the optimization tool. The optimization tool results themselves could be enhanced by assessing the resolution dependency of the computed PtH_2 element capacities. Further, the significance of the AuxS assessment could be increased by implementing the Non–Negative–Integers (NNI) variables which might lead to increased computing times. To close, the importance of projections and scenario–based forecasts are highlighted. The implementation of forecasts could furthermore increase the significance of the results obtained by the optimization tool.

Bibliography

[1] 50Hertz Transmission GmbH, Amprion GmbH, TenneT TSO GmbH, and TransnetBW GmbH, *Allgemeines zur Regelleistung - Technische Aspekte*, 2022. [Online]. Available: `https://www.regelleistung.net/ext/static/technical` (visited on 10/30/2022).

[2] 50Hertz Transmission GmbH, Amprion GmbH, TenneT TSO GmbH, and TransnetBW GmbH, Eds., *FAQ Regelleistung*, 2022. [Online]. Available: `https://www.regelleistung.net/ext/` (visited on 11/23/2022).

[3] Agora Energiewende and Agora Industry, Eds., *12 Insights on Hydrogen: IMPULSE*. Berlin, 2021.

[4] Agora Energiewende and Wuppertal Institute, Eds., *Estimated CO_2 abatement costs of selected key technologies*. 2019.

[5] All NEMOs Committee, *About the All NEMO Committee*, 2022. [Online]. Available: `https://www.nemo-committee.eu/contact` (visited on 10/17/2022).

[6] Arbeitsgemeinschaft für sparsamen und umweltfreundlichen Energieverbrauch e.V., Ed., *Wasserstoff-anwendung in Industrie und Energiewirtschaft*. Bonn, 2020.

[7] Aurubis AG, Ed., *Umweltschutz im Arubis-Konzern und aktualisierte Umwelterklärung 2019 der Aurubis AG der Standorte Hamburg und Lünen*. Hamburg, Lünen, 2019. [Online]. Available: `https://www.emas.de/fileadmin/user_upload/ue/reg/DE-131-00035_Aurubis-AG.pdf` (visited on 11/08/2022).

[8] BAFA, *Informationsblatt CO2-Faktoren: Merkblatt*, 2021. [Online]. Available: `https://www.bafa.de/SharedDocs/Downloads/DE/Energie/eew_infoblatt_co2_faktoren_2021.pdf?__blob=publicationFile&v=5` (visited on 04/27/2022).

[9] M. Beg, J. Taka, T. Kluyver, *et al.*, "Using Jupyter for Reproducible Scientific Workflows," *Computing in Science & Engineering*, vol. 23, no. 2, pp. 36–46, 2021. DOI: `10.1109/mcse.2021.3052101`.

[10] Bundeskartellamt and Bundesnetzagentur, "Monitoringbericht," *Monitoringbericht gemäß § 63 Abs. 3 i.V.m. § 35 EnWG und § 48 Abs. 3 i.V.m. § 53 Abs. 3 GWB*, 2021.

[11] Bundesministerium für Wirtschaft und Klimaschutz, *The EU emissions trading system – essential for the energy transition*, 2022. [Online]. Available: `https://www.bmwk.de/Redaktion/EN/Artikel/Energy/emissions-trading.html` (visited on 11/21/2022).

[12] Bundesministerium für Wirtschaft und Technologie, *Bekanntmachung zur Änderung der Richtlinie für Beihilfen für Unternehmen in Sektoren bzw. Teilsektoren, bei denen angenommen wird, dass angesichts der mit den EU-ETS-Zertifikaten verbundenen Kosten, die auf den Strompreis abgewälzt werden, ein erhebliches Risiko der Verlagerung von CO2-Emissionen besteht (Beihilfen für indirekte CO2-Kosten)*, 2013.

[13] Bundesministerium für Wirtschaft und Technologie, *Energiewirtschaftsgesetz, last change of article 3 at October 8, 2022: EnWG*, 2005.

[14] Bundesnetzagentur and SMARD.de, *Marktdaten*, Bonn, 2022. [Online]. Available: `https://www.smard.de/home/downloadcenter/` (visited on 10/08/2022).

[15] Bundesnetzagentur and SMARD.de, Eds., *So funktioniert der Strommarkt*, 2022. [Online]. Available: `https://www.smard.de/page/home/wiki-article/446/384` (visited on 11/21/2022).

[16] A. Buttler, R. Koltun, R. Wolf, and H. Spliethoff, "A detailed techno-economic analysis of heat integration in high temperature electrolysis for efficient hydrogen production," *International Journal of Hydrogen Energy*, vol. 40, no. 1, pp. 38–50, 2015. DOI: `10.1016/j.ijhydene.2014.10.048`.

[17] A. Buttler and H. Spliethoff, "Current status of water electrolysis for energy storage, grid balancing and sector coupling via power-to-gas and power-to-liquids: A review," *Renewable and Sustainable Energy Reviews*, vol. 82, pp. 2440–2454, 2018. DOI: `10.1016/j.rser.2017.09.003`.

[18] M. L. Bynum, G. A. Hackebeil, W. E. Hart, *et al.*, Eds., *Pyomo–optimization modeling in python* (67), 3rd ed. pringer Science & Business Media, 2021.

[19] W. Cole, W. A. Frazier, and C. Augustine, Eds., *Cost Projections for Utility-Scale Battery Storage: 2021 Update*. 2021.

[20] Consentec GmbH, Ed., *Beschreibung von Konzepten des Systemausgleichs und der Regelreservemärkte in Deutschland: Erläuterungsdokument im Auftrag der deutschen regelzonenverantwortlichen Übertragungsnetzbetreiber*. Aachen, 2022.

[21] Consentec GmbH, Ed., *Beschreibung von Konzepten des Systemausgleichs und der Regelreservemärkte in Deutschland: im Auftrag der deutschen Übertragungsnetzbetreiber*. Aachen, 2020.

[22] F. D'Ettorre, M. Banaei, R. Ebrahimy, *et al.*, "Exploiting demand-side flexibility: State-of-the-art, open issues and social perspective," *Renewable and Sustainable Energy Reviews*, no. 165, 2022. DOI: `10.1016/j.rser.2022.112605`.

[23] Danish Energy Agency and Energinet, Eds., *Technology Data - Renewable Fuels: Technology descriptions and projections for long-term energy system planning*, 9th ed. Copenhagen, 2017. [Online]. Available: `https://ens.dk/sites/ens.dk/files/Analyser/technology_data_for_renewable_fuels.pdf` (visited on 12/22/2022).

[24] DEHSt, *Treibhausgasemissionen 2021: Emissionshandelspflichtige stationäre Anlagen und Luftverkehr in Deutschland: VET-Bericht 2021*, Berlin, 2022. [Online]. Available: `https://www.dehst.de/SharedDocs/downloads/DE/publikationen/VET-Bericht-2021_Summary.pdf?__blob=publicationFile&v=3` (visited on 08/08/2022).

[25] Deutsche Bundesbank, Ed., *EZB-Rat erhöht Leitzinsen erneut um 75 Basispunkte*, 2022. [Online]. Available: https://www.bundesbank.de/de/aufgaben/themen/ezb-rat-erhoeht-leitzinsen-erneut-um-75-basispunkte-899350 (visited on 12/06/2022).

[26] Deutsche Emissionshandelsstelle (DEHSt), *Europäischer Emissionshandel*, Umweltbundesamt, Ed., 2018. [Online]. Available: https://www.dehst.de/DE/Europaeischer-Emissionshandel/EU-Emissionshandel-verstehen/eu-emissionshandel-verstehen_node.html (visited on 11/21/2022).

[27] Deutsche Energie-Agentur, Ed., *Tech for Net Zero Allianz: CCfD zur Skalierung von Klimatechnologien in Deutschland*. Berllin, 2022.

[28] Deutscher Bundestag, *Erneuerbare-Energien-Gesetz*, 2014. [Online]. Available: http://www.gesetze-im-internet.de/eeg_2014/EEG_2021.pdf (visited on 11/29/2022).

[29] Deutsches Zentrum für Luft- und Raumfahrt e. V. (DLR), Ed., *Electrical Grid Service Catalogue for Water Electrolyser: Standardized qualifying tests of electrolysers for grid services*. 2017. [Online]. Available: https://www.qualygrids.eu/app/uploads/sites/5/2017/02/Deliverable-1.1-Electrical-Grid-Service-Catalogue-for-Water-Electrolysers-27-11-2017.pdf (visited on 12/22/2022).

[30] Deutsches Zentrum für Luft- und Raumfahrt e. V. (DLR), Ed., *Wasserstoff als ein Fundament der Energiewende: Teil 2: Sektorenkopplung und Wasserstoff: Zwei Seiten der gleichen Medaille*. Oldenburg, 2020. [Online]. Available: https://www.dlr.de/content/de/downloads/publikationen/broschueren/2020/wasserstoffstudie-teil-2.pdf?__blob=publicationFile&v=6.

[31] Die Wissenschaftlichen Dienste des Deutschen Bundestages, Ed., *Gestehungskosten von Strom im Vergleich: Ausarbeitung*. Berlin, 2022. DOI: 10.5281/zenodo.6326972.

[32] F.-M. Dittes, *Optimierung*. Berlin, Heidelberg: Springer Berlin Heidelberg, 2015. DOI: 10.1007/978-3-642-53889-6.

[33] S. Drünert, U. Neuling, S. Timmerberg, and M. Kaltschmitt, "Power-to-X (PtX) aus „Überschussstrom" in Deutschland – Ökonomische Analyse," *Zeitschrift für Energiewirtschaft*, vol. 43, no. 3, pp. 173–191, 2019. DOI: 10.1007/s12398-019-00256-7.

[34] ecoinvent, *The ecoinvent Database*, Zürich, 2019. [Online]. Available: www.ecoinvent.org.

[35] T. Edens and S. Johnn, "Using Hydrogen as a Reductant in Fire Refining at Aurubis Hamburg's "Down-town" Smelter," *The 61st Annual Conference of Metallurgists, COM 2022, Montréal QC*, 2022.

[36] Energy Brainpool GmbH & Co. KG, Ed., *Anreiz einer energiewendedienlichen Fahrweise von Elektrolyseuren*. Berlin, 2019.

[37] ENTSO-E, *Transparency Platform*, 2022. [Online]. Available: https://transparency.entsoe.eu/ (visited on 10/08/2022).

[38] EPEX SPOT SE, *Time–series data of the SPOT–market*, Paris, 2022. [Online]. Available: https://www.epexspot.com/de/node/118 (visited on 12/03/2022).

[39] EPEX SPOT SE, *Trading Products*, Paris, 2022. [Online]. Available: https://www.epexspot.com/en/tradingproducts.

[40] Europäische Zentralbank, Ed., *Geldpolitische Instrumente*, Frankfurt am Main, 2022. [Online]. Available: https://www.ecb.europa.eu/ecb/tasks/monpol/html/index.de.html (visited on 12/05/2022).

[41] European Commission, *Directive (EU) 2018/2001 of the European Parliament and of the Council of 11 December 2018 on the promotion of the use of energy from renewable sources*, 2018.

[42] European Commission, *Guidelines on certain State aid measures in the context of the system for greenhouse gas emission allowance trading post 2021*, 2021. [Online]. Available: https://www.euractiv.com/wp-content/uploads/sites/2/2020/09/ets_guidelines_2021_en.pdf.

[43] European Commission, *Market analysis: The Commission produces quarterly reports on EU gas and electricity markets.* 2022. [Online]. Available: https://energy.ec.europa.eu/data-and-analysis/market-analysis_en (visited on 10/30/2022).

[44] European Parliament and of the Council, *Directive 2003/54/EC of the European Parliament and of the Council of 26 June 2003 concerning common rules for the internal market in electricity and repealing Directive 96/92/EC - Statements made with regard to decommissioning and waste management activities: 2003/54/EG.*

[45] European Union Agency for the Cooperation of Energy Regulators, Ed., *ACER's Final Assessment of the EU Wholesale Electricity Market Design.* 2022.

[46] K. Fasshauer, F. Steffner, H.-J. Dauerstedt, M. Albrecht, and E. Wernicke, "Verfahren zum Polen von Kupfer mit Wasserstoff und Stickstoff: European Patent," EP 0 992 597 B1.

[47] FfE München, Ed., *Daily updated Specific Greenhouse Gas Emissions of the German Electricity Mix*, München, 2022. [Online]. Available: https://opendata.ffe.de/dataset/specific-greenhouse-gas-emissions-of-the-electricity-mix%5C (visited on 09/23/2022).

[48] FfE München, Ed., *Entwicklung der Energie- und CO2-Preise*, München, 2022. [Online]. Available: https://www.ffe.de/veroeffentlichungen/entwicklung-der-energie-und-co2-preise-2022/ (visited on 10/13/2022).

[49] FfE München, Ed., *Veränderungen der Merit Order und deren Auswirkungen auf den Strompreis*, München, 2022. [Online]. Available: https://www.ffe.de/veroeffentlichungen/veraenderungen-der-merit-order-und-deren-auswirkungen-auf-den-strompreis/ (visited on 11/23/2022).

[50] FfE München, Ed., *Was ist der Regelarbeitsmarkt (RAM)?* München, 2022. [Online]. Available: https://www.ffe.de/veroeffentlichungen/was-ist-der-regelarbeitsmarkt-ram/ (visited on 11/22/2022).

[51] FfE München, Ed., *Was ist Netzdienlichkeit?* München, 2021. [Online]. Available: https://www.ffe.de/veroeffentlichungen/was-ist-netzdienlichkeit/ (visited on 12/27/2022).

[52] Fraunhofer, Ed., *Cost Forecast for Low-Temperature Electrolysis - Technology Driven Bottom-Up Prognosis for PEM and Alkaline Water Electrolysis Systems.* Freiburg, 2022.

[53] M. Friedrich, *Energie des Nordens kauft Windgas-Elektrolyseur*, Greenpeace Energy eG, Ed., 2019. [Online]. Available: https://green-planet-energy.de/news-politik/publikationen/pressebereich/artikel/energie-des-nordens-kauft-windgas-elektrolyseur.html (visited on 10/19/2022).

[54] K. Ganz and T. Kern, *Was ist der Regelarbeitsmarkt (RAM)?* 2022. [Online]. Available: https://www.ffe.de/veroeffentlichungen/was-ist-der-regelarbeitsmarkt-ram/ (visited on 11/23/2022).

[55] Gasnetz Hamburg GmbH, Ed., *Netzbezogene Daten: Abrechnungsbrennwert/Gasbeschaffenheit/Gas analyse*, Hamburg, 2022. [Online]. Available: https://www.gasnetz-hamburg.de/fuer-unternehmen/netzzugang-nutzung/netzbezogene-daten (visited on 10/05/2022).

[56] German Environment Agency, Ed., *Power-to-Liquids: Potentials and Perspectives for the Future Supply of Renewable Aviation Fuel*. Dessau-Roßlau, 2016.

[57] M. Graebing and M. Wolfram, "Das Schaufenster für intelligente Energie aus dem Nordosten Deutschlands 2017 - 2020," *WindNODE*, 2020.

[58] K.-H. Grote and J. Feldhusen, Eds., *Dubbel Taschenbuch für den Maschinenbau*, 24th ed. Berlin, Heidelberg: Springer Vieweg, 2014.

[59] N. Gunantara, "A review of multi-objective optimization: Methods and its applications," *Cogent Engineering*, vol. 5, no. 1, 2018. DOI: 10.1080/23311916.2018.1502242.

[60] L. L. Gurobi Optimization, *Gurobi Optimizer Reference Manual*, 2022. [Online]. Available: www.gurobi.com (visited on 10/11/2022).

[61] L. L. Gurobi Optimization, *Mixed-Integer Programming (MIP) - A Primer on the Basics*, 2022. [Online]. Available: https://www.gurobi.com/resources/mixed-integer-programming-mip-a-primer-on-the-basics/ (visited on 11/26/2022).

[62] H-TEC Systems GmbH, Ed., *Data Sheet - Parameter 4 MW HCS*, Augsburg, 2022. [Online]. Available: https://www.h-tec.com/produkte/detail/h-tec-pem-elektrolyseur-hcs/10-mw-hcs/ (visited on 12/13/2022).

[63] H&R GROUP, *Hansen & Rosenthal weiht weltgrössten Elektrolyseur für umweltfreundlichen Wasserstoff ein*, 2017. [Online]. Available: https://www.hur.com/de/veranstaltungen/thema/hansen-rosenthal-weiht-weltgroessten-elektrolyseur-fuer-umweltfreundlichen-wasserstoff-ein (visited on 12/19/2022).

[64] Hamburg Wasser, *Allgemeiner Wasserpreis je Kubikmeter*, 2022. [Online]. Available: https://www.hamburgwasser.de/privatkunden/service/gebuehren-abgaben-preise (visited on 05/06/2022).

[65] C. R. Harris, K. J. Millman, S. J. van der Walt, *et al.*, "Array programming with NumPy," *Nature*, vol. 585, no. 7825, pp. 357–362, 2020. DOI: 10.1038/s41586-020-2649-2.

[66] W. E. Hart, Jean-Paul Watson, and David L. Woodruff, *Pyomo: modeling and solving mathematical programs in Python.* (Mathematical Programming Computation). 2011, vol. 3.

[67] P. Haug, "Experimental and theoretical investigation of gas purity in alkaline water electrolysis," Dissertation, Clausthal University of Technology, Clausthal, 2019. [Online]. Available: https://dokumente.ub.tu-clausthal.de/servlets/MCRFileNodeServlet/clausthal_derivate_00000598/Db114036.pdf (visited on 12/22/2022).

[68] H.-M. Henning and A. Palzer, "What will the Energy Transformation Cost? Pathways for transforming the German energy system by 2050," *Fraunhofer ISE*, 2015.

[69] M. Hirscher, Ed., *Handbook of Hydrogen Storage*. Weinheim: Wiley-VCH Verlag GmbH & Co. KGaA, 2010. [Online]. Available: https://application.wiley-vch.de/books/sample/3527322736_c01.pdf (visited on 11/19/2022).

[70] M. Hölling, M. Grasenack, L. Jürgens, and H. Schäfers, "Projektbericht "Windstahl aus Norddeutschland" (WiSaNo)," 2021. DOI: 10.13140/RG.2.2.12721.10084. [Online]. Available: http://rgdoi.net/10.13140/RG.2.2.12721.10084 (visited on 03/24/2022).

[71] J. Huber, K. Lohmann, M. Schmidt, and C. Weinhardt, "Carbon efficient smart charging using forecasts of marginal emission factors," *Journal of Cleaner Production*, vol. 284, p. 124 766, 2021. DOI: 10.1016/j.jclepro.2020.124766.

[72] International Energy Agency, Ed., *Global Hydrogen Review*. Abu Dhabi, 2021.

[73] International Energy Agency, Ed., *Projected Costs of Generating Electricity 2020*. Paris, 2020. [Online]. Available: https://www.iea.org/reports/projected-costs-of-generating-electricity-2020.

[74] International Energy Agency, Ed., *The Future of Hydrogen*. Paris, 2019. [Online]. Available: https://www.iea.org/reports/the-future-of-hydrogen (visited on 10/12/2022).

[75] International Renewable Energy Agency, Ed., *Demand-side flexibility for power sector transformation*. Abu Dhabi, 2019. [Online]. Available: https://www.irena.org/-/media/Files/IRENA/Agency/Publication/2019/Dec/IRENA_Demand-side_flexibility_2019.pdf (visited on 10/10/2022).

[76] International Renewable Energy Agency, Ed., *Green Hydrogen Cost Reduction: Scaling up Electrolysers to Meet the 1.5^{0}C Climate Goal*. Abu Dhabi, 2020. [Online]. Available: https://www.irena.org/publications/2020/Dec/Green-hydrogen-cost-reduction (visited on 08/05/2022).

[77] International Renewable Energy Agency, Ed., *Hydrogen: A renewable energy perspective*. Abu Dhabi, 2019. [Online]. Available: https://www.iea.org/reports/the-future-of-hydrogen.

[78] Investing.com, Ed., *Carbon Emissions Futures Historical Data*, 2022. [Online]. Available: https://www.investing.com/commodities/carbon-emissions-historical-data (visited on 12/01/2022).

[79] Investing.com, Ed., *Coal (API2) CIF ARA (ARGUS-McCloskey) Futures - (MTFc1)*, 2022. [Online]. Available: https://www.investing.com/commodities/coal-(api2)-cif-ara-futures-historical-data (visited on 12/01/2022).

[80] Investing.com, Ed., *Dutch TTF Natural Gas Futures Historische Daten*, 2022. [Online]. Available: https://www.investing.com/commodities/dutch-ttf-gas-c1-futures (visited on 12/13/2022).

[81] B. D. İskeceli, G. Kayakutlu, T. U. Daim, and A. Shaygan, "Optimization of battery and wind technologies: Case of power deviation penalties," *Technology in Society*, vol. 63, p. 101 322, 2020. DOI: 10.1016/j.techsoc.2020.101322.

[82] M. Kiaee, A. Cruden, D. Infield, and P. Chladek, "Utilisation of alkaline electrolysers to improve power system frequency stability with a high penetration of wind power," *IET Renewable Power Generation*, vol. 8, no. 5, pp. 529–536, 2012. DOI: 10.1049/iet-rpg.2012.0190.

[83] M. Klell, *Wasserstoff in der Fahrzeugtechnik: Erzeugung, Speicherung, Anwendung: ATZ/MTZ-Fachbuch*, 4th ed. Wiesbaden: Springer Vieweg, 2018.

[84] M. Kopp, *Strommarktseitige Optimierung des Betriebs einer PEM-Elektrolyseanlage: Dissertation*. Kassel: kassel university press GmbH, 2018.

[85] C. Kost, S. Shammugam, V. Fluri, D. Peper, A. D. Memar, and T. Schlegl, Eds., *Stromgestehungskosten Erneuerbare Energien: Juni*. Freiburg, 2021. [Online]. Available: https://www.ise.fraunhofer.de/content/dam/ise/de/documents/publications/studies/DE2021_ISE_Studie_Stromgestehungskosten_Erneuerbare_Energien.pdf.

[86] C. Kost, S. Shammugam, V. Jülch, H.-T. Nguyen, and T. Schlegl, Eds., *Stromgestehungskosten Erneuerbare Energien: März*. Freiburg, 2018. [Online]. Available: https://www.ise.fraunhofer.de/content/dam/ise/de/documents/publications/studies/DE2018_ISE_Studie_Stromgestehungskosten_Erneuerbare_Energien.pdf.

[87] D. Krieg, *Konzept und Kosten eines Pipelinesystems zur Versorgung des deutschen Straßenverkehrs mit Wasserstoff*. Aachen: Forschungszentrum Jülich, 2012.

[88] P. Kurzweil and O. Dietlmeier, *Elektrochemische Speicher: Superkondensatoren, Batterien, Elektrolyse-Wasserstoff, rechtliche Rahmenbedingungen* (Lehrbuch), 2., aktualisierte und erweiterte Auflage. Wiesbaden: Springer Vieweg, 2018. DOI: 10.1007/978-3-658-21829-4.

[89] Kyros Hydrogen Solutions GmbH, Ed., *Technical specifications: Kyros turnkey electrolyzer*, Föritztal, 2022. [Online]. Available: https://kyroshydrogensolutions.com/technology-decentralized-turnkey-hydrogen-solution/#technicalspecifications (visited on 12/13/2022).

[90] N. Lehmann and N. Lanzrath, "An estimation of hard coal transport costs in Germany, France, Italy and Spain," *International Ruhr Energy Conference (INREC)*, 2018. (visited on 11/09/2022).

[91] T. Longden, F. Jotzo, M. Prasad, and R. Andrews, "Green hydrogen production costs in Australia: implications of renewable energy and electrolyser costs: CCEP Working Paper 20-07, ZCEAP Working Paper ZCWP03-20," 2020.

[92] T. Makalska, R. Varfolomejeva, and R. Oleksijs, "The Impact of Wind Generation on the Spot Market Electricity Pricing," in *2018 IEEE International Conference on Environment and Electrical Engineering and 2018 IEEE Industrial and Commercial Power Systems Europe (EEEIC / I&CPS Europe)*, IEEE, 2018, pp. 1–6. DOI: 10.1109/EEEIC.2018.8494539.

[93] L. Mauler, F. Duffner, W. G. Zeier, and J. Leker, "Battery cost forecasting: a review of methods and results with an outlook to 2050," *Energy & Environmental Science*, vol. 14, no. 9, pp. 4712–4739, 2021. DOI: 10.1039/D1EE01530C.

[94] S. Milanzi, C. Spiller, B. Grosse, L. Hermann, J. Kochems, and J. Müller-Kirchenbauer, "Working Paper Energie und Ressourcen: Technischer Stand und Flexibilität des Power-to-Gas-Verfahrens," *Fachgebiet Energie- und Ressourcenmanagement*, 2018.

[95] Mukund_Bhagwat, *The Needs of the Industrial Electricity Consumers*, Corporate Energy and Climate Affairs Aurubis Belgium, Ed., Brussels, 2016. [Online]. Available: http://bestres.eu/wp-content/uploads/2016/11/2.-BestRES_IFIEC-and-Demand-Flexibility_Aurubis_Mukund-Bhagwat.pdf (visited on 11/23/2022).

[96] National Renewable Energy Laboratory, Ed., *Hydrogen Station Compression, Storage, and Dispensing Technical Status and Costs*. Denver, 2014. [Online]. Available: https://www.nrel.gov/docs/fy14osti/58564.pdf.

[97] Nexant Inc, Air Liquide, Argonne National Laboratory, Chevron Technology Venture, and Gas Technology Institute, Eds., *H2A Hydrogen Delivery Infrastructure Analysis Models and Conventional Pathway Options Analysis Results*. 2008.

[98] Next Kraftwerke GmbH, *Wissen: Unser Energie Glossar*, 2022. [Online]. Available: https://www.next-kraftwerke.de/wissen/netzfrequenz (visited on 11/20/2022).

[99] M. Nicolosi and M. Fürsch, "The Impact of an increasing share of RES-E on the Conventional Power Market — The Example of Germany," *Zeitschrift für Energiewirtschaft*, vol. 33, no. 3, pp. 246–254, 2009. DOI: 10.1007/s12398-009-0030-0.

[100] Oesterreichische Nationalbank, *Fremdwährungs-Referenzkurse zum Euro*, 2022. [Online]. Available: https://www.oenb.at/zinssaetzewechselkurse/zinssaetzewechselkurse (visited on 10/19/2022).

[101] G. Parks, R. Boyd, J. Cornish, and R. Remick, *Hydrogen Station Compression, Storage, and Dispensing Technical Status and Costs: Systems Integration*, 2014. DOI: 10.2172/1130621.

[102] J. Paulus, *Präqualifikation für den Regelenergiemarkt: Was ist das und wie funktioniert es?* Next Kraftwerke GmbH, Ed., 2013. [Online]. Available: https://www.next-kraftwerke.de/energie-blog/praequalifikation-regelenergiemarkt (visited on 11/22/2022).

[103] J. L. J. Pereira, G. A. Oliver, M. B. Francisco, S. S. Cunha, and G. F. Gomes, "A Review of Multi-objective Optimization: Methods and Algorithms in Mechanical Engineering Problems," *Archives of Computational Methods in Engineering*, vol. 29, no. 4, pp. 2285–2308, 2022. DOI: 10.1007/s11831-021-09663-x.

[104] M. Pieper, *Mathematische Optimierung: Eine Einführung in die kontinuierliche Optimierung mit Beispielen*. Wiesbaden: Springer Spektrum, 2017.

[105] Prognos, Öko-Institut, and Wuppertal-Institut, *Klimaneutrales Deutschland 2045. Wie Deutschland seine Klimaziele schon vor 2050 erreichen kann. Studie im Auftrag von Stiftung Klimaneutralität, Agora Energiewende und Agora Verkehrswende (inkl. Datenanhang, Version 1.0.)* 2021. [Online]. Available: https://www.agora-energiewende.de/veroeffentlichungen/klimaneutrales-deutschland-2045-datenanhang/.

[106] Prognos AG, Ed., *Kosten und Transformationspfade für strombasierte Energieträger: Studie im Auftrag des Bundesministeriums für Wirtschaft und Energie: Endbericht zum Projekt „Transformationspfade und regulatorischer Rahmen für synthetische Brennstoffe“*. [Online]. Available: https://www.bmwk.de/Redaktion/DE/Downloads/Studien/transformationspfade-fuer-strombasierte-energietraeger.pdf?__blob=publicationFile.

[107] Reiner Lemoine Institut, Ed., *Netzdienliche Wasserstofferzeugung: Studie zum Nutzen kleiner, dezentraler Elektrolyseure*. Berlin, 2022.

[108] M. Reuß, T. Grube, M. Robinius, P. Preuster, P. Wasserscheid, and D. Stolten, “Seasonal storage and alternative carriers: A flexible hydrogen supply chain model,” *Applied Energy*, vol. 200, pp. 290–302, 2017. DOI: 10.1016/j.apenergy.2017.05.050.

[109] M. Reuß, T. Grube, M. Robinius, and D. Stolten, “A hydrogen supply chain with spatial resolution: Comparative analysis of infrastructure technologies in Germany,” *Applied Energy*, vol. 247, pp. 438–453, 2019. DOI: 10.1016/j.apenergy.2019.04.064.

[110] E. Rivard, M. Trudeau, and K. Zaghib, “Hydrogen Storage for Mobility: A Review,” *Materials*, vol. 12, no. 12, 2019. DOI: 10.3390/ma12121973.

[111] F. T. Röben, N. Schöne, U. Bau, M. A. Reuter, M. Dahmen, and A. Bardow, “Decarbonizing copper production by power-to-hydrogen: A techno-economic analysis,” *Journal of Cleaner Production*, vol. 306, pp. 127–191, 2021. DOI: 10.1016/j.jclepro.2021.127191.

[112] B. Rohland, “Massenbilanyierung der Anodenofen einer Kupferprimärhütte,” Diplomarbeit, Montanuinversität Leoben, Montanuinversität Leoben, 2009.

[113] A. Ryota Keeley, K. Matsumoto, K. Tanaka, Y. Sugiawan, and S. Managi, “The Impact of Renewable Energy Generation on the Spot Market Price in Germany: Ex-Post Analysis using Boosting Method,” *The Energy Journal*, vol. 41, no. 01, 2020. DOI: 10.5547/01956574.41.SI1.akee.

[114] Sachverständigenrat für Umweltfragen, Ed., *Wasserstoff im Klimaschutz: Klasse statt Masse: Stellungnahme*. Berlin, 2021.

[115] M. Schalenbach, G. Tjarks, M. Carmo, W. Lueke, M. Mueller, and D. Stolten, “Acidic or Alkaline? Towards a New Perspective on the Efficiency of Water Electrolysis,” *Journal of The Electrochemical Society*, vol. 163, no. 11, F3197–F3208, 2016. DOI: 10.1149/2.0271611jes.

[116] M. E. Schlesinger, M. J. King, and K. C. Sole, *Extractive Metallurgy of Copper*, 65. Aufl. Amsterdam: Elsevier, 2011.

[117] C. Schütte, N. Neubauer, F. Röben, *et al.*, “Decarbonization of the Metal Industry in Hamburg - Demand, Efficiency and Costs of Green Hydrogen,” *European Energy Markets Conference (EEM22)*, 2022. DOI: 10.13140/RG.2.2.15874.96961.

[118] N. Seckinger, "Methodische Weiterentwicklung dynamischer, prospektiver Treibhausgasemissionsfaktoren zur Analyse von Technologien der Sektorkopplung," Dissertation, Universität Stuttgart, Stuttgart, 2021. DOI: 10.18419/opus-12172.

[119] A. Seidler, *„FOKUS Nachhaltigkeit": Aurubis veröffentlicht umfangreichen Nachhaltigkeitsbericht: Pressemitteilung*, Aurubis AG, Ed., 2021. [Online]. Available: https://www.aurubis.com/medien/pressemitteilungen/pressemitteilungen-2021/-FOKUS-Nachhaltigkeit---Nachhaltigkeitsbericht (visited on 04/10/2022).

[120] T. Seilnacht, *Bildungsenthalpien (DHB) und Entropien (S0)*, Gwatt, 2022. [Online]. Available: https://www.seilnacht.com/Lexikon/dhtabell.htm.

[121] T. Senoner, H. Aghaie, and R. Wendtner, *Das EU-Strommarktdesign unter der Lupe*, Wien Energie GmbH, Ed., Wien, 2021. [Online]. Available: https://positionen.wienenergie.at/blog/strommarktdesign/ (visited on 11/23/2022).

[122] L. Sens, Y. Piguel, U. Neuling, S. Timmerberg, K. Wilbrand, and M. Kaltschmitt, "Cost minimized hydrogen from solar and wind – Production and supply in the European catchment area," *Energy Conversion and Management*, no. 265, 2022. DOI: 10.1016/j.enconman.2022.115742.

[123] Siemens Energy AG, Ed., *Silyzer 300: The next paradigm of PEM electrolysis*, Erlangen, 2020. [Online]. Available: https://assets.siemens-energy.com/siemens/assets/api/uuid:a193b68f-7ab4-4536-abe2-c23e01d0b526/datasheet-silyzer300.pdf (visited on 12/07/2022).

[124] R. Sioshansi, P. Denholm, J. Arteaga, *et al.*, "Energy-Storage Modeling: State-of-the-Art and Future Research Directions," *IEEE Transactions on Power Systems*, vol. 37, no. 2, pp. 860–875, 2022. DOI: 10.1109/TPWRS.2021.3104768.

[125] T. Smolinka, N. Wiebe, S. Philip, *et al.*, "Studie IndWEDe: Industrialisierung der Wasserelektrolyse in Deutschland: Chancen und Herausforderungen für nachhaltigen Wasserstoff für Verkehr, Strom und Wärme," 2018. [Online]. Available: https://www.now-gmbh.de/wp-content/uploads/2020/09/indwede-studie_v04.1.pdf.

[126] J. A. Snyman and D. N. Wilke, *Practical Mathematical Optimization: Basic Optimization Theory and Gradient-Based Algorithms*, 2nd ed. Cham: Springer Nature, 2018.

[127] Spyder Doc Contributors, *Welcome to Spyder's Documentation*, 2022. [Online]. Available: https://docs.spyder-ide.org/current/index.html (visited on 10/11/2022).

[128] Statistisches Bundesamt (Destatis), *Preisentwicklung in den EU-Staaten*, 2022. [Online]. Available: https://www.destatis.de/Europa/DE/Thema/Wirtschaft-Finanzen/Inflation.html#:~:text=Die%20Inflationsrate%20in%20der%20EU,Jahresdurchschnitt%20bei%202%2C9%20%25. (visited on 10/19/2022).

[129] Stromnetz Hamburg GmbH, *Preisblatt für den Anschluss an das Niederspannungsnetz*, Stromnetz Hamburg GmbH, Ed., Hamburg, 2022. [Online]. Available: https://www.stromnetz-hamburg.de/fuer-bauherren/spannungsebenen/niederspannung (visited on 10/20/2022).

[130] The pandas development team, *Python Pandas*, 2022. [Online]. Available: pandas.pydata.org.

[131] Thomas A Caswell, Antony Lee, Michael Droettboom, *et al.*, *matplotlib/matplotlib: REL: v3.6.0*, 2022. DOI: 10.5281/zenodo.7084615.

[132] thyssenkrupp Uhde Chlorine Engineers, Ed., *Hydrogen from large-scale electrolysis*, Dortmund, 2019. [Online]. Available: https://ucpcdn.thyssenkrupp.com/_legacy%20/UCPthyssenkruppBAISUhdeChlorine%20Engineers%20/assets.files/products/%20water_electrolysis/tk_19_0820_hydrogen_broschuere_2019_03.pdf (visited on 12/22/2022).

[133] G. H. Tjarks, *PEM-electrolysis-systems for the integration in power-to-gas applications*. RWTH Aachen University, 2017. DOI: 10.18154/RWTH-2017-04470.

[134] W. G. Tuschewitzki, "Modeling and Evaluation of the Dynamic Behavior of Electrolyzers with Fluctuating Energy Supply," Project Work, TU Hamburg, Hamburg, 2021.

[135] W. G. Tuschewitzki, "Optimized Hydrogen Production – A Techno-Economic Analysis of Low- and High-Temperature Electrolysis," Master Thesis, TU Hamburg, Hamburg, 2022.

[136] UBA, *Treibhausgas-Emissionen in Deutschland*, 2022. [Online]. Available: https://www.umweltbundesamt.de/daten/klima/treibhausgas-emissionen-in-deutschland#nationale-und-europaische-klimaziele (visited on 05/24/2022).

[137] Umweltbundesamt, Ed., *Daten und Fakten zu Braun- und Steinkohlen*. 2017. [Online]. Available: https://www.umweltbundesamt.de/sites/default/files/medien/1410/publikationen/171207_uba_hg_braunsteinkohle_bf.pdf.

[138] Umweltbundesamt, *Schutz vor Carbon Leakage*, 2022. [Online]. Available: https://www.dehst.de/DE/Europaeischer-Emissionshandel/Reform-Perspektiven/Carbon-Leakage-Schutz/carbon-leakage-schutz_node.html#:%C2%A0:text=Au%C3%9Ferdem%20wird%20in%20Deutschland%20und,Kommission%20ein%20Grenzausgleichsmechanismus%20eingef%C3%BChrt%20werden. (visited on 08/09/2022).

[139] G. van Rossum, *The Python language reference* (Documentation for Python), Release 3.0.1 [Repr.] Hampton, NH and Redwood City, Calif.: Python Software Foundation and SoHo Books, 2010, vol. Pt. 2.

[140] C. Varela, M. Mostafa, and E. Zondervan, "Modeling alkaline water electrolysis for power-to-x applications: A scheduling approach," *International Journal of Hydrogen Energy*, vol. 46, no. 14, pp. 9303–9313, 2021. DOI: 10.1016/j.ijhydene.2020.12.111.

[141] E. Vartiainen, G. Masson, C. Breyer, D. Moser, and E. Román Medina, "Impact of weighted average cost of capital, capital expenditure, and other parameters on future utility–scale PV levelised cost of electricity," *Progress in Photovoltaics: Research and Applications*, vol. 28, no. 6, pp. 439–453, 2020. DOI: 10.1002/pip.3189.

[142] Verein Deutscher Ingenieure, *Wirtschaftlichkeit gebäudetechnischer Anlagen: Grundlagen und Kostenberechnung*, Berlin, 2000.

[143] L. P. Wagner, Reinpold, Lasse, Matthias, L. Scholz, *et al.*, "Generic Model Structure for the Representation of Flexible Energy Resources and Their Joint Optimization," in *dtec.bw-Beiträge der Helmut-Schmidt-Universität / Universität der Bundeswehr Hamburg: Forschungsaktivitäten im Zentrum für Digitalisierungs- und Technologieforschung der Bundeswehr dtec.bw - Band 1 · 2022*, pp. 254–259.

[144] M. Waskom, "Seaborn: statistical data visualization," *Journal of Open Source Software*, vol. 6, no. 60, p. 3021, 2021. DOI: 10.21105/joss.03021.

[145] B. Willems and Y. Yu, "Bidding and Investment in Wholesale Electricity Markets: Pay-as-Bid versus Uniform-Price Auctio," 2022.

[146] T. Willner, *Lecture Script: Biofuels: 2.4.3 Compression*. Hamburg: HAW Hamburg.

[147] P. Wörner, A. Müller, and D. Sauerwein, "Dynamische CO2 –Emissionsfaktoren für den deutschen Strom–Mix," *Bauphysik*, vol. 41, no. 1, pp. 17–29, 2019. DOI: 10.1002/bapi.201800034.

[148] Wuppertal Institut and DIW Econ, Eds., *Bewertung der Vor- und Nachteile von Wasserstoffimporten im Vergleich zur heimischen Erzeugung*. 2020. [Online]. Available: https://wupperinst.org/fa/redaktion/downloads/projects/LEE-H2-Studie.pdf (visited on 10/12/2022).

[149] B. Zakeri, I. Staffell, P. Dodds, *et al.*, "Energy Transitions in Europe – Role of Natural Gas in Electricity Prices," *SSRN Electronic Journal*, 2022. DOI: 10.2139/ssrn.4170906.

Statutory Declaration

I herewith declare that I have composed the present thesis myself and without using any other than the cited sources and aids. Sentences or parts of sentences quoted literally are marked as such; other references with regard to the statement and scope are indicated by full details of the publications concerned. The thesis in the same or similar form has not been submitted to any examination body or published. This thesis was not yet, even in part, used in another examination or as a course performance. Furthermore, I declare that the submitted written (bound) copies of the present thesis and the version submitted on a data carrier are consistent with each other in contents.

03.07.23 N. Neu

Date, Nicolas Neubauer

Acknowledgements

The author of this work would like to thank his supervising tutor Carsten Schütte for the numerous discussions, suggestions and constructive criticism. Furthermore, the author would like to thank the supervising professor Dr. Marc Hölling and the supervisor Mike Blicker for their professional feedback and evaluations. Thanks are also to all persons who repeatedly gave me new ideas and suggestions in discussions. This includes the industry partner Aurubis and, in particular, the counterparts Luisa Genz, Kelly Westphal and Annemarie Bruns in charge of the Northern German Living Lab (NRL) project.

Last but not least, I would like to thank my colleagues and friends who contributed to this master thesis by proofreading it. Thereby I would like to point out my supervising tutor Carsten Schütte, my fellow student and colleague Hagen Barkow and especially my mother Doris Neubauer.

Date, Nicolas Neubauer

Appendix

Contents in appendix

List of figures in appendix

List of tables in appendix

A Gas composition

The gas composition is taken from the local gas distributor Gasnetz Hamburg GmbH [55]. These compositions can be used to calculate the actual reduction potential of natural gas (f_{red} in mol_{Cu_2O}/mol_{CH_4}). The average values from Gasnetz Hamburg are given in figure A.1. The corresponding values for the gas composition are summarized in table A.1 and A.2. The first two graphs show the main components of natural gas. The third graph is about the shares of CO_2, N_2 and H_2. The fourth graph is about the Wobbe Index, which is an indicator for the volumetric energy flow and is applied to characterize the natural gas quality [83].

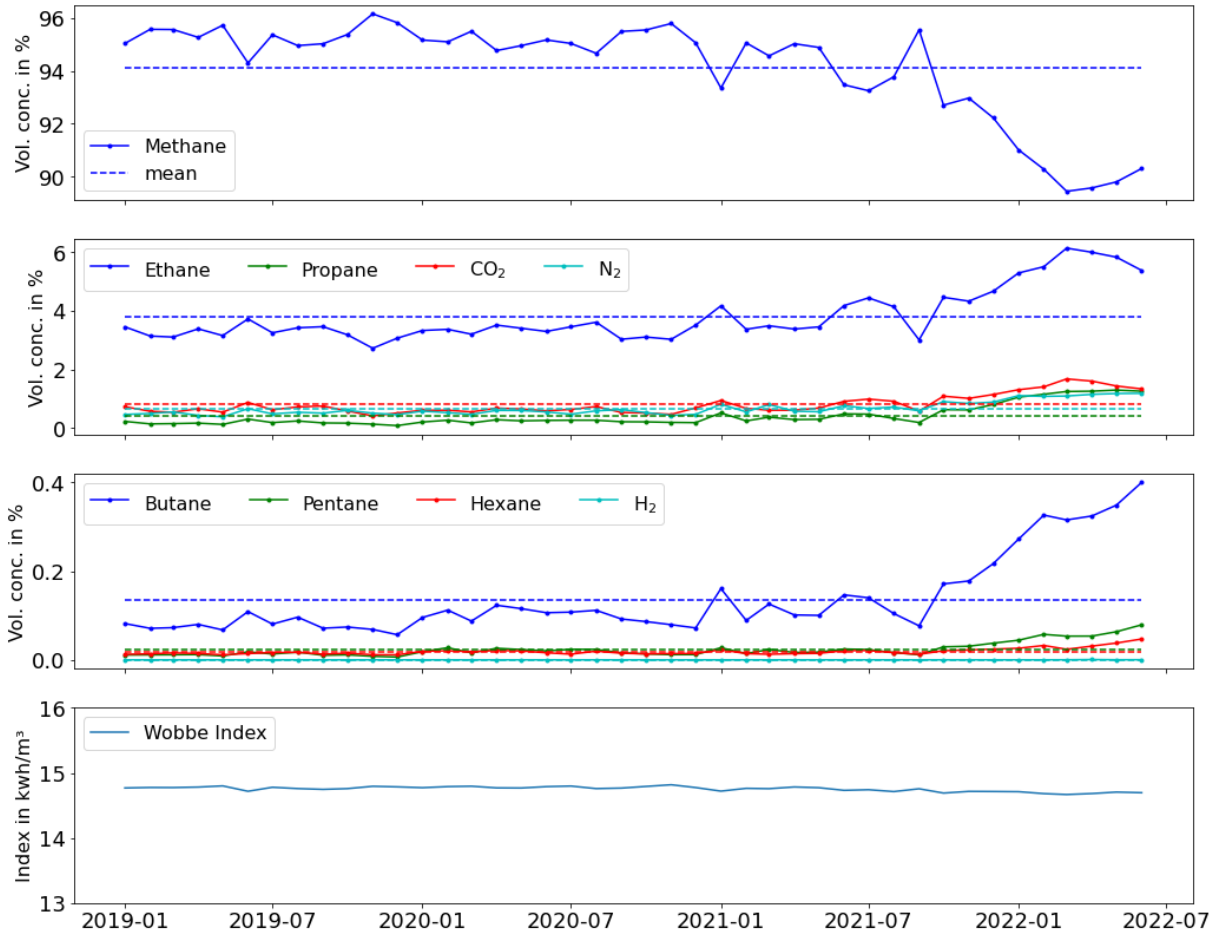

Figure A.1: Monthly gas composition and the specific averages as dashed lines at standard conditions in Hamburg plotted next to the Wobbe Index. Own visualization based on measurements provided by Gasnetz Hamburg [55].

The average x for each ci is calculated according to the formula 1 which includes the sum of the

monthly concentration of each component $x_{M,ci}$ divided by the number of months.

$$x_{av,comp} = \sum_{t=1}^{t_{end}=45} \frac{x_{M,ci}}{t_{end}} \tag{1}$$

Based on the averaged composition $x_{av,comp}$, given in table A.1 and A.2, the actual ratio formula of the "natural gas molecule" (C / H / N / O = x_C / x_H / x_N / x_O) in mol-% (consumed in Hamburg in the respective time frame) is calculated. This ratio formula can be calculated by applying formulas 2 to 5.

$$x_C = \sum_{ci}^{all} x_{C,ci} \tag{2}$$

$$x_H = \sum_{ci}^{all} x_{H,ci} \tag{3}$$

$$x_N = \sum_{ci}^{all} x_{N,ci} \tag{4}$$

$$x_O = \sum_{ci}^{all} x_{O,ci} \tag{5}$$

The ratio formula of the NG consumed in Hamburg during the respective time frame is determined by the equations above. This yields the results shown in equation 6.

$$x_C/x_H/x_N/x_O = 1.041/4.044/0.013/0.015 \quad mol-\% \tag{6}$$

The reaction equation for this is the ratio formula of the "natural gas molecule" is stated in the following equation 7.

$$C_{x_C}H_{x_H}N_{x_N}O_{x_O} + \nu_{Cu_2O}Cu_2O \longrightarrow \nu_{CO_2}CO_2 + \nu_{H_2O}H_2O + \nu_{N_2}N_2 + \nu_{Cu}Cu \tag{7}$$

The stochiometric factors ν for the components of natural gas are derived from the ratio formula in equation 6 by applying individual balances. The determination of the missing factors for equation 7 of are shown in the following equation 14. The variable element in equation 7 is the ν_{Cu_2O} copper oxide.

$$Product\ side: \tag{8}$$

$$\nu_{CO_2} = x_C \tag{9}$$

$$\nu_{H_2O} = \frac{x_H}{2} \tag{10}$$

$$\nu_{N_2} = \frac{x_N}{2} \tag{11}$$

$$\nu_{Cu} = \frac{\nu_{Cu_2O}}{2} \tag{12}$$

$$Educt\ side: \tag{13}$$

$$\nu_{Cu_2O} = 2 \cdot \nu_{CO_2} + 1 \cdot \nu_{H_2O} - x_O \tag{14}$$

The considerations explained in equations 1 to 14 yield to the reaction equation 15. With this equation, the actual reducing factor can be determined by dividing the stochiometric factor of the copper oxide by the stochiometric factor of natural gas which is one in this case. Therefore, the reduction potential of natural gas consumed in Hamburg during the respective time frame is reducing factor $f_{red} = 4.094\,mol_{Cu_2O}/mol_{CH_4}$.

$$C_{1.044}H_{4.044}N_{0.013}O_{0.015} + 4.094Cu_2O \longrightarrow 1.044CO_2 + 2.022H_2O + 0.013N_2 + 2 \cdot 4.094Cu \tag{15}$$

To calculate the CO_2–exhaust caused by burning the gas, a similar approach can be used. The reaction equation 16 is set up with the ratio formula for natural gas reacting with oxygen.

$$C_{1.044}H_{4.044}N_{0.013}O_{0.015} + \frac{4.094}{2}O_2 \longrightarrow 1.044CO_2 + 2.022H_2O + 0.013N_2 \tag{16}$$

Literature data such as the German federal office for economics determined an average CO_2–exhaust factor for natural gas to be $201.0\,g_{CO2}/kwh$ [8]. Transforming the CO_2–value of equation 16 to the same unit, a CO_2–factor of $201.2\,g_{CO2}/kwh$ is derived which fits the literature data. The averaged LHV of the NG discussed in this is calculated to be $10.20\,KWh/m^3_{NG}$ or $13.39\,kWh/kg_{NG}$ as shown in table A.2.

Table A.1: Measurement values provided by Gasnetz Hamburg in vol–% [55]. Note that the components Butan and Pentane are displayed as the sum of their isomers. The full data is available in the digital appendix

	CO_2	N_2	H_2	Methane	Ethane	Propane	Butane	Pentane	Hexane
2019-01	0.726	0.462	0.000	95.031	3.456	0.224	0.082	0.011	0.013
2019-02	0.570	0.495	0.000	95.565	3.141	0.139	0.071	0.011	0.014
2019-03	0.538	0.548	0.000	95.559	3.107	0.149	0.073	0.012	0.016
2019-04	0.655	0.430	0.000	95.262	3.386	0.165	0.080	0.012	0.014
2019-05	0.541	0.381	0.000	95.719	3.156	0.122	0.067	0.009	0.012
2019-06	0.872	0.657	0.000	94.297	3.726	0.303	0.109	0.018	0.014
2019-07	0.621	0.481	0.000	95.358	3.252	0.184	0.081	0.013	0.016
2019-08	0.720	0.537	0.000	94.952	3.423	0.239	0.096	0.017	0.017
2019-09	0.750	0.506	0.000	95.020	3.461	0.172	0.071	0.010	0.013
2019-10	0.581	0.602	0.000	95.371	3.184	0.164	0.074	0.011	0.015
2019-11	0.413	0.505	0.000	96.150	2.723	0.130	0.069	0.008	0.012
2019-12	0.511	0.458	0.000	95.817	3.069	0.081	0.057	0.006	0.011
2020-01	0.605	0.575	0.000	95.160	3.331	0.203	0.096	0.018	0.019
2020-02	0.605	0.521	0.000	95.093	3.370	0.266	0.112	0.027	0.021
2020-03	0.549	0.466	0.000	95.491	3.204	0.172	0.087	0.016	0.018
2020-04	0.679	0.601	0.000	94.763	3.515	0.281	0.123	0.026	0.021
2020-05	0.648	0.596	0.000	94.949	3.408	0.243	0.115	0.023	0.020
2020-06	0.585	0.547	0.000	95.166	3.298	0.258	0.106	0.020	0.016
2020-07	0.632	0.471	0.000	95.032	3.457	0.265	0.108	0.024	0.013
2020-08	0.732	0.585	0.000	94.660	3.613	0.265	0.112	0.024	0.020
2020-09	0.529	0.627	0.000	95.487	3.032	0.212	0.092	0.016	0.015
2020-10	0.511	0.524	0.000	95.541	3.107	0.209	0.086	0.013	0.014
2020-11	0.465	0.429	0.000	95.785	3.029	0.190	0.079	0.012	0.014
2020-12	0.685	0.464	0.000	95.057	3.515	0.182	0.072	0.012	0.014
2021-01	0.938	0.810	0.000	93.349	4.173	0.515	0.161	0.027	0.023
2021-02	0.669	0.549	0.000	95.054	3.372	0.242	0.089	0.014	0.014
2021-03	0.606	0.800	0.000	94.563	3.492	0.368	0.126	0.023	0.013
2021-04	0.605	0.573	0.000	95.023	3.380	0.286	0.101	0.017	0.014
2021-05	0.681	0.554	0.000	94.882	3.454	0.296	0.100	0.017	0.015
2021-06	0.909	0.760	0.000	93.470	4.182	0.482	0.146	0.024	0.021
2021-07	0.985	0.665	0.000	93.246	4.446	0.472	0.140	0.023	0.021
2021-08	0.913	0.715	0.000	93.771	4.144	0.323	0.104	0.016	0.016
2021-09	0.576	0.586	0.000	95.545	3.011	0.187	0.077	0.012	0.012
2021-10	1.086	0.899	0.000	92.702	4.465	0.624	0.171	0.029	0.021
2021-11	1.011	0.836	0.000	92.969	4.332	0.617	0.178	0.031	0.022
2021-12	1.143	0.883	0.000	92.222	4.672	0.800	0.217	0.038	0.024
2022-01	1.307	1.104	0.000	91.012	5.296	1.051	0.272	0.044	0.026
2022-02	1.405	1.080	0.000	90.280	5.511	1.152	0.326	0.057	0.032
2022-03	1.676	1.092	0.000	89.445	6.146	1.246	0.315	0.053	0.024
2022-04	1.601	1.149	0.001	89.575	6.003	1.256	0.324	0.054	0.031
2022-05	1.434	1.177	0.000	89.801	5.836	1.295	0.349	0.063	0.038
2022-06	1.334	1.183	0.000	90.307	5.383	1.256	0.400	0.079	0.047
Average	0.800	0.664	0.000	94.131	3.816	0.412	0.136	0.024	0.019

Table A.2: Calculated values based on the measurements provided by Gasnetz Hamburg [55]. The standard density is considered to be at 0 °C and 1.013 bar.

	Standard Density in kg/m^3	Wobbe Index kWh/m^3	Lower Heating Value (LHV) in kg/kWh
2019-01	0.756	14.768	10.185
2019-02	0.751	14.775	10.156
2019-03	0.751	14.774	10.156
2019-04	0.754	14.781	10.180
2019-05	0.751	14.800	10.166
2019-06	0.762	14.717	10.196
2019-07	0.753	14.779	10.172
2019-08	0.757	14.758	10.184
2019-09	0.756	14.746	10.168
2019-10	0.752	14.758	10.154
2019-11	0.747	14.794	10.134
2019-12	0.749	14.785	10.144
2020-01	0.754	14.772	10.179
2020-02	0.755	14.789	10.202
2020-03	0.752	14.795	10.179
2020-04	0.759	14.769	10.204
2020-05	0.757	14.767	10.192
2020-06	0.755	14.788	10.193
2020-07	0.758	14.797	10.210
2020-08	0.759	14.758	10.201
2020-09	0.752	14.766	10.158
2020-10	0.751	14.791	10.171
2020-11	0.749	14.817	10.176
2020-12	0.755	14.774	10.186
2021-01	0.771	14.719	10.257
2021-02	0.756	14.762	10.181
2021-03	0.760	14.757	10.205
2021-04	0.756	14.783	10.197
2021-05	0.757	14.772	10.199
2021-06	0.770	14.731	10.255
2021-07	0.772	14.741	10.274
2021-08	0.769	14.712	10.218
2021-09	0.751	14.755	10.146
2021-10	0.777	14.689	10.275
2021-11	0.774	14.715	10.280
2021-12	0.782	14.714	10.329
2022-01	0.794	14.711	10.402
2022-02	0.793	14.681	10.424
2022-03	0.808	14.667	10.469
2022-04	0.800	14.682	10.435
2022-05	0.799	14.704	10.445
2022-06	0.799	14.695	10.438
Average	0.764	14.753	10.230

B Case Study: Standard H_2 demand

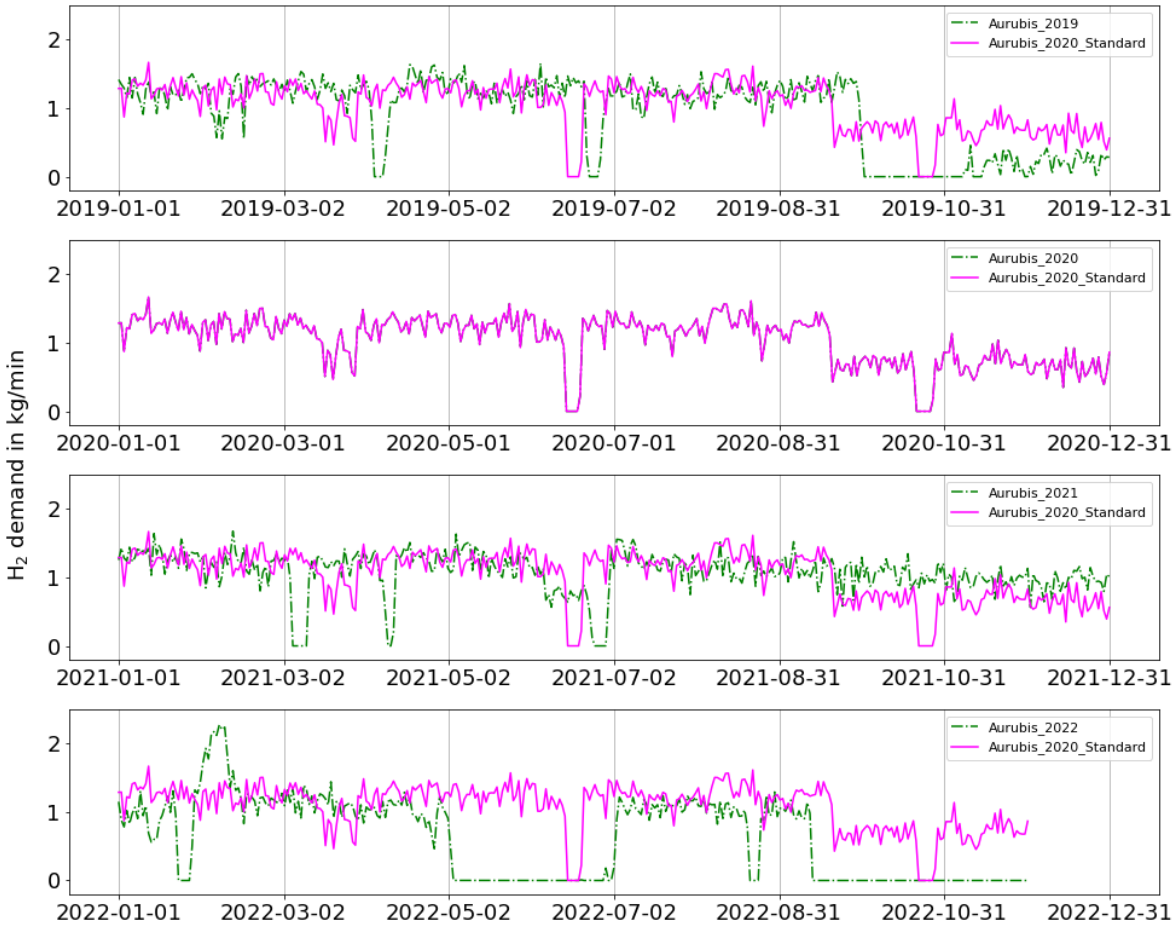

Figure B.1: The annual H_2 consumption time–series (daily averages) in the case study compared with the consumption of the standard year 2020. Note that the values for 2022 are only present in parts, the missing data is interpolated.

C Power system data

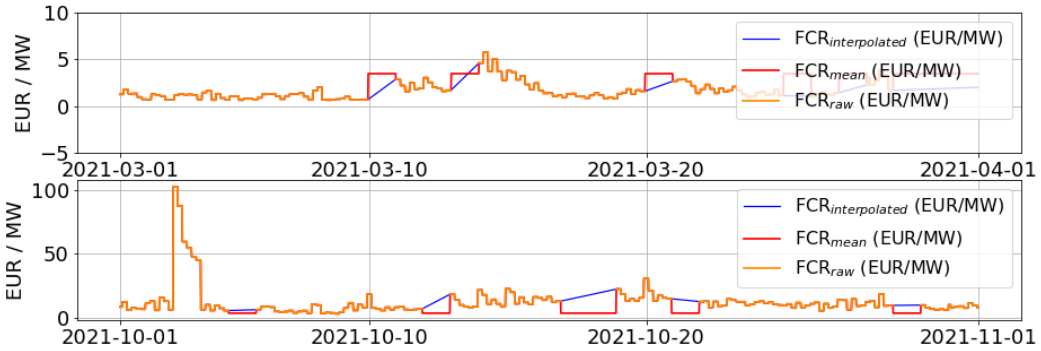

Figure C.1: Visiualization of NaN treatment by interpolation and average fill on the example of the FCR time–series.

Figure C.1 visualizes the interpolation applied to the FCR time–series data. In addition, an alternative method is shown which fills NaN with the global mean. This graphical plot should represent the interpolation applied to all the time–series data. Note, that the visualization does not achieve optimal results. This can be clearly seen in the time–series covering 2022 where the price spikes are completely ignored by the interpolation function. Although there are issues with the interpolation, the function is applied as it is the best alternative to the global mean.

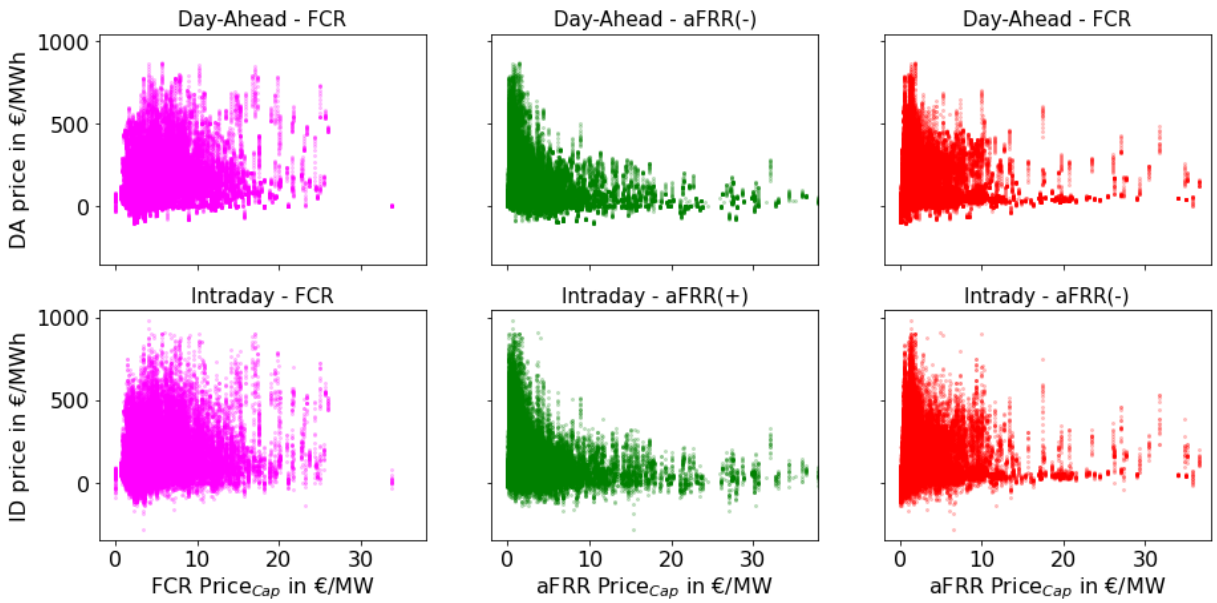

Figure C.2: Correlation between the auction results for AuxS and the spot market price for all observed years based on data from the BNetzA and EPEX [38], [47].

The figure extends the discussion of section 4.3.4 which aims to find a correlation between the AuxS and the spot market prices.

D Evaluation of the combined objective ($LCoH_2$ and $F_{CO2,H2}$)

The subsequent graphs illustrate the optimized timelines resulting from generic test data based on a MOO approach. The behavior of the optimization tool can be compared to the single–objective approach analyzed in section 6.2.

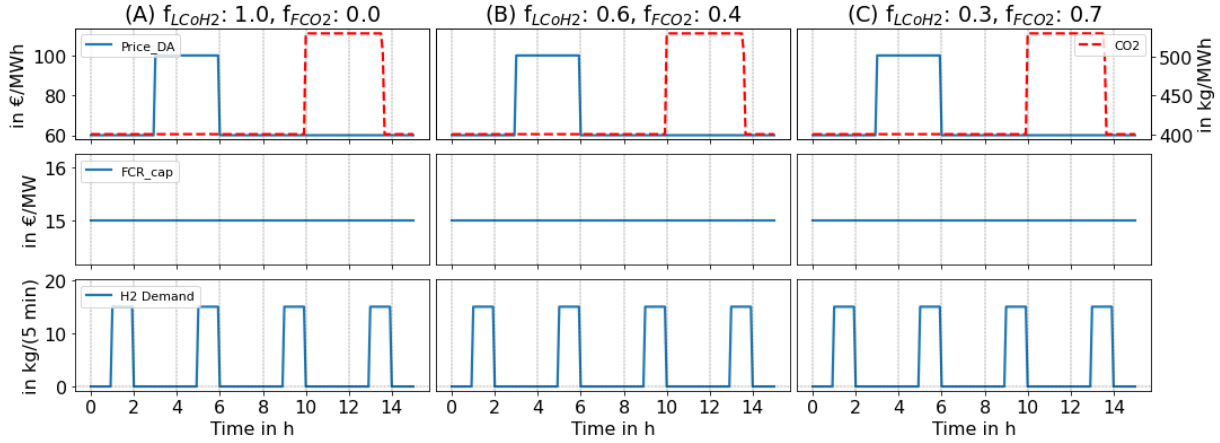

Figure D.1: Generic input data for the analysis of the MOO behavior for three different scenarios.

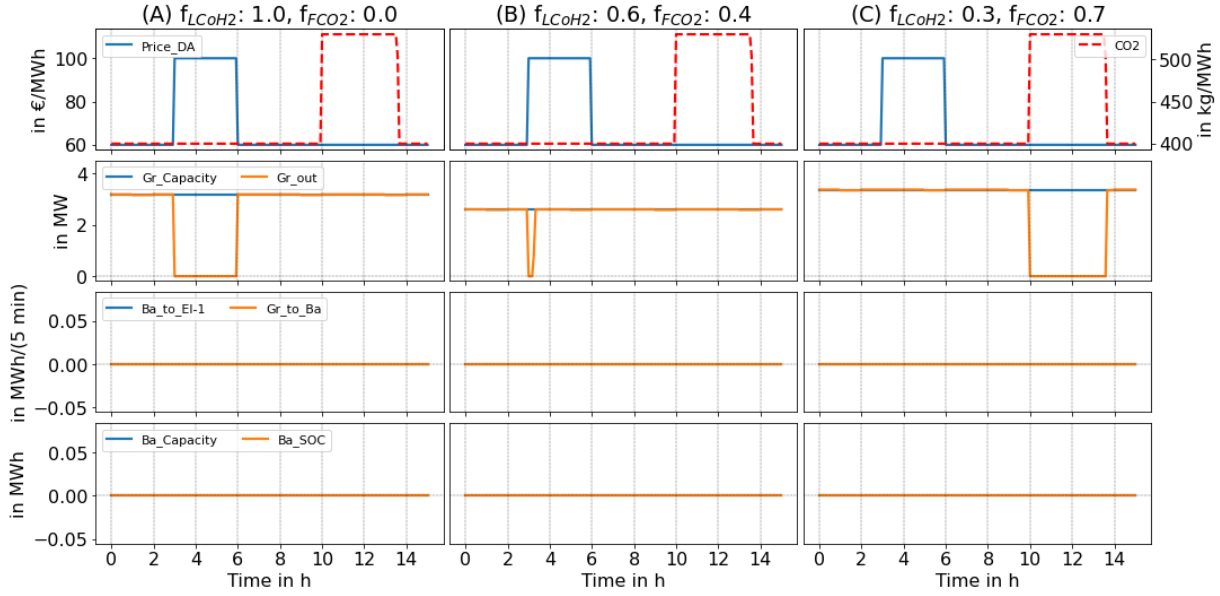

Figure D.2: Graphical evaluation of the results concering the Gr and the Ba dispatch for three defined test cases with an combined objective ($LCoH_2$ and $F_{CO2,H2}$, MOO approach).

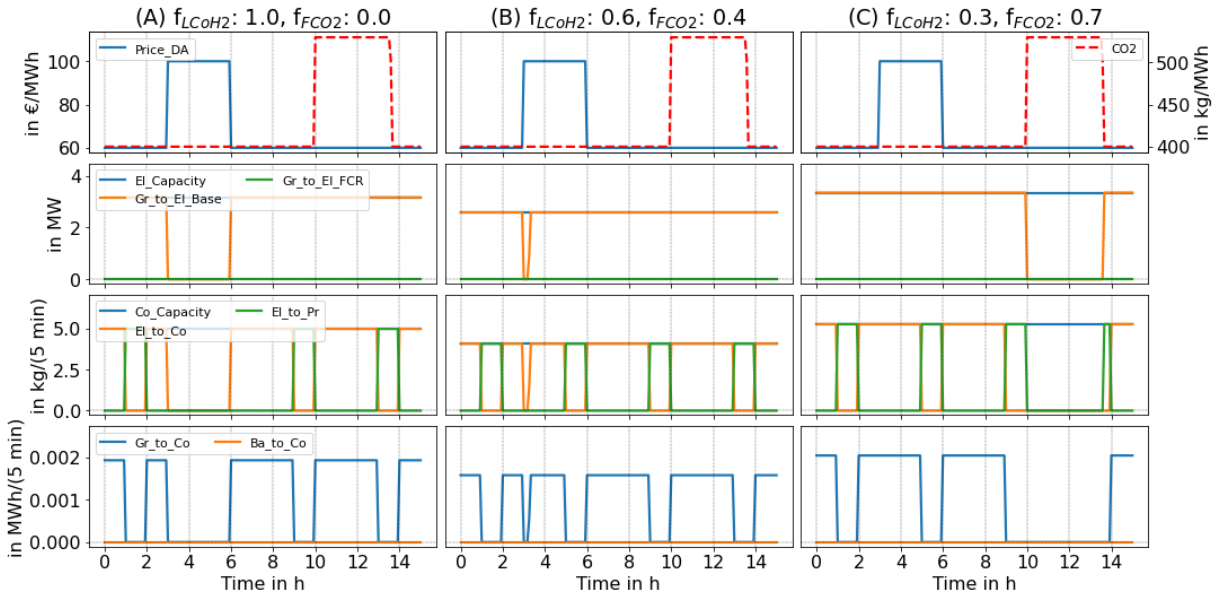

Figure D.3: Graphical evaluation of the results concering the El and the Co dispatch for three defined test cases with an combined objective ($LCoH_2$ and $F_{CO2,H2}$, MOO approach).

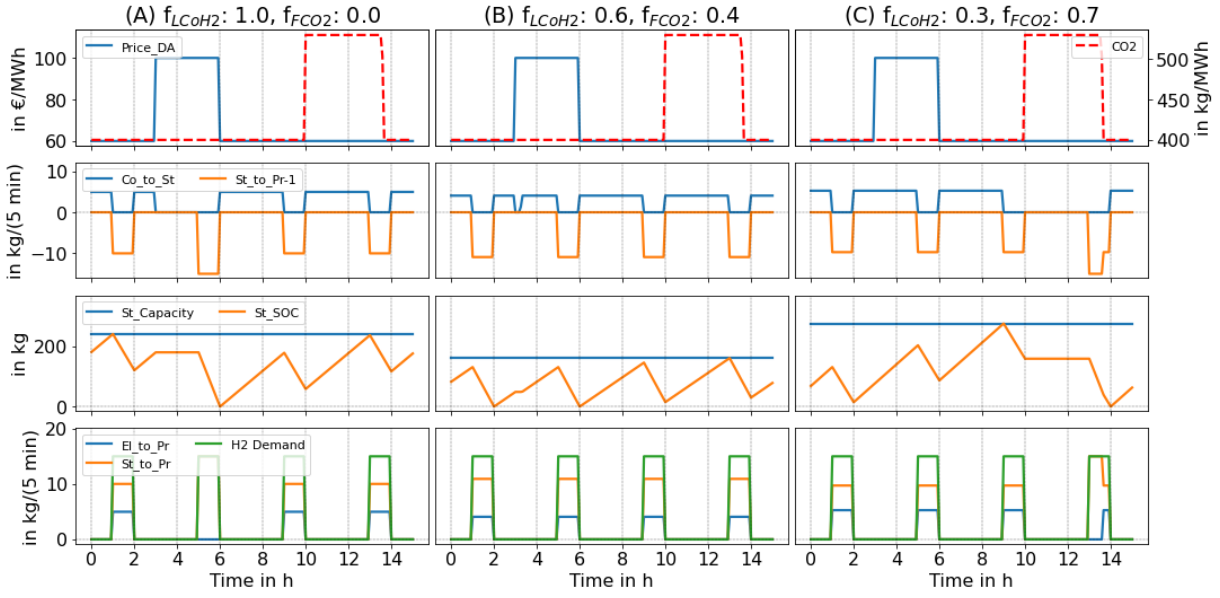

Figure D.4: Graphical evaluation of the results concering the St and the Pr dispatch for three defined test cases with an combined objective ($LCoH_2$ and $F_{CO2,H2}$, MOO approach).

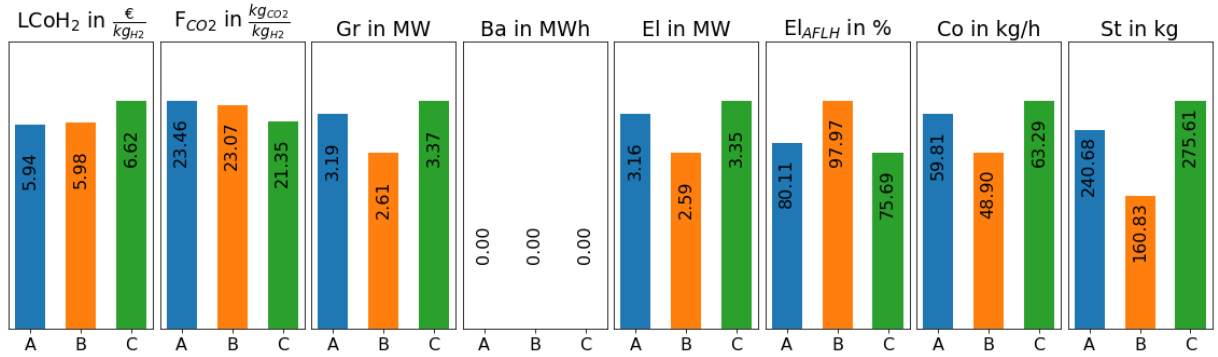

Figure D.5: Summary of the optimization tool results concering the objective values and the PtH_2 component sizes for three defined test cases with an combined objective ($LCoH_2$ and $F_{CO2,H2}$, MOO approach).

E Sensitivities of the resolution interval

The subsequent graphs include the sensitvity analysis of the resolution t_{int} discussed in section 7.1. The graphs inlude different scenarios for the year 2020 and 2022 and the two El technologies PEMEL and AEL.

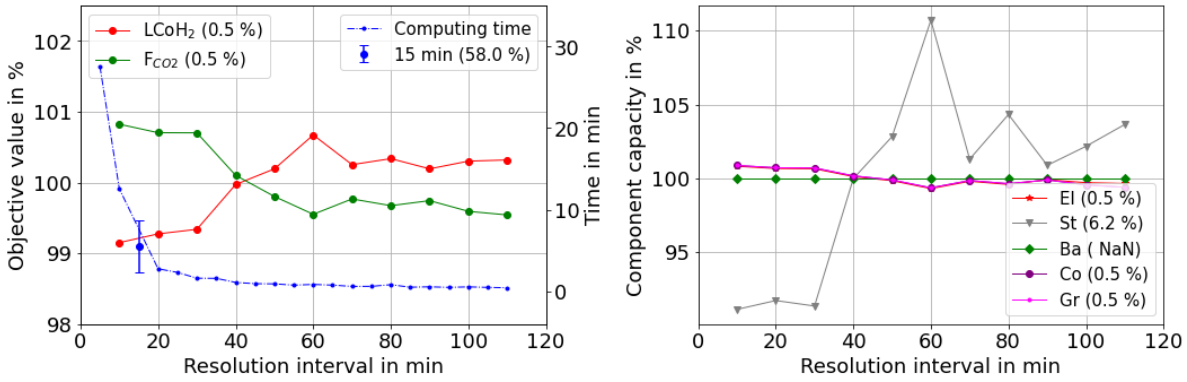

Figure E.1: The sensitivity of the normalized objective values $LCoH_2$ and F_{CO2} on the primary y–axis and the corresponding computing time on the secondary y–axis related to the resolution t_{int} (left). The resulting normalized component sizes (right). Both diagrams are based on an AEL operating in the year 2020. The StD_{rel} is shown in brackets.

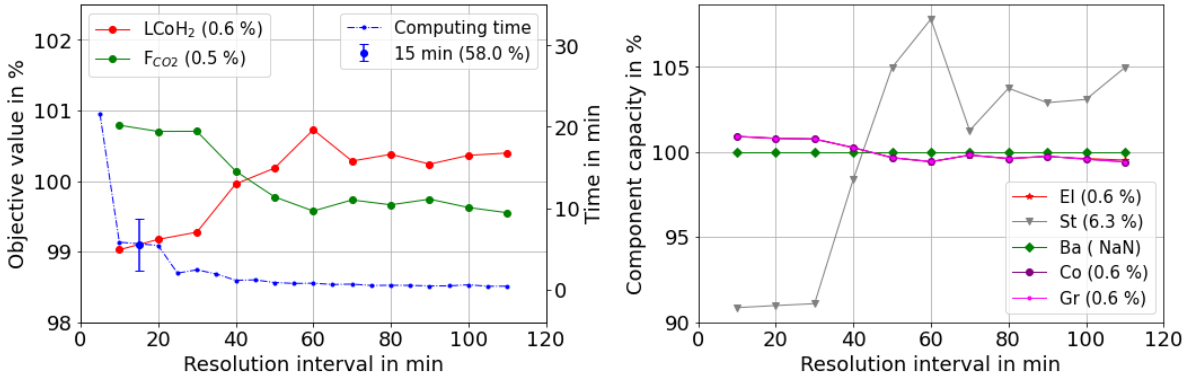

Figure E.2: The sensitivity of the normalized objective values $LCoH_2$ and F_{CO2} on the primary y–axis and the corresponding computing time on the secondary y–axis related to the resolution t_{int} (left). The resulting normalized component sizes (right). Both diagrams are based on an PEMEL operating in the year 2020. The StD_{rel} is shown in brackets.

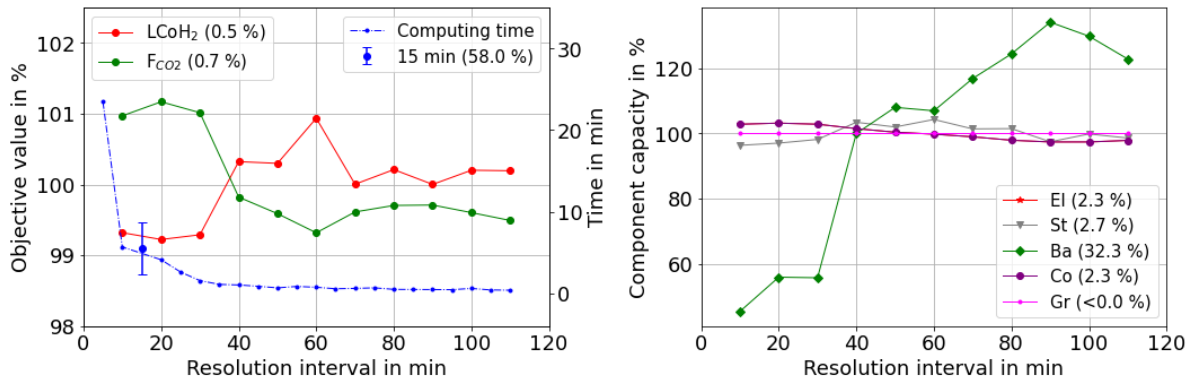

Figure E.3: The sensitivity of the normalized objective values $LCoH_2$ and F_{CO2} on the primary y–axis and the corresponding computing time on the secondary y–axis related to the resolution t_{int} (left). The resulting normalized component sizes (right). Both diagrams are based on an AEL operating in the year 2022. The StD_{rel} is shown in brackets.

F Sensitivities of the economic parameters

The subsequent graphs include the sensitvity analysis of the economic parameters discussed in section 7.2. The graphs inlude different scenarios for the year 2020 and 2022 and the two El technologies PEMEL and AEL.

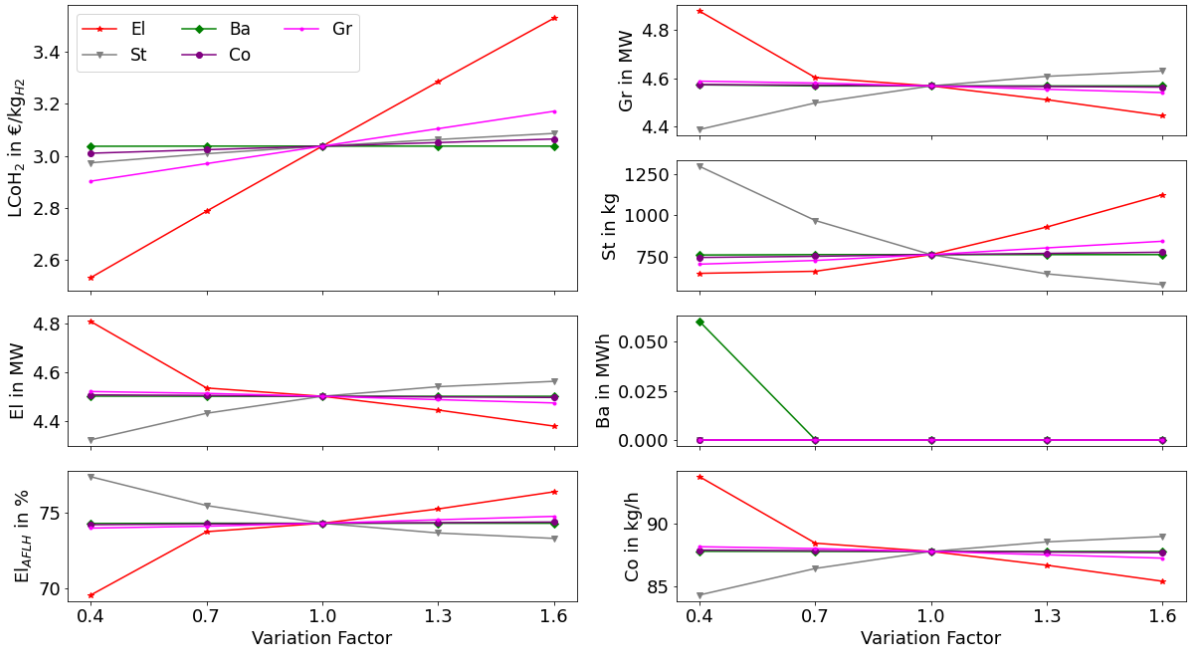

Figure F.1: Sensitivity of the optimization tool results in respect to an economic objective with regard to individual varied specific investment costs of the PtH_2 elements. Based on the year 2020 and an AEL system.

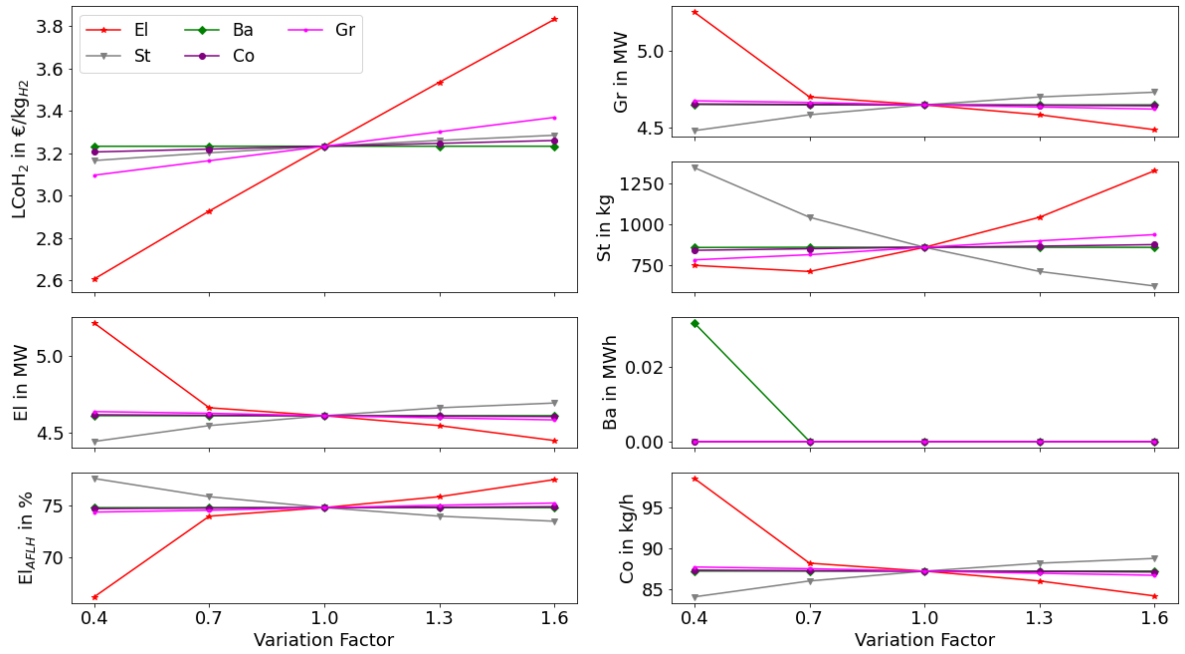

Figure F.2: Sensitivity of the optimization tool results in respect to an economic objective with regard to individual varied specific investment costs of the PtH_2 elements. Based on the year 2020 and a PEMEL system.

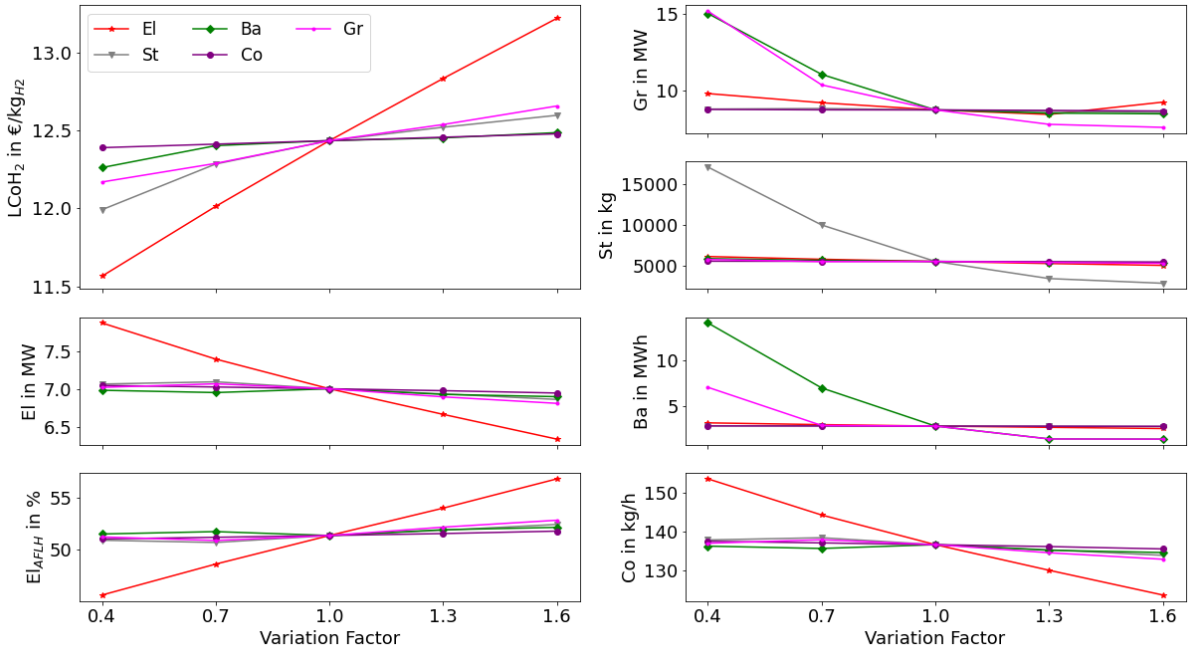

Figure F.3: Sensitivity of the optimization tool results in respect to an economic objective with regard to individual varied specific investment costs of the PtH_2 elements. Based on the year 2022 and an AEL system.

G Sensitivities of the technological parameters

The subsequent graphs include the sensitvity analysis of the technological parameters discussed in section 7.2. The graphs inlude different scenarios for the year 2020 and 2022 and the two El technologies PEMEL and AEL.

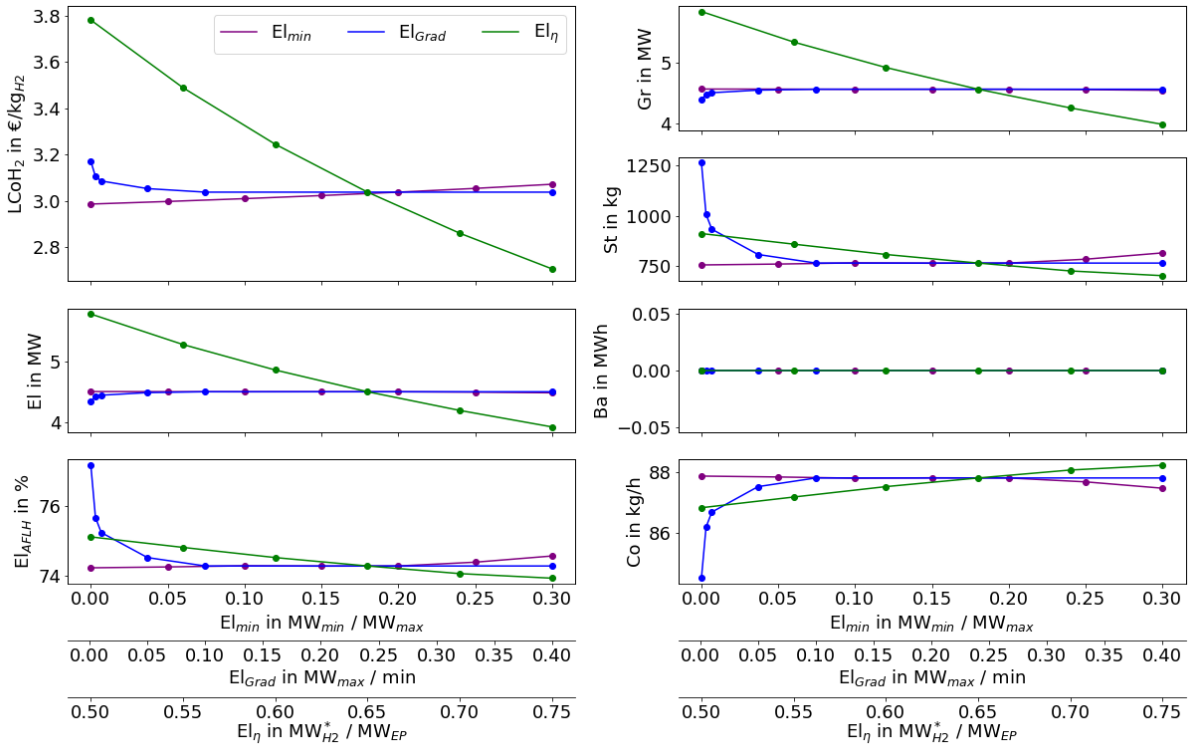

Figure G.1: Sensitivity of the optimization tool results for an economic objective with regard to the technical parameters of the El such as the El_{min}, the El_{Grad} and the efficiency El^*_η based on the LHV. Incorporating an AEL and electricity prices of the year 2020.

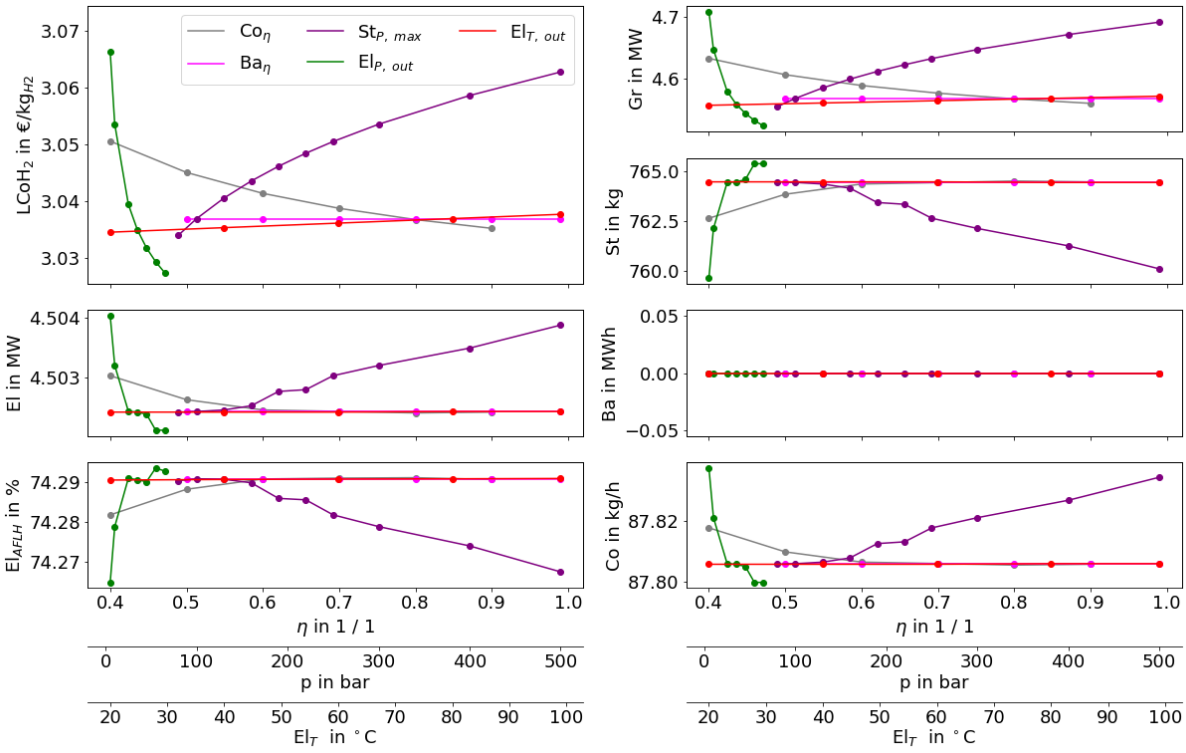

Figure G.2: Sensitivity of the results incorporating an economic objective with regard to the technical parameters of the compression stage covering the in and output pressures of the Co, its efficiency Co_η and the output temperature of the El. In addition, the Ba_η is analyzed. Incorporating an AEL and electricity prices of the year 2020.

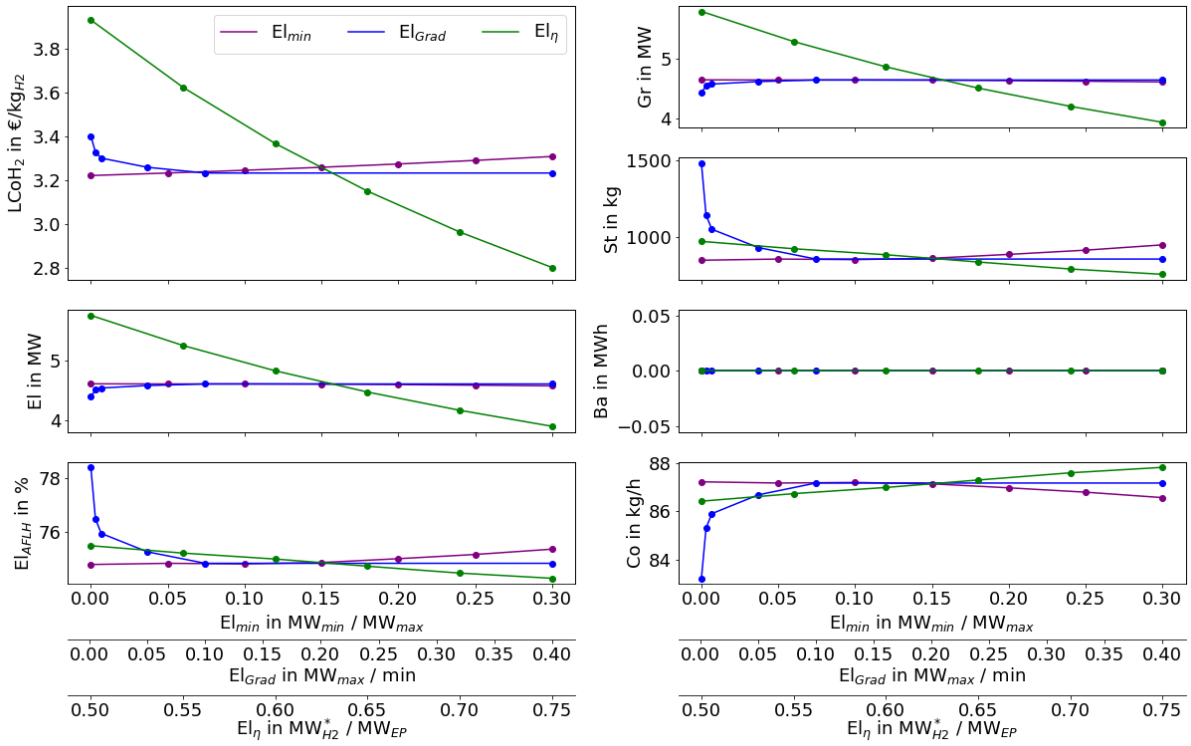

Figure G.3: Sensitivity of the optimization tool results for an economic objective with regard to the technical parameters of the El such as the El_{min}, the El_{Grad} and the efficiency El^*_η based on the LHV. Incorporating a PEMEL and electricity prices of the year 2020.

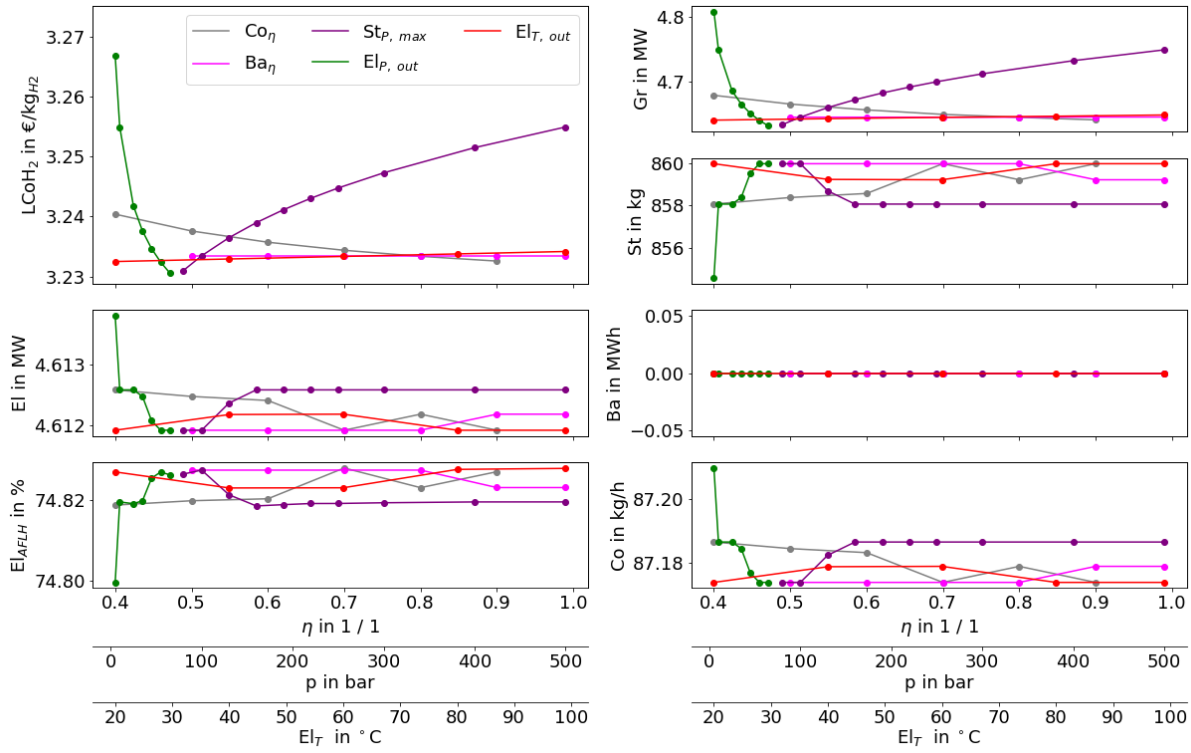

Figure G.4: Sensitivity of the results incorporating an economic objective with regard to the technical parameters of the compression stage covering the in and output pressures of the Co, its efficiency Co_η and the output temperature of the El. In addition, the Ba_η is analyzed. Incorporating a PEMEL and electricity prices of the year 2020.

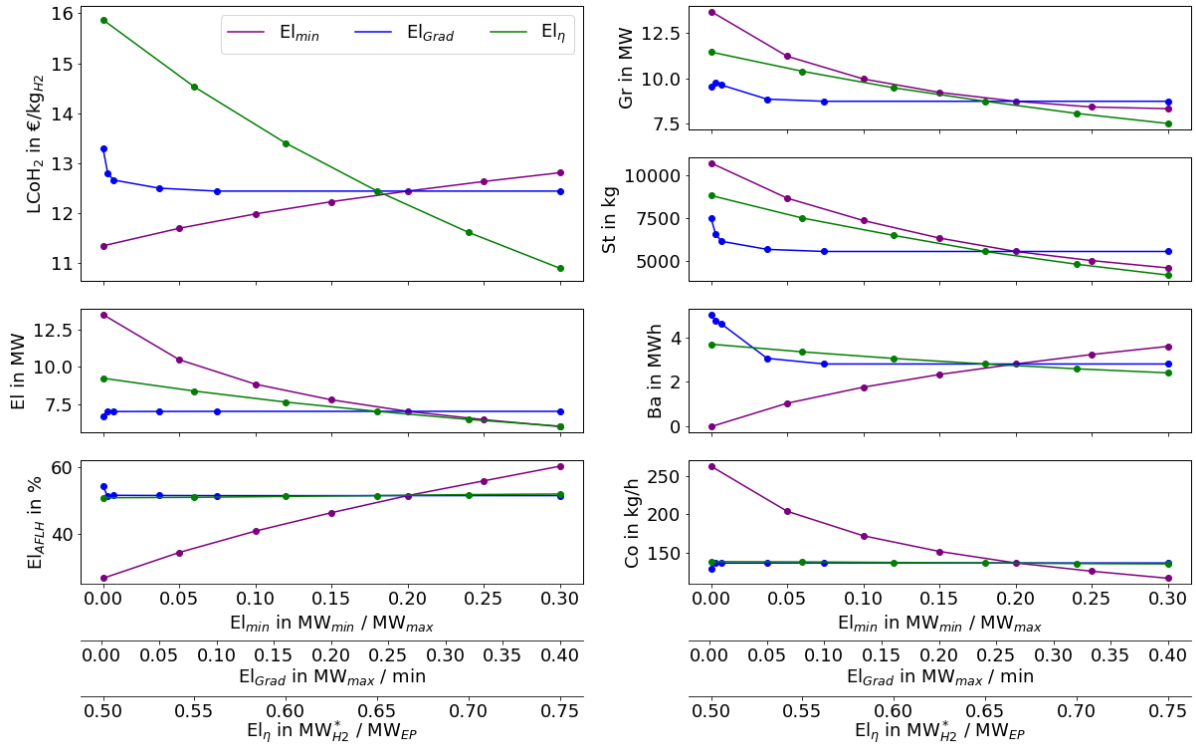

Figure G.5: Sensitivity of the optimization tool results for an economic objective with regard to the technical parameters of the El such as the El_{min}, the El_{Grad} and the efficiency El^*_η based on the LHV. Incorporating an AEL and electricity prices of the year 2022.

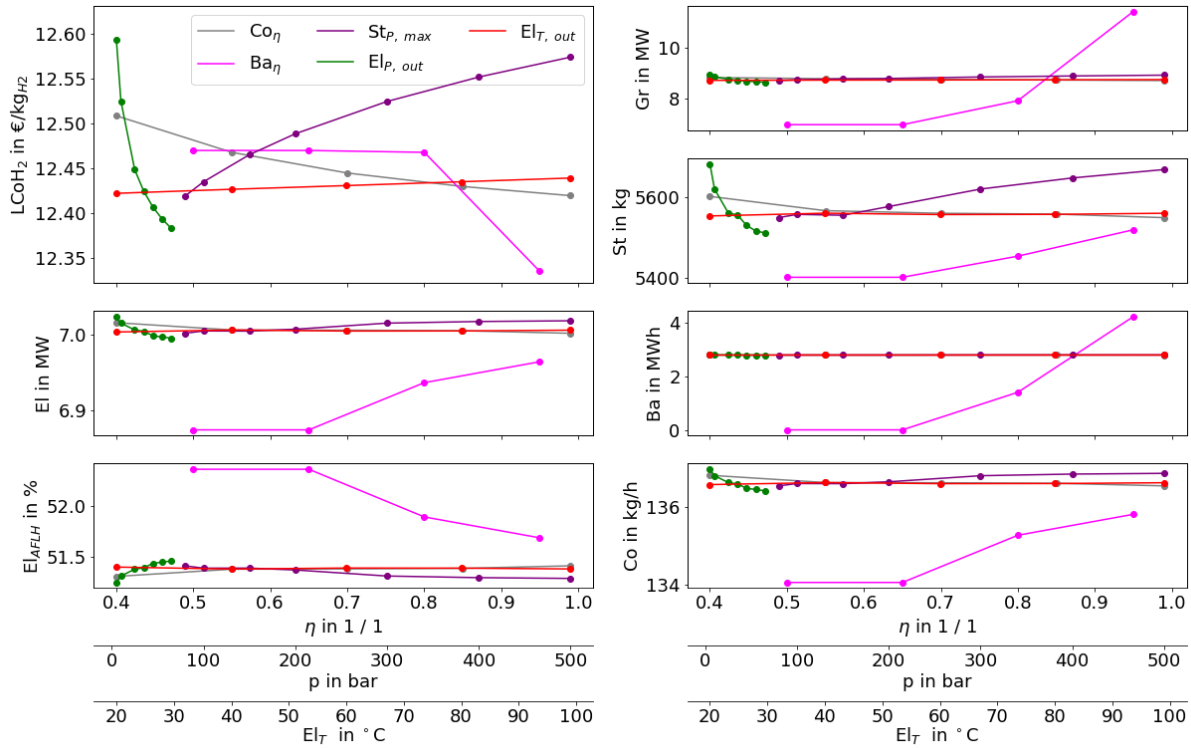

Figure G.6: Sensitivity of the results incorporating an economic objective with regard to the technical parameters of the compression stage covering the in and output pressures of the Co, its efficiency Co_η and the output temperature of the El. In addition, the Ba_η is analyzed. Incorporating an AEL and electricity prices of the year 2022.

H Scenario analysis

The subsequent figures are listed to extend section 7.2. This includes a discussion of the H_2 demand influence and the results of the performed analysis.

H.1 Influence of the H_2 demand

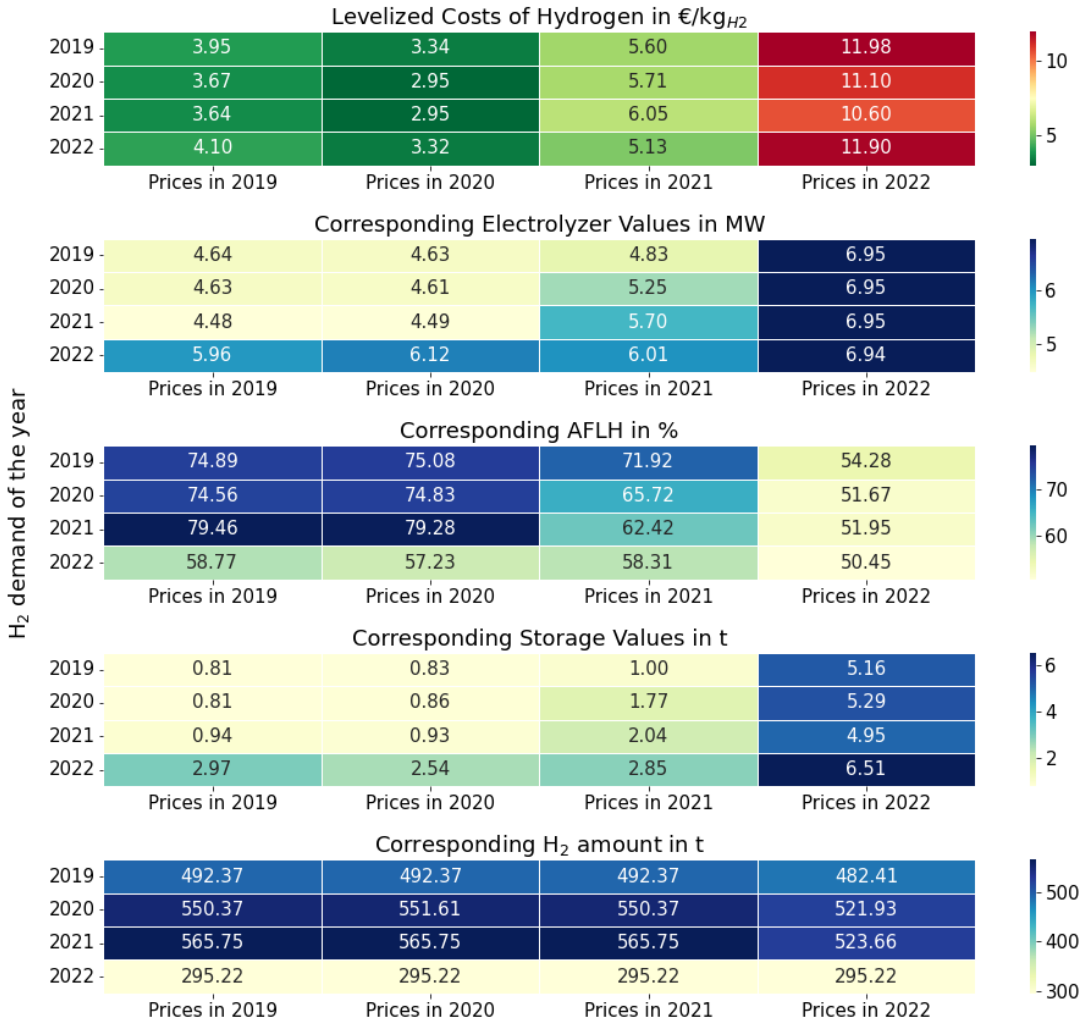

Figure H.1: Sensitivity of the H_2 demand time–series and the energy market price time–series based on a PEMEL system participating at the ID market including EPC and GoO.

Figure H.1 analyzes the influence of the H_2 demand in different years. It shows, that the most significant influence on the $LCoH_2$ are the energy–market prices varied at the x–axis in the plot. However, the H_2 demand time–series influence the obtained results. For example, the calculated $LCoH_2$ for the energy–market in 2019 and different H_2 demands, varies between 3.67 to 4.10 €/kg$_{H2}$. These differences are expected to result from the different downtime periods experienced in the respective year. The tool

is influenced by whether times of high prices are skipped by a production downtime (for example due to maintenance). Based on these results, the thesis concludes that a standard year has to be considered to allow an appropriate discussion of different energy market (price) scenarios.

H.2 Energy markets analysis

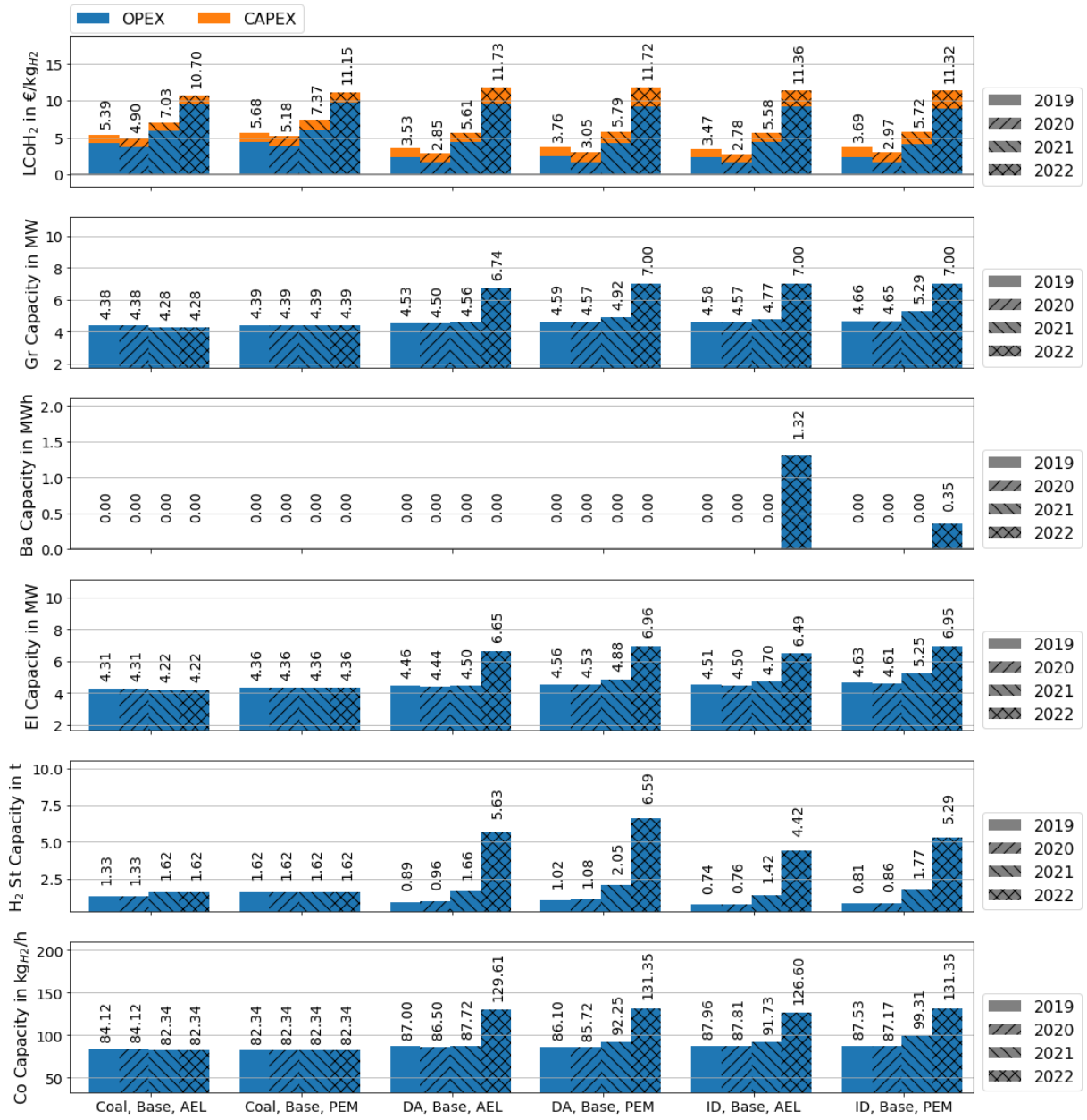

Figure H.2: Global results of the scenario analysis focusing on the energy markets incorporating a coal–power contract and the DA and ID markets. The AEL and PEMEL are considered without participation at the AuxS markets.

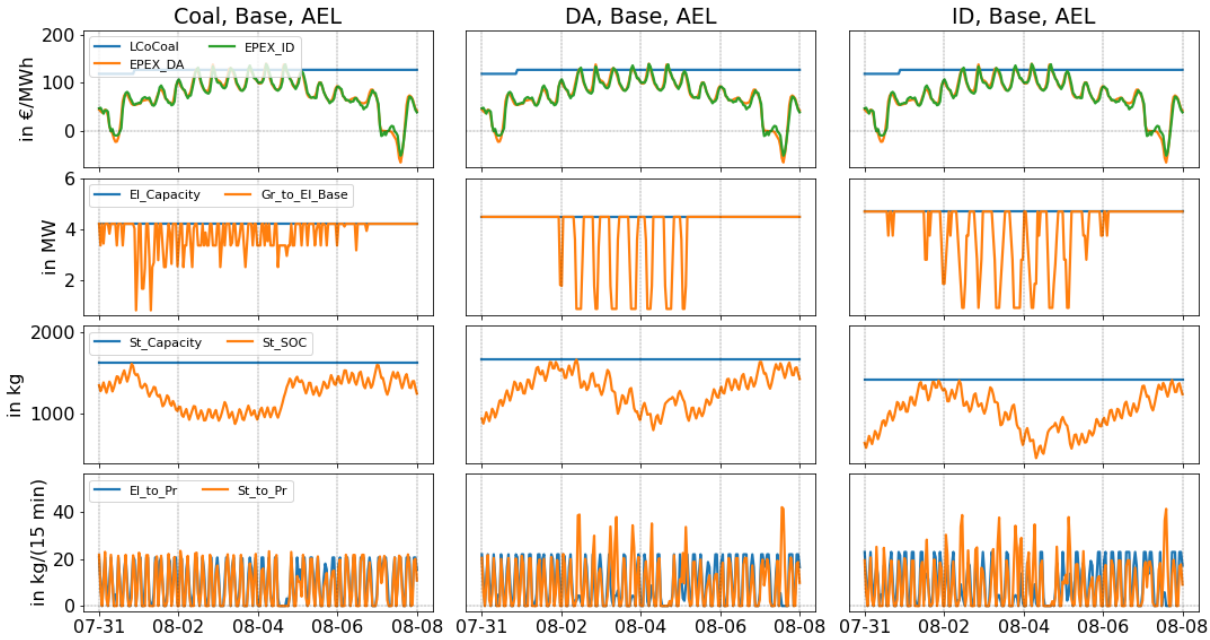

Figure H.3: Comparision of three AEL based scenarios in 2021 with the specific electricity prices, the dispatch of the El and the SOC of the H_2 St. The price time–series are retrieved from EPEX among others [38], [78], [79].

H.3 AuxS markets analysis

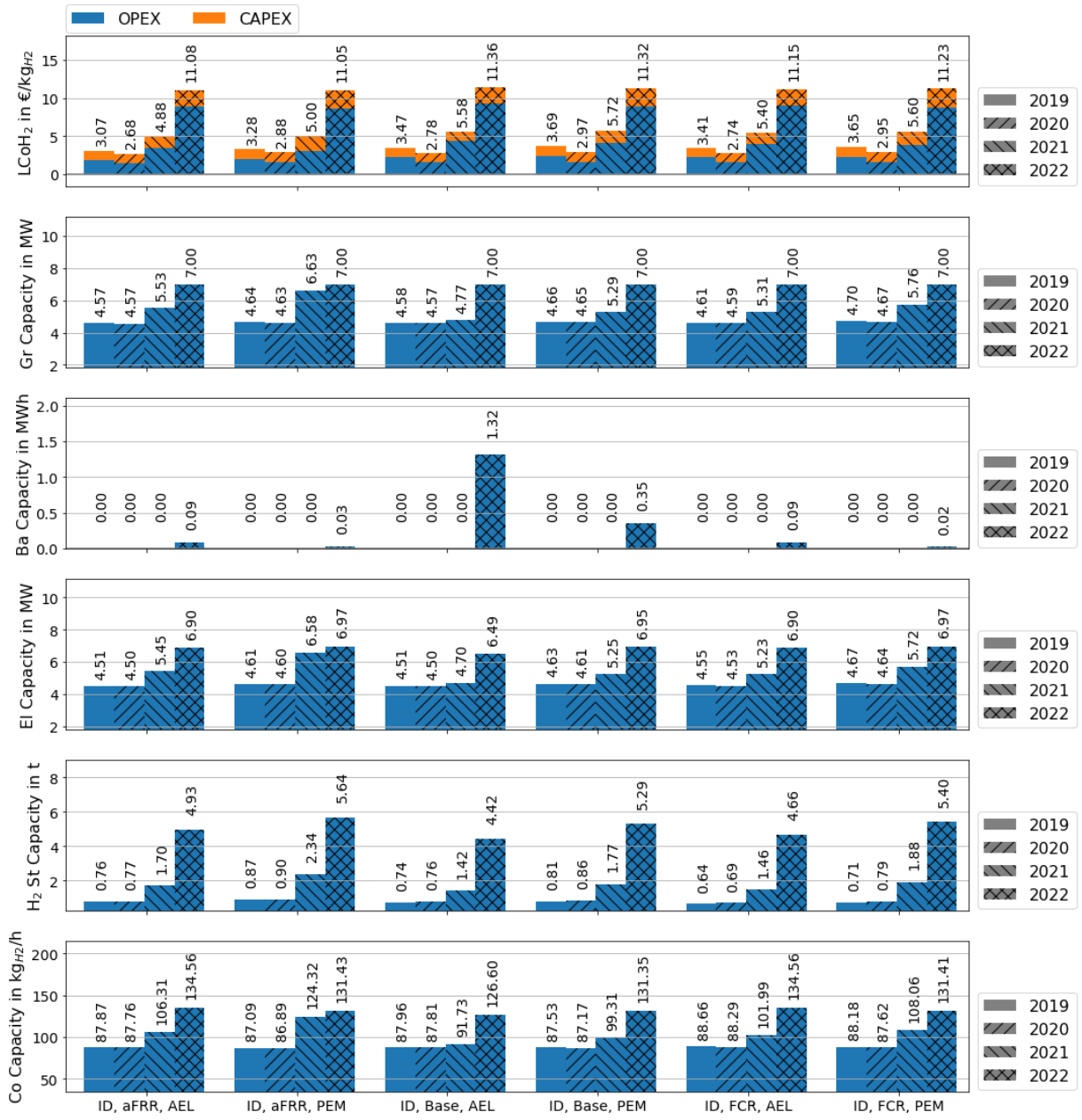

Figure H.4: Comparision of three AEL based scenarios in 2021 with the specific electricity prices, the dispatch of the El and the SOC of the H_2 St. The price time–series are retrieved from EPEX among others [38], [78], [79].

I MOO analysis

The subsequent figures supplement the MOO approach discussed in section 7.4. The figures inlude the Environmental weighting factor (f_{FCO2}) and its economic counter part while stating the representive objective values $LCoH_2$, $F_{CO2,H2}$ and the corresponding PtH_2 component sizes.

I.1 AEL based PtH_2 units

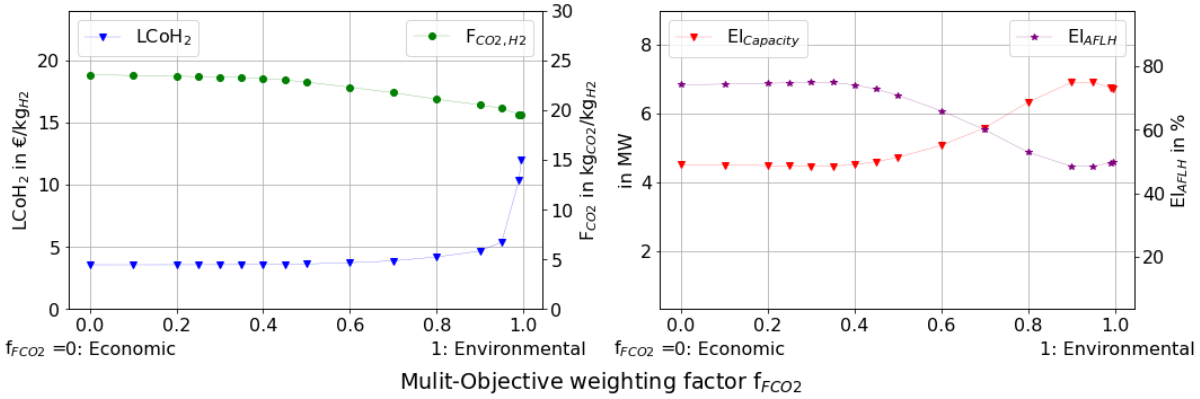

Figure I.1: Results of the MOO analysis of the PtH_2 unit with an AEL operating at the ID market in the year 2019.

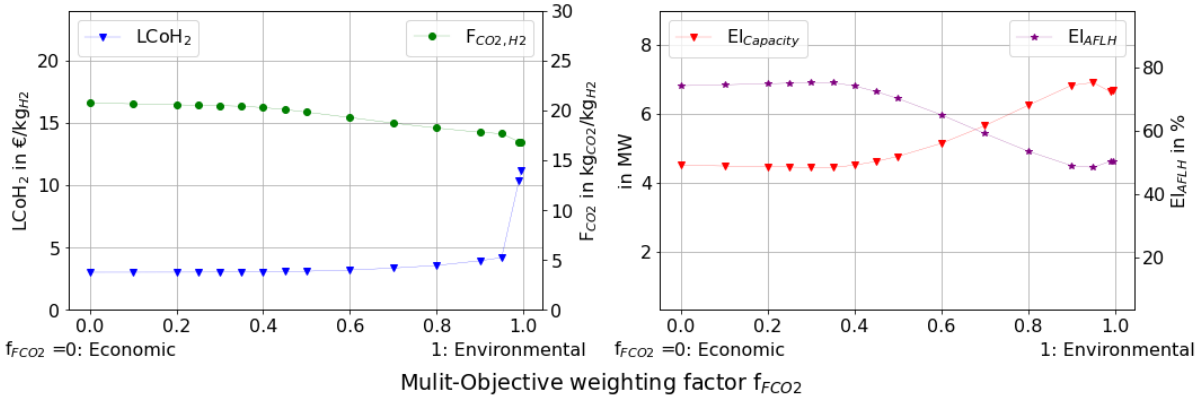

Figure I.2: Results of the MOO analysis of the PtH_2 unit with an AEL operating at the ID market in the year 2020.

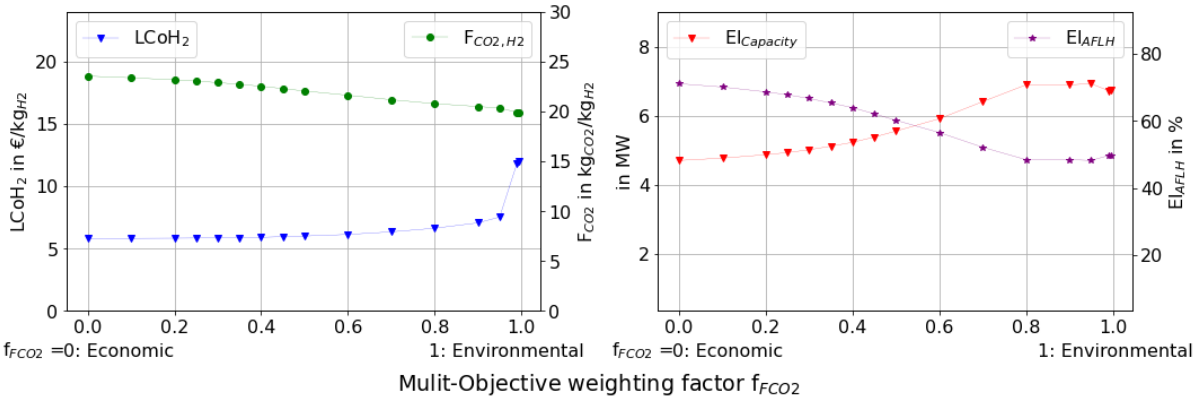

Figure I.3: Results of the MOO analysis of the PtH_2 unit with an AEL operating at the ID market in the year 2021.

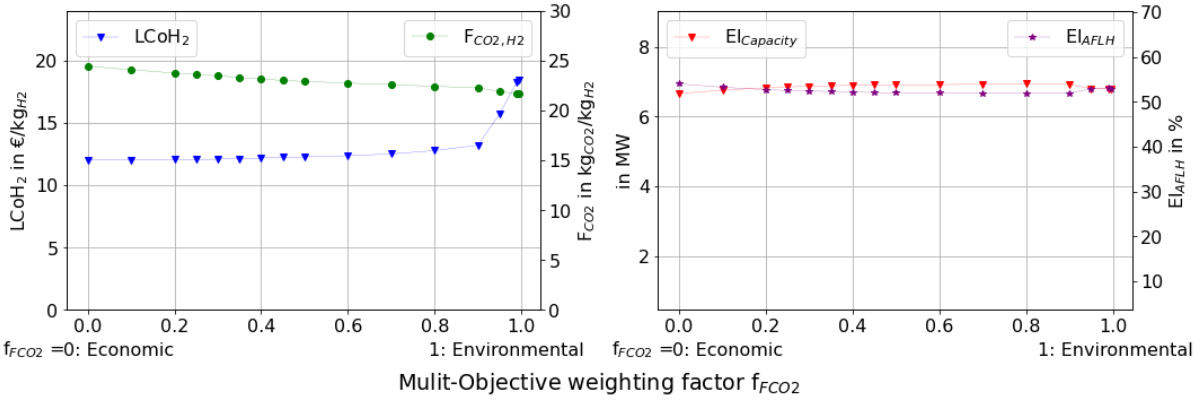

Figure I.4: Results of the MOO analysis of the PtH_2 unit with an AEL operating at the ID market in the year 2022.

I.2 PEMEL based PtH_2 units

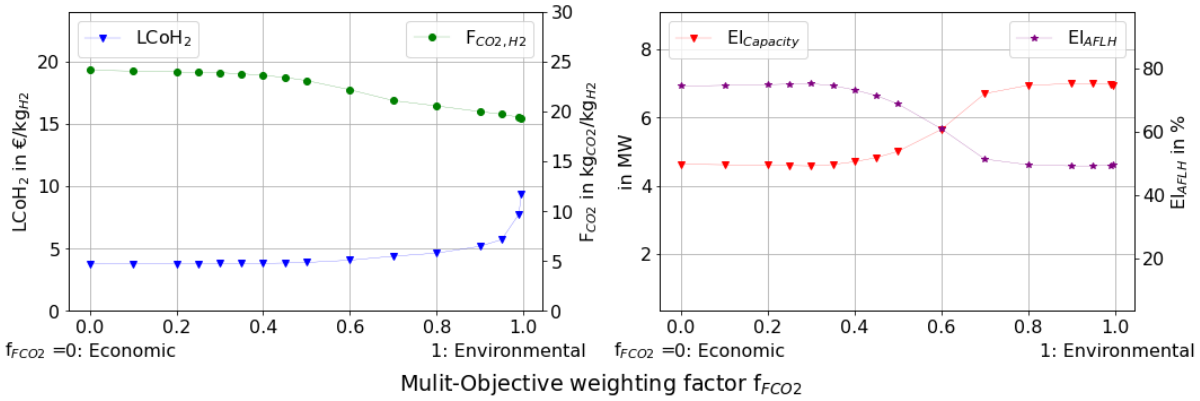

Figure I.5: Results of the MOO analysis of the PtH_2 unit with a PEMEL operating at the ID market in the year 2019.

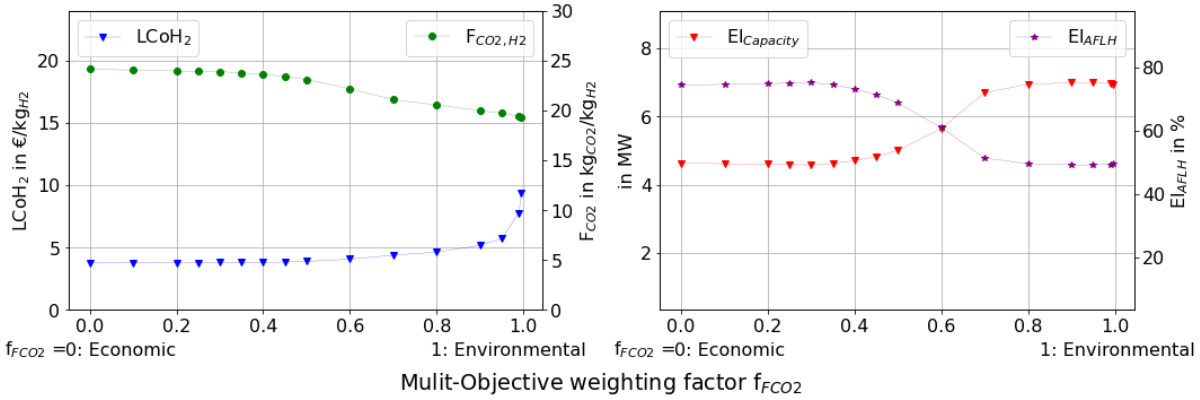

Figure I.6: Results of the MOO analysis of the PtH_2 unit with a PEMEL operating at the ID market in the year 2020.

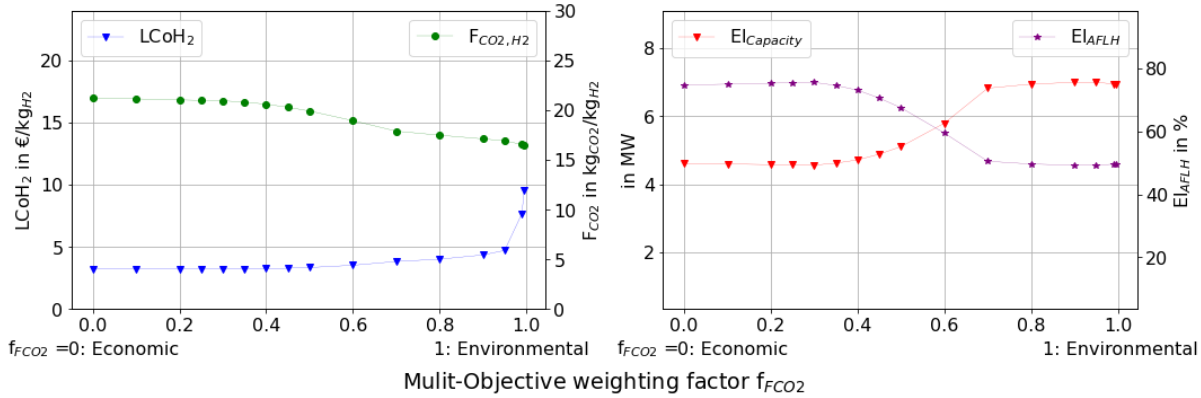

Figure I.7: Results of the MOO analysis of the PtH_2 unit with a PEMEL operating at the ID market in the year 2021.

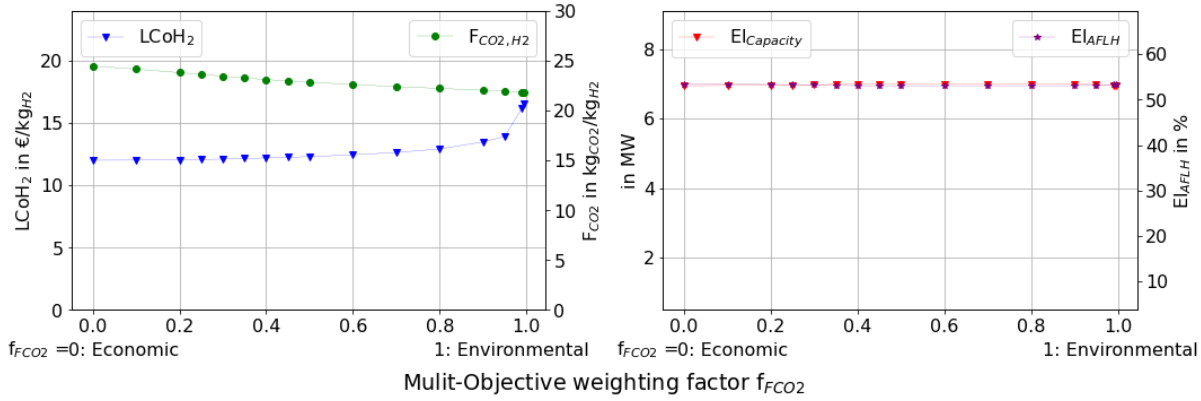

Figure I.8: Results of the MOO analysis of the PtH_2 unit with a PEMEL operating at the ID market in the year 2022.

J Digital Appendix

The elements to be found in the digital appendix attached to this thesis are listed subsequently. There are two preliminary notes. The flash drive data contains the optimization tool developed within the thesis whereas the relevant time–series can only be published partly as the data is considered sensitive. Further, the optimization results are stored in serialized data which can be extracted with the Python "pickle" function.

a) Digital version of this thesis

b) Optimization Tool (.py) and time–series data (.csv)

c) Data results of the performed analysis (serialized data)

d) Figures of the technical analysis

e) Figures of the implementation and tests procedure

f) Figures of the obtained results for different scenarios

   (i) Sensitivity figures

   (ii) Scenario figures

   (iii) MOO figures

   (iv) Influence of the H_2 demand time–series